IRON-RELATED MOLECULAR PHYSIOLOGY OF MARINE DIATOMS: INDIVIDUAL GENES TO COMMUNITY TRANSCRIPTOMES

Natalie Rachel Eve Cohen

A dissertation submitted to the faculty at the University of North Carolina at Chapel Hill in partial fulfillment of the requirements for the degree of Doctor of Philosophy in the Department of Marine Sciences in the Colleges of Arts and Sciences.

Chapel Hill
2017

Approved by:

Adrian Marchetti

Marc Alperin

Hans Paerl

Barbara MacGregor

William G. Sunda

© 2017
Natalie Rachel Eve Cohen
ALL RIGHTS RESERVED

ABSTRACT

Natalie Rachel Eve Cohen: Iron-related molecular physiology of marine diatoms: Individual genes to community metatranscriptomes
(Under the direction of Adrian Marchetti)

This dissertation aims to elucidate the molecular and physiological adaptations that determine the survival of diatoms under iron stress – an outcome with pronounced biogeochemical implications for nutrient cycling and carbon transfer between the atmosphere and the ocean. The following research has demonstrated that *Pseudo-nitzschia*, a genus of marine pennate diatoms, is unique among studied diatoms in its strategies for coping with iron stress and quickly responding to bioavailable iron, and highlights the mechanisms by which its competitive tendencies are achieved.

Community-wide bioinformatic analyses of natural diatom communities within the Northeast (NE) Pacific Ocean indicate changes in iron bioavailability may influence vitamin, nitrate and iron metabolism, with responses varying by algal taxa and geographical region. In particular, laboratory analyses support a direct iron effect on diatom B_7 synthesis, but show no iron influence on B_{12}-sensitive protein machinery. Therefore, molecular indications of B_{12}-stress in the NE Pacific Ocean following iron enrichment are likely a result of B_{12} consumption by blooming taxa offsetting B_{12} production. Furthermore, chronically iron-limited NE Pacific Ocean diatoms demonstrate a distinct transcriptomic response following iron enrichment as compared to coastal diatoms of the California Upwelling Zone receiving sporadic iron supplies. Genes highly expressed following iron addition in oceanic diatoms correspond to processes including iron storage and vitamin B_7 synthesis, with these expression patterns not shared by diatoms from

coastal locations. In addition, genes of interest involved in iron and nitrogen metabolism exhibit divergent expression patterns as a function of iron status between the two diatom genera investigated, *Pseudo-nitzschia* and *Thalassiosira*. Although some strategies appear universal, we report here distinct mechanisms among regions and taxa for dealing with iron stress and responding to iron enrichment events.

Using targeted physiological and gene expression approaches on the oceanic diatom *Pseudo-nitzschia granii*, the molecular bases underlying this organism's exceptional ability to cope in low-iron environments are explored. Iron storage abilities and associated ferritin gene expression in this oceanic diatom and several other coastal diatoms were investigated within laboratory studies. *Pseudo-nitzschia granii* was unique in its broad iron quota range and ferritin transcript response, consistent with long-term luxury iron storage. Several of the other diatoms examined contain two distinct putative ferritin genes that differ in their expression patterns as a function of iron status, with some ferritins increasing in expression under iron limiting conditions. Our results suggest that diatom ferritins may serve multiple functional roles among marine diatoms. Finally, a combination of transcriptomic sequencing and proteomic approaches was performed on *P. granii* under iron-replete and iron-limited conditions. Findings suggest the success of this species during periods of iron enrichment and its persistence under iron limitation stems from its competitive physiological and genetic characteristics, including constitutive use of iron-independent proteins, coordinated use of iron-dependent and –independent proteins depending on iron status, and enhanced vitamin biosynthesis under iron-replete conditions. Collectively, this research increases our understanding of how diatoms, with an emphasis on *Pseudo-nitzschia,* restructure their iron metabolism, respond to iron scarcity, and in turn alter their environment.

To the president and vice president of my fan club, my mom and dad, for their unconditional support and unwavering belief in my abilities

ACKNOWLEDGEMENTS

The work presented in this dissertation has been supported by the Department of Marine Sciences at UNC Chapel Hill, UNC Graduate School, and the National Science Foundation Grants OCE1334935 to A.M, OCE1334632 to B.S.T, OCE1334387 to M.B, OCE1333929 to K.T and OCE1259776 to K.B.

The completion of this degree would not have been possible without the guidance and support of my colleagues, collaborators, mentors and family. I give many thanks to my advisor Adrian Marchetti, for allowing me the opportunity to challenge myself beyond what I imagined possible and providing me with a priceless education. Thank you to my committee member Bill Sunda for sharing hours of his time and years of knowledge regarding photosynthesis and iron chemistry, and my committee members Marc Alperin, Barbara MacGregor, and Hans Paerl, for their guidance and encouragement over the years. The Department of Marine Sciences has provided the most supportive network of individuals (including faculty, staff and students) I could have hoped for during this challenging journey and I am especially grateful to Harvey Seim for creating an atmosphere conducive to my success.

To the girls of the Marchetti lab – I am eternally grateful for your support. Special thanks to Kelsey Ellis for being a dedicated editor, collaborator, lab mate and friend, Carly Moreno for teaching me not to take myself so seriously, and Kimberly DeLong for countless thought-provoking conversations regarding science, philosophy, and everything in between. And to the boys of the Marchetti lab, Rob Lampe and Weida Gong, for answering my never-ending stream

of differential expression-related questions. JP Balmonte is credited for strengthening my scientific and moral character. John Ramsey is credited for strengthening my smile.

A *huge* thank you to all of my collaborators for their phenomenal contributions to these research projects: Benjamin S. Twining (Bigelow), William Sunda (UNC), Kelsey Ellis (UNC), Elizabeth Mann (Bigelow), Brooke Stemple (UNC), Robert H. Lampe (UNC), Sergio Sañudo-Wilhelmy (USC), Wilton G Burns (UNC), Nina Schuback (UBC), Zackary Johnson (Duke), Sara Rauschenberg (Bigelow), Jeremy E Jacquot (Bigelow), Heather McNair (UCSB), Fedor I. Kuzminov (Rutgers), Mark A. Brzezinski (UCSB), Kimberlee Thamatrakoln (Rutgers), Maria T. Maldonado (UBC), Claire P. Till (UCSC), Sibel Bargu (LSU), Kenneth W. Bruland (UCSC), Weida Gong (UNC) and Mak Saito (WHOI). I am grateful to the scientists from the Institute of Ocean Sciences as well as the crews of the CCGS J.P. Tully for their support at sea during the 2013 and 2015 Line-P cruises, and to the scientific party and staff of the 2014 research cruise onboard the R/V Melville (IRNBRU).

Finally I thank my family members for continuing to invite me to holiday parties despite my lack of presence over the last six years: Mom and Dad, Lisa and Gary, Eric and Sean, Michelle, Leah, Sara, Shana, Jared, Jordan, Dylan and my brother Todd, who I have been trying to emulate since I was 6 years old. Thank you for being my academic trail blazer.

TABLE OF CONTENTS

LIST OF TABLES

LIST OF FIGURES

LIST OF ABBREVIATIONS

ACT	Actin
AMT	Ammonium transporter
B_7	Biotin
B_{12}	Cobalamin
BIOB	Biotin synthase
CUZ	California Upwelling Zone
DIC	Dissolved inorganic carbon
DFB	Desferrioxamine B
Fe	Iron
FLDA	Flavodoxin
FTN	Ferritin
HNLC	High-nutrient, low-chlorophyll
ISIP	Iron-starvation-induced-protein
METE	B_{12}-independent methionine synthase
METH	B_{12}-dependent methionine synthase
NIRA	Ferredoxin-nitrite reductase
NIRB	NADPH-nitrite reductase
NR	Nitrate reductase
NRT2	Nitrate transporter
NO_3	Nitrate
PETC	Cytochrome b_6/f complex

PETE	Plastocyanin
PETF	Ferredoxin
PETH	Ferredoxin-NADP+ reductase
PETJ	Cytochrome c_6
RHO	Rhodopsin
RBCL	RubisCO (large subunit)
SOD	Superoxide dismutase

INTRODUCTION

Phytoplankton serve as the base of the marine food web and are therefore integral to the survival of microbes, zooplankton, fish, and large marine mammals. They provide approximately half the planet's fixed carbon and oxygen supply through photosynthesis, and drive climate change over geologic timescales by transferring carbon from the atmosphere to the deep ocean. However, phytoplankton growth is constrained by the availability of the micronutrient iron in approximately 30% of the global ocean (Moore et al. 2002). When iron is added to previously iron-limited surface waters through either natural or artificial fertilization, certain phytoplankton groups, including the silicified microalgae diatoms, rapidly respond to form dense blooms (Boyd *et al.*, 2007).

Diatoms respond to favorable environmental conditions, including iron availability, more efficiently and quickly than other phytoplankton groups (Marchetti et al. 2012; Alexander et al. 2015). Even among diatoms, rapidly changing environmental conditions may select for the growth of particular species, depending on nutrient requirements. A seemingly minor physiological characteristic, such as the thickness of a diatom's silica shell, can substantially influence the efficiency of the biological carbon pump. Heavier, thicker cells transport more carbon to the deep ocean, altering ocean chemistry and leading to decreases in atmospheric carbon dioxide (Honjo et al. 2008). Therefore changes in diatom growth dynamics may influence global biogeochemical processes. Understanding the iron-specialized adaptations controlling diatom growth is increasingly relevant as we begin to predict how surface phytoplankton

communities will be affected by rapidly warming and acidifying marine environments, which may lead to changes in the ocean's iron supply (Shi et al. 2010; Hutchins and Boyd 2016).

Diatoms are diverse organisms; the two main lineages, centrics and pennates, share approximately 57% of their genomes with one another (Bowler et al. 2008). By sequencing the expressed genes of marine diatom species, we gain insight into molecular machinery that is sensitive to factors influencing growth. To date, hundreds of diatoms have been genetically characterized by high-throughput sequencing techniques, yielding genomic, transcriptomic and proteomic ('omic) data from phylogenetically- and geographically-diverse species (Keeling et al. 2014; Malviya et al. 2016). 'Omics approaches, including the ones implemented in the studies presented here, allow us the opportunity to examine changes in diatom metabolism as a function of environmental perturbation through the thousands of expressed genes or proteins present within natural communities. The following community-wide and taxa-specific studies leverage the power of 'omic technology and established reference databases to address how diverse diatoms differ in their iron, nitrate and vitamin strategies, with varying implications for phytoplankton community composition and primary production.

The overall aims of this dissertation are to expand on the important role of iron in influencing diatom metabolism and to explore how diatom taxa may differ in their molecular responses to varying iron supplies. The dissertation work presented here will address these aims through the following chapters: 1) influence of iron bioavailability on B-vitamin production and utilization dynamics in diatoms, 2) diverse strategies for coping with iron stress or quickly responding to iron enrichment between taxa and regions, 3) diversity in functional roles of the iron storage protein, ferritin, among diatom taxa, and 4) the physiological and molecular bases allowing for the exceptional competitiveness of the oceanic diatom *Pseudo-nitzschia granii*.

CHAPTER 1: IRON AND VITAMIN INTERACTIONS IN MARINE DIATOM ISOLATES AND NATURAL ASSEMBLAGES OF THE NORTHEAST PACIFIC OCEAN[1]

Introduction

Diatoms are responsible for approximately 20% of global carbon fixation each year and as much as 40% of marine organic carbon production (Armbrust 2009; Nelson et al. 1996). Over geologic timescales, it is hypothesized that varying rates of deep ocean carbon sequestration due to changes in diatom growth have influenced climate on a global scale (de Baar et al. 2005). Micronutrients such as iron are scarce enough to limit growth in vast areas of the ocean, called high-nutrient, low-chlorophyll (HNLC) regions (de Baar et al. 2005). These HNLC regions comprise approximately 30% of the ocean's surface waters and include large regions of the Southern Ocean, equatorial Pacific, and northeast Pacific Ocean (Boyd et al. 2007). During artificial iron fertilization, the introduction of bioavailable iron to HNLC waters creates diatom-dominated phytoplankton blooms with the potential to sequester large amounts of carbon in the deep ocean and seafloor sediments (de Baar et al. 2005; Boyd et al. 2007; Smetacek et al. 2012). Natural iron addition events occur when iron enters surface waters through aeolian transport,

[1]The content of this chapter has been accepted for publication in the peer-reviewed journal *Limnology and Oceanography* and is currently in press. The citation is as follows: Cohen NR, Ellis KA, Burns W, Lampe RH, Schuback N, Johnson Z, Sañudo-Wilhelmy S, Marchetti A. Iron and vitamin interactions in marine diatom isolates and natural assemblages of the Northeast Pacific Ocean. Slight modifications have been made to the text to facilitate reading. NRC and AM designed the study; NRC and KAE maintained experimental cultures and performed RNA analyses; WB provided diatom cell counts via light microscopy; RHL contributed bioinformatic support; NS obtained F_v:F_m measurements onboard the *CCGS John P. Tully*; ZJ provided bacterial cell count measurements; SS assisted with vitamin preconcentration and quantified concentrations; and NRC and AM wrote the manuscript.

vertical mixing of the water column, inputs from coastal sediments and rivers, and active hydrothermal venting along fast and slow-spreading tectonic plate boundaries (Moore et al. 2002; Saito et al. 2013). In HNLC waters of the Northeast Pacific Ocean, iron inputs from atmospheric dust from arid continental regions and volcanic continental margins are major sources, with continental margin inputs fueling winter phytoplankton blooms when dust deposition is low (Lam et al. 2006; Lam and Bishop 2008).

In addition to macro- and micro-nutrients, biosynthesized molecules such as B-vitamins serve as irreplaceable co-factors in enzymes and are required for proper cellular metabolism. These biologically-derived compounds may be growth-limiting to microorganisms unable to synthesize or acquire them from the environment. It has been proposed that B-vitamins influence microbial community composition, where during bloom events, seawater may be depleted or enriched in vitamins consumed or produced by the blooming species, thereby influencing species succession by creating optimal environmental conditions for organisms producing the depleted vitamin and/or requiring the enriched vitamin (Provasoli 1963; Bertrand et al. 2007, 2015; Gobler et al. 2007; Sanudo-Wilhelmy et al. 2014). In particular, instances of iron and B_{12} co-limitation on phytoplankton growth have been documented in the Southern Ocean (Bertrand et al. 2007, 2011, 2015). These findings collectively support the notion that vitamin availability can be an important driver of phytoplankton community dynamics and primary productivity in marine environments.

Vitamin B_7 (biotin) is required as a cofactor in carboxylation enzymes, most notably those involved in fatty acid synthesis, and is produced through a series of reactions beginning with the compound pimeloyl-coenzyme A (Streit and Entcheva 2003). Four genes are involved in the B_7 biosynthetic pathway, which that begins with the compound pimeloyl-CoA: *BIOF*

(encoding KAPA synthase), *BIOA* (DAPA synthase), *BIOD* (dethiobiotin synthase), and *BIOB* (biotin synthase) (Webb et al. 2007). Orthologs for all of the necessary genes are found in algae with the exception of *BIOD* (Croft et al. 2006). Because diatoms in culture are able to grow without B_7 added to the medium, it is assumed there is a *BIOD*-like homolog present that provides the end product of the *BIOD* reaction and the precursor to B_7, dethiobiotin. The last enzyme in the pathway, *BIOB*, is an iron-dependent enzyme containing multiple iron-sulfur clusters. The iron-sulfur clusters facilitate binding of dethiobiotin and donate a sulfur atom to the B_7 molecule itself (Jarrett 2005). Therefore, it is hypothesized that iron limitation in marine diatoms could alter the production, function and activity of *BIOB* enzymes. Interestingly, in the yeast *Saccharomyces cerevisiae*, iron limitation causes a decrease in B_7 biosynthesis and activates a transporter that functions in the acquisition of external B_7 (Shakoury-elizeh et al. 2004). If a similar mechanism for B_7 uptake is present in diatoms, this would allow intracellular iron in short supply to be redistributed towards other necessary iron-dependent processes, although such a mechanism has yet to be verified in diatoms.

B_{12}, or cobalamin, in eukaryotes plays a major role in methionine synthesis as it is required in the B_{12}-dependent enzyme, methionine synthase (METH). Alternatively, some phytoplankton possess a B_{12}-independent methionine synthase (METE). Both forms of the enzyme catalyze the transfer of a methyl group from methyltetrahydrofolate to homocysteine, the final step in methionine biosynthesis (Pejchal and Ludwig 2005). While some eukaryotic phytoplankton have the ability to produce vitamins B_1 and B_7, there is no evidence for *de novo* eukaryotic B_{12} synthesis. Thus, these microorganisms must either alleviate their B_{12} demand (e.g., by possessing *METE*) or obtain it from their environment (Croft et al. 2005; Sanudo-Wilhelmy et al. 2014). B_{12} is an energetically costly molecule to synthesize, requiring

approximately 21 biosynthetic enzymes (Warren et al. 2002). In eukaryotes, in addition to being used as a cofactor in METH, it is also utilized in succinyl Coenzyme A (CoA) production through methylmalonyl-CoA mutase, although since this enzyme is found in diatoms that do not require B_{12}, it is not the primary determinant of B_{12} auxotrophy (Croft et al. 2006). Instead, there is a strong correlation between the absence of a functional *METE* gene and B_{12} auxotrophy among examined microalgae (Helliwell et al. 2011). The B_{12} used by eukaryotic marine phytoplankton is produced by select prokaryotes; 35% of marine bacteria with sequenced genomes have the full B_{12} biosynthetic pathway (Sanudo-Wilhelmy et al. 2014). Recent studies have found that marine prokaryotes synthesize various forms of B_{12}. Photoautotrophic cyanobacteria likely produce only pseudocobalamin, a variant less bioavailable to marine eukaryotes compared to cobalamin, which is produced by select heterotrophic bacteria and Thaumarchaeota (Helliwell et al. 2016; Heal et al. 2017).

B_{12} availability may influence photosynthesis via production of phylloquinones, electron carriers involved in photosystem I, which require methionine for synthesis (Lohmann et al. 2006). Because B_{12} limitation has been observed to increase cellular iron requirements of B_{12}-requiring diatoms, potentially through increases in cytochromes and ferredoxins to replace phylloquinones. It is hypothesized iron and B_{12} co-limitation could impair photosynthesis by reducing the availability of both iron- and methionine-dependent electron carriers (King et al. 2011).

Even when iron and B_{12} do not limit primary production, increases in iron can influence phytoplankton B_{12} consumption and bacterial B_{12} production (Bertrand et al. 2011). 62% of available Southern Ocean diatom transcriptomes contain putative *METE*, compared to only 11% of diatom transcriptomes from other regions of the ocean (Ellis et al. 2017). This suggests there

may be a biogeographical basis for the presence of METE, in that phytoplankton may have reduced their B_{12} requirements where B_{12} availability is low and possibly growth limiting. Furthermore, B_{12} levels within coastal regions can influence community composition, as dinoflagellates have been observed to outcompete diatoms after B_{12} addition, creating a phytoplankton community that may be less likely to export carbon from the upper ocean when compared to diatom-dominated communities (Koch et al. 2012; Agusti et al. 2015).

In this study we investigated the influence of iron status on B_7 production, B_{12} utilization and METE activity in diatom isolates and natural assemblages from HNLC waters in the Northeast Pacific Ocean. We quantified the transcriptional response of *BIOB* under variable iron and B_7 growth conditions through targeted gene expression approaches in the diatom *Pseudo-nitzschia granii*. In addition, gene expression of *METH* in the B_{12}-auxotroph *P. granii*, and *METH* and *METE* in *Grammonema cf. islandica*, a diatom without a B_{12} requirement, were measured in response to variable iron and B_{12} status. This laboratory work complements previous studies investigating the influence of external B_{12} scarcity on *METH* and *METE* gene expression within laboratory cultures of model diatom species *Phaeodactylum tricornutum* and *Thalassiosira pseudonana* (Bertrand et al. 2012). Even more importantly, our laboratory studies serve as a basis for interpreting natural assemblage metatranscriptomic responses to iron/B_{12} and iron/B_7 incubation experiments performed at Ocean Station Papa in the Northeast Pacific Ocean. Iron and B-vitamin dynamics are explored in order to better understand how naturally occurring iron fertilization events could influence B-vitamin production and consumption and ultimately phytoplankton community growth and composition.

Methods

Culture conditions

The pennate diatoms *Pseudo-nitzschia granii* (UNC1102) and *Grammonema cf. islandica* (UBC1301) used in the laboratory experiments were isolated from Ocean Station Papa (OSP; 50°N, 145°W) in the Northeast Pacific in 2011 and 2013, respectively. Only *P. granii* was used for B_7 experiments. Both species were used for B_{12} experiments: *P. granii* is auxotrophic for B_{12} and *G. cf. islandica* is facultative, possessing *METE* (Ellis et al. 2017). *G. cf. islandica* was identified based on a 99% homology to an 18S rDNA sequence deposited in Genbank (accession number AJ535190).

Diatom cultures were maintained in the artificial seawater medium Aquil using trace metal clean (TMC) techniques according to Marchetti et al. (2006). Cells were grown in 28 mL acid-cleaned polycarbonate centrifuge tubes for a minimum of three growth cycles while in exponential phase (≥ 18 cell divisions) in order to pre-acclimate them to treatment conditions before use in large experimental cultures, with the exception of *P. granii* under B_{12}-limitation and *G. cf. islandica* under iron limitation (see below). Macronutrients were added to Aquil medium in final concentrations of 300 μmol L^{-1} NO_3^-, 10 μmol L^{-1} PO_4^{3-}, and 100 μmol L^{-1} $Si(OH)_4$. Media were dispensed into 2 L acid-cleaned, Milli-Q H_2O-rinsed polycarbonate bottles and supplemented with filter-sterilized (0.2-μm Acrodisc) trace metals, vitamins, and iron bound to EDTA in a 1:1 ratio. Growth-replete vitamin treatments (+B_7 or +B_{12}) were added in concentrations established for Aquil medium: 333 nmol L^{-1} B_1, 2,047 pmol L^{-1} B_7, 406 pmol L^{-1} B_{12} (Price et al. 1989). For treatments where B_7 was absent from the media (-B_7) all vitamins except B_7 were added in Aquil concentrations, and likewise within treatments where B_{12} was absent (-B_{12}), all vitamins except for B_{12} were added to growth media.

In iron-replete treatments (+Fe), Aquil was buffered with 100 µmol L^{-1} EDTA, yielding 1,370 nmol L^{-1} of total iron (Marchetti et al. 2009). In order to iron limit the growth rate of *Pseudo-nitzschia granii,* the iron chelator desferroxiamine B (DFB) was used in Fe:DFB ratios of 1.5:200 nmol L^{-1}. The Fe:DFB solution was allowed to equilibrate overnight before being added to medium. For *G. cf. islandica,* iron limitation of growth rate was achieved by adding premixed Fe-EDTA (1:1) at total iron concentrations of approximately 6.2 nmol L^{-1}. The +Fe and iron-limited (-Fe) media were allowed to chemically equilibrate overnight before use.

Four laboratory treatments were prepared to test the physiological and molecular responses of *P. granii* to varying iron/B_7 conditions: 1) +Fe/+B_7; 2) +Fe/-B_7; 3) -Fe/+B_7; and 4) -Fe/-B_7. Laboratory treatments prepared to test the response of *P. granii* and *G. cf. islandica* to iron/B_{12} conditions consisted of the following treatments: 1) +Fe/+B_{12}; 2) +Fe/-B_{12}; 3) -Fe/+B_{12}; 4) -Fe/-B_{12}. All experiments were inoculated when seed cultures were in mid-exponential growth phase, except in the cases of B_{12}-limited *P. granii* and iron-limited *G. cf. islandica*. Because *P. granii* growth ceased after approximately two transfers in -B_{12} medium regardless of antibiotic treatment, +B_{12}-grown *P. granii* cultures (18 mL) were used as the inoculum for the -B_{12}/+Fe and -B_{12}/-Fe treatments. A similar procedure was used to grow iron-limited *G. cf. islandica*. Exponential phase cultures were transferred from 8.6 nmol L^{-1} medium into medium containing a slightly lower iron concentration of 6.2 nmol L^{-1}.

All cultures were grown under a continuous, growth-saturating photon flux density of 110-120 µmol photons m^{-2} s^{-1}, with the exception of three iron-replete, light-limited *P. granii* cultures (+Fe/+B_7/LL) used as a reduced-growth rate comparison to iron-limited *P. granii* cultures. Light-limitation was obtained by growing these cells under a light intensity of 40 µmol photons m^{-2} s^{-1}(El-Sabaawi and Harrison 2006). The length of experiments varied among diatom

species and experimental treatments, but was typically between 5 and 15 days. Cultures were maintained at 12°C and mixed on a stir plate for the duration of the pre-acclimation and experimental period in order to prevent cells from settling. Subsamples were taken daily to monitor changes in cell biomass via fluorescence measurements and to ensure cells remained in the exponential phase of growth throughout the duration of the culture period.

Growth rates combined with photophysiology served as indicators of iron and vitamin stress or limitation. Exponential-phase growth rates (μ) were determined from *in vivo* chlorophyll *a* (chl *a*) fluorescence measurements using a Turner Designs model 10-AU fluorometer (*in vivo* chlorophyll optical kit). Growth rates were calculated using the linear regression of the natural log of chl *a* fluorescence versus time as described in Marchetti and Harrison (2007). In our *P. granii* cultures, the r^2 values of *in vivo* fluorescence versus cell concentration derived from light microscopy counts were > 0.9 for both iron-limited and iron-replete treatments, demonstrating fluorescence was proportional to cell concentrations.

Estimates of variable to maximum chlorophyll fluorescence (F_v:F_m) were obtained by measuring fluorescence induction with a Satlantic FIRe fluorometer (Gorbunov and Falkowski 2005). Before each measurement, a subsample (5mL) of each culture was placed in the dark for 20 minutes. A short, saturating pulse of blue light (450 nm) was applied to dark-acclimated phytoplankton for a 100 μs duration to measure fluorescence induction from minimum (F_o) to maximum (F_m) fluorescence yields. F_o and F_m were used to estimate F_v:F_m from $(F_m - F_o)\ F_m^{-1}$. Values were calculated for each culture upon harvesting during the mid-exponential growth phase. Iron/B_{12} culture measurements were obtained using single-turnover flash (STF), while iron/B_7 measurements were performed using multiple-turnover flash (MTF), which resulted in the differences in ranges of F_v:F_m observed between experiments (Kromkamp

and Forster 2003; Behrenfeld and Milligan 2013). Relative decreases in F_v:F_m due to iron limitation remained apparent within each set of experiments.

Iron addback experiments

To further investigate whether iron status triggers transcriptomic regulation of B_7 production genes, an iron add-back experiment was performed on a 2 L iron-limited *P. granii* culture with B_7 present in the growth medium. Growth rates were recorded to ensure iron limitation and monitor the response to iron addition. In a low biomass culture, 1.5 L of culture was harvested on 3 µm polycarbonate filters and stored at -80°C until RNA extraction. Approximately 49 µL of 1.4 x 10^{-2} M Fe:EDTA (1:1) was added to the remaining 500 mL of –Fe/+B_7 cells to achieve a final iron concentration of 1,370 nmol L^{-1}. Upon reaching mid-exponential phase, all but 1 mL of the exponentially-growing culture was harvested for RNA extraction and F_v:F_m determination. The remaining 1 mL of the culture was inoculated into 1L of fresh +Fe/+B_7 1 L medium in order to serve as a longer-term addback comparison. This post addback culture was harvested after 6 days of exponential growth and samples were again collected for F_v:F_m and RNA analysis.

Changes in gene expression of methionine synthase genes (*METH* and *METE*) in response to short-term iron addition were assessed for *P. granii* (*METH* only) and *G. cf. islandica* by performing an iron addback to previously iron-limited 1 L cultures. During early exponential growth phase, F_v:F_m was obtained and then 400 mL of iron-limited cells were filtered for RNA acquisition. Approximately 39 µL of 1.4 x 10^{-2} M Fe:EDTA (1:1) was then added to the remaining cells immediately following the first filtration to achieve a final iron concentration of 1,370 nmol L^{-1}. Cultures were incubated for an additional 24 hours before the

same set of measurements were obtained using the remainder of the culture. +Fe/+B_{12} and +Fe/-B_{12} cultures were grown using the same protocol but without additional added iron and subsequent second filtration. Before the final filtration of all cultures, a 2 mL subsample was collected to check for bacterial contamination using the SYBR-stain method described below.

Axenic culture conditions for iron/B_{12} experiments

Antibiotic-treated cultures were prepared by adding an antibiotic cocktail consisting of 50 µg mL^{-1} streptomycin, 100 µg mL^{-1} ampicillin, 67 µg mL^{-1} gentamycin, 20 µg mL^{-1} ciprofloxacin, and 2.2 µg mL^{-1} chloramphenicol (S. Amin, New York Univ). Antibiotics were added to 5 mL of cell culture and incubated for 24 hours before a 1 mL aliquot was transferred into fresh sterile Aquil medium of the corresponding treatment (+/-Fe, +/-B_{12}). Following equilibration to medium, bacteria were detected by the use of bacteriological peptone broth in conjunction with SYBR green staining and epifluorescent microscopy (Noble and Fuhrman 1998). Cultures were deemed low or free of bacteria when bacteriological peptone broth remained clear after 3 days and a substantial reduction in bacterial cells could be observed following SYBR staining. The reduction in bacteria was quantified by performing cell counts using Olympus Metamorph Basic v.7.6.0.0 software's integrated morphometry analysis on 10 randomly chosen fields of view from each SYBR-stained filter, which were then averaged. In all cultures, bacterial abundances were substantially reduced (93-99%) after incubation with antibiotics.

Targeted gene expression analysis

RNA extractions were performed on frozen filters using the RNAqueous 4-PCR kit

(Ambion). In order to remove DNA contamination, the RNA was then incubated with deoxyribonuclease (DNase) I at 37°C for 45 minutes and purified by DNase inactivation reagent (Ambion). RNA concentrations were measured using a NanoDrop spectrophotometer and samples with concentrations <250 ng μL^{-1} were concentrated using the RNeasy MinElute Cleanup Kit (Qiagen). Quantitative PCR (qPCR) with the RNA samples was used to determine DNA contamination levels, with samples containing >10 DNA copies per mL of RNA given additional incubation and purification with DNase I. Two µg of total RNA was reverse transcribed using the SuperScript III First-Strand cDNA Synthesis kit with oligo-dT primers (Invitrogen).

P. granii BIOB primers were designed from a *BIOB* partial gene sequence obtained from an Expressed Sequence Tag (EST) library (Marchetti et al. 2012) to target a 189 bp region, within the size range suitable for qPCR analysis (<250 bp). *P. granii ACT* and *METH* primers were previously designed from ESTs (Marchetti et al. 2015; Ellis et al. 2017). *G. cf. islandica METH*, *METE* and *ACT* primers for qPCR were designed from gene sequences obtained from the *G. cf. islandica* transcriptome to target 183, 172 and 175 bp regions, respectively. Primers were developed using Primer 3 and tested using PCR, gel electrophoresis, and PCR product sequencing (Table 1.1). Actin was chosen as the housekeeping gene as its expression has been reported to remain stable during varying physiological states in diatoms (Alexander et al. 2012). Standards were created for quantification purposes by PCR amplification at 94°C for 2 minutes, followed by 40 cycles of 30 seconds at 95°C, 30 seconds at the specific primer's annealing temperature, and 1 minute at 72°C. Reactions consisted of 1 µL DNA, 1 µL Taq Buffer, 1 µL $MgCl_2$, 0.5 µL dNTP, 0.4 µL of forward and reverse primers, 0.075 µL Taq polymerase, and 4.625 µL UV-treated water. Amplified fragments were cloned and transformed into *Escherichia*

coli using the TOPO TA Cloning Kit (Life Technologies). Colonies containing the cloned gene fragment were incubated at 37°C overnight in liquid Luria broth media, and plasmids were extracted using the QIAprep Spin Miniprep Kit (Qiagen). Plasmids were linearized by incubation with *SpeI* at 37°C for 1 hour and enzyme denaturation at 80°C for 20 minutes. Linearized plasmids were quantified with a Qubit using the Qubit RNA Assay Kit (Life Technologies) to create a set of standards for each gene of interest ranging between 10^1-10^6 copies μL^{-1}. Copies per µL of cDNA were determined by performing triplicate 20 µL qPCR reactions with a Mastercycler ep gradient S (Eppendorf) on each sample and normalizing each gene to Actin (*ACT*) expression from the same sample. Reactions were composed of 2 µL DNA standard or cDNA unknown, 10 µL SyberFast Universal qPCR mastermix (Kapa), 4.8 □L Milli-Q water, and 1.6 µL each of the forward and reverse primers.

Organism	Gene	Forward Primer (5' to 3')	Reverse Primer (5' to 3')	Target Length	GenBank accession
Pseudo-nitzschia granii	*BIOB*	TGTCACCGTTGAAAATGGAA	GAACTCCTTTGGGGGAAGAC	189	KX255663
Pseudo-nitzschia granii	*ACT*	ACTCGTTGACTACCACCGCT	GGACATCTGAATCGCTCGTTT	181	FJ004969
Grammonema cf. islandica	*METH*	AGCCTCGGAGGTAGGAAGAG	GGCAACTGAAGACATGCTGA	183	KX255664
Grammonema cf. islandica	*METE*	CTGGAACGACACCCAGAAAT	GAAGCACTGGAAAGGTCAGC	172	KX255665
Grammonema cf. islandica	*ACT*	AGTTGTTGCTTCGTCGGTCT	GATAGCTCGACTGCCTGACC	175	KX255666

Table 1.1. qPCR primers used in laboratory culture experiments.

Statistical analyses on culture experiments

To test for significant differences in growth rates, F_v:F_m values, and gene expressions among iron/B_7 treatments, a two-way ANOVA was used followed by Tukey multiple comparison tests. To test for significant differences between iron/B_{12} treatments, two-tailed homoscedastic t-tests within each species were performed on growth rate, gene expression and

F_v:F_m values. Significant differences in chlorophyll *a*, F_v:F_m, and diatom densities among incubation treatments was determined through one-way RM ANOVA followed by Holm-Sidak comparison tests. The level of statistical significance for all tests was $p < 0.05$. All tests were performed in Sigmaplot v12.5 (Systat Software Inc.).

Field experimental design and RNA extraction

Near-surface seawater was collected onboard the CCGS John P. Tully from June 7-25th 2013 as a part of the Line-P program that transects coastal to open ocean waters in the subarctic Northeast Pacific Ocean. Samples were collected at stations P2 (48°36N, 126°00W), P4 (48°39N 126°40W), P12 (48°58.2N, 130°40W), P16 (49°17N, 134°40W), P20 (49°34, 138°40W) and P26 (OSP; 50°N, 145°W). At each station, samples for size-fractionated chl *a*, dissolved nutrients and dissolved vitamin concentrations, flow cytometry and phytoplankton preservations were collected (detailed methods of each measurement are provided below). At OSP, microcosm iron and B_7/B_{12} enrichment experiments were conducted. Seawater was collected from a depth of 10 meters, corresponding to 33% surface irradiance, using a trace metal clean sampling system consisting of Teflon tubing connecting to an air bellows pump as described in Marchetti et al. (2012). Seawater was pumped directly into a positive-pressure laminar flow hood and used to rinse and fill trace metal clean (TMC) cubitainers. Prior cleaning procedures for the cubitainers included 1.2 mol L^{-1} hydrochloric acid (reagent grade) soaking for three days followed by three rinses with Milli-Q water, soaking with 1.2 mol L^{-1} hydrochloric acid (trace metal grade) for one week, three rinses with Milli-Q, and finally a 0.1 mol L^{-1} acetic acid (trace metal grade) soak. Immediately before use, cubitainers were rinsed three times with ambient low-iron OSP seawater. Approximately 30 L of seawater was immediately collected for initial

measurements, and served as the initial time point (T_0).

Cubitainers (~10 L) were prepared in triplicate for each treatment and incubated for 96 hours. The following treatments were performed: 4 nmol L^{-1} iron chloride (Fe), 200 pmol L^{-1} biotin (B_7), 200 pmol L^{-1} cyanocobalamin (B_{12}), 4 nmol L^{-1} iron chloride and 200 pmol L^{-1} biotin (FeB_7), and 4 nmol L^{-1} iron chloride and 200 pmol L^{-1} cyanocobalamin (FeB_{12}). Three cubitainers received no additions and served as an unamended control (Ctl). Cubitainers were placed in two on-deck Plexiglass incubators and cooled with flow-through seawater at 33% irradiance for 96 hours. Subsamples from each cubitainer were collected following the 96 hour incubation and used for measurements of size-fractionated chl *a*, diatom cell counts, F_v:F_m and RNA.

Seawater (9-10 L) for RNA analysis was filtered directly from each cubitainer onto Supor Pall 0.45µm porosity filters (142 mm) using a peristaltic pump. Filters were wrapped in aluminum foil and immediately flash frozen in liquid nitrogen. Samples were later transferred to storage in -80°C freezers until RNA extractions were performed. Filters were briefly thawed on ice before being extracted individually using the ToTALLY RNA Kit (Ambion). The extraction procedure followed manufacturer protocols with the modified first step of glass bead addition in order to facilitate disruption of cells. Removal of DNA was performed with DNAse 1 (Ambion) followed by qPCR on total RNA to ensure DNA contamination was not present in total RNA samples.

Physiological assessment: chlorophyll a, F_v:F_m, cell counts, bacterial counts

For estimates of size fractionated chl *a*, 300 mL of seawater was vacuum filtered through a 5 µm pore-sized polycarbonate filter, and the filtrate was re-passed through a GF/F filter (0.7

μm pore size). Filters were frozen at -80°C until analysis. Chl *a* extraction was performed in the laboratory using 90% acetone at -20°C overnight and concentrations were determined fluorometrically using a Turner Designs 10-AU fluorometer (Brand et al. 1981). While it is true that chl *a* content varies by taxa and with changes in cellular physiology (thus affecting the C:chl *a* cellular ratio), chl *a* is a relatively good proxy for phytoplankton carbon concentrations at values above 0.14 μg L^{-1}, and therefore chl *a* concentrations are interpreted as an equivalent measurement to phytoplankton biomass (Behrenfeld et al. 2005). Photophysiology measurements were performed on a bench-top fast repetition rate fluorometer (FRRF, Solience Instruments). Background fluorescence blanks were prepared by syringe filtering <5 mL of seawater through a GF/F. A single turnover (ST) fluorescence induction protocol (100 flashlets with 1.0 μs length and 2.5 μs interval, 46,200 μmol quanta m^{-2} s^{-1} peak power intensity, providing ~5-10 quanta per RCII in 250 μs) was applied. The fluorescence yields F_o and F_m were estimated from the mean of 22 consecutive ST acquisitions. In the study region, iron addition has been shown to increase the F_v:F_m of phytoplankton communities from less than 0.4 to approximately 0.6 (Schuback et al. 2015).

Diatom cell densities were estimated by preserving 250 mL of seawater with 4% Lugol's solution in amber glass bottles and kept in the dark until analysis. In the laboratory 50-100 mL of the preserved samples were settled in Utermöhl settling chambers for at least 24 hours. Diatom cell counts were performed via light microscopy and at least 10 fields of view were counted. Cell counts were determined based on volume settled, magnification used, and slide area. Diatoms were sorted into one of the following groups: 1) *Pseudo-nitzschia* (large; 20 μm in length), 2) *Pseudo-nitzschia* (small; <20 μm in length), 3) centrics, and 4) other pennates. "Centrics"

included both large and small centrics, e.g. *Proboscia sp.*, and *Chaetoceros sp*. "Other pennates" included pennates visually distinct from *Pseudo-nitzschia*.

To measure bacterial cell densities along the Line-P transect, 2 mL surface seawater was collected and preserved using a 10% flow cytometry preservative cocktail consisting of 40% PBS, 10% formalin and 0.5% glutaraldehyde. Samples were refrigerated at 4°C for 15 minutes to allow for fixative to permeate membranes before being flash frozen with liquid nitrogen and stored at -80°C until analysis. Thawed fractions were injected into a Becton Dickson FACSCalibur flow cytometer (San Jose, CA, USA). Total bacteria were targeted using a SYBR green stain fluorescing at 530 nm. *Synechococcus* populations were captured via fluorescence at 585 nm, with the addition of alignment beads for calibration. *Prochlorococcus* was not detected in any of the samples. FlowJo v7.6.5 was used for quantitative analysis (Johnson et al. 2010). Total bacterial populations subtracted from the cyanobacteria populations are referred to as non-photosynthetic (non-ps) bacteria.

Dissolved vitamins

For determination of dissolved B-vitamin (B_1 [thiamine hydrochloride], B_2 [riboflavin], B_6 [pyridoxal hydrochloride], B_7 [biotin], and B_{12} [cyanocobalamin]) concentrations, duplicate 2 L seawater samples from 5 m depth were collected during the day using rosette Niskins at stations P2, P4, P12, P16, P20 and OSP along the Line-P transect. Seawater was filtered using a sterile, methanol-cleaned Whatman Polycap AS 0.2 µm porosity filter into dark HDPE bottles and frozen at -20°C onboard the vessel. Samples were shipped on dry-ice and stored at -80°C until pre-concentration in the laboratory.

Vitamin preconcentration was performed via a solid phase extraction (SPE) technique developed by Sañudo-Wilhelmy et al. (2012). Briefly, Bondesil-C18 resin (Agilent) was prepared by mixing with reagent grade methanol in a 1:1 ratio to create a resin slurry. Next a series of two rinses was performed on the resin by allowing particles to settle, decanting off the methanol, and resupplying fresh methanol. Resin was subsequently rinsed with Milli-Q water in the same manner three times, and 6-7 mL of this 1:1 resin:water slurry was packed into polypropylene chromatography columns (Bio-Rad). Resin columns were further conditioned by passing through 20 mL HPLC grade methanol, 20 mL of pH adjusted 6.5 Milli-Q, followed by 20 mL of seawater sample adjusted to pH 6.5. These seawater samples were thawed overnight and acidified to a pH of 6.5 with 6 M hydrochloric acid. Following resin conditioning, the remainder of seawater samples were passed through the columns at a rate of approximately 1 mL min^{-1} in the dark at room temperature. Seawater was subsequently acidified to a pH of 2 and re-passed through the resin, again under dark conditions at room temperature. All vitamins aside from B_7 are bound to resin at pH of 6.5, while B_7 requires a pH of 2 in order to more effectively bind resin. Significant loss of vitamin fractions over the duration of the resin passing has not been observed using this method, and the vitamin fractions appear to be stable at room temperature given our satisfactory spike recoveries (see below). The only vitamin found to be light sensitive was riboflavin, and to minimize loss, the pre-concentrations were performed in the dark. Column resin pH was neutralized by passing through 30 mL of pH 7 Milli-Q water. The addition of water to the resin column does not cause elution to occur and is solely for removal of salt that could interfere in the LC/MS quantification.

Immediately before analysis, samples were eluted with 10 mL of methanol, dried under vacuum pressure at 40°C, and dissolved in 250 mL of LCMS water (pH adjusted to 6.5).

Standard addition was performed on every sample in order to account for matrix effects and prepare a five-point standard curve. Negative and positive controls consisted of a blank (comprised of only 2 L synthetic seawater, no vitamins added) and a spike (1 pmol L^{-1} spike of each B-vitamin into synthetic seawater), respectively. LC/MS analysis was performed with a Thermo TSQ Quantum Access triple quadrupole mass spectrometer with electro-spray ionization and a Thermo Accela High Speed Liquid Chromatography set-up using LCMS water as the injection solvent (Sañudo-Wilhelmy et al. 2012). Excalibur software was used for computational quantitative analysis. Instrumental detection limits were used due to traditional analytical detection limits based on 3X-standard deviation of the procedural blank being essentially zero. The instrumental detection limits are defined as 3X-standard deviation of the lowest detectable concentration of standard used for each vitamin, and were as follows: 0.25 pmol L^{-1} for thiamine hydrochloride and biotin, 0.13 pmol L^{-1} for riboflavin and cyanocobalamin, and 0.38 pmol L^{-1} for pyridoxal hydrochloride. SPE recoveries were determined by dividing the amount measured via LC/MS (multiplied by the concentration factor) by the amount added in the spiked control: 100% for thiamine hydrochloride, 63% for riboflavin, 75% for pyridoxal hydrochloride, 180% for biotin, and 72% for cyanocobalamin. These recoveries are comparable to those obtained in previous vitamin studies even with much lower spike concentrations used (Sañudo-Wilhelmy et al. 2012; Heal et al. 2014). The high biotin recovery indicates up to 1 pmol L^{-1} of biotin contamination may have been introduced via reagents used in the seawater preconcentration procedure. Therefore, biotin concentrations reported may be artificially slightly higher than naturally occurring along the Line P transect.

Metatranscriptomic sequencing analysis

For metatranscriptomic sequencing, mRNA in each sample was concentrated using the Poly(A)Purist MAG Kit (Ambion) followed by library preparation with the Illumina TruSeq Stranded mRNA Library Preparation Kit and HiSeq v4 reagents. To obtain sequences for all incubations, RNA was pooled by treatment for all triplicate samples (duplicate for the control). Sequencing of barcoded samples was performed on a single lane on an Illumina HiSeq 2000 (125bp, paired-end). Sequencing statistics are provided in Table 1.2. Raw sequences are deposited in the Sequence Reach Archive (SRA) database under accession number SRP074366.

Raw reads were trimmed for quality bases and removal of adapters using Trimmomatic v0.32 (paired-end mode, adaptive quality trim with 40bp target length and strictness of 0.6, minimum length of 36bp; Bolger et al. 2014). Trimmed paired reads were merged into single reads with BBMerge v8.0. The resulting merged pairs and non-overlapping paired-end reads were assembled using ABySS v1.5.2 with a multi-kmer approach (Birol et al. 2009). Assemblies were merged to remove redundant contigs using Trans-ABySS v1.5.3 (Robertson et al. 2010). Read counts were obtained by mapping raw reads to contigs with Bowtie2 v2.2.6 (end-to-end alignment; Langmead and Salzberg 2012; Table 1.2). Alignments were filtered by mapping quality score (MAPQ) of 10 or higher as determined by SAMtools v1.2 (Li et al. 2009). Taxonomic and functional annotations were assigned based on sequence homology via BLASTx v2.3.0 with an E-value cutoff of 10^{-3} (Altschul et al. 1990). Functional annotations were assigned using the Kyoto Encyclopedia of Genes and Genomes (KEGG; Release 75), while taxonomic assignments were obtained with MarineRefII (Laboratory of Mary Ann Moran, University of Georgia), a custom-made database comprised of protein sequences of marine microbial prokaryotes and eukaryotes including all sequenced transcriptomes from the Marine Microbial

Eukaryote Transcriptome Sequencing Project (MMETSP; Keeling et al. 2014). Taxonomic information was obtained from the National Center for Biotechnology Information's (NCBI) Taxonomy Database (each isolate in MarineRefII is assigned a NCBI taxonomic ID). The information from NCBI was manually curated to ensure proper assignment and use of common phytoplankton taxonomic ranks.

All diatom-assigned counts were summed by genus and KEGG Orthology (KO). For genes without KO assignments but possessing an annotated gene definition (i.e. *CBA1*, *ISIP2A*, *ISIP2B)*, raw counts corresponding to KEGG gene definitions were summed. edgeR v3.12.0 was used to calculate normalized fold change and counts-per-million (CPM) from pairwise comparisons (Robinson and Smyth 2008; Robinson et al. 2010). For pathway-level analysis, read counts corresponding to KOs contained within each KEGG vitamin biosynthetic module were summed. Heatmaps were produced with the R package pheatmap v1.0.8, and the dendrogram was created using the default settings of Euclidean distance and hierarchical clustering. MA plots with taxonomic pies were created with edgeR output and a custom script available at www.github.com/marchettilab/mantaPlot. Assembled contigs, functional and taxonomic annotations, and read counts information are available at marchettilab.web.unc.edu/data/.

	Assembly	Control		B_7		B_{12}		Fe		FeB_7		FeB_{12}	
Read data													
No. of paired end reads post trimming		22,957,272		14,562,574		27,625,670		23,884,208		15,503,378		28,374,140	
No. of paired reads mapped		11,902,742	52%	8,312,483	57%	14,069,792	51%	13,112,327	55%	9,326,955	60%	16,584,419	58%
Avg length of trimmed forward read (bp)		84		86		85		84		87		88	
Assembly													
No. of contigs	5,207,452												
Annotation													
KEGG KO													
No. of contigs with functional annotation	931,727 (18%)												
No. of raw reads with functional annotation		4,102,357	34%	2,740,350	33%	5,083,629	36%	4,776,724	36%	3,125,834	34%	5,677,431	34%
MarineRefII													
No. of contigs with taxonomic annotation	2,323,607 (45%)												
No. of raw reads with taxonomic annotation		8,484,766	71%	5,500,115	66%	10,166,209	72%	9,500,463	72%	6,517,429	70%	11,557,063	70%
Diatoms													
MarineRefII													
No. of contigs	378,177 (7%)												
No. of reads		1,670,600	14%	1,092,236	13%	2,880,331	20%	3,767,865	29%	2,796,625	30%	5,303,939	32%
KEGG KO													
No. of contigs	128,876 (2%)												
No. of reads		667,810	6%	429,353	5%	1,120,147	8%	1,691,535	13%	1,234,002	13%	2,331,084	14%
% of diatom reads with KEGG annotations		39.97%		39.31%		38.89%		44.89%		44.12%		43.95%	

Table 1.2. Metatranscriptomic sequencing statistics

Results

BIOB gene expression in response to iron limitation within laboratory cultures

Iron-replete *P. granii* cultures grew at a specific growth rate of 1.70 ± 0.04 d^{-1} while iron-limited cultures maintained a specific growth rate of approximately 0.60 ± 0.08 d^{-1}, 65% less than the maximum growth rate (Fig. 1.1A; $p < 0.001$). There was no significant difference in growth rate between cultures with and without B_7 added to the growth media, either under iron-replete or iron-limited conditions. Assessment of F_v:F_m further supports a physiological response to iron treatment and a negligible effect of external B_7 on photophysiology as iron-replete cultures maintained an F_v:F_m of approximately 0.71 ± 0.002 while iron-limited cultures produced ratios of approximately 0.59 ± 0.01, an approximate 17% reduction (Fig. 1.1B*;* $p < 0.036$).

Relative *BIOB* gene expression, obtained by normalizing *BIOB* to *ACT* transcripts (*BIOB/ACT*), indicated an approximate 2-fold decrease in -Fe/+B_7 relative to the +Fe/+B_7 treatment (Fig. 1.1C; $p = 0.009$). *BIOB* expression in -Fe/-B_7 was also reduced although not significantly different from either the +Fe/+B_7 ($p = 0.092$), or -Fe/+B_7 ($p = 0.058$). Iron resupply experiments showed an increase in *BIOB* expression following the addition of iron to –Fe/+B_7 cells, with expression levels increasing >3-fold over the duration of 6 days (Fig. 1.1C).

Light limitation, in which cultures were grown under 40 µmol photons m^{-2} s^{-1}, resulted in a significantly reduced growth rate as compared to control cultures exposed to growth-saturating light conditions (110 µmol photons m^{-2} s^{-1}; Fig. 1.2A; $p = 0.05$). *BIOB* expression levels were not significantly different between the low-light (+Fe/+B_7/LL) treatment and +Fe/+B_7 ($p = 0.106$), suggesting decreases in *BIOB* expression under iron limitation are not a general response to a decrease in growth rate (Fig. 1.2B).

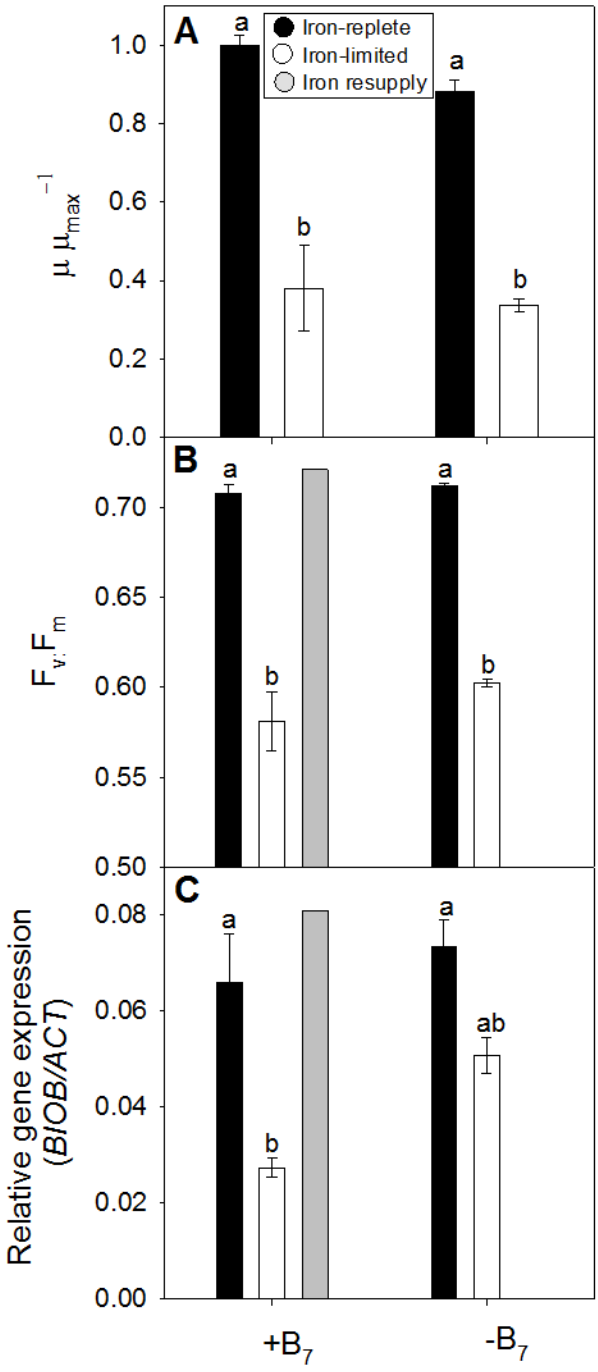

Fig. 1.1. *P. granii* growth rates, F_v:F_m, and BIOB/ACT gene expression as a function of iron and B_7 status. **A**) Relative growth rates compared to the maximum growth rate (μ_{max}), **B**) Maximum photochemical yield of PSII (F_v:F_m), and **C**) Relative gene expression of biotin synthase normalized to Actin (BIOB/ACT) of iron-replete (+Fe), iron-limited (-Fe) and iron resupplied *P. granii* in the presence (+B_7) or absence (-B_7) of vitamin B_7. Letters denote significant differences among treatments as determined via one-way ANOVA and Tukey multiple comparison tests ($p < 0.05$). Error bars represent ±1 standard error associated with the mean (n = 3, except in the iron resupply experiment where n = 1)

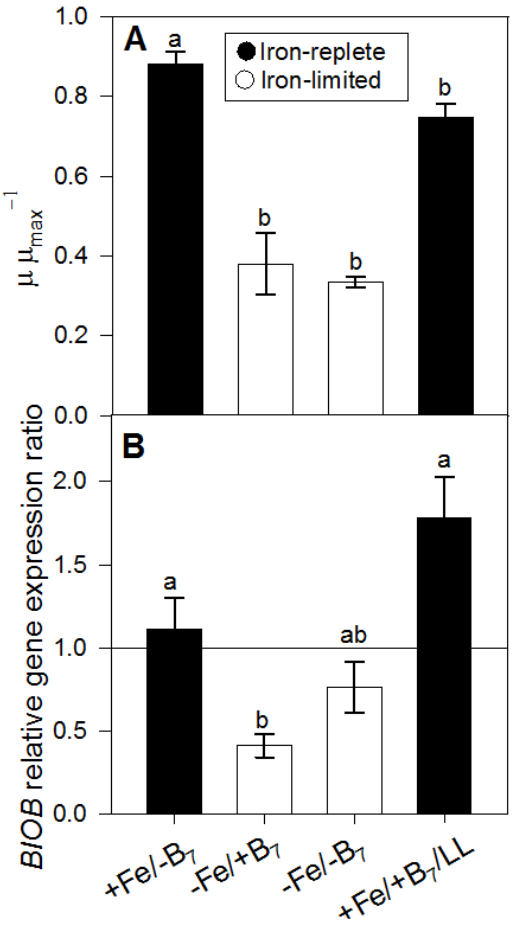

Fig. 1.2. *P. granii* growth rates and *BIOB/ACT* gene expression as a function of iron, B_7, and light status. (+Fe/–B_7): iron-replete, without B_7; (–Fe/+B_7): iron-limited, with B_7; (–Fe/–B_7): iron-limited, without B_7; (+Fe/+B_7/LL) = iron-replete, with B_7, 40 µmol photons $m^{-2}s^{-1}$ (all other cultures grown under growth-saturating light intensity of 110 µmol photons $m^{-2}s^{-1}$, see methods). **A**) Relative growth rates of iron-replete (+Fe) and iron-limited (-Fe) *P. granii* compared to the maximum growth rate (μ_{max}) obtained under +Fe/+B_7, growth-saturating light conditions. The letter "b" denotes a significant decrease in growth rate as compared to the +Fe/+B_7, growth-saturating light treatment "a" as determined via two-way ANOVA and Tukey multiple comparison tests ($p < 0.05$). **B**) Normalized *BIOB* expression in each treatment relative to the growth-replete control (+Fe/+B_7, growth-saturating light). Values <1 indicate decreased *BIOB* expression as compared to the growth-replete control. Letters indicate statistically different treatments determined through two-way ANOVA and Tukey tests ($p < 0.05$). Error bars represent ±1 standard error associated with the mean ($n = 3$).

METE and METH gene expression in response to iron limitation within laboratory cultures

P. granii iron-replete cultures with B_{12} supplied in the media (+Fe/+B_{12}) grew at 0.85 ± 0.11 d^{-1}, while iron-limited cultures (-Fe/+B_{12}) had reduced growth rates by 50% (0.45 ± 0.10 d^{-1}; $p = 10^{-3}$; Fig. 1.3A). *P. granii* cultures without B_{12} supplied in the medium were not able to survive more than two transfers (see methods). F_v:F_m analysis supports a physiological response

to iron limitation with a 40% decrease in F_v:F_m within iron-limited treatments, regardless of B_{12} status (Fig. 1.3B; $p < 0.004$). Gene expression analysis of *METH* (*METH/ACT*) demonstrates a >3-fold increase in the absence of B_{12} (+Fe/-B_{12}) relative to B_{12}-replete cultures (Fig. 1.4A; +Fe/+B_{12}: $p = 0.001$; -Fe/+B_{12}: $p = 0.0008$; and +B_{12}/Fe resupply: $p = 0.007$). *P. granii* has previously been found to increase *METH* expression in the absence of B_{12} (Ellis et al. 2017). Here we report that iron has no significant effect on *METH* expression with or without B_{12} in the medium.

G. cf. islandica iron-replete cultures with B_{12} supplied in the medium (+Fe/+B_{12}) grew at approximately 0.88 ± 0.19 d^{-1}, while iron-limited cultures (-Fe/+B_{12}) experienced a 67% reduction in growth (0.29 ± 0.12 d^{-1}; $p = 0.004$; Fig. 1.3C). B_{12} absence (+Fe/-B_{12}) significantly decreased growth rates by 35% as compared to +Fe/+B_{12} conditions with cultures experiencing growth rates of 0.57 ± 0.08 d^{-1}. Furthermore, iron-limited cultures without B_{12} present (-Fe/-B_{12}) grew at significantly reduced rates as compared to their iron-replete counterparts, at approximately 0.35 ± 0.02 d^{-1} ($p = 0.014$). F_v:F_m decreased in iron-limited *G. cf. islandica* by 27%, with -B_{12} cultures having a negligible effect (Fig. 1.3D; $p < 0.002$). B_{12} absence decreased *G. cf. islandica METH* expression by 3-fold, as observed between –Fe/+B_{12} and –Fe/-B_{12} treatments ($p = 0.007$). Furthermore *METH/ACT* expression was significantly influenced by iron status, with expression decreasing by >2-fold under iron-limited conditions (-Fe/+B_{12} and -Fe/-B_{12}) when compared to iron-replete treatments (+Fe/+B_{12}; $p = 0.03$ and 0.02 respectively; Fig. 1.4B). It remains unclear whether *METH* expression in *G. cf. islandica* is indirectly influenced by growth rate or directly affected by iron availability. In contrast, *METE/ACT* expression was primarily affected by B_{12} status with no significant differences due to iron treatment; there was a

>15-fold increase in expression in –B_{12} medium (+Fe/-B_{12}; -B_{12}/Fe-resupply) when compared to treatments containing B_{12} ($p < 0.03$; Fig. 1.4C).

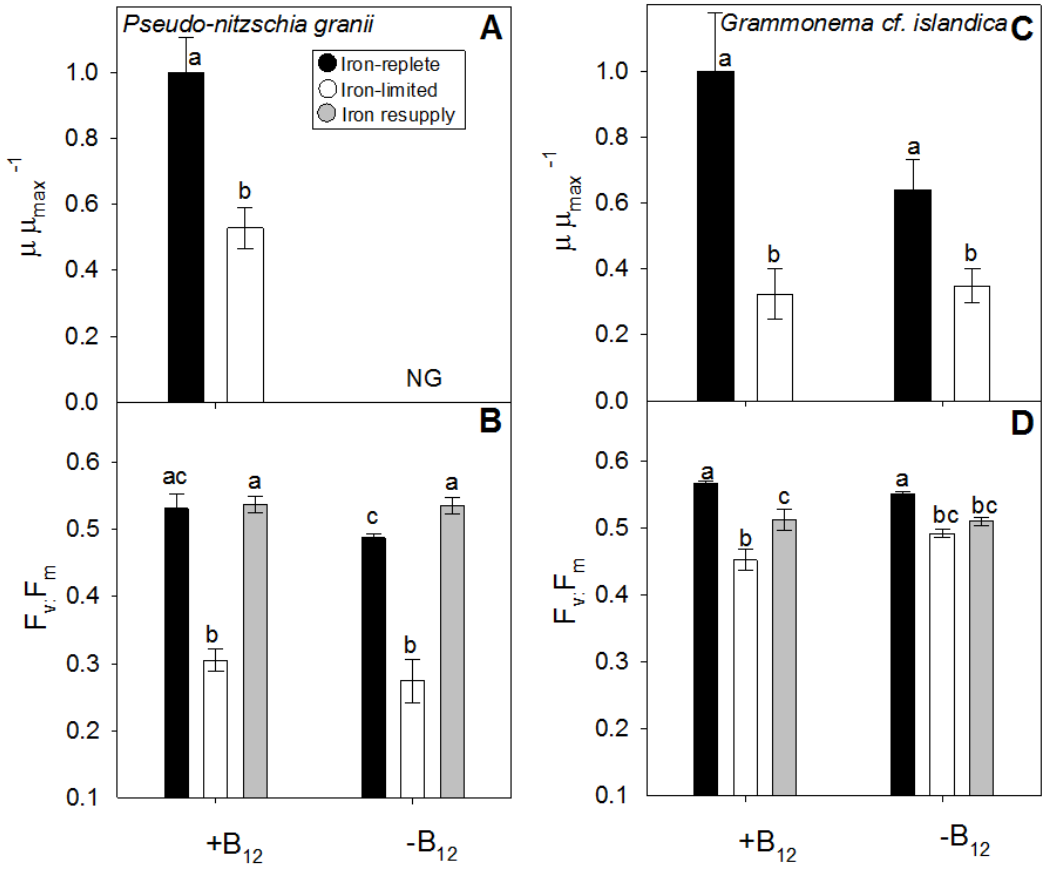

Fig. 1.3. Growth rates and F_v:F_m of laboratory cultures as a function of iron and vitamin B_{12}. **A**) Relative growth rates of iron-replete (+Fe) and iron-limited (-Fe) *P. granii* in the presence (+B_{12}) and absence (-B_{12}) of vitamin B_{12} compared to the maximum growth rate (μ_{max}) obtained under +Fe/+B_{12} conditions. NG denotes no steady-state growth rates were achieved. **B**) Maximum photochemical yield of PSII (F_v:F_m) within *P. granii*. **C**) Relative growth rates of iron-replete and iron-limited *G. cf. islandica* in the presence (+B_{12}) and absence (-B_{12}) of vitamin B_{12} compared to the maximum growth rate (μ_{max}) obtained under +Fe/+B_{12} conditions. **D**) Maximum photochemical yield of PSII (F_v:F_m) within *G. cf. islandica*. Letters indicate statistically different treatments determined through two-tailed homoscedastic t-tests ($p < 0.05$). Error bars represent ±1 standard error associated with the mean ($n \geq 3$, except within the -B_{12}/-Fe and -B_{12}/+Fe-resupply treatments, where $n = 2$).

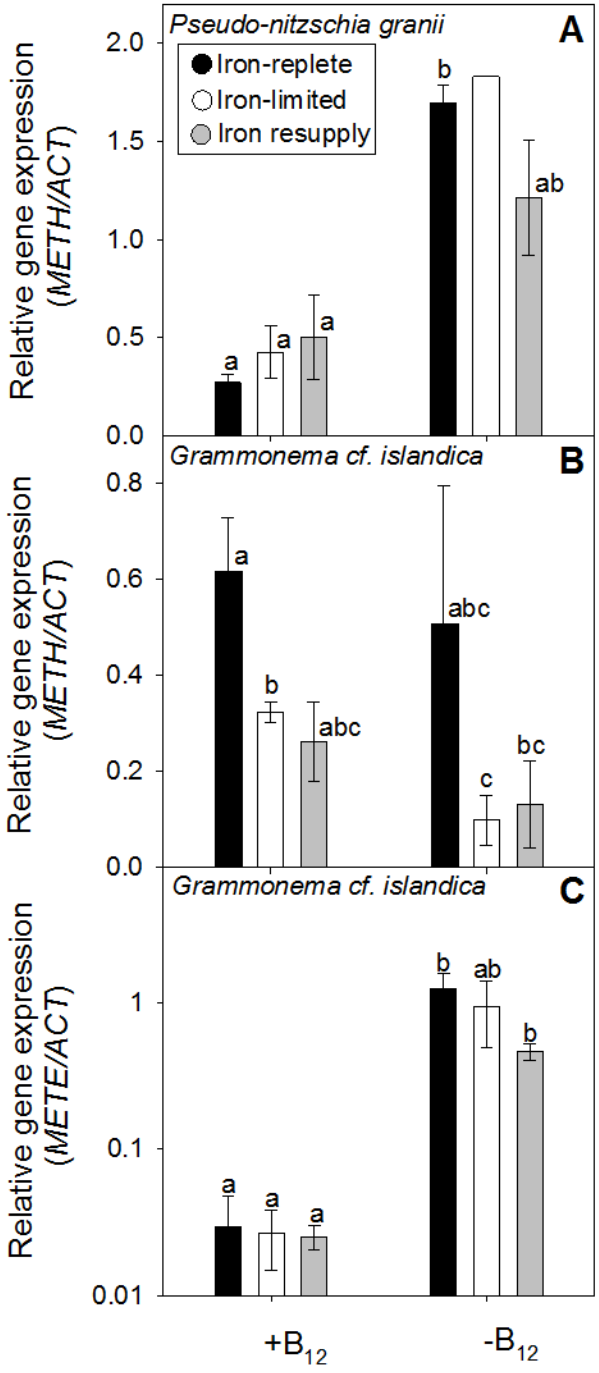

Fig. 1.4. Relative gene expression of **A**) *P. granii METH*, **B**) *G. f. islandica METH* and **C**) *G. cf. islandica METE* under iron-replete (+Fe), iron-limited (-Fe) and iron-resupplied conditions in the presence (+B_{12}) or absence (-B_{12}) of vitamin B_{12}. All genes are normalized to Actin (*ACT*) transcripts. Letters denote significant differences among treatments as determined through two-tailed homoscedastic t-tests ($p < 0.05$). Error bars represent ±1 standard error associated with the mean [$n \geq 3$ except within the following treatments: *P. granii METH* +Fe/+B_{12}, -B_{12}/+Fe-resupply ($n = 2$); *P. granii METH* –Fe/-B_{12} ($n = 1$), *G. cf. islandica METE* –Fe/-B_{12} and -B_{12}/+Fe-resupply ($n = 2$)].

Growth dynamics and B-vitamin patterns along the Line-P transect

Trends along the natural iron gradient of the Line-P transect indicate phytoplankton biomass decreased whereas dissolved nitrate concentrations increased with distance from the shore (Fig. 1.5A). Larger phytoplankton (>5µm) decreased in biomass 7-fold from 1.85 ± 0.03 µg chl *a* L^{-1} at the most coastal station (P2) to 0.26 ±0.01 µg chl *a* L^{-1} at OSP. Small phytoplankton (<5 □m) similarly decreased by >3-fold along the transect, reaching highest concentrations of 1.87 ± 0.29 µg chl *a* L^{-1} at P2 and gradually decreasing to 0.48 ± 0.02 µg chl *a* L^{-1} at OSP. Based on size-fractionated chl *a* measurements, larger phytoplankton comprised about half of the phytoplankton biomass at coastal stations whereas small phytoplankton dominated at all other stations along the transect. Total chlorophyll concentrations were elevated at OSP relative to the adjacent station P20. This may have been associated with a recent iron deposition event within the vicinity of OSP near the time of sampling due to the eruption of Mt. Pavlof, a frequently active volcano within the Aleutian Range of the Alaskan Peninsula (see discussion for more details).

Diatom cell densities were highest at the coastal stations and substantially decreased along the Line-P transect, consistent with the declines in large phytoplankton chl *a* concentrations (Fig. 1.5B). Diatom density was relatively high at P2 with $6.2x10^4$ cells L^{-1}, decreased to $2x10^4$ cells L^{-1} at P4, and remained below $3x10^3$ cells L^{-1} at stations P12 through P20. Counts were elevated at OSP as compared to the preceding stations. The assemblage at the coastal stations was comprised mainly of centric diatoms, while the diatom population at OSP was mostly pennate diatoms, in particular, members of the genus *Pseudo-nitzschia*.

Neither cyanobacteria nor the non-photosynthetic (non-ps) bacteria cell counts followed any obvious spatial trends along the Line-P transect (Fig. 1.5B). Cyanobacteria counts were

attributed to *Synechococcus* – cell densities fluctuated from approximately $3x10^7 \pm 0.2x10^7$ cells L^{-1} at OSP to $12x10^7 \pm 0.9x10^7$ cells L^{-1} at P12. Non-ps bacterial abundance was elevated at P16, with $14x10^8 \pm 3x10^8$ cells L^{-1}, while cell densities were comparatively lower at all other stations.

B-vitamin concentrations varied substantially along the Line-P transect (Figs. 1.5C-D). Vitamin B_1 (thiamine hydrochloride) concentrations ranged from 3.3 to 9.5 pmol L^{-1}, with stations P4 and P12 having the highest concentrations. Vitamin B_7 (biotin) similarly fluctuated along the transect varying between 4.3 and 14.7 pmol L^{-1}, with the highest concentration located at P16. Due to the large error associated between replicates and the SPE recovery reaching 180%, trace B_7 contamination from reagents used during preconcentration was possible. Vitamin B_2 (riboflavin) concentrations ranged from 1.3 to 9 pmol L^{-1} with the highest concentration at OSP. Vitamin B_6 (pyridoxal hydrochloride) ranged from 0.48 to 5.49 pmol L^{-1} with a peak concentration at P20, and below the detection limit at stations at P4 and P26. The form of vitamin B_{12} measured, cyanocobalamin, fell below the limit of quantification (0.13 pmol L^{-1}) at all stations except P4 and P20, in which concentrations were 0.18 and 0.25 pmol L^{-1} respectively. B_1 and B_7 concentrations at OSP were on the lower end of those measured along the Line-P transect, while B_6 and B_{12} were below the detection limit.

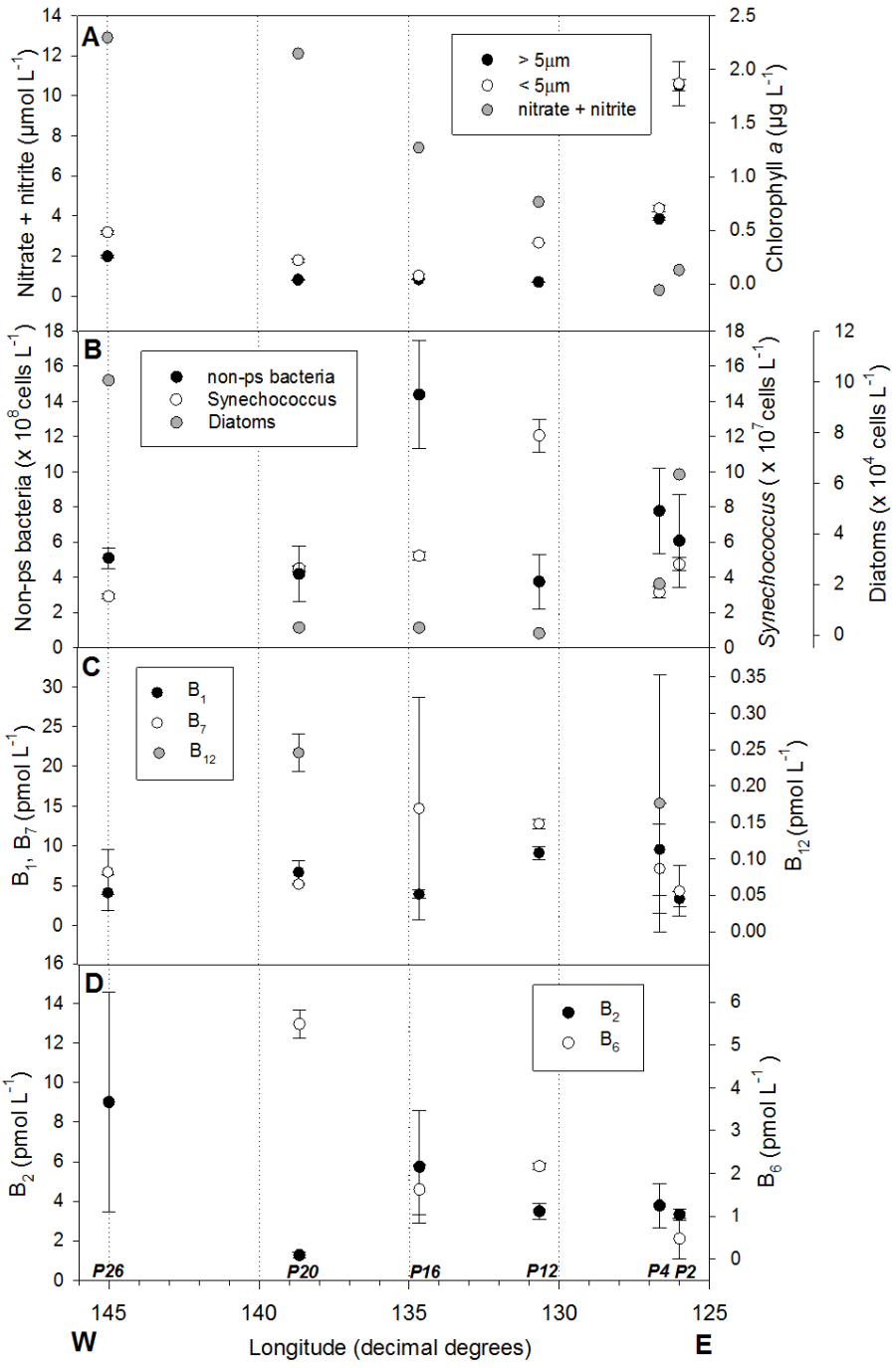

Fig. 1.5. Surface nitrate concentrations, phytoplankton biomass, cell densities and dissolved concentrations for select vitamin forms along the Line-P transect. **A**) Nitrate and nitrite concentrations and size-fractionated chlorophyll *a*. **B**) *Synechococcus*, non-photosynthetic (non-ps) bacteria and diatom cell densities. **C**) Dissolved B_1, B_7 and B_{12} concentrations in surface seawater. **D**) Dissolved B_2 and B_6 concentrations in surface seawater. The instrumental detection limit for each vitamin were as follows: 0.25 pmol L^{-1} for thiamine hydrochloride (B_1) and biotin (B_7), 0.13 pmol L^{-1} for riboflavin (B_2) and cyanocobalamin (B_{12}), and 0.38 pmol L^{-1} for pyridoxal hydrochloride (B_6). Error bars represent ±1 standard error associated with the mean (for A and B, n=3, for C and D, n=2).

Phytoplankton response to iron and vitamin enrichment experiments at OSP

Phytoplankton biomass increased during the incubation experiments in all treatments as indicated by chl *a* within two size fractions (Fig. 1.6A). Initial chl *a* concentrations were predominantly attributable to small phytoplankton (< 5 µm; 0.65 ± 0.25 µg chl *a* L^{-1}) with large phytoplankton (>5 µm) comprising approximately 24% of the biomass. The contribution of the large size fraction significantly increased following iron addition, reaching over 4 µg chl *a* L^{-1} following 96 hours of incubation ($p \leq 0.002$). Small phytoplankton biomass was approximately 4-fold lower than large phytoplankton in incubations receiving iron. F_v:F_m assessment indicated iron limitation was alleviated following iron addition with a significant increase in ratios ($p < 0.001$; Fig. 1.6B). F_v:F_m values of initial communities and treatments without iron ranged from 0.37-0.40, while treatments with iron achieved maximum values of 0.50-0.53.

Diatom populations in incubations with iron addition increased appreciably, reaching 40-fold higher densities (approximately 15 x 10^5 cells L^{-1}) compared to the initial diatom cell densities (4 x 10^4 cells L^{-1}; Fig. 1.6C). Total diatom abundance was the highest in the community receiving both iron and B_{12}, reaching 16 x 10^5 cells L^{-1}, and was the only treatment considered significantly different from initial diatom densities (T_0) and all incubations where iron was not added ($p < 0.03$). Diatom cell densities in treatments without iron also increased from those in the ambient seawater although concentrations were approximately 2-fold lower compared to the iron addition treatments. All incubations were dominated by *Pseudo-nitzschia* spp. Other diatom groups observed were comparatively less abundant across treatments and time points (Fig. 1.6C).

High-throughput sequencing of transcripts allowed for comparisons of relative community composition among the treatments. Consistent with light microscopy data, diatoms increased from 8% of the eukaryotic plankton community to 20-28% in treatments without iron

and 40-46% in treatments with iron addition (Fig. 1.6D). Apart from diatoms and dictyochocophytes, all other major phytoplankton groups decreased in relative proportions compared to the initial community following incubation.

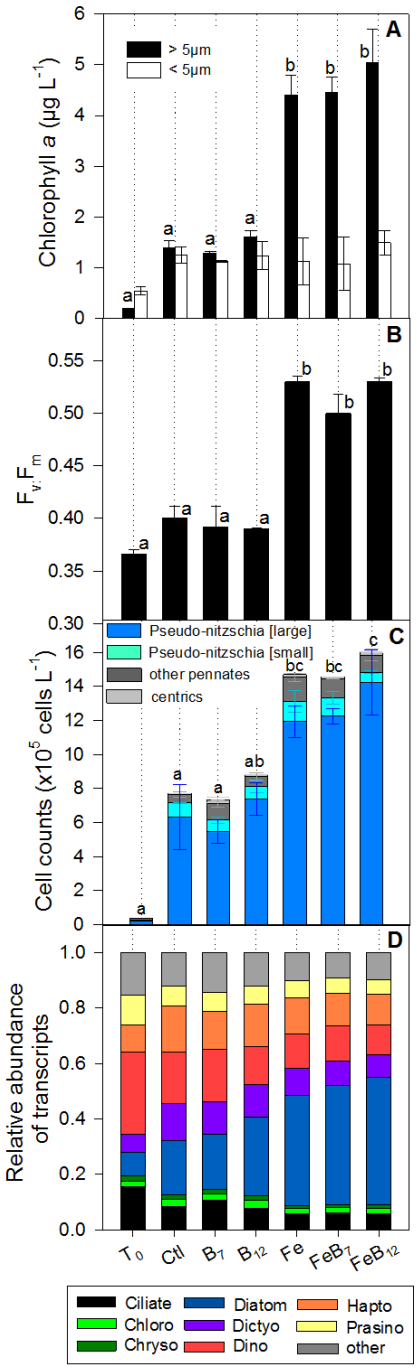

Fig. 1.6. Growth characteristics, diatom cell densities, and transcript abundances of iron and/or vitamin incubation experiments. **A**) Size-fractionated chlorophyll *a* concentrations, **B**) Maximum photochemical yield of PSII (F_v:F_m), **C**) Diatom cell counts obtained via light microscopy, and **D**) Relative transcript abundance of eight major taxonomic groups in the initial seawater (T_0), unamended control (Ctl), B_7-only (B_7), B_{12}-only (B_{12}), iron-only (Fe), iron and B_7 (FeB_7) and iron and B_{12} (FeB_{12}) treatments following 96 hours of incubation as obtained through metatranscriptomic analysis. For D) Ciliate, ciliates; Chloro, chlorophytes; Chryso, chrysophytes; Diatom, diatoms; Dictyo, dictyochophytes; Dino, dinoflagellates; Hapto, haptophytes; Prasino, prasinophytes. Where present, error bars represent ±1 standard error associated with the mean ($n \geq 2$). Letters denote significant differences among treatments as determined via one-way RM ANOVA and Holm-Sidak comparison tests ($p < 0.05$). For A) only the >5 µm fraction was tested for significant differences among treatments.

Metatranscriptomic community response to iron/vitamin additions

Key indicator genes encoding proteins involved in iron and vitamin metabolism were used to determine diatom community response to iron/vitamin enrichments (Fig. 1.7). Iron played a large role in driving expression changes, with B_7 and B_{12} additions alone having less of an impact on overall gene expression. In all iron-amended treatments, transcript abundance of the gene encoding the iron storage protein ferritin (*FTN*), involved in maintaining iron homeostasis in marine protists (Marchetti et al. 2009; Botebol et al. 2015; Pfaffen et al. 2015), increased at least 7-fold (Fig. 1.7A). Similarly, fructose-bisphosphate aldolase class II (*class II FBA*), a metal-dependent aldolase involved in gluconeogenesis, glycolysis and the Calvin Cycle, increased approximately 8-fold as compared to the unamended control treatment (Fig. 1.7; Horecker et al. 1972). *Class II FBA* transcripts have been previously demonstrated to be abundant under iron-replete conditions in diatoms; this protein is hypothesized to contain Fe^{2+} as a metal cofactor (Lommer et al. 2012; Allen et al. 2012). The iron-starvation induced proteins 2A (*ISIP2A*), responsible for iron acquisition in diatoms (Morrissey et al. 2015), and *ISIP2B* decreased by approximately 3-fold and 73-fold, respectively, with very few transcripts associated with *ISIP2B* within iron addition treatments. Gene expression of fructose-bisphosphate aldolase class I (*class I FBA*), the metal-independent version of class II FBA found to be abundant under iron limitation in diatoms (Lommer et al. 2012; Allen et al. 2012), similarly decreased by 8-fold after iron addition as compared to the control treatment. Flavodoxin (*FLDA*), an iron-independent photosynthetic electron acceptor and proposed iron stress indicator gene in certain diatoms (Chappell et al. 2015), did not change in expression within iron-amended treatments compared to the control.

B_7 metabolism was also affected by iron addition, as *BIOB* transcripts increased 2-fold in treatments receiving iron compared to the unamended control treatment (Fig. 1.7B). However, two other genes involved in biotin metabolism, *BIOA* and *BIOF*, were not similarly overrepresented following iron addition. B_{12} status was assessed via transcript changes in the genes encoding METE and CBA1. Expression of both genes increased in treatments where iron was added without B_{12} (Fe and FeB_7). *CBA1* increased by approximately 2-fold compared to the control, while *METE* increased by 30-fold (Fig. 1.7). In contrast, transcripts of *METH* did not change in abundance within all iron and/or vitamin amended treatments. The *METE* gene is present in some, but not all, diatoms with the gene being absent from sequenced transcriptomes of *Pseudo-nitzschia* species as well as the genome of *Pseudo-nitzschia multiseries* (Ellis et al. 2017). Thus, there was a clear distinction in the taxonomic assignment for *METE* in these diatom communities where transcripts were assigned to the raphid pennate diatom *Attheya septentrionalis* as opposed to most of the other diatom transcripts assigned to *Pseudo-nitzschia*, the dominant diatom genera following iron addition (Fig. 1.7; Fig. 1.6D).

Pairwise comparison between the iron-amended and unamended control treatments revealed the differential expression of several other genes indirectly related to iron or vitamin metabolism, including nitrite reductase (*NIRB*), nitrate reductase (*NR*), 3-hydroxyacyl-acyl-carrier-protein (ACP) dehydratase (*FABZ*), and acetyl-coenzyme A (CoA) carboxylase (*ACACA*). Increased abundance of nitrogen assimilation transcripts *NR* and *NIRB* following iron addition likely allow previously iron-limited diatoms to take advantage of bioavailable iron in order to metabolize readily available nitrate from HNLC waters (Marchetti et al. 2012), while increases in *FABZ* and *ACACA* transcripts following iron addition may play a role in B_7 metabolism (see discussion).

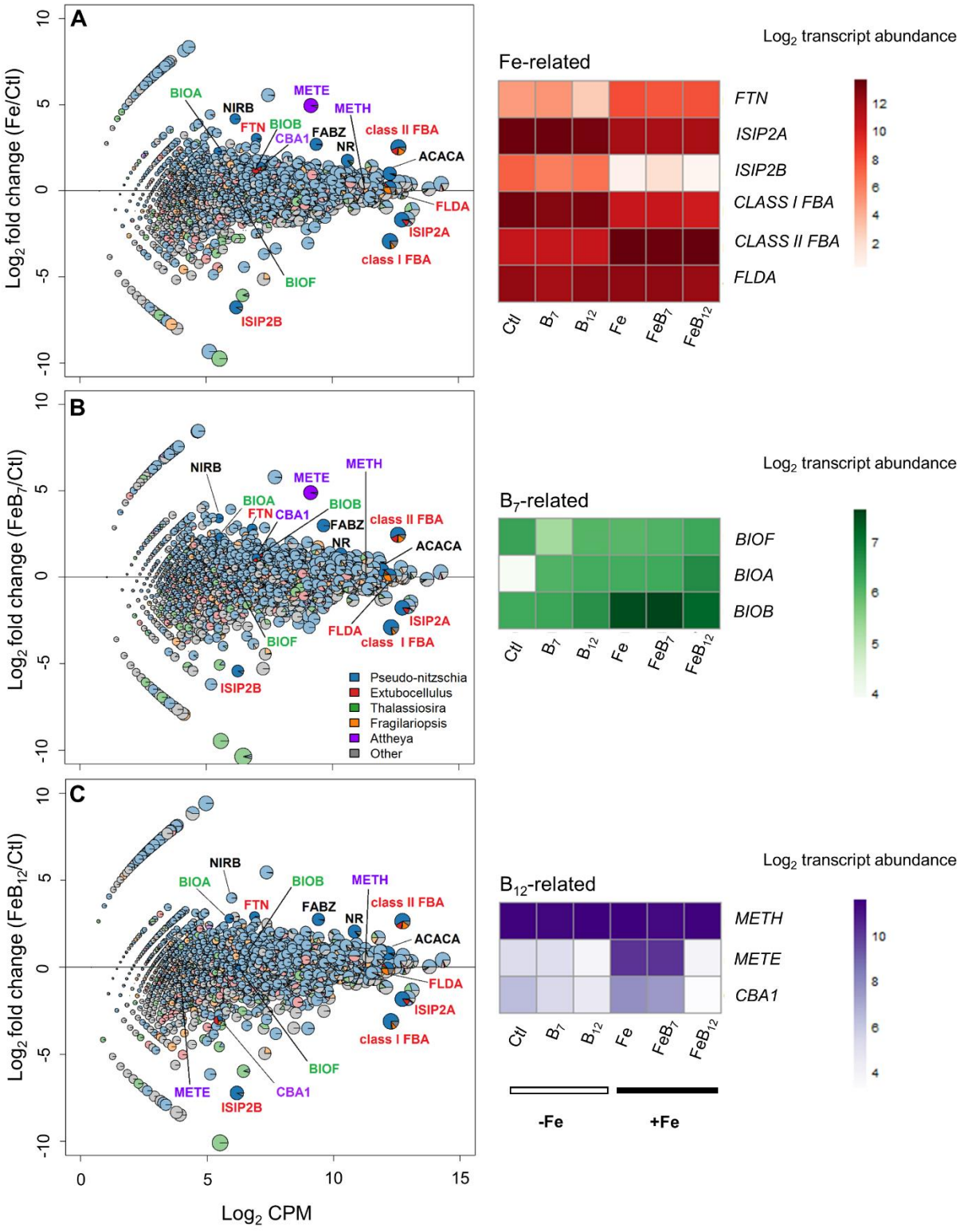
A
B
C
Log2 fold change (Fe/Ctl)
Log2 fold change (FeB7/Ctl)
Log2 fold change (FeB12/Ctl)
Log2 CPM
BIOA
NIRB
METE
METH
FTN
BIOB
CBA1
FABZ
NR
class II FBA
ACACA
FLDA
ISIP2A
class I FBA
BIOF
ISIP2B
Pseudo-nitzschia
Extubocellulus
Thalassiosira
Fragilariopsis
Attheya
Other
Log2 transcript abundance
Fe-related
FTN
ISIP2A
ISIP2B
CLASS I FBA
CLASS II FBA
FLDA
B7-related
BIOF
BIOA
BIOB
B12-related
METH
METE
CBA1
Ctl
B7
B12
Fe
FeB7
FeB12
-Fe
+Fe

Fig. 1.7. Diatom-specific gene expression responses to iron and/or vitamin additions. **A**) Fe versus control (Ctl) **B**) FeB_7 versus Ctl **C**) FeB_{12} versus Ctl. The y-axis corresponds to the log_2 fold change ratio of normalized transcripts between the two treatments, while the x-axis represents the average log_2 counts per million (CPM), or transcript abundance. Each pie represents transcripts associated with a single gene (KEGG KO or gene definition, see methods). Pies increase in size with increasing CPM and absolute value of the fold change. Pies are colored by distribution of transcripts from each of the four most abundant diatom genera as well as the diatom genus *Attheya*. In each graph, genes with transcripts within only one of the treatments are displayed on arms to the left. Iron and vitamin-related genes, along with a few other genes of interest are labeled: iron-related (red): *FTN*, ferritin; *ISIP2A*, iron-starvation induced protein A; *ISIP2B*, iron-starvation induced protein B; *FLDA*, flavodoxin I; *class I FBA*, fructose-bisphosphate aldolase class I; *class II FBA*, fructose-bisphosphate aldolase class II. B_7-related proteins (green): *BIOB*, biotin synthase; *BIOA*, DAPA synthase; *BIOF*, KAPA synthase. B_{12}-related proteins (purple): *METH*, B_{12}-dependent methionine synthase; *METE*, B_{12}-independent methionine synthase; *CBA1*, cobalamin acquisition protein 1. Other proteins indirectly related to iron and/or vitamins (black): *FABZ*, 3-hydroxyacyl-acp dehydratase; *ACACA*, acetyl-coenzyme A; *NR*, nitrate reductase; *NIRB*, nitrite reductase. Pies corresponding to genes not mentioned in the text are lightly shaded. Displayed in adjacent heatmaps are the log_2 normalized transcript abundances of genes of interest partitioned into iron/vitamin categories within all treatments.

Classifying genes based on their KEGG Orthology (KO) assignment and grouping them into module-level classifications enables a broader assessment of vitamin synthesis genes among treatments. Transcript abundance within treatments receiving iron additions (Fe, FeB_7, FeB_{12}) responded similarly and clustered together (Fig. 1.8). All B-vitamin modules were enriched to varying degrees following iron addition as compared to the unamended control or vitamin-only treatments. A putative B_{12} synthesis/repair/salvage module in diatoms was elevated 2-fold within the Fe and FeB_7 treatments as compared to the control, with FeB_{12}, B_{12}, and B_7 treatments also demonstrating elevated expression as compared to the control, though to a lesser extent. The methionine synthesis module (which contains the *METH* and *METE* genes) followed a similar pattern to the B_{12} module, with enrichment of 1.5- and 1.3-fold in the Fe and FeB_7 treatments respectively, largely driven by changes in *METE* transcript abundance (See tables in Appendix I). The B_7 synthesis module was elevated 2-fold after iron addition, with enrichment also apparent in the B_7 and B_{12} treatments but to a lesser extent. Both vitamin B_6 and B_2 modules were enriched by approximately 1.6- and 1.4-fold respectively within all three iron-amended treatments, while the B_1 module increased 1.5-fold in the FeB_7 treatment but was only slightly increased in the Fe and FeB_{12} treatments.

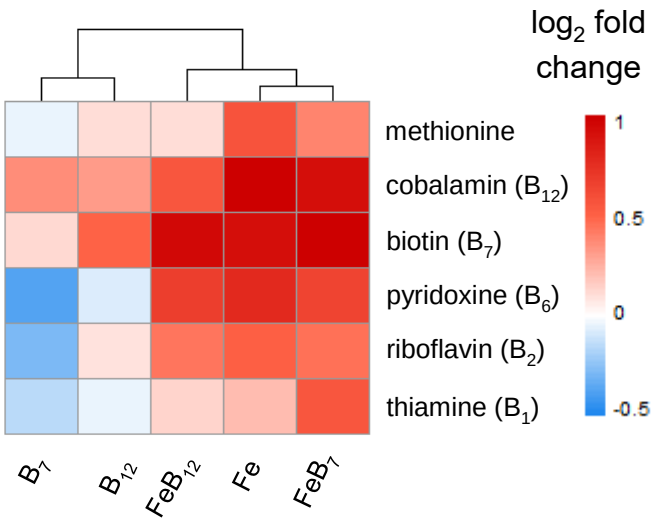

Fig. 1.8. Module-level expression responses of biosynthetic vitamin pathways in diatoms. Diatom read counts contained within each KEGG vitamin synthesis module were summed within a treatment and expressed as the log2 fold change compared to the unamended control treatment. Genes contained within each vitamin module and the associated contigs with the most reads mapped are provided in Appendix I. The dendrogram reflects similarity in expression responses among treatments and was created using Euclidean distance and hierarchical clustering.

Discussion

Line-P transect and vitamin dynamics

During the June 2013 cruise, we observed higher than typical chl *a* concentrations at OSP (0.75 µg L^{-1} Chl *a*; Fig. 1.5A), which generally supports lower phytoplankton biomass (0.3 – 0.5 µg L^{-1} Chl *a*; Harrison et al. 2004). In May of 2013 one of Alaska's most active volcanoes, Mt. Pavlof, began erupting and released ash up to 22,000 feet above sea level. NOAA HYSPLIT (Hybrid Single-Particle Lagrangian Integrated Trajectory model; Stein et al. 2015) particle trajectories estimated that the ash cloud may have reached OSP by late May. Based on these observations, we suspect the OSP phytoplankton community was exposed to a higher than usual amount of iron input in the form of volcanic ash deposition due to the eruption, resulting in relatively high chl *a* concentrations when compared to adjacent Line P stations and the historical average. Regardless, our iron-amended treatments indicated increases in chl *a*, F_v:F_m, and diatom cell counts as compared to the unamended control treatment, suggesting that the ambient phytoplankton community at OSP was still iron-limited (Fig. 1.6A-D).

Our Line-P transect analysis began at coastal station P2 and ended at OSP, following expected trends of increasing nitrate and decreasing phytoplankton biomass and diatom abundance (with the exception of OSP as previously discussed). This is consistent with the transition from coastal to HNLC waters occurring along the transect, where surface dissolved iron concentrations at P4 are typically >0.1 nmol L^{-1}, and decrease westward to approximately <0.05 nmol L^{-1} at OSP (Harrison et al. 2004). However, select forms of B-vitamins measured and bacteria densities did not follow any obvious onshore-offshore trends. Localized peaks in *Synechococcus* cell densities occurred at the transition station P12, and in non-ps bacteria cell densities at P16, but these hotspots of bacterial biomass did not strongly co-vary with either

diatom abundance, vitamin concentrations, or chl *a* concentrations (Fig. 1.5). Alternatively, it is possible that non-ps bacterial growth was primarily influenced by organic matter availability, which was not measured in this study. Grazing by microzooplankton, which was also not measured, may have additionally influenced both non-ps and *Synechococcus* abundances (Zöllner et al. 2009). Additionally these vitamin measurements represent only a fraction of the total dissolved vitamin pool, and multiple forms exist in varying abundances and importance in the marine environment (Helliwell et al. 2016; Heal et al. 2017). Therefore quantification of remaining vitamin fractions are necessary in order to gain a comprehensive understanding of the relationships between macro- and micro-nutrients, bacterial and phytoplankton biomass, and dissolved vitamins along the Line P transect. However, the measured dissolved vitamin concentrations reported here are useful in defining ranges in concentrations along the transect in comparison to other regions of the coastal Pacific Ocean in which vitamin quantification has been performed in a consistent manner (Sañudo-Wilhelmy et al. 2012).

B_{12} (cyanocobalamin) was detected in the highest concentration at station P20 (0.25 ± 0.03 pmol L^{-1}) and was below the detection limits of 0.13 pmol L^{-1} at all other locations apart from P4, where variability was high due to lack of detection in one replicate (0.18 ± 0.18 pmol L^{-1}). This is in contrast to the cyanocobalamin concentrations obtained within the California Current System (CCS), which ranged from below detection to as high as 15 pmol L^{-1} in surface waters (Sañudo-Wilhelmy et al. 2012). These comparatively lower cyanocobalamin concentrations alone however do not indicate B_{12} limitation of the ambient phytoplankton community in the NE Pacific Ocean. The other forms of B_{12} not measured in this study, including the other cobalamin upper-ligand variants and all variants of pseudocobalamin, could have been more abundant than cyanocobalamin in these waters. Given that in a number of

cobalamin and pseudocobalamin producers the cyano- upper ligand has not been detected but all others have, these other variants may be more abundant and important in fueling growth of B_{12}-dependent microorganisms (Heal et al. 2017).

Although evidence of widespread B_{12} limitation was not observed through our chlorophyll *a* measurements in the incubation experiments (i.e., treatments with B_{12} addition did not achieve significantly higher chlorophyll *a* versus non-B_{12} treatments), the FeB_{12} treatment was the only incubation to achieve diatom cell densities significantly higher than all of the non-iron containing treatments. Furthermore, our transcriptomic findings indicate that there is potential for species-specific B_{12} limitation in phytoplankton with obligate B_{12} requirements following alleviation of iron limitation (see further discussion below). We interpret this to suggest that since iron was the primarily limiting nutrient, B_{12} enrichment alone could not result in increased growth. However, the combination of iron and B_{12} resulted in the highest diatom abundances observed, and given the transcriptomic response of certain diatom community members following iron addition, we speculate differences in phytoplankton biomass between the FeB_{12} treatment and those in which iron and B_{12} were added independently might have occurred with a longer incubation.

Interestingly, B_6 (pyridoxal hydrochloride) concentrations reached a maximum of 5.49 ± 0.33 pmol L^{-1} at station P20 and were below detection at P4 and OSP. These concentrations were considerably lower than the maximum of 400 pmol L^{-1} observed within the CCS surface waters (Sañudo-Wilhelmy et al. 2012). B_6 requirements in phytoplankton are not well defined, though the stark contrast in vitamin concentrations between the coastal and open ocean environments suggests pronounced differences in production and/or consumption of this vitamin possibly due to differences in community composition of bacteria, phytoplankton or both.

Vitamin synthesis in diatoms

During our incubation experiments at OSP, B-vitamin genes encompassed within KEGG biosynthesis and synthesis/repair/salvage vitamin pathways were overrepresented in phytoplankton communities receiving iron additions as compared to the unamended control (Fig. 1.8). These results suggest that initially iron-limited diatom communities do not produce as many vitamins due to either having reduced demand while growing at a slower rate, or not having the iron necessary to fuel iron-dependent vitamin synthesis. The increase in vitamin transcript abundance following iron addition likely represents a combination of the increased vitamin production required to fuel elevated rates of metabolic activity and relief of iron-stress on vitamin biosynthesis.

Three of the four genes involved in biotin B_7 biosynthesis were identified in our metatranscriptomes, with the B_7 biosynthesis module increasing 2-fold in expression after iron addition. Although this study provides strong support for B_7 biosynthesis in *Pseudo-nitzschia*, it remains unclear how this genus and others are producing the precursor to B_7, dethiobiotin, given the absence of a *BIOD* ortholog (Croft et al. 2006). The gene *BIO3-BIO1*, which encodes for a bifunctional fusion protein with the functionality of both *BIOD (BIO3)* and *BIOA (BIO1),* may be a likely candidate (Muralla et al. 2008). This gene has been previously identified in the *Phaeodactylum tricornutum* genome (Bowler et al. 2008) and is also present in our metatranscriptome sequences, albeit with very low transcript abundance and only present in the iron-enriched treatments. In addition, the majority of *BIO3-BIO1* transcripts belong to the genus *Chaetoceros,* which was not an abundant taxon in the incubations, while the majority of transcripts for all other B_7 biosynthesis genes (*BIOF, BIOA, BIOB*) were taxonomically

associated with *Pseudo-nitzschia*.. It remains unclear whether *Pseudo-nitzschia* may additionally utilize *BIO3-BIO1* or instead relies on an unidentified enzyme to synthesize dethiobiotin.

Based on the presence of vitamin transcripts for genes involved in vitamin synthesis within our metatranscriptomes, diatoms at OSP are likely able to produce vitamins B_2 and B_7. However, only incomplete pathways for vitamins B_1, B_6, and B_{12} synthesis were identified. This may suggest that diatoms are either auxotrophs for these latter vitamins; that they possess the ability to process intermediates in order to relieve auxotrophy; that vitamin-independent metabolic alternative pathways are invoked (i.e., METE); or that transcripts were missed by our methods. As it is possible that transcriptome sequencing depth did not capture the presence of the full biosynthetic pathways associated with vitamin B_1 or B_6 production, it should not be assumed that diatoms present within the incubations are truly missing key components of certain vitamin synthesis pathways.

Unexpectedly, transcripts for genes encoding 8 out of approximately 21 enzymes involved in the production of B_{12} were identified within diatoms, mainly belonged to the genus *Pseudo-nitzschia.* These include genes within the KEGG final synthesis/repair/salvage module and two additional synthesis genes responsible for production of intermediates that are not included in the KEGG module (Warren et al. 2002; Fig. 1.9). All but 2 of these 8 genes (*COBB*, cobyrinic acid a,c-diamide synthase, and *COBA*, cob(I)alamin adenosyltransferase; the only two genes with the majority of transcripts associated with genera other than *Pseudo-nitzschia)* were also identified in the genome of *Pseudo-nitzschia multiseries* (JGI Genome Portal; see tables in Appendix I). Module expression was elevated by 2-fold in the Fe and FeB_7 treatments compared to the unamended control, with a comparatively reduced response in the FeB_{12} treatment. It is unlikely that diatoms possess the ability to synthesize B_{12} *de novo* since the full biosynthetic

pathway has not yet been identified in any eukaryote (Warren et al. 2002). However, the pattern of increased transcript abundance of genes involved in B_{12} synthesis/repair/salvage in diatoms under conditions consistent with B_{12} stress and/or limitation suggests diatoms may have some capacity to process B_{12} intermediates.

Although bacterial contamination during eukaryotic-targeted sequencing is possible, sequence homology analyses indicated all environmental *COB* genes found in the metatranscriptomes presented here closely match unannotated genes within genomes and transcriptomes of diatoms, green algae, cryptophytes and other protists available within GenBank's non-redundant and MMETSP protein databases (e-value < 0.001). Additionally, these environmental *COB* contigs contained conserved domain regions diagnostic of each *COB* protein, verifying their role within B_{12} synthesis. We therefore argue against bacterial contamination resulting in the presence of these genes in our metatranscriptomes or non-specific functional assignments for the contigs identified in diatoms. Instead we speculate *COB* presence within marine eukaryotes is widespread. *COB*-like genes have been observed in eukaryotes previously, particularly in diatoms, dinoflagellates and haptophytes (Helliwell et al. 2011; Bertrand et al. 2012; Zhang et al. 2013; Helliwell et al. 2016). Furthermore recent evidence suggests divergent lineages of phytoplankton are capable of chemically modifying the lower axial ligand of the B_{12} molecule by incorporating 5, 6-di- methylbenzimidazole (DMB) acquired exogenously from growth medium (Helliwell et al. 2016), and thereby converting a form unable to support maximum growth (pseudocobalamin) to one that can (cobalamin). The genes encoding proteins thought to be involved in the remodeling process include *COBT, COBC* and *COBS*, identified within the genome of *Chlamydomonas reinhardtii* and transcriptome of *Pavlova lutheri*, both of which exhibit remodeling behavior in culture (Fig. 1.9; Anderson et al.

2008; Helliwell et al. 2016). *COBT* and *COBS* were identified in the diatom metatranscriptomes presented here, with increased transcripts following iron-enrichment (Fig. 1.9), suggesting marine diatoms in the NE Pacific may be utilizing these genes for remodeling purposes. Further studies are necessary to determine whether pseudocobalamin detected in the NE Pacific Ocean is bioavailable and whether members of the diatom community are able to modify it in order to fulfill their vitamin requirements as has been demonstrated in laboratory cultures with the chlorophyte *Chlamydomonas reinhardtii* and haptophyte *Pavlova lutheri* for B_{12} (Helliwell et al. 2016; Heal et al. 2017).

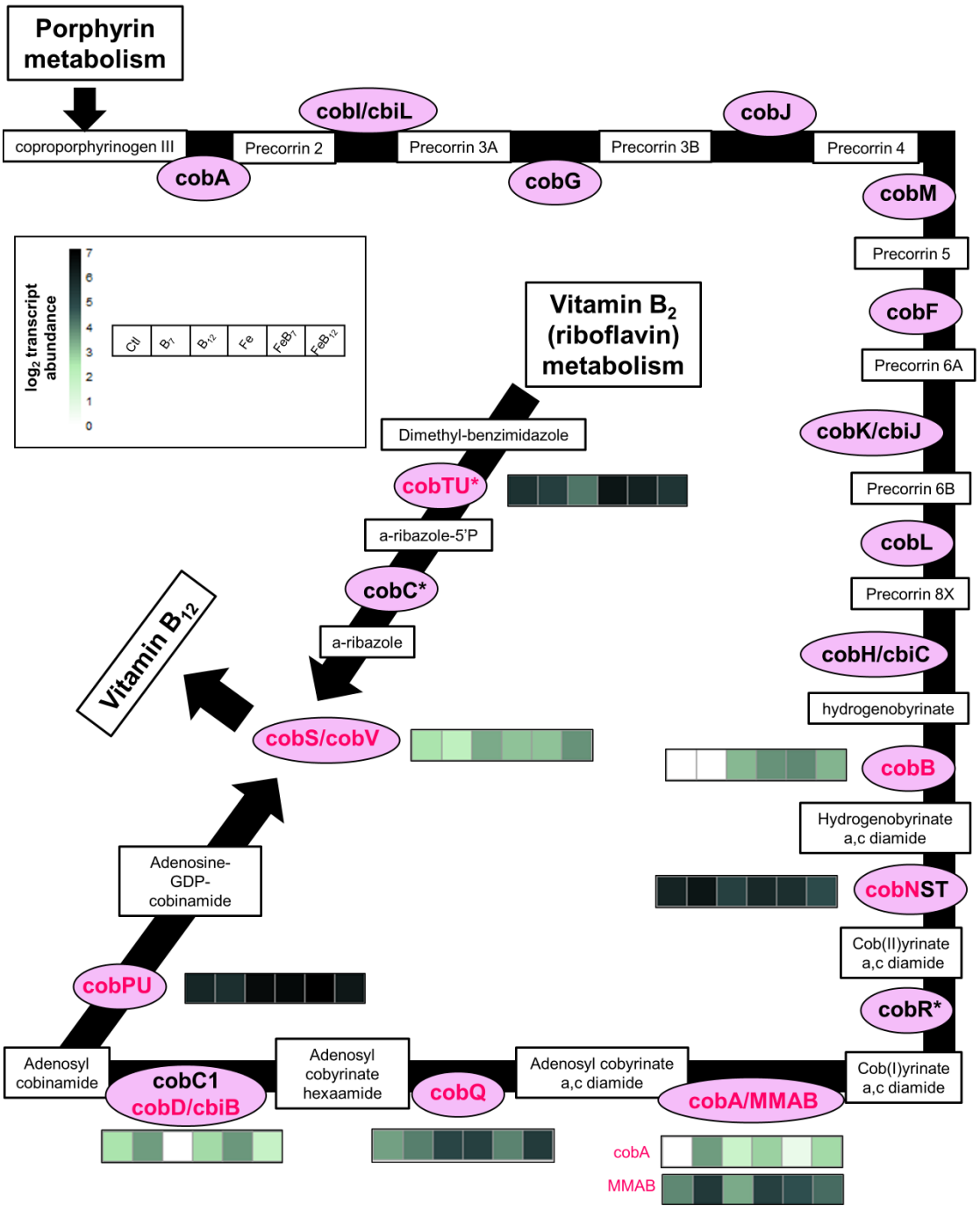

Fig. 1.9. The aerobic vitamin B_{12} biosynthesis pathway based on KEGG cobalamin final synthesis/repair/salvage (module M00122), porphyrin and chlorophyll metabolism (reference pathway map00860), and Warren et al. (2002). COB enzymes are displayed in ovals, reactant and product compounds in rectangles. Diatom-associated genes found within the metatanscriptomes from the OSP iron and/or vitamin incubation experiments are shown in pink. Color maps indicate the $\log_2$ transcript abundance, or normalized read counts as obtained through edgeR, for COB genes present within each treatment: control (Ctl), B_7-only (B_7), B_{12}-only (B_{12}), iron-only (Fe), iron and B_7 (FeB_7) and iron and B_{12} (FeB_{12}). *COB* genes with an asterisk (*) indicate genes not consistently identified within genomes of cobalamin-producers (Rodionov et al. 2003; Mera and Escalante-Semerena 2010; Lawrence et al. 2014).

Implications of iron status on B_7 production by diatoms

We demonstrate here for the first time that *BIOB* expression and presumably B_7 production in *P. granii* is reduced under iron-limiting growth conditions. This was further supported by the laboratory iron resupply experiments, in which previously iron-limited *P. granii* cells increased *BIOB* expression following the addition of iron. Similar to our laboratory experiments, iron-limited natural diatom communities increased transcript abundance of *BIOB* following iron addition at OSP. The implications of being in a growth-limited state must be taken into consideration when comparing gene expression across treatments (Bremer and Dennis, 1996). In our laboratory experiments, reductions in growth rate alone did not control *BIOB* expression, as light-limited *P. granii* cells exhibited expression levels consistent with replete cultures. This suggests that *BIOB* expression is directly regulated by iron status and is in agreement with previous studies reporting that iron limitation can trigger a transcriptional change in iron-dependent genes within *P. granii* and effectively induce an alternative gene repertoire (Marchetti et al. 2012). A reduction in B_7 biosynthesis may thus be an additional strategy used to conserve iron within iron-limited diatoms.

In addition to the three genes directly involved in B_7 biosynthesis, other B_7-related genes were identified and found to be affected by iron addition at OSP. One abundant gene, 3-hydroxyacyl-ACP dehydratase (*FABZ*), was overrepresented by approximately 7-fold in all iron-amended treatments as compared to the control. FABZ is a component of fatty acid synthesis, a pathway linked to B_7 biosynthesis due to its role in producing the precursor pimeloyl-ACP methyl ester, used by *BIOH* to initiate biotin production (Lin et al. 2010). Similarly, acetyl-CoA carboxylase (*ACACA*), a biotin-dependent enzyme that catalyzes the transfer of carboxyl groups critical during fatty acid synthesis (also known as biotin carboxylase) was overrepresented

following iron addition by 1.7-fold. Although expression patterns indicate iron-enriched diatoms increase expression of *ACACA*, this trend is not necessarily due to iron as previous studies report *ACACA* transcript abundance is a direct function of cellular growth rate (Li and Cronan 1993). Increased BIOB following iron addition, perhaps in conjunction with FABZ, may lead to elevated B_7 production by rapidly blooming diatoms and subsequently result in increased B_7 availability to auxotrophs within their surrounding environment.

There are multiple possibilities for how iron-limited marine diatoms may be compensating for decreased B_7 biosynthetic production. Intracellular B_7 quotas could decrease to allow cells to persist with less B_7, similar to steady-state diatoms under iron limitation decreasing cellular iron quotas (Harrison and Morel 1986). Alternatively, cells may switch modes of B_7 metabolism from production to uptake when iron is in limited supply (although biotin uptake was not observed in acclimated iron-limited *P. granii* laboratory cultures, see Appendix II). *Pseudo-nitzschia pungens* has been found to be auxotrophic for B_7 (Tang et al. 2010), therefore an uptake mechanism must exist in diatoms and may be present in other B_7-producing diatoms as well. Interestingly, the yeast *Saccharomyces cerevisiae* decreases B_7 biosynthesis under iron limitation and activates the acquisition of external B_7 through the proton-dependent permease vitamin-H transporter 1 (VHT1) (Shakoury-Elizeh et al. 2004). This allows intracellular iron to be allocated to crucial iron-dependent metabolic pathways, reducing overall cellular iron demand, while still maintaining an adequate supply of B_7 for continued growth. A similar response to iron limitation may also occur in *P. granii*, which under iron-limited conditions, has higher *BIOB* transcript abundance when B_7 is absent as compared to when B_7 is present. This pattern in gene expression may suggest an ability to take up B_7 from their external environment. Such a response was not tested for in our acclimated, biotin-replete, biotin uptake experiments (See Appendix II), nor was

observed within our iron addition experiments in the Northeast Pacific Ocean, with *BIOB* expression levels remaining constant under iron-limiting conditions with or without B_7 addition. This is likely due to there being sufficient B_7 at OSP (6.7 ± 2.8 pmol L^{-1}), resulting in similar B_7 dynamics between the B_7 addition treatment and the unamended control.

Implications of iron status on B_{12} utilization by diatoms

Laboratory studies presented here with *Grammonema cf. islandica* under varying iron/B_{12} conditions demonstrate *METE* gene expression is primarily regulated by B_{12} status with minimal to no influence of iron status (Fig. 1.4C). Therefore, we must interpret the 30-fold increase in transcript abundance of *METE* we observed in natural diatom assemblages following iron addition to be due to B_{12} concentrations becoming limiting for iron-stimulated diatoms. Insufficient acquisition from their environment would have caused METE-possessing diatoms to begin producing the B_{12}-independent form of methionine synthase (Fig. 1.7). In addition, *CBA1*, another gene demonstrated to increase under B_{12} limitation (Bertrand et al. 2012), increased 3-fold in treatments where iron was added without vitamin B_{12}. The community was furthermore relieved of B_{12} limitation when B_{12} was added in conjunction with iron; both *METE* and *CBA1* transcripts decreased in the FeB_{12} treatment as compared to the unamended control (by 2.5- and 8.2-fold respectively). Taken together, we conclude that the subarctic NE Pacific Ocean diatom community we examined was driven into B_{12} limitation following iron addition. The emergence of increased expression in B_{12}-sensitive indicator genes following iron addition co-occurs with surface dissolved cyanocobalamin concentrations below 0.13 pmol L^{-1} at OSP (Fig. 1.5). Because *METE* and *CBA1* were not abundant in the unamended control or ambient seawater, sufficient concentrations of B_{12} were likely present to support growth of iron-limited cells but

were quickly depleted as the *Pseudo-nitzschia*-dominated bloom progressed. As all examined transcriptomes of *Pseudo-nitzschia* species lack *METE* (Ellis et al. 2017), the iron-stimulated *Pseudo-nitzschia* bloom may have consumed and outpaced the B_{12} supply. These conditions allowed for a diatom containing *METE* that was not initially abundant in the community, most likely belonging to or closely-related to the genus *Attheya*, to increase their abundance of *METE* transcripts (Fig. 1.7A-B).

This work serves as compelling support for iron-induced vitamin B_{12} limitation in the Northeast Pacific Ocean. Several studies have demonstrated that low concentrations of vitamins can control phytoplankton biomass, with communities stimulated following vitamin enrichment experiments (Sañudo-Wilhelmy et al. 2006; Gobler et al. 2007; Bertrand et al. 2012; Koch et al, 2012; Bertrand et al. 2015). In such experiments, addition of B_1 and B_{12} resulted in community composition shifts (Gobler et al. 2007, Koch et al. 2012). Although in our study there were no obvious differences in the biomass as a result of B_{12} enrichment, either with or without iron, we hypothesize shifts in community composition may have occurred if more time had elapsed, given the molecular indications of B_{12} limitation following iron addition within certain members of the diatom community by the end of our experiments.

Conclusions

Given the results of this study, it is likely that iron limitation reduces the amount of diatom-produced vitamins B_7 available to other auxotrophic microorganisms. The consequences would be most profound in regions where diatoms are a major supplier. Under iron-limiting conditions, auxotrophic microbes may then be forced to compete for a scarce resource as iron-

limited diatoms reduce B_7 production and possibly transition to taking up vitamins from their environment. Conversely, following ephemeral iron enrichment events such as those observed during our field study with the eruption of Mt. Pavlof, increased demands for vitamin B_{12} may result in surface water depletion and subsequent community composition shifts. In our study, the emergence of METE-containing diatoms along with the increased expression of *METE* following iron enrichment provided evidence for B_{12} limitation in at least some members of the diatom community. Furthermore we report that iron-limited diatoms produce fewer vitamin synthesis transcripts (for B_1, B_2, B_6, B_7 and B_{12}) as compared to cells enriched with iron, suggesting they either require less vitamins when growing more slowly, or they may lack the essential resources necessary to fuel their production.

CHAPTER 2: VARIATIONS IN DIATOM TRANSCRIPTIONAL RESPONSE TO CHANGES IN IRON AVAILABILITY ACROSS OCEAN PROVINCES[2]

Introduction

Phytoplankton growth is limited by iron (Fe) availability in approximately 30-40% of the ocean (Moore et al. 2002). The subarctic Northeast (NE) Pacific Ocean is one of the most well-characterized of these Fe-limited areas, commonly referred to as a high-nutrient, low chlorophyll (HNLC) regions. Productivity in the NE Pacific Ocean remains low regardless of ample nitrate (NO_3) concentrations and is typically dominated by small cells such as *Synechococcus* and other picophytoplankton (Varela and Harrison 1999). In this region, Fe is supplied to surface waters mainly through atmospheric dust deposition and volcanic inputs, with continental margins fueling winter phytoplankton blooms when atmospheric deposition is low (Lam et al. 2006; Lam and Bishop 2008). A gradient in surface nutrient concentrations is observed from this oceanic region eastwards towards the continent; bioavailable Fe increases and supports higher phytoplankton biomass, while NO_3 concentrations concomitantly decrease and periodically limit growth (Taylor and Haigh 1996; Harris et al. 2009; Ribalet et al. 2010).

[2]The contents of this chapter will soon be submitted for publication at the peer-reviewed journal *Environmental Microbiology*. The working citation is as follows: Cohen NR, Lampe RH, McNair H, Ellis KA, Kuzminov FI, Brzezinksi MA, Thamatrakoln K, Maldonado MT, Till CP, Bruland KW, Twining BS, Marchetti A. Variations in diatom transcriptional response to changes in iron availability across ocean provinces. AM, BST and KB designed the study; NRC, KAE, BST and AM performed the incubation experiments; NRC performed RNA and bioinformatic analyses; RHL provided bioinformatic support; FIK and KT measured F_v:F_m onboard the *R/V Melville*; MAB and HM quantified biogenic silica; MMT contributed primary productivity measurements; CPT quantified trace metals; NRC and AM wrote the manuscript.

Iron-limited growth of phytoplankton may also occur in coastal waters, a notable example being the California Upwelling Zone (CUZ; Hutchins *et al.* 1998; Bruland *et al.* 2001). This region is characterized by high concentrations of upwelled macronutrients, but relatively low dissolved Fe (dFe) due to lack of riverine input and a narrow continental shelf that does not allow for mixing of upwelled water with Fe derived from iron-rich shelf sediments (Johnson et al. 1999). The primary Fe source in the CUZ is winter river sediment deposition (Hutchins et al. 2002; Chase et al. 2005). The phytoplankton community tends to be dominated by diatoms during the early upwelling season, with dinoflagellates dominating towards the end (Du and Peterson 2014).

Phytoplankton that subsist in Fe-limited environments are equipped with strategies to sustain growth during periods of physiological Fe stress and to rapidly respond to sudden increases in bioavailable Fe (Marchetti et al. 2012). Strategies employed by phytoplankton include increasing usage of Fe-independent proteins and protein complexes to decrease cellular Fe requirements (La Roche et al. 1996; Peers and Price 2006; Allen et al. 2008; Lommer et al. 2012), increasing Fe uptake rates through high affinity Fe uptake systems (Shaked et al. 2005; Morrissey et al. 2015) and the use of Fe storage proteins or within cell vacuoles (Marchetti et al. 2009; Nuester et al. 2012). Some laboratory isolates and natural communities rapidly reverse these Fe-limited strategies when Fe concentrations increase (Kustka et al. 2007; Lommer et al. 2012), whereas in other organisms these strategies are permanent (Lommer et al. 2010; Marchetti et al. 2012). While we have an understanding of certain phytoplankton physiological and molecular responses to Fe limitation within laboratory isolates, it is not clear how the strategies invoked by intermittently Fe-limited coastal taxa differ from those used by species that reside in

chronic Fe-limited oceanic regions in the open ocean when present within natural mixed phytoplankton assemblages.

Within the diatoms, a large amount of genetic diversity exists among lineages, likely due to differences in environmental pressures at the time of their evolutionary emergence. The earliest centric lineage (radial) evolved around 250 million years ago when atmospheric carbon dioxide levels were higher and dissolved oxygen was lower compared to contemporary conditions (Armbrust 2009). In contrast, the youngest pennate diatom linage (raphid) evolved 30 million years ago as atmospheric carbon dioxide continued to decrease and oxygen increased. Due to the reactivity of oxygen with Fe resulting in Fe oxides that rapidly precipitate out of seawater, this pennate lineage likely emerged when Fe availability in the ocean was the lowest. A genomic comparison of between the more primitive coastal centric *Thalassiosira pseudonana* and the younger coastal pennate *Phaeodactylum tricornutum* demonstrates the two diatoms share only 57% of their genes with each other, suggesting a tremendous amount of genomic diversity exists between members of these two diatom lineages (Bowler et al. 2008). Additionally, it is often observed that pennate diatoms, especially those belonging to the genus *Pseudo-nitzschia,* tend to dominate large Fe-induced blooms (Boyd et al. 2007; Marchetti et al. 2012). These observations may suggest that diatoms emerging following the stabilization of oxygen levels in the atmosphere have evolved distinct strategies for sustaining Fe-limited growth, resulting in a competitive advantage over more primitive diatoms and other types of phytoplankton.

While a large subset of examined phytoplankton respond consistently to increases in Fe availability, some taxa differ in their response. For instance, the Fe storage protein ferritin increases in gene and protein expression under high-Fe conditions in the diatom *Pseudo-nitzschia* (Marchetti et al. 2009). In contrast, some diatoms have been found to harbor multiple

ferritin genes (e.g., *Amphora coffeaeformis* (raphid pennate) and *Thalassiosira rotula* (bimultipolar centric)), one of which increases under Fe limitation while the other is constitutive (Cohen *et al*., submitted). In addition, while flavodoxin, an Fe-independent replacement for the iron containing protein ferredoxin in photosynthetic electron transport, is an indicator of Fe-limitation in the centric diatom *Thalassiosira oceanica* (Chappell et al. 2015), it does not appear to be influenced by Fe status in the closely related coastal diatom *Thalassiosira pseudonana* (Whitney et al. 2011). Thus differences in molecular responses can be observed even within similar taxonomic groups, and therefore gene and protein expression in response to Fe status cannot be assumed constant across taxa or environments. Given the large amount of genetic diversity and observed physiological variation between the major diatom lineages (Bowler et al. 2008; Marchetti et al. 2009; Sutak et al. 2012), differences in molecular (and thus inferred physiological) responses to changing nutrient availabilities within identical environments are anticipated on a wide scale.

Combining gene expression analyses with physiological measurements increases our ability to decipher the responses of diatoms to varying nutrient availability and better predict the implications for large scale ecological processes. Indeed, relationships between gene expression and nutrient uptake rates can be uncoupled (Thamatrakoln and Hildebrand 2008). However, when in concert, these relationships may provide a mechanism for observed rapid changes in nutrient inventories. Furthermore since phytoplankton taxa can differ in nutrient uptake kinetics and gene transcriptional patterns (Bender et al. 2014), the ability to differentiate expression activity by taxa provides a better coupling of processes to specific microbial members within mixed natural assemblages.

To better understand whether coastal and oceanic diatom communities differ in their responses to variable Fe availability, a comparative analysis among diverse taxa and nutrient regimes was performed and assessed through combined molecular and physiological approaches. Microcosm incubation experiments were conducted at geographically diverse sites with vastly different Fe and macronutrient concentrations and phytoplankton community compositions. Gene expression responses to Fe status identified among sites and between the diatom genera *Pseudo-nitzschia* and *Thalassiosira* demonstrate that several strategies for handling Fe stress are distinct among regions and diatom taxa. Furthermore, two of the methodological approaches used in this analysis – metatranscriptomics and nutrient uptake rates – gave consistent results at several locations. Since Fe bioavailability to phytoplankton is predicted to change with increasing temperature and acidification of surface seawater (Shi et al. 2010; Hutchins and Boyd 2016), the findings presented here will aid in predicting the consequences of changing ocean conditions on phytoplankton productivity, community composition, and the biological carbon pump.

Experimental Procedures

Experimental Design

Incubation experiments were conducted on two separate cruises: within regions of the CUZ during July 3-26th 2014 onboard the *R/V Melville* and along the Line-P transect of the subarctic NE Pacific during June 7-23rd 2015 onboard the *Canadian Coast Guard Ship (CCGS) John P. Tully* (Fig. 2.1). The incubated phytoplankton community response was assessed using a combination of physiological measurements and metatranscriptomics in order to examine the effects of Fe status on diatom physiology and gene expression. Each experiment included three

treatments consisting of a 5 nmol L^{-1} $FeCl_3$ addition (Fe), a 200 nmol L^{-1} desferroxamine B (DFB) addition, and an unamended control (C), each sampled at two time points.

During the CUZ cruise, three incubation experiments were performed at separate locations corresponding to distinct Fe and macronutrient regimes (Table 2.1), including sites of high dFe, macronutrients, and phytoplankton biomass (C1: 38°39.30N, 123°39.87W), relatively low dFe, high macronutrients and phytoplankton biomass (C2: 38°15.31N, 123°57.98W), and relatively low dFe with high macronutrients and low phytoplankton biomass (C3: 42°40.00N, 125°0.00W) (Fig. 2.2). Near-surface seawater (2-5 m) was collected using a trace-metal clean sampling system consisting of a tow-fish sampler attached to Kevlar™ line, PFA Teflon tubing and a Teflon dual-diaphragm pump that pumped seawater directly into a positive pressure trace-metal clean bubble. The seawater was placed into a large 200L acid-cleaned HDPE drum for homogenization before being distributed into 10L flexible acid-cleaned polyethylene cubitainers. Cleaning protocols for the cubitainers included soaking in 1.2 mol L^{-1} hydrochloric acid (reagent grade) for 3 days, 1.2 mol L^{-1} hydrochloric acid (trace metal grade) for 1 week and soaking in 0.1 mol L^{-1} acetic acid (trace-metal grade) until use. Prior to filling the cubitainers with seawater, the dilute acetic acid was removed and the cubitainers were rinsed thoroughly three times with ambient seawater from the collection site. As the primary objective of these experiments was to elucidate the phytoplankton (diatom) responses to variable Fe conditions, sites were targeted that would ensure adequate macronutrient concentrations to support a potential increase in phytoplankton biomass. However in C2, 15 µmol L^{-1} of $Si(OH)_4$ was added to all cubitainers to support growth of diatoms due to initially low $Si(OH)_4$ concentrations (<4.7 µmol L^{-1}).

During the Line-P cruise, incubation experiments were conducted at the low-NO_3 coastal station P4 (48°39N, 126°40W) and at the chronically Fe-limited, HNLC oceanic station P26,

also known as Ocean Station Papa (OSP, 50°00N, 145°00W; Harrison 2002). Seawater was collected at depths corresponding to approximately 30% of incident irradiance (8-12 m) at both stations using a trace-metal clean sampling system consisting of a Teflon air bellows pump and PTFE lined Kevlar™ tubing (0.75 in diameter) attached to Kevlar™ line. The seawater was pumped directly into 10 L acid-cleaned polyethylene cubitainers with an on-deck trace-metal clean positive pressure flowhood. At C4, 10 μmol L^{-1} of NO_3 was added to all cubitainers to support growth of diatoms due to the initially low NO_3 concentrations (<1.5 μmol L^{-1}).

At the start of the experiments, ambient seawater was filtered for all initial measurements (T_0). For each incubation experiment, cubitainers were filled and amended with $FeCl_3$ or DFB (depending on treatment) just prior to dawn. All treatment cubitainers were placed in on-deck Plexiglass incubators with flow-through seawater to maintain near-ambient surface water temperatures and were covered with neutral density screening to achieve approximately 30% of the incident irradiance (Fig. 2.3). Following 24-96 hours of incubation (Table 2.1; depending on the measured macronutrient drawdown) the cubitainers for a specific time point were removed from the incubators and filtered immediately. The goal for each time point was to achieve measureable drawdowns in macronutrients that would infer stimulation of phytoplankton growth without complete macronutrient depletion. However for certain experiments and time points, depletion of a particular macronutrient (typically NO_3) occurred (Table 2.1). All filtrations were conducted at dawn. Subsamples for dissolved and particulate nutrients, size-fractionated dissolved inorganic carbon (DIC) and NO_3 uptake rates, size-fractionated chlorophyll *a*, F_v/F_m and RNA were collected at T_0 and from each cubitainer according to the protocols described below.

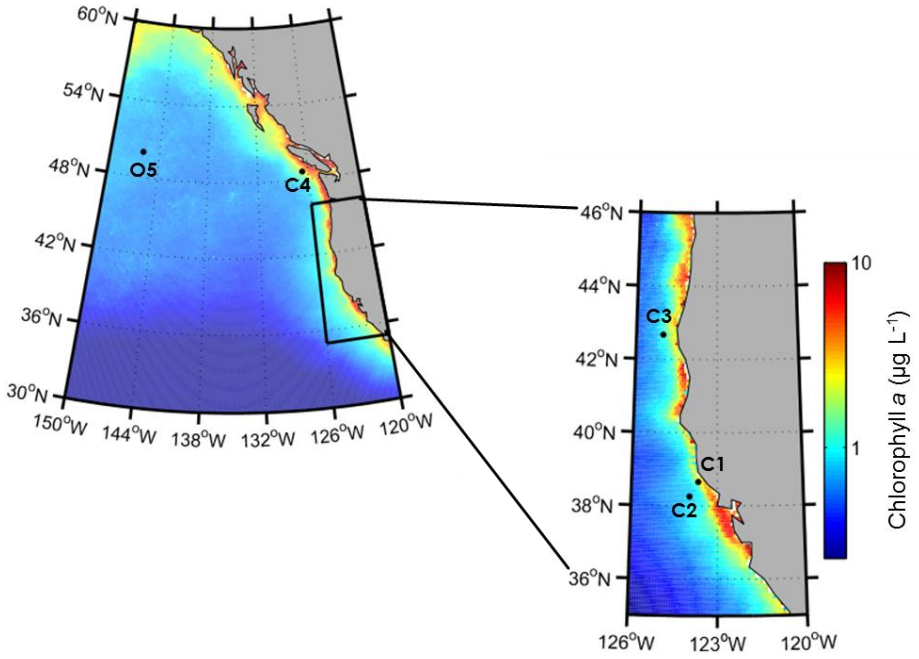

Fig. 2.1. Locations of incubation experiments in the California Upwelling Zone (C1, C2, C3) and Northeast Pacific Ocean (C4, O5). Color bar indicates climatological averaged chlorophyll *a* concentrations (µg L^{-1}) from SeaWiFS (1997-2010).

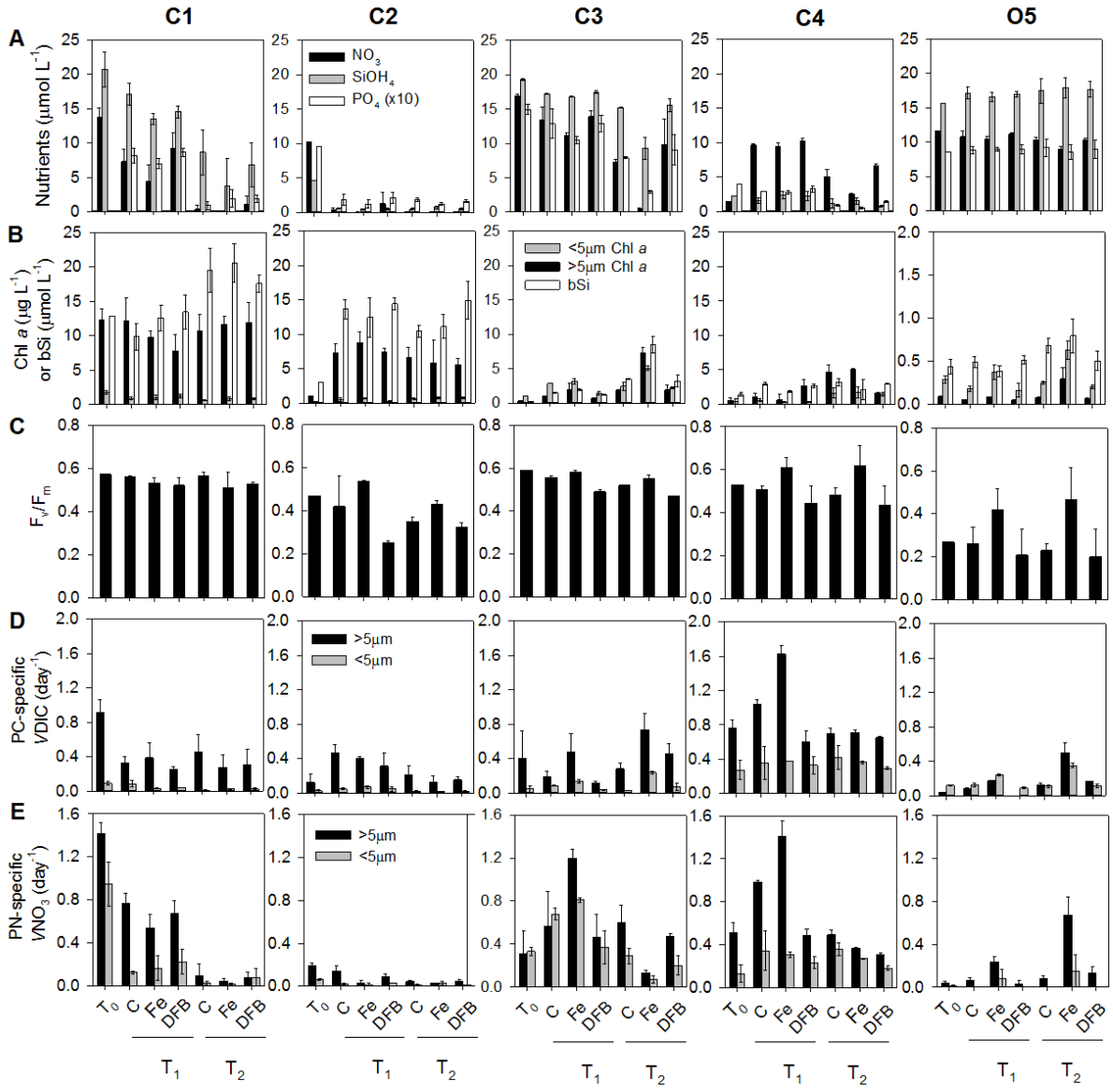

Fig. 2.2. Physiological assessment of incubation experiments. **A**. Dissolved macronutrient concentrations: nitrate (NO_3), silicic acid ($SiOH_4$), and phosphate (PO_4), **B**. Size-fractionated chlorophyll a (µg L^{-1}) within the large (>5 µm) and small (<5 µm) size fractions or bSi (µmol L^{-1}), **C**. Maximum photochemical yield of PSII (F_v/F_m), **D**. Particulate organic carbon (PC)-specific dissolved inorganic carbon (DIC) uptake rates [VDIC (day^{-1})] within the large and small size fractions, and **E**. particulate organic nitrate (PN)-specific nitrate uptake rates [VNO_3 (day^{-1})] within the large and small size fractions in each treatment across sites and sample time points (see Table 2.1). Where present, error bars represent ±1 standard deviation associated with the mean of triplicate incubations.

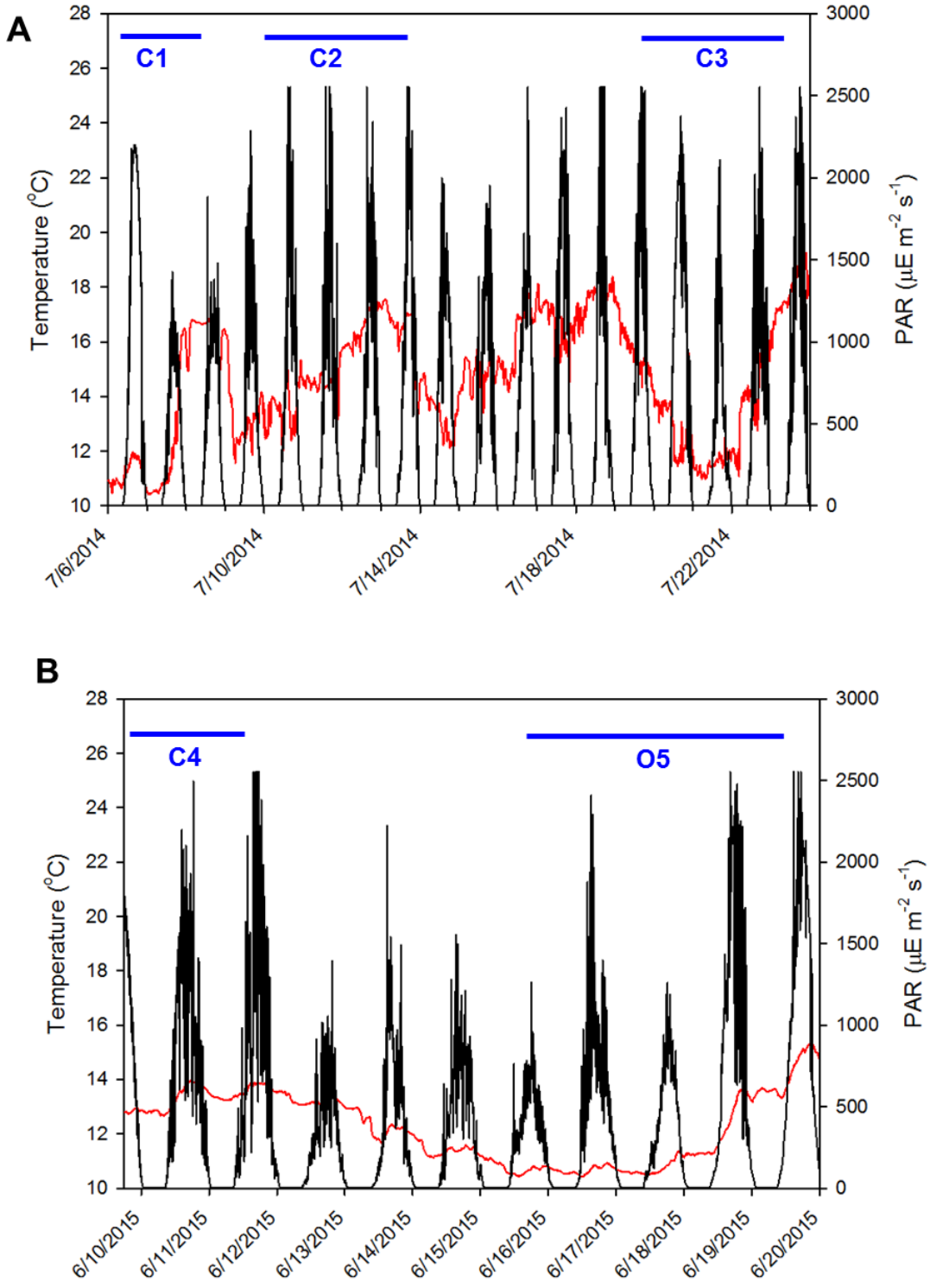

Fig. 2.3. Irradiance and temperature of flow-through seawater Plexiglass incubators containing mesocosom incubations onboard the CUZ (**A**) and Line-P (**B**) cruises. Incubators were used to maintain near-ambient surface water temperatures and irradiance during the incubation period (48-96 hours; Table 2.1). Plexiglass incubators were covered with neutral density screening to achieve approximately 30% of the incident irradiance. PAR (µE) is shown in black, temperature (°C) in red. Time periods corresponding to each incubation experiment are denoted in blue.

Site ID	Location of incubation	Coastal/oceanic	% large cells in T_O	T_1/T_2 (hours)	Macronutrient depletion at T_1 or T_2?	dFe (nmol L^{-1})	NO_3:Fe at T_0 (µmol:nmol)	Fe effect?
C1	California Upwelling Zone (38°39.30N, 123°39.87W)	coastal	88%	T_1 = 24 T_2 = 48	NO_3 (T_2)	3.48	3.9	-
C2	California Upwelling Zone (38°15.31N, 123°57.98W)	coastal	83%	T_1 = 48 T_2 = 72	NO_3 and Si (T_1)	0.43	24	-
C3	California Upwelling Zone (42°40N, 125°W)	coastal	30%	T_1 = 48 T_2 = 72	NO_3 (T_2)	0.28	60	+
C4	Line-P (P4) (48°39N, 126°40W)	coastal	57%	T_1 = 24 T_2 = 48	Si (T_1)	0.64	2.3 18.8*	+/-
O5	Line-P (OSP) (50°N, 145°W)	oceanic	22%	T_1 = 48 T_2 = 96	-	0.05	234	+

*Ratio after 10 µmol L^{-1} NO_3 was added to incubation experiments to support diatom growth in initially low NO_3 seawater (see methods).

Table 2.1. Summary of bulk parameters measured within incubation experiments. Percent large cells corresponds to the percent of >5 µm chl *a* as compared to the total pool encompassing picoplankton (<5 µm chl a). T_1/T_2 represents timing of incubation harvesting. A NO_3:Fe ratio >12 µmol:nmol indicates a phytoplankton community is likely to be driven into Fe limitation (King and Barbeau, 2007). A positive Fe effect (+) represents that the community demonstrated a physiological response to Fe addition as observed through increases in bulk measurements (chl *a*, PN-specific VNO_3 and PC-specific VDIC), while (+/-) indicates a positive response in PN-specific VNO_3 and PC-specific VDIC though not in chl *a*, and (-) represents no change.

Nutrient concentrations, uptake rates and biogenic silica

For CUZ experiments, dissolved nitrate and nitrite ($NO_3^- + NO_2^-$), phosphate (PO_4^{3-}), and silicic acid (H_4SiO_4) concentrations were measured onboard using a Lachat Quick Chem 8000 Flow Injection Analysis system (Parsons et al. 1984). Particles were removed via filtration through a Whatman GF/F filter. Reference materials for nutrients in seawater were run for quality control. During Line-P sampling, approximately 15 mL of seawater was filtered through a Whatman GF/F filter into acid-rinsed polypropylene tubes and frozen at −20 °C in aluminum blocks until onshore analysis. Shortly following the cruise, the dissolved $NO_3^- + NO_2^-$, PO_4^{3-}, and H_4SiO_4 concentrations were determined using an Astoria analyzer (Barwell-Clarke et al. 1996).

Size-fractionated particulate nitrogen (PN), particulate carbon (PC), and NO_3^- uptake rates were obtained by spiking 618 mL of seawater placed within clear polycarbonate bottles with ^{15}N-$NaNO_3$ at no more than 10% of ambient NO_3 concentration within CUZ incubations, and at 1 µmol L^{-1} within Line-P incubations. DIC uptake within Line-P incubations was measured by additionally spiking subsamples with 120 µmol L^{-1} $NaH^{13}CO_3$. Bottles were incubated in the same flow-through Plexiglass incubators where cubitainers were kept. Following 8 h of incubation, seawater samples were gravity filtered through a polycarbonate filter (5 µm pore size, 47 mm), and then through a pre-combusted (450°C for 5 h) GF/F filter (0.7 µm nominal pore size, 25 mm) by gentle vacuum (< 100 mg Hg). Particulates collected on the 5 µm polycarbonate filter were then rinsed onto a separate pre-combusted GF/F filter using an artificial saline solution. Filters were stored at -20°C until onshore analysis. In the laboratory, filters were heated to 50°C for 24 hours and pelletized in tin capsules (Elemental Microanalysis) in preparation for analysis of the atom % ^{15}N, atom % ^{13}C (for Line-P), particulate organic nitrogen (PN) and particulate organic carbon (PC) using an elemental analyzer paired with an

isotope ratio mass spectrometer (EA-IRMS). Biomass-normalized NO_3 uptake rates (PN-*V*NO3) and DIC uptake rates (PC-*V*DIC) for the Line-P experiments were obtained by dividing by PN and PC concentrations, respectively.

To quantify *V*DIC in CUZ incubations, incorporation of ^{14}C was determined using a protocol adapted from Taylor *et al.* (2013). Briefly, 60 mL of seawater from each cubitainer was distributed into acid-cleaned light and dark polycarbonate bottles. In each bottle, 1.2 µCi of $NaH^{14}CO_3$ was added. Bottles were incubated in the same flow-through Plexiglass incubators where cubitainers were kept for 6.5-8 h. Following incubation, samples were filtered through stacked polycarbonate filters (5 µm, 1 µm and 47 mm) separated with a mesh spacer during filtration. Filters were vacuum dried, placed in 7 mL scintillation vials containing 0.5 mL of 6M HCl and permitted to degas for 24h. Disintegrations per minute (DPM) retained on the filters were measured using a Beckman Coulter LS 6500 scintillation counter. Reported values are light bottle DPMs minus dark bottle DPMs. To obtain *V*DIC, DIC uptake rates were normalized to PC within each incubation and size fraction.

For biogenic silica (bSi) measurements, 335 mL (CUZ) or 250 mL (Line P) of seawater was filtered onto polycarbonate filters (1.2 µm pore size for CUZ and 0.6 µm pore size for Line-P, 25 mm), digested with NaOH in Teflon tubes, and measured with the colorimetric ammonium molybdate method (Nelson et al. 1995).

Dissolved Fe concentrations

Seawater samples for Fe analysis within the CUZ were acidified at sea with the equivalent of 4 mL 6N quartz-distilled HCl L^{-1} of seawater and stored in acid-cleaned LDPE bottles, and subsequently analyzed using an adaption of Biller and Bruland (2012) on a Thermo-

Element high resolution XR ICP-MS (Parker et al. 2016). Line-P dissolved Fe measurements were obtained via ICP-MS.

Chlorophyll a

Four hundred mL of seawater was gravity-filtered through a polycarbonate filter (5 µm pore size, 47 mm diameter) followed by a GF/F filter (0.7 µm nominal pore size, 25 mm diameter) under vacuum pressure using a series filter cascade for size fractionation. Filters were frozen at -80°C until analysis. Chlorophyll *a* extraction was performed using 90% acetone at -20°C for 24 h and determined via *in vitro* fluorometry on a Turner Designs 10-AU fluorometer using the acidification method (Parsons et al. 1984).

Domoic acid

Approximately 250 mL of seawater from each CUZ site was GF/F filtered (25 mm) via vacuum pressure (<100 mm Hg) and frozen at -80°C. Filters were extracted using 20% methanol (MeOH) in water, sonicated (2 min, 30-40 W) in an ice bath with a Sonicator 3000, followed by centrifugation (10 min, 1399 x g). The supernatant was collected and passed through a 0.22 µm syringe filter. Samples were stored at -20°C until analysis. Concentrations with a detection limit of 0.01 µg L^{-1} were obtained using an enzyme-linked immunosorbent assay (Abraxis, Warminster, PA, USA) following the manufacturer's protocol, including running each sample in duplicate at several dilutions. Final concentrations (pg DA mL $extract^{-1}$) were calculated using the manufacturer supplied analysis spreadsheet.

Photophysiology

The maximum photochemical yield of PSII (F_v/F_m), were obtained by measuring fluorescence induction with a Satlantic FIRe fluorometer (Kobler et al. 1998; Gorbunov and Falkowski 2005). Before each measurement, a 5mL subsample of seawater from each cubitainer

was placed in the dark for 20 minutes. A saturating pulse (20,000 µmol photons m^{-2} s^{-1}) of blue light (450 nm) was applied to dark-acclimated cells for a duration of 100-200 µs. Measurements were obtained using the single-turnover flash (STF) setting with 50 iterations in the CUZ experiments, and 1 iteration within the Line-P experiments.

RNA extraction and bioinformatic analysis

Seawater samples were filtered onto 0.8 µm Pall Supor filters (0.8 µm pore size, 142 mm diameter) via peristaltic pumping, immediately flash frozen in liquid nitrogen and stored at -80°C until extraction onshore. Filters were briefly thawed on ice before being extracted individually using the ToTALLY RNA Kit (Ambion). The extraction procedure followed manufacturer protocols with the modified first step of glass bead addition and vortexing in order to facilitate disruption of cells. Removal of DNA was performed with one round of DNAse I (Ambion) incubation. For the Line P experiments, due to low yields in treatments, RNA from the triplicate cubitainers was pooled prior to sequencing. Within CUZ experiments all triplicate incubation samples were sequenced separately. Metatranscriptomic library preparation was performed with the Illumina TruSeq Stranded mRNA Library Preparation Kit and HiSeq v4 reagents. Samples were barcoded and run across three lanes of Illumina HiSeq 2000 (125 bp, paired-end) yielding on average 23,156,648 paired-end reads per sample. Sequencing statistics are available at http://marchettilab.web.unc.edu/data/.

Raw reads were trimmed for quality bases and removal of adapters using Trimmomatic v0.32 (paired-end mode, adaptive quality trim with 40bp target length and strictness of 0.6, minimum length of 36bp; Bolger et al. 2014). Trimmed paired reads were merged into single reads with BBMerge v8.0. For each site, the resulting merged pairs and non-overlapping paired-end reads were assembled using ABySS v1.5.2 with a multi-kmer approach (Birol et al. 2009).

The different k-mer assemblies were merged to remove redundant contigs using Trans-ABySS v1.5.3 (Robertson et al. 2010). Read counts were obtained by mapping raw reads to assembled contigs with Bowtie2 v2.2.6 (end-to-end alignment; Langmead and Salzberg 2012). Alignments were filtered by mapping quality score (MAPQ) of 10 or higher as determined by SAMtools v1.2 (Li et al. 2009). Taxonomic and functional annotations were assigned based on sequence homology to reference databases via BLASTx v2.3.0 with an e-value cutoff of 10^{-3} (Altschul et al. 1990). Functional annotations were assigned according to the top hit using the Kyoto Encyclopedia of Genes and Genomes (KEGG; Release 75), while taxonomic assignments were obtained according to the top hit using MarineRefII (Laboratory of Mary Ann Moran, University of Georgia), a custom-made database comprised of protein sequences of marine microbial prokaryotes and eukaryotes including all sequenced transcriptomes from the Marine Microbial Eukaryote Transcriptome Sequencing Project (MMETSP; Keeling et al. 2014). Taxonomic information was obtained from NCBI's Taxonomy Database (each isolate in MarineRefII is assigned a NCBI taxonomic ID). The information from NCBI was manually curated to ensure proper assignment and use of common phytoplankton taxonomic ranks.

All diatom-assigned counts were summed to the genus taxonomic rank and KEGG Orthology (KO) functional annotation level. For genes of interest without a KO assignments but with an annotated gene definition (i.e. ISIPs and rhodopsin), raw counts corresponding to KEGG gene definitions were summed. edgeR v3.12.0 was used to calculate normalized fold change and counts-per-million (CPM) from pairwise comparisons using the exactTest (Robinson and Smyth 2008; Robinson et al. 2010). Significance ($p < 0.05$) was calculated with edgeR's estimate of tagwise dispersions across all samples within CUZ sites. Heatmaps were produced with the R package pheatmap v1.0.8, and dendrograms created using Euclidean distance and hierarchical

clustering. Contigs, read counts, and functional annotations of contigs are available at http://marchettilab.web.unc.edu/data/.

In order to compare transcript abundance across locations and data sets for principal component analysis (PCA), the assemblies for all sites were merged with Trans-ABySS. The removal of redundant contigs was verified with GenomeTools v.1.5.1. Counts were obtained by aligning raw reads against this merged metatranscriptome using Salmon v.0.7.3-beta. Normalized counts were then obtained with edgeR v3.12.0. PCA biplots were creating using the R package ggbiplot v.0.5

Results

Initial nutrient regimes of experimental sites

California Upwelling Zone (CUZ) site C1 consisted of a high biomass, high macronutrient and Fe-replete phytoplankton community in the mixed layer. The system was dominated by phytoplankton cells in the >5 µm chlorophyll *a* (chl *a*) size fraction, constituting 88% of the total chl *a* concentration (Fig. 2.2B; Table 2.1). Macronutrient concentrations were initially high and were rapidly consumed following 24 hours of incubation (T_1), and the resulting phytoplankton community depleted most of the NO_3 by 48 hours with $\leq$1 µmol L^{-1} remaining (T_2; Fig. 2.2A). Our measurements suggest this initially Fe-replete phytoplankton community (dFe: 3.48 nmol L^{-1}) was mostly unaffected by the additions of Fe or DFB as demonstrated through relatively constant F_v/F_m, phytoplankton biomass, particulate organic nitrate (PN)-specific nitrate uptake rates (VNO_3, or nitrogen assimilation rates), and particulate organic carbon (PC)-specific dissolved inorganic carbon uptake rates (VDIC, or carbon assimilation rates) across all treatments (Fig. 2.2C-E). Furthermore, the NO_3:Fe ratio of initial seawater (T_0)

was substantially below the established threshold ratio for Fe stress of 12 µmol:nmol (Table 2.1; King and Barbeau, 2007; Brzezinski *et al.*, 2015), indicating this phytoplankton community was not likely to be driven into Fe limitation. However, indications of molecular-level responses to Fe and DFB additions were observed with 74 genes differentially expressed ($p < 0.05$) in *Pseudo-nitzschia* between Fe and DFB treatments (Fig. 2.4A; see discussion below).

CUZ site C2 was located in close geographical proximity to C1 (Fig. 2.1), yet exhibited different mixed layer properties in relation to phytoplankton biomass, silicic acid ($Si[OH]_4$) and dFe concentrations (0.43 nmol L^{-1}). NO_3 and phosphate (PO_4) concentrations were similarly high (10.3 and 0.96 µmol L^{-1}, respectively) as found at site C1, although $Si(OH)_4$ levels were much lower and possibly growth-limiting to some diatoms (4.69 mol L^{-1}; Nelson *et al.*, 1996). Therefore, incubations were amended with 15 µmol L^{-1} $Si(OH)_4$ to support potential diatom growth with added Fe (Brzezinski, 1985). Although the >5 µm chl *a* size fraction was initially <1 µg L^{-1}, concentrations reached >7 µg L^{-1} in all treatments by 48 hours (T_1), accompanied by appreciable decreases in NO_3, PO_4, and $Si(OH)_4$ concentrations (Fig. 2.2A&B). Since this community quickly depleted NO_3 concentrations during the experimental period, this site presented a unique opportunity to couple the physiological indicators of NO_3 stress with N-related assimilation and transport genes shown to be elevated in NO_3 limited laboratory cultures of diatoms (Rogato et al. 2015). Although indications of an Fe-stress responses were mostly absent in the bulk biochemical and physiological measurements across treatments, the NO_3:Fe ratio of the inital seawater was 24 µmol:nmol, suggesting this community may have been driven into Fe limitation if $Si(OH)_4$ was not depleted. In addition 414 genes associated with *Pseudo-nitzschia* were significantly differentially expressed ($p <0.05$) by T_1 between Fe and DFB treatments (Fig. 2.4B). This greater number of differentially expressed genes in *Pseudo-nitzschia*

when compared to C1 suggests the C2 diatom community experienced a higher degree of Fe stress during the incubation time course. The initially low dissolved $Si(OH)_4$:NO_3 ratio at this site furthermore implies a history of Fe limitation and previous upwelling activity (Brzezinski et al. 2015). Interestingly, concentrations of the *Pseudo-nitzschia*-produced neurotoxin, domoic acid (DA), were 90 pg mL^{-1} in initial seawater (T_0) and exceeded 3,000 pg mL^{-1} following incubation by T_1 (Fig. 2.5), supporting the finding that DA production in *Pseudo-nitzschia* may be linked to $Si(OH)_4$ starvation (Pan et al. 1996).

Site C3 contained the lowest dFe concentrations (0.28 nmol L^{-1}) among the CUZ sites whereas the macronutrient concentrations were initially high, with approximately 17 µmol L^{-1} NO_3, 19 µmol L^{-1} $Si(OH)_4$, and 1.5 µmol L^{-1} PO_4 (Fig. 2.2A). The corresponding NO_3:Fe ratio of this initial seawater was approximately 60 µmol:nmol. Following incubation, the chl *a*, PN-specific *V*NO_3, and PC-specific *V*DIC were all higher in Fe-amended treatments relative to the unamended control (Fig. 2.2B,D-E). NO_3 was completely drawn down only within the Fe treatment by 72 hours (T_2). Despite the pronounced influence of Fe enrichment on bulk parameters, F_v/F_m values were only slightly higher in the Fe treatments relative to the control but were substantially higher than the DFB treatments (Fig. 2.2C). This is likely a reflection of the different phytoplankton composition at this location compared to site C2, which did not show indications of an Fe addition response on the measured bulk parameters, but did demonstrate elevated F_v/F_m values in treatments where Fe was added. Thus, site C3 represented the only phytoplankton community that displayed a definitive physiological response to Fe addition in the CUZ (Table 2.1). The Fe-induced molecular response in diatoms was demonstrated by the differential expression ($p < 0.05$) of 458 genes in *Pseudo-nitzschia* and 1,223 in *Thalassiosira* between the Fe and DFB treatments (Fig. 2.4C).

Coastal site C4 was located at station P4 of the Line-P transect in the subarctic NE Pacific Ocean. Initial mixed layer conditions were characterized by low phytoplankton biomass, macronutrient concentrations and dFe. NO_3 concentrations were initially 1.5 µmol L^{-1}, thus in order to facilitate a potential phytoplankton growth response to added Fe, 10 µmol L^{-1} of NO_3 was added to each incubation. Consequently, $Si(OH)_4$ concentrations were also initially low (2.18 µmol L^{-1}) and incubation concentrations dropped to <2 µmol L^{-1} by the second incubation time point (T_2; Fig. 2.2A). Therefore, it is likely the resulting diatom community experienced $Si(OH)_4$ limitation by the end of the incubation period. Despite its relatively close proximity to land and relatively high dFe concentrations (0.64 nmol L^{-1}), there was a pronounced response to Fe addition at C4 as demonstrated through higher F_v/F_m, PN-specific VNO_3, and PC-specific *V*DIC in the Fe treatment when compared to the control by T_1 (Fig. 2.2D-E; Table 2.1). Accordingly, the NO_3:Fe ratio following artificial NO_3 addition of was 18.8 µmol:nmol.

Oceanic site O5 was located at Ocean Station Papa (OSP) or station P26 of the Line-P transect. This site demonstrated characteristically high macronutrients and low dFe (0.05 nmol L^{-1}), resulting in the highest NO_3:Fe ratio observed across sites (234 µmol:nmol; Table 2.1). Phytoplankton biomass was initally low, consistent with historical observations from this well-characterized Fe-limited region (Fig. 2.2A; Table 2.1; Boyd and Harrison 1999). In contrast to most of the coastal sites, the majority of the phytoplankton biomass was dominated by picophytoplankton initially and throughout the incubation period (<5 µm; Table 2.1; Fig. 2.6). Both large and small chl *a* size fractions, F_v/F_m, PN-specific VNO_3, and PC-specific *V*DIC reached their highest values within the Fe treatment by T_2 and were substantially higher as compared to the unamended control, confirming the initial phytoplankton community and those in all treatments without added Fe were experiencing Fe limitation (Fig. 2.2B-E).

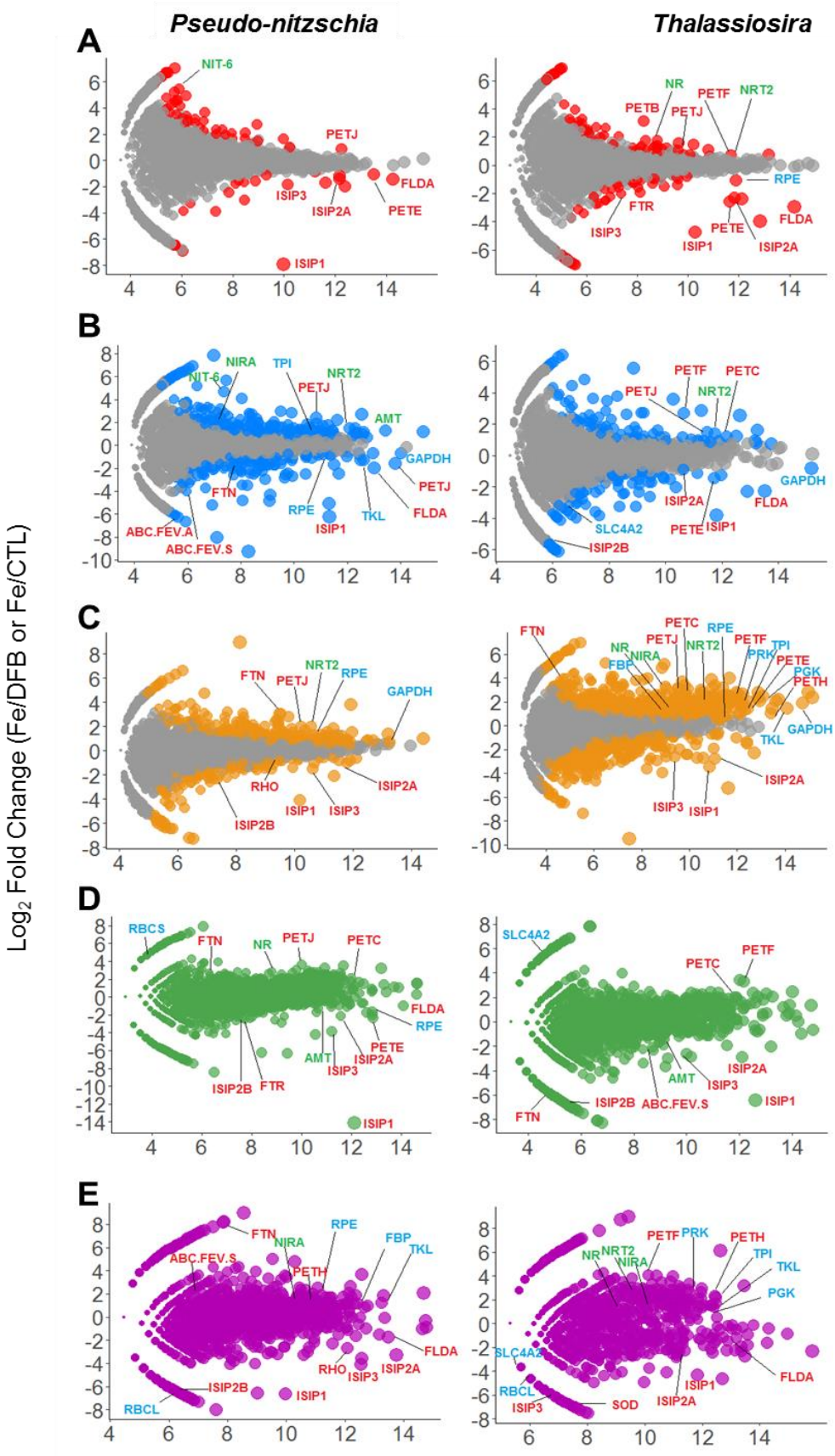
Pseudo-nitzschia
Thalassiosira
A
B
C
D
E
Log2 Fold Change (Fe/DFB or Fe/CTL)
NIT-6
PETJ
FLDA
ISIP3
ISIP2A
PETE
ISIP1
NR
PETB
PETF
NRT2
RPE
FTR
NIRA
TPI
AMT
GAPDH
FTN
TKL
ABC.FEV.A
ABC.FEV.S
PETC
SLC4A2
ISIP2B
RHO
RBCS
PRK
PETH
FBP
RBCL
SOD

Fig. 2.4. MA plots depicting the differential expression response of KOs within the diatom genera *Pseudo-nitzschia* or *Thalassiosira* between Fe-addition (Fe) and DFB-addition (DFB) treatments across sites C1 (**A**), C2 (**B**), C3 (**C**), C4 (**D**) and O5 (**E**). Each point corresponds to a unique KO. Points are shaded gray if transcripts were not significantly differentially expressed ($p<0.05$; A-C only). Genes of interest involved in nitrogen (N; green), carbon (C; blue) or iron (Fe; red) metabolism are annotated only if differentially expressed ($p<0.05$: A-C only) or exhibiting a >2-fold change within treatments (D-E). The unamended control treatment was used at site O5 in place of a DFB-addition treatment.

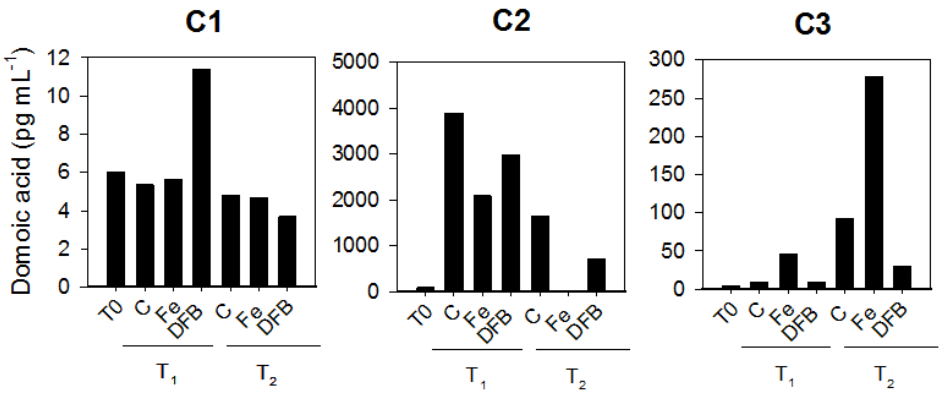

Fig. 2.5. Domoic acid (DA) concentrations within initial phytoplankton communities (T_0) and incubated treatments at CUZ sites C1-C3.

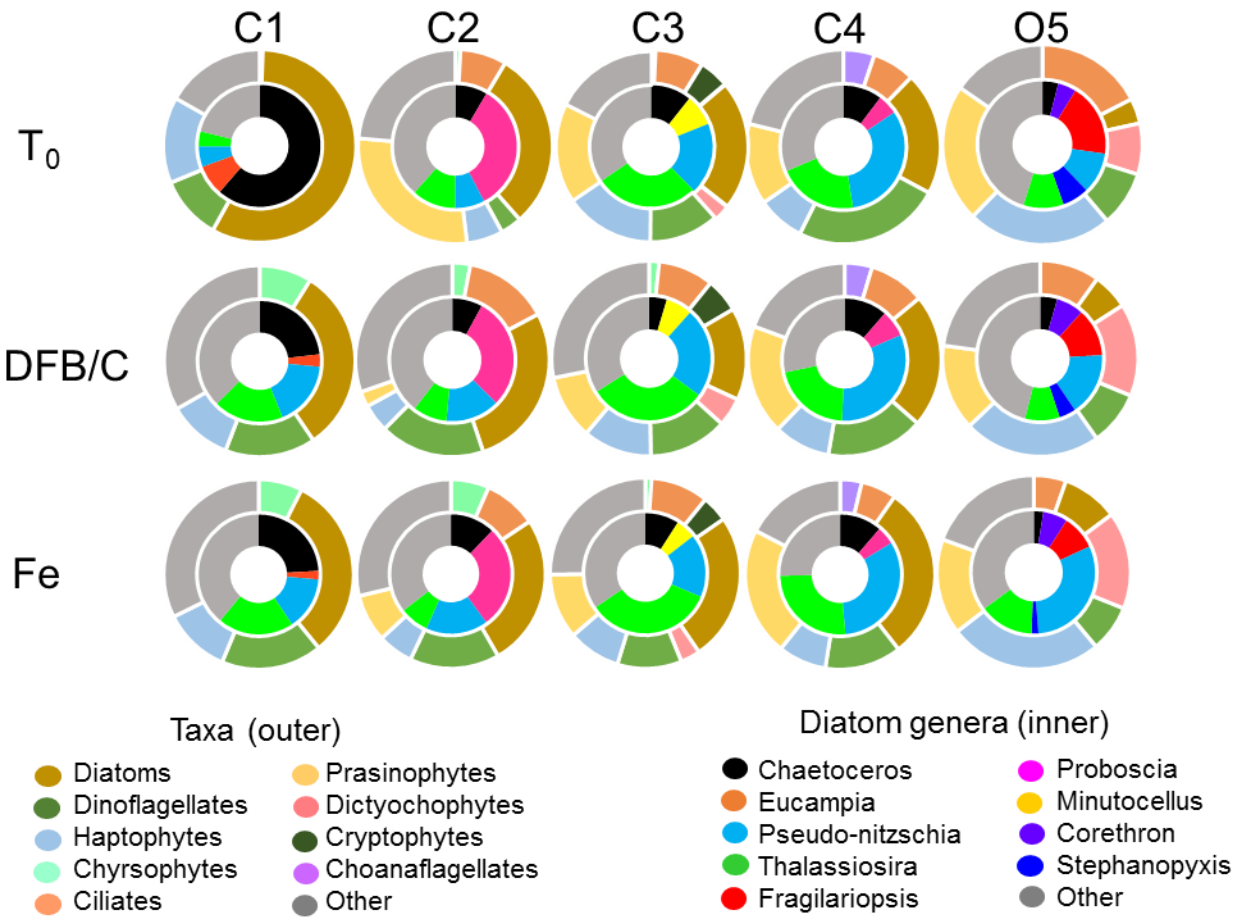

Fig. 2.6. The average normalized transcript proportions of phytoplankton taxa (outer charts) and diatom genera (inner charts) from initial seawater (T_0) and during the first time point (T_1; see Table 2.1) within the Fe addition (Fe) and DFB addition (DFB) treatments at each site. O5 communities are shown from T_2, did not have a DFB treatment performed at this time point, and therefore the control (C) treatment is provided as the Fe-limited comparison .

Community composition and gene expression responses to Fe status

Metatranscriptomic assembly of sequence data and subsequent taxonomic annotation yielded the relative transcript proportions of phytoplankton functional groups, with treatment-induced changes in transcript proportions varying depending on site (Fig. 2.6). The CUZ site C1 was initially yielded mostly comprised of diatom transcripts; however, there was a 26% decrease in both the Fe and DFB treatments by T_1, accompanied by genus-level shifts within the diatoms. This included a relative decrease in *Chaetoceros* and increase in *Thalassiosira* and *Pseudo-nitzschia* transcripts. In contrast, CUZ site C2 initially yielded a phytoplankton community transcript pool dominated equally by diatoms (30%) and prasinophytes (28%), with diatoms remaining a dominant taxa following incubation (26-28%) and prasinophyte transcripts substantially decreasing from 28% to 3-8% within both Fe and DFB incubations. Within the diatom community, *Proboscia, Thalassiosira* and *Pseudo-nitzschia* were initially the most abundant genera and remained so by T_1 in both treatments. CUZ site C3 contained a phytoplankton community transcript pool almost equally represented by diatoms, prasinophytes, haptophytes and dinoflagellates with little change in community composition following incubation in either treatment. *Thalassiosira* dominated the diatom community, representing approximately 30% of the diatom transcripts both in the initial seawater and following incubation. The coastal subarctic Pacific site C4 yielded an initial phytoplankton community transcript pool dominated by dinoflagellate-assigned sequences (24%), though they decreased by approximately 10% in the Fe treatment, concurrent with 9% increases in diatom transcript proportions. Within the diatom community, the genus *Pseudo-nitzschia* was the most dominant based on relative transcript abundance (32%), at T_0 and in both incubated treatments. At the oceanic site O5, there were initially equal proportions of prasinophyte (22%), haptophyte (23%),

and ciliate (17%) transcripts, with little representation by diatoms (4%), although diatom-assigned transcripts constituted 9% of the community transcript pool by T_2 following Fe addition. Within the diatom community the relative abundance of *Pseudo-nitzschia* transcripts increased from 9% at T_0 to 16% in the DFB treatment and 31% in the Fe treatment. Overall, members of the diatom genera *Pseudo-nitzschia* and *Thalassiosira* were present and among the top five most abundant genera in all sites examined (Fig. 2.6). Based on relative transcript abundance, these two genera combined constituted between 9 and 53% of the initial diatom communities, and 25-58% of the Fe enriched diatom communities. In addition, these two taxa were determined by the *Tara* Oceans circumnavigation expedition to be two of the eight most abundant diatom genera in the global ocean (Malviya et al. 2016). With *Pseudo-nitzschia* being a pennate diatom and *Thalassiosira* a centric, they were therefore ideal candidates for examining diatom lineage differences in molecular responses to varying Fe availability.

Gene expression responses among sites were compared using Euclidian distance similarity analyses between Fe and DFB treatments within the diatom genera *Pseudo-nitzschia* and *Thalassiosira* (Fig. 2.7). Expression responses within coastal sites clustered together, whereas the oceanic site O5 was the most distinct for both genera (Fig. 2.7). At site O5, 83 out of 1,334 KEGG Orthology genes (KOs) in *Pseudo-nitzschia* were more highly expressed by >16-fold following Fe enrichment as compared to the DFB treatment (Fig. 2.7). Comparatively, 155 out of 1,241 KOs in *Thalassiosira* were more highly expressed by >16-fold following Fe enrichment as compared to DFB conditions. Highly expressed *Pseudo-nitzschia* genes in the Fe enriched treatment at O5 corresponded to Fe storage and metal transport, whereas in *Thalassiosira*, these included heme utilization and components of sulfate reduction. Both genera increased expression of genes involved in photosynthetic processes by >16-fold exclusively at

this location. In addition, both genera increased expression of the Fe-dependent vitamin B_7 synthesis protein biotin synthase (*BIOB*) in the Fe enriched treatment relative to DFB, by 84- and 49-fold in *Pseudo-nitzschia* and *Thalassiosira* respectively, only in the oceanic community. This is consistent with previous field observations demonstrating that Fe enrichment of previously Fe-limited diatom communities stimulates B_7 synthesis (Cohen et al. in press). Furthermore *Pseudo-nitzschia* and *Thalassiosira* contained 48 out of 1334 and 77 out of 1241 genes, respectively, that increased expression by >16-fold in the DFB treatment as compared to Fe, and these patterns were again not found within diatoms from the examined coastal sites (Fig. 2.7). These genes encoded for proteins including superoxide dismutase (*SOD*), which is involved in the oxidative stress response, and ribulose-1,5-bisphosphate carboxylase oxygenase (RubisCO; large subunit; *RBCL*), which is involved in the first step of C fixation through the Calvin cycle.

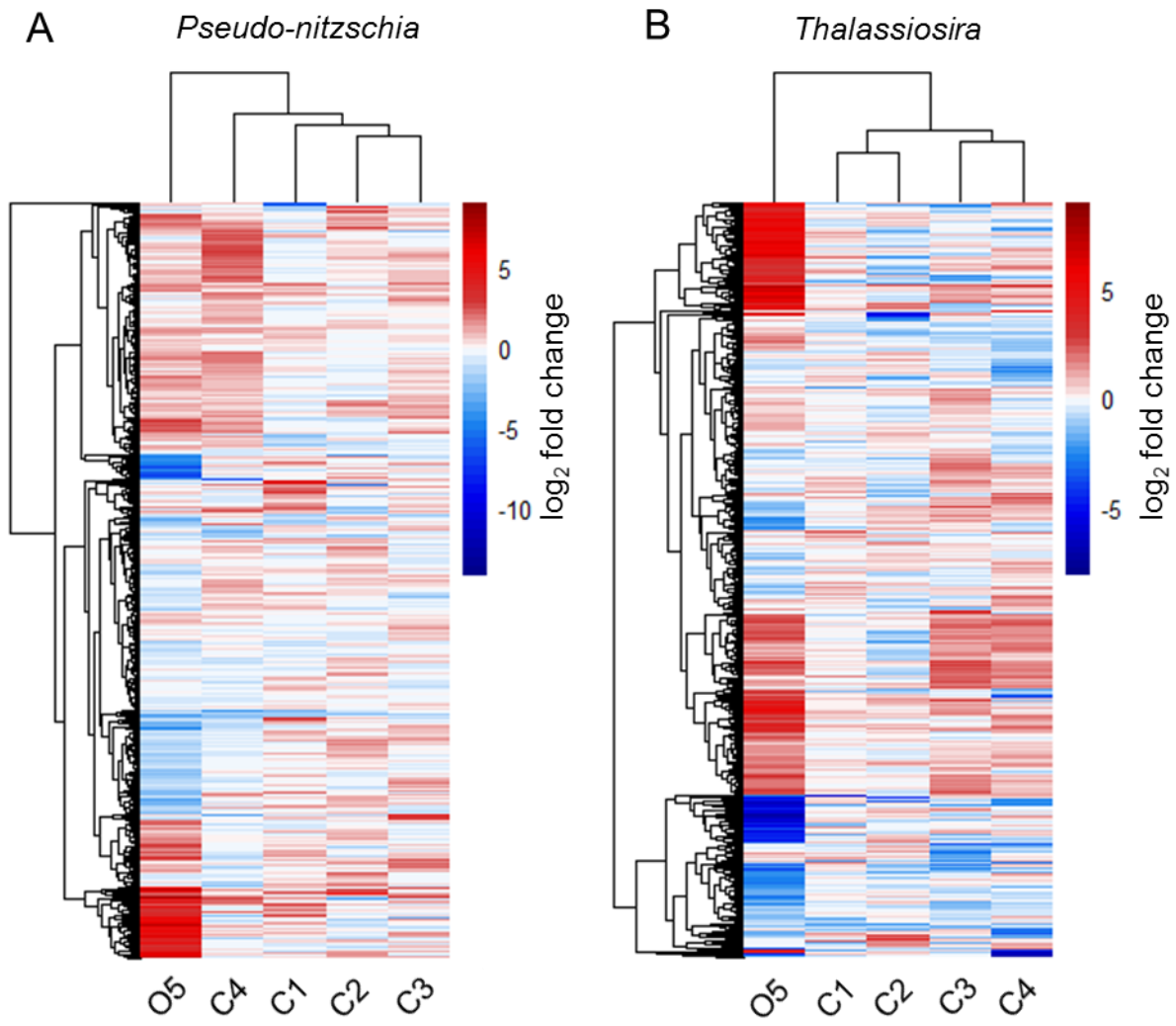

Fig. 2.7. Differential expression response of shared KEGG Orthology genes (KOs) between the Fe and DFB treatment by T_1 in the diatom genera **A**) *Pseudo-nitzschia* and **B**) *Thalassiosira*. Heatmap represents the $\log_2$ fold change in gene expression within the Fe addition treatment relative to the DFB addition treatment at each site. For site O5, the Fe-limited diatom community is depicted using control (C) instead of the DFB treatment at T_2. Only abundant transcripts are considered ($\log_2$CPM > 5). Dendrograms were created using Euclidean distance and hierarchical clustering and reflect similarity in expression responses among sites (columns) or genes (rows).

Iron, nitrate and carbon metabolism in response to treatments

The expression of genes involved in Fe, N and C acquisition and metabolism were compared between the diatom genera *Pseudo-nitzschia* and *Thalassiosira*. Fe-related genes of interest generally displayed more strongly divergent expression patterns in response to Fe treatments between diatom taxa, as compared to N- and C-related genes (Fig. 2.8). Genes encoding proteins involved in binding and transporting Fe (*ABC.FEV.S, ABC.FEV.A, TC.FEV.OM*) were intermittently detected among sites (Fig. 2.8). *Pseudo-nitzschia* increased expression of the Fe transporter *ABC.FEV.S* by >2-fold under Fe enrichment as compared to DFB conditions at all locations demonstrating a physiological Fe effect (C3, C4, O5; Table 2.1). Transcripts for another Fe uptake facilitator, the high affinity iron permease *FTR*, were generally more abundant under DFB conditions, although the gene was more highly expressed following Fe enrichment in *Pseudo-nitzschia* at sites C2, C3 and O5 (Fig. 2.8). In relation to Fe homeostasis, transcripts for the Fe storage protein ferritin (*FTN*) increased in the Fe addition treatment as compared to the DFB treatment at all sites except for C2 and C4, consistent with its role as a long-term Fe storage protein (Marchetti et al. 2009). At sites C2 and C4 *FTN* transcripts were more abundant in the DFB treatment in both taxa (3.5-fold in *Pseudo-nitzschia*., $p = 1x10^{-3}$ and 90-fold in *Thalassiosira*, respectively). *FTN* transcripts were not detected at all in *Thalassiosira* at O5, although they were detected and extremely abundant following Fe enrichment in *Pseudo-nitzschia* at this location (Fig. 2.8). Transcripts for the iron starvation induced proteins (*ISIP*s), including the recently-identified iron acquisition protein *ISIP2A* that binds Fe at the cell surface and is though to be involved in intracellular Fe transport (Morrissey et al. 2015), were highly abundant in Fe-limited treatments across all sites (Fig. 2.8). In particular, *ISIP1* was one of the most differentially expressed genes within each experimental

site under DFB conditions (Fig. 2.4). Oceanic site O5 was the only location in which *Thalassiosira* highly expressed metal-containing superoxide dismutase (*SOD;* copper-zinc family) by >100-fold under DFB conditions, while diatoms at all other sites either increased *SOD*-encoding genes following Fe addition or constitutively expressed them (Fig. 2.8).

Transcriptional responses of Fe-dependent and independent genes involved in energy synthesis, either through photosynthesis or proteorhodopsins, were examined within both diatom genera (Fig. 2.8). Transcripts for the photosynthetic Fe-independent electron acceptor flavodoxin (*FLDA*), which functionally replaces the Fe-protin ferredoxin in photosynthetic electron transport, were generally more abundant in the DFB treatments as compared to Fe treatments in both genera (Fig. 2.8). Conversely transcripts of ferredoxin (*PETF*) increased by >2-fold following Fe enrichment only in *Thalassiosira* across all sites apart from C2. In *Pseudo-nitzschia*, *PETF* transcripts were either constitutively expressed, more highly expressed in the DFB treatment, or not present (Fig. 2.8). Cytochrome c_6 (*PETJ*) transcripts were more abundant under Fe enrichment at all sites except for O5, where it was more abundant in the Fe-limited treatments (Fig. 2.8). Transcripts for plastocyanin (*PETE*), the Fe-independent electron transfer protein that can substitute for *PETJ*, displayed inconsistent expression trends in response to Fe status across sites, being relatively more abundant under Fe enrichment in both genera at C3 (1.4-fold in *Pseudo-nitzschia*.; 1.9-fold in *Thalassiosira*, $p = 5x10^{-4}$) and at the initially Fe-limited site, O5 (1.4-fold in *Thalassiosira*; Fig. 2.8). At all other locations *PETE* transcripts were either more abundant under DFB conditions or not detected. Lastly, transcripts for the proteorhodopsin gene (*RHO*), an Fe-independent light-harvesting proton pump mechanism recently identified in some diatoms (Marchetti et al. 2015), were not detected in *Thalassiosira* at any location, while expression increased in *Pseudo-nitzschia* by >2-fold following DFB addition

relative to Fe treatment at the two lowest dFe sites [C3 (p = 0.01) and O5; Fig. 2.8; Fig. 2.2C&E].

Relationships among Fe-related transcript abundance, experimental site and treatment were determined using Principal Components Analysis (PCA) individually for each diatom genus. In *Pseudo-nitzschia*, transcripts for the photosynthetic genes ferredoxin-NADP+ reductase (*PETH*), *PETJ*, a cytochrome b_6/f complex protein (*PETC*), *FTN*, and *SOD* were in higher relative abundance within Fe addition treatments while *RHO*, *ISIPs*, *FLDA*, *PETE* and *FTR* were generally more abundant in the low-Fe treatments. In *Thalassiosira*, a similar response was observed, although *RHO* was not detected, and *PETF*, which was sporadically found and not abundant in *Pseudo-nitzschia*, strongly co-varied with the other genes highly expressed in the treatments where Fe was added (Fig. 2.9C).

Genes involved in N transport and metabolism were investigated to assess the influence of varying Fe status on N assimilation. Transcripts for genes encoding nitrate (*NRT2*) and ammonium (*AMT*) transporters were detected at all locations, with *NRT2* increasing in expression by >2-fold in response to Fe addition relative to the DFB treatment at all sites except O5 in *Pseudo-nitzschia*, while *AMT* expression varied depending on site (Fig. 2.8). For instance, C4 was the only location with a >2-fold increase in *AMT* expression under DFB conditions in both *Pseudo-nitzschia* and *Thalassiosira*. In contrast to these two genes in which transcripts were present at all sites investigated, transcripts for another ammonium transporter (*SLC42A)* and a urea transporter (*URTA*) were intermittently detected (Fig. 2.8). Transcripts for genes encoding components of NO_3 assimilation, including nitrate (*NR*) and nitrite reductases (*NIRA, NIRB, NIT-6*) were additionally more abundant in the treatments with added Fe, although *NIRA* and *NIRB* had opposite expression patterns in *Pseudo-nitzschia* and *Thalassiosira* at site C3 (Fig. 2.8).

Pseudo-nitzschia increased gene expression of one form of nitrite reductase [*NIRB* and *NIT-6*, NADP+ as acceptors (Brown et al. 2009)] by 11-fold and 3.6-fold, respectively, following added Fe addition. In *Thalassiosira*, expression *NIT-6* similarly increased by 7-fold following Fe addition, whereas *NIRB* expression increased 3.7-fold under the DFB conditions (Fig. 2.8). In addition, *Thalassiosira* increased gene expression of another form of nitrite reductase [*NIRA*, ferredoxin as acceptor (Brown et al. 2009)] by 8-fold ($p = 3x10^{-22}$) under Fe enrichment while *Pseudo-nitzschia* constitutively expressed *NIRA* at this location. Noticeably, transcripts for the genes encoding *NIRB* and *NIT-6* were present from at least one of the two diatom taxa examined at all sites except O5.

The relationships among the transcript abundance for N uptake and assimilation-related genes, experimental sites, treatments and PN-specific $V NO_3$ measurements within the >5 µm size fraction of the phytoplankton community were examined via PCA bi-plots (Fig. 2.9A). Sites C2, C3, C4, and O5 contained high transcript abundances of *NRT2* and *NR* in the Fe treatments, with the two genes strongly co-varying with one another in both *Pseudo-nitzschia* and *Thalassiosira.* The two sites that experienced NO_3 depletion, C2 and C3, contained the highest *AMT* transcript abundance following Fe addition during T_1 and T_2, respectively, coinciding with low PN-specific $V NO_3$ measurements (0.03 – 0.13 day^{-1}; Fig. 2.9A). The highest PN-specific $V NO_3$ were observed in the Fe treatment at site C4 during T_1 and at C1 within the initial phytoplankton community (1.4 day^{-1}), which coincided with high abundances of *NIRA* transcripts in both genera from these locations (Fig. 2.9A).

Genes involved in C transport and fixation were examined among sites and between the diatom genera. Transcripts for carbonic anhydrase (*CA*), involved in the carbon concentrating mechanism (CCM) within photosynthetic eukaryotes (Reinfelder 2011), were intermittently

detected among sites and generally not abundant. However, patterns indicate higher expression under DFB conditions as compared to Fe enrichment in *Thalassiosira* at C1, *Pseudo-nitzschia* at C2 and both diatoms at C3 (Fig. 2.8). Members of the solute carrier (SLC) family of bicarbonate transporters, also involved in the CCM (*SLC4A-1*, *-2*, and *-4*), were also detected intermittently among sites, though in low in transcript abundance (Fig. 2.8). *RBCL* gene expression increased by >24-fold in the DFB treatment in both genera at site O5 while at other sites the gene was either constitutively expressed, increased expression in the added Fe treatment, or not detected (Fig. 2.8). In addition, genes involved in the Calvin Cycle, including phosphoglycerate kinase (*PGK*), transketolase (*TKL*), ribulose-phosphate 3-epimerase (*RPE*), and phosphoribulokinase (*PRK*), generally increased in expression following Fe addition compared to the DFB treatment at one or more of the three sites experiencing some degree of Fe limitation (C3, C4, and O5; Table 2.1; Fig. 2.8). At the CUZ sites C1 and C2, transcripts for these genes were either not differentially expressed or were more abundant under DFB conditions within both diatom genera.

The relationships in transcript abundance among C fixation-related genes, experimental sites, incubated treatments and PC-specific *V*DIC measurements were assessed using PCA bi-plots (Fig. 2.9B). Site C4 had some of the highest PC-specific *V*DIC within the >5 µm size fraction (0.65 – 1.6 day^{-1}), and coincided with the highest transcript abundances of *PGK*, *PRK*, *FBP*, *TKL*, *RPE* and *GAPDH* in *Pseudo-nitzschia* (Fig 6B). Conversely, DFB treatments from C3 and O5 had the lowest transcript abundances of these genes in both *Pseudo-nitzschia* and *Thalassiosira,* concurrent with some of the lowest measurements of PC-specific *V*DIC (0.11 - 0.17 day^{-1}).

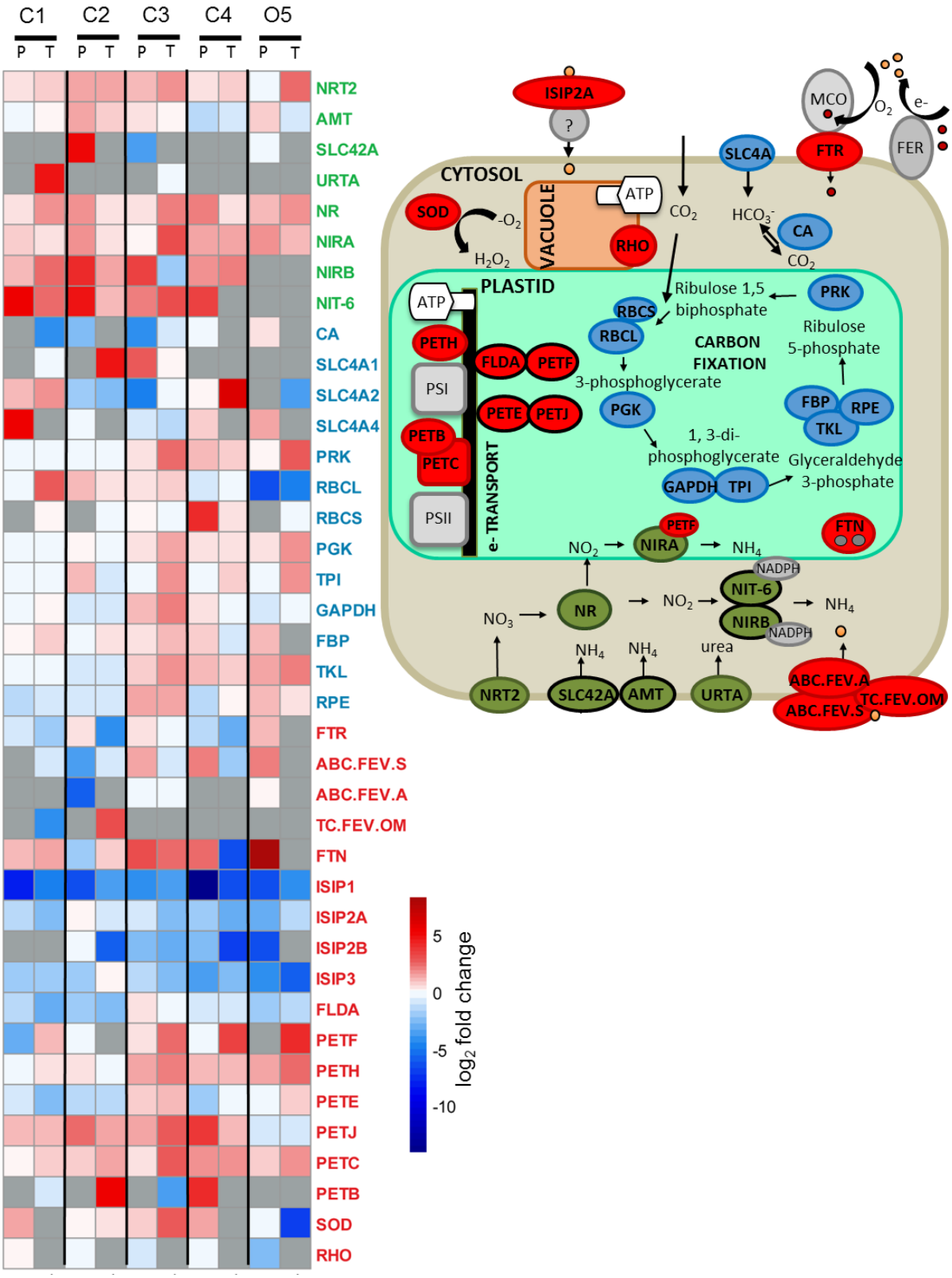
C1
C2
C3
C4
O5
P T
NRT2
AMT
SLC42A
URTA
NR
NIRA
NIRB
NIT-6
CA
SLC4A1
SLC4A2
SLC4A4
PRK
RBCL
RBCS
PGK
TPI
GAPDH
FBP
TKL
RPE
FTR
ABC.FEV.S
ABC.FEV.A
TC.FEV.OM
FTN
ISIP1
ISIP2A
ISIP2B
ISIP3
FLDA
PETF
PETH
PETE
PETJ
PETC
PETB
SOD
RHO
5
0
-5
-10
log2 fold change
ISIP2A
?
CYTOSOL
VACUOLE
SOD
-O2
H2O2
ATP
RHO
CO2
SLC4A
HCO3-
CA
MCO
O2
e-
FTR
FER
PLASTID
ATP
PETH
FLDA
PETF
PSI
PETE
PETJ
PETB
PETC
PSII
e- TRANSPORT
RBCS
RBCL
Ribulose 1,5 biphosphate
PRK
Ribulose 5-phosphate
CARBON FIXATION
3-phosphoglycerate
PGK
1, 3-di-phosphoglycerate
FBP
RPE
TKL
GAPDH
TPI
Glyceraldehyde 3-phosphate
FTN
NO2
NIRA
PETF
NH4
NADPH
NIT-6
NIRB
NO3
NR
NO2
NH4
NADPH
NH4
NH4
urea
NRT2
SLC42A
AMT
URTA
ABC.FEV.A
ABC.FEV.S
TC.FEV.OM

Fig. 2.8. Transcriptional response of diatoms to varying Fe status. **A**) Differential expression responses of select genes involved in nitrogen (N; green), carbon (C; blue) and iron (Fe; red)-related processes between the Fe and DFB treatments within the diatom genera *Pseudo-nitzschia* (P) and *Thalassiosira* (T). Heatmap represents the $\log_2$ fold change of gene expression within the Fe addition treatment relative to the DFB treatment at each site. For site O5, the Fe-limited diatom community is depicted using control (C) instead of DFB, and during T_2. White boxes signify no change in expression between treatments. Gray boxes indicate transcripts were not detected in either treatment. **B**) A schematic representation of cellular Fe-, N- and C-related transport and assimilation within a typical diatom cell, color-coded by genes of interest is shown to the right of the heatmap in A. Adjacent proteins with black borders indicate they perform similar cellular functions (e.g., *SLC42A* and *AMT*). Gene abbreviations are NRT2: nitrate transporter; AMT: ammonium transporter; SLC42A: solute carrier family (ammonium transporter); URTA: urea transporter; NR: nitrate reductase; NIRA: ferredoxin-nitrite reductase; NIRB: nitrite reductase; NIT-6: nitrite reductase; CA: carbonic anhydrase; SLC4A: solute carrier family (bicarbonate transporters); PRK: phosphoribulokinase; RBCL: RubisCO large subunit; RBCS: RubisCO small subunit; PGK: phosphoglycerate kinase; TPI: triseophosphate isomerase; GAPDH: glyceraldehyde 3-phosphate dehydrogenase; FBP: fructose-1,2-bisphosphatase I; TKL: transketolase; RPE: ribulose-phosphate 3-epimerase; FTR: high affinity iron permease; ABC.FEV.S: iron complex transport system substrate-binding protein; ABC.FEV.A: iron(III) dicitrate transport ATP-binding protein; TC. FEV.OM: iron complex outermembrane receptor protein; FTN: ferritin; ISIP1: iron starvation induced protein 1; ISIP2A: iron starvation induced protein 2A; ISIP2B: iron starvation induced protein 2B; ISIP3: iron starvation induced protein 3; FLDA: flavodoxin I; PETF: ferredoxin; PETH: ferredoxin-NADP+ reductase; PETE: plastocyanin; PETJ: cytochrome c6; PETC: cytochrome b6/f complex; PETB: cytochrome b6; SOD: superoxide dismutase (Cu/Zn); RHO: rhodopsin. Note the localization of RHO within the vacuole membrane is speculative.

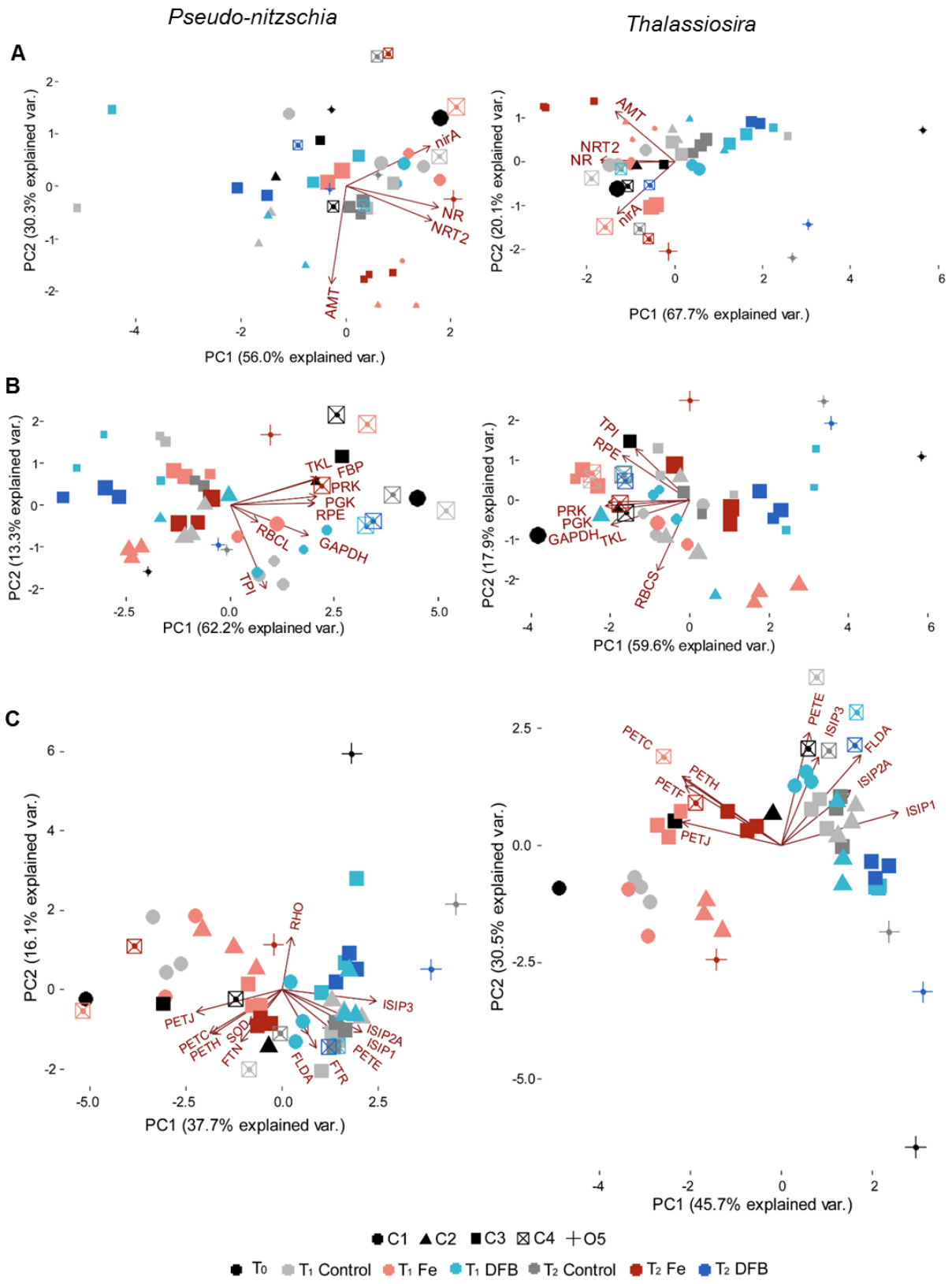
Pseudo-nitzschia
Thalassiosira
A
PC2 (30.3% explained var.)
PC1 (56.0% explained var.)
nirA
NR
NRT2
AMT
PC2 (20.1% explained var.)
PC1 (67.7% explained var.)
B
PC2 (13.3% explained var.)
PC1 (62.2% explained var.)
TKL
FBP
PRK
PGK
RPE
RBCL
GAPDH
TPI
PC2 (17.9% explained var.)
PC1 (59.6% explained var.)
RBCS
C
PC2 (16.1% explained var.)
PC1 (37.7% explained var.)
RHO
PETJ
PETC
PETH
SOD
FTN
FLDA
FTR
PETE
ISIP1
ISIP2A
ISIP3
PC2 (30.5% explained var.)
PC1 (45.7% explained var.)
PETF
C1 C2 C3 C4 O5
T0 T1 Control T1 Fe T1 DFB T2 Control T2 Fe T2 DFB

Fig. 2.9. PCA bi-plots depicting the relationship between treatment (color), site (shape), and biomass-normalized uptake rates (size) for transcript abundances of genes involved with N, C, and Fe-related processes in *Pseudo-nitzschia* and *Thalassiosira*. Size of points increase with increasing PN-specific VNO_3 (day^{-1}) from 0.04 to 1.63 day^{-1} (**A**), and increase with increasing PC-specific VDIC (day^{-1}) from 0.01 to 1.50 day^{-1} (**B**). For the Fe-related genes transcript abundance PCA bi-plot, sizes remain constant across samples (**C**). See Fig. 2.8 for list of gene abbreviations.

Discussion

Iron-related gene expression responses across sites

Our study captured coastal upwelling diatom communities under various natural phases of Fe stress and/or limitation. Site C1 contained a phytoplankton community that was generally not affected by Fe addition, with bulk measurements not significantly different across treatments (Fig. 2.2). Only 74 genes were differentially expressed between Fe and DFB treatments at this location in contrast to the other CUZ sites, C2 and C3, which differentially expressed more genes by >5-fold (414 and 458, respectively; Fig. 2.4A-C). These other CUZ sites additionally displayed physiological signs of Fe stress on the diatom communities. C2 exhibited low $Si(OH)_4$:NO_3 and high NO_3:Fe ratios, both of which may indicate an aged upwelled water mass with a history of Fe limitation. Similarly, site C3 exhibited elevated phytoplankton biomass, PN-specific *V*NO_3, and PC-specific *V*DIC after Fe addition relative to both the control and DFB treatments. However, although there were fewer differentially expressed genes and little indication of physiological Fe stress was observed at C1 than at C2 and C3, Fe-stress bioindicator genes (*FLDA*, *PETE* and *ISIP2A;* Whitney *et al.*, 2011; Morrissey *et al.*, 2015; Graff van Creveld *et al.*, 2016) did increase in expression following the addition of DFB relative to Fe addition in the C1 incubations. This is consistent with there being a mild degree of Fe stress that may have occurred by the final time point at site C1 in the DFB treatment, and these genes may therefore be involved in the initial stages of the Fe limitation response by the diatoms.

Differences in gene expression patterns in response to Fe addition or chelation were observed between the coastal and oceanic sites examined in this study. Expression responses were strongly driven by Fe status in the oceanic but not coastal diatom communities. These included the 16-fold overexpression of protein-encoding genes biotin synthase (*BIOB*) and ferritin (*FTN*) in the added Fe treatment, and super-oxide dismutase (*SOD*) and RubisCO (*RBCL*) in the DFB treatment. This emphasis on select metabolic processes likely reflects how the oceanic diatom communities have adapted to the very distinct set of environmental conditions present, with oceanic diatoms better adapted to chronic Fe limitation and coastal diatoms better-suited for highly variable Fe concentrations.

Many photosynthetic genes were highly expressed following Fe addition regardless of location. However, a subset of these genes displayed distinct expression responses depending on whether incubated communities experienced Fe limitation of growth (e.g., C3 and O5) or Fe stress (C4; Table 2.1). Flavodoxin *(FLDA)* transcripts were generally more abundant in the DFB treatment in both diatom genera across sites, consistent with flavodoxin'a role as an Fe-independent photosynthetic electron carrier. However at CUZ site C3, *FLDA* was either constitutively expressed or slightly more abundant after Fe addition, depending on the diatom. Plastocyanin (*PETE)* transcripts were more abundant after Fe addition in both diatom genera at C3 and in *Thalassiosira* at O5, while at all other locations plastocyanin transcripts were more abundant under DFB conditions, suggesting some diatoms may temporarily replace cytochrome c_6 (*PETJ)* with plastocyanin because of the scarcity of Fe in the environment. Finally, the putative Fe transporter *ABC.FEV.S* increased in expression after Fe addition in *Pseudo-nitzschia* only at sites C3, C4, and O5. Collectively these patterns suggest that diatoms from Fe-limited or Fe–stressed communities will continue to express their Fe-limited gene repertoires regardless of

Fe status artificially imposed in the experiments, likely in attempts to conserve cellular Fe, while diatoms from initially Fe-replete communities temporary replace their Fe-dependent proteins under low Fe conditions (Marchetti et al. 2012).

Fe-related gene expression responses between diatoms

Several genes encoding Fe-related proteins demonstrated divergent expression responses to Fe status between the two diatom taxa investigated, *Pseudo-nitzschia* and *Thalassiosira.* Ferredoxin (*PETF*) transcripts were more abundant in *Thalassiosira* at all sites following Fe addition, and this pattern was absent in *Pseudo-nitzschia*. In contrast, ferredoxin in *Pseudo-nitzschia* was either constitutively expressed, transcripts were not detected, or more highly expressed under DFB conditions. Therefore, *Pseudo-nitzschia* seems to either utilize ferredoxin regardless of Fe status or while experiencing Fe stress, while *Thalassiosira* preferentially utilizes it under Fe-replete conditions. In addition, oceanic site O5 was the only location in which *Thalassiosira* increased gene expression of a zinc/copper-containing superoxide dismutase (*SOD*) under DFB conditions. This pattern was not shared by oceanic *Pseudo-nitzschia* or by either genus in coastal sites, suggesting a role for *SOD* specific to oceanic *Thalassiosira*. Transcripts for the gene encoding rhodopsin (*RHO)* increased in abundance in *Pseudo-nitzschia* after DFB addition at the two sites experiencing pronounced Fe limitation in incubation experiments (C3, O5), but were not identified in *Thalassiosira* from any location. This is consistent with rhodopsin being undetected in sequenced *Thalassiosira* spp. transcriptomes (Marchetti et al. 2015) and suggests *Pseudo-nitzschia* may have a competitive advantage over non-rhodopsin containing taxa, allowing for an Fe-independent alternative to photosynthesis for ATP generation during times of Fe stress. Ferritin (*FTN)* gene expression patterns also diverged between the two taxa at the coastal Line-P site C4, with high expression following Fe addition in

Pseudo-nitzschia but high expression under DFB addition in *Thalassiosira*. This suggests that *FTN* may serve multiple functions, at times differing between the two taxa from the same location. Lastly *ABC.FEV.S*, encoding an iron transport system protein, displayed different expression patterns between the genera. *Pseudo-nitzschia* increased *ABC.FEV.S* expression after Fe addition at all locations with initial phytoplankton communities that experienced Fe stress in incubation experiments (C3, C4, O5), while in *Thalassiosira* the gene was either constitutively expressed or more abundant after DFB addition. Taken together, these patterns in gene expression demonstrate that members of the pennate diatom genus *Pseudo-nitzschia* and the centric diatom genus *Thalassiosira* may respond to changes in Fe status in very distinct manners regardless of their ability to co-exist under the same environmental conditions, likely due to these two diatom lineages containing different gene repertoires and Fe adaptation strategies.

Nitrogen-related diatom response to Fe status

The majority of genes investigated involved in N transport and assimilation increased in expression in both *Pseudo-nitzschia* and *Thalassiosira* following Fe addition. Several site- and taxa-specific patterns were identified, with some trends also possibly explained by each site's initial NO_3 concentrations. For example, the gene encoding the nitrate transporter, *NRT2*, has been demonstrated in laboratory cultures to increase in gene expression within NO_3-stressed diatoms (Rogato et al. 2015), and transcripts corresponding to this gene were some of the most abundant detected in both *Pseudo-nitzschia* and *Thalassiosira* at C2 ($log_2CPM > 12$; Fig. 2.4B), the CUZ site where NO_3 concentrations were depleted in all incubations by the T_1 sampling time. This gene also showed expression trends that correlated with Fe status; *NRT2* transcripts were more abundant after Fe addition in both genera at all locations except in the oceanic Line-P site O5, regardless of initial NO_3 concentrations. Based on these observations, *NRT2* in diatoms also

appears to be linked to Fe status, following the expression of other N-related genes involved in Fe-dependent NO_3 assimilation, including those encoding nitrate reductase (*NR)* and nitrite reductase (*NIRA*; Marchetti *et al.*, 2012)

Diatoms were perhaps relying on NH_4 in place of NO_3 as a source of N based on gene expression patterns at CUZ sites C2 and C3, based on gene expression patterns. Following Fe enrichment at C2, NO_3 became depleted by T_1, and genes encoding ammonium transporters, *AMT* and *SLC42A,* increased in expression relative to the DFB treatment. At C3, Fe-enriched communities entered NO_3 stress by T_2, as evidenced by increased *AMT* expression in *Pseudo-nitzschia* relative to expression one day earlier, during T_1. NO_3 assimilation rates at C3 co-varied with NO_3 concentrations in the Fe treatments, with high rates during T_1, but substantially lower rates one day later when NO_3 concentrations were depleted. This negative relationship between NO_3 availability and *AMT* transcript abundance in natural diatom assemblages is consistent with those in laboratory diatom cultures (Rogato et al. 2015). In contrast, high *AMT* transcript abundance at some of these locations could represent NH_4 rather than NO_3 being preferred as an N source by Fe-stressed diatoms conserving their cellular Fe supply, as NO_3 reduction depends on various Fe-dependent processes, including NO_3 and NO_2 reduction. This is supported by the increased expression of *AMT* transcripts in *Thalassiosira* from the Fe-stressed coastal Line-P site C4. However, *Thalassiosira* from the two other sites that experienced Fe stress within incubation experiments (C3 and O5) did not follow this pattern.

Several N-related genes demonstrated divergent expression responses between *Pseudo-nitzschia* and *Thalassiosira.* At the CUZ site C3, expression of the nitrite reductase genes, *NIRA* and *NIRB*, displayed opposite patterns between *Pseudo-nitzschia* and *Thalassiosira*. Following Fe addition, *Pseudo-nitzschia* highly expressed the gene *NIRB* encoding the non-ferredoxin-

utilizing nitrite reductase, while *Thalassiosira* highly expressed gene *NIRA* encoding the ferredoxin-utilizing nitrite reductase. Furthermore, *Pseudo-nitzschia* increased expression of *AMT* following Fe addition while *Thalassiosira* increased expression of *NRT2* following Fe addition at site O5, suggesting oceanic *Pseudo-nitzschia* may rely upon NH_4 as an N source while oceanic *Thalassiosira* preferentially relies upon NO_3. Based on these observations, we conclude *Pseudo-nitzschia* may prefers the non-Fe intensive metabolic pathways (*NIRB, AMT*) for assimilating N as compared to *Thalassiosira*. These expression patterns collectively support that variations exist between the two diatom taxa in terms of N acquisition and assimilation strategies following changes in Fe supply.

Carbon-related diatom response to Fe status

Genes encoding proteins involved in C uptake and assimilation were surveyed in order to determine the influence of Fe addition or stress on C metabolism. Multiple structures of RubisCO have been characterized (Andersson and Backlund 2008) and diverse diatoms have been shown to possess different RubisCO enzymes with varying kinetics (Young et al. 2016). Correspondingly, we observed site-specific expression patterns of the diatom RubisCO (*RBCL)* gene, in which gene expression was higher at site O5 following DFB addition relative to the response with Fe addition in both diatom genera. In contrast, at the coastal sites, *RBCL* expression was either constitutive, increased following Fe addition, or was not detected. Based on our gene expression results, we hypothesize iron-limited oceanic diatoms may be relying on a distinct form of RubisCO compared to coastal diatoms. High affinity RubisCO enzymes, corresponding to weak carbon concentrating mechanisms and enhanced expression responses of *RBCL* (Tortell et al. 2000), may be preferentially utilized iron-limited oceanic diatoms.

Other Calvin cycle-related genes such as *PGK*, *TKL*, *RPE*, and *PRK* did not exhibit similar site-specific expression patterns to *RBLC*, but instead increased in expression following Fe enrichment at one or more of the three sites where unamended treatments exhibited signs of Fe stress during the incubation period (C3, C4, O5). Increased expression of these genes is likely a result of alleviated Fe stress and subsequent increases in rates of C fixation and growth . Furthermore, transcripts corresponding to members of the SLC family of bicarbonate transporters (*SLC4A-1*, *-2*, and *-4*), which import DIC from the environment, were also present. These genes share sequence homology with the *Phaeodactylum tricornutum* genes *PtSLC4-1*, *-2* and *-4* in (BLASTP; $E < 2x10^{-69}$), which were recently found to be transcriptionally active under low CO_2 conditions. One of these genes, *PtSLC4-2*, aids in CO_2 acquisition in by stimulating bicarbonate uptake (Nakajima et al. 2013). However transcripts for these genes in *Pseudo-nitzschia* and *Thalassiosira* were intermittently detected between sites and displayed inconsistent patterns of gene expression with each another, with no clear relationship to carbon assimilation rates.

Positive relationships were identified between some C fixation-related transcript abundances and carbon assimilation rates, particularly following Fe addition. One of the highest fixation rates measured occurred at CUZ site C1 in the initial phytoplankton community (T_0; 0.91 day^{-1}), and coincided with high relative abundances of *PGK*, *PRK*, *TKL* and *GAPDH* transcripts in both genera. At the two sites where Fe-limitation of diatom growth was evident, C3 and O5, carbon assimilation rates increased following Fe addition, again coinciding with increases in expression of the C fixation genes investigated. These expression patterns are in agreement with laboratory cultures of the diatom *Phaeodactylum tricornutum*, which increased expression of genes involved in C fixation during the light portion of their diel cycle, when DIC

is being taken up to support photosynthesis (Chauton et al. 2013). Interestingly, *Thalassiosira* contained one of the highest transcript abundances of C fixation genes after Fe was added at C3, where members of this genus were the most abundant, while transcript abundances of C fixation genes in *Pseudo-nitzschia* were the highest at C4, also the site in which members of this genus were most abundant. Assuming gene expression correlates to enzymatic activity, this may suggest that the most abundant genus at a single location will possess the majority of C assimilation machinery and will subsequently be the most responsible for DIC uptake and fixation. We conclude that C fixation-related gene expression patterns were largely consistent with C assimilation rates, and generally varied as a function of both Fe status and ocean province.

Conclusion

Gene expression characterization coupled with physiological assessment of diverse diatom communities suggests both regional- and taxa-specific strategies are utilized when rapidly responding to variations in Fe status. In particular, our analysis demonstrates that chronically Fe-limited oceanic diatoms will restructure Fe, N, and C metabolism in a distinctive manner following Fe addition when compared to the response of coastal diatom communities that receive inherently more variable Fe inputs. *Pseudo-nitzschia* and *Thalassiosira*, two cosmopolitan diatom taxa (Malviya *et al.*, 2016) found at all locations investigated, at times demonstrate divergent responses to changes in Fe status in terms of Fe, N and C metabolism, even within identical environmental conditions. This supports the notion that a tremendous degree of genetic diversity is contained within even a single diatom lineage, and thus caution should be used when extrapolating responses to environmental perturbations observed in one diatom to other diatom species.

CHAPTER 3: EVIDENCE FOR MULTIPLE FUNCTIONAL ROLES OF FERRITIN IN DIATOMS[3]

Introduction

Diatoms are a critical component of the oceans' biological carbon pump, which consists of the photosynthetic fixation of carbon dioxide (CO_2) into organic matter by phytoplankton in the ocean's surface layer and the subsequent transport of this carbon to the deep ocean. This biological pump plays a major role in the regulation of atmospheric CO_2 and hence global climate (Sarmiento and Bender 1994). The strength and efficiency of the biological carbon pump in large areas of the oceans, including the equatorial Pacific, subarctic Pacific, and Southern Ocean, is substantially reduced by the limited availability of the micronutrient iron for phytoplankton. Low iron inputs from a variety of sources (including aeolian transport of continental dust, vertical mixing, inputs from coastal sediments and rivers and active hydrothermal venting) are unable to meet the biological demand for iron in these regions (Moore et al. 2002; Saito et al. 2013). Diatoms typically dominate algal blooms when iron is introduced into iron-limited ocean waters (Boyd et al. 2007). They possess a range of strategies for coping with iron limitation that allow them to persist under low iron conditions and rapidly bloom in

[3]The contents of this chapter are currently in review for publication at *ISME Journal*. The citation is as follows: Cohen NR, Mann, E, Stemple B, Raushenberg S, Jacquot J, Moreno C, Sunda W.G, Twining B.S, Marchetti A. Evidence for multiple functional roles of ferritin in diatoms. BST and AM designed the study; NRC and BS performed RNA analyses; EM and JJ obtained cellular iron quotas; CM provided the map of diatom ferritin transcript possession shown in Fig. 3.9; WGS contributed intellectual content; NRC and AM wrote the manuscript.

response to ephemeral iron inputs (Sunda and Huntsman 1995; Marchetti et al. 2012). These mechanisms include decreasing metabolic iron demands through a decrease in the abundance of iron-rich photosynthetic protein complexes (Strzepek and Harrison 2004); increasing usage of iron-independent alternative proteins and complexes (LaRoche et al. 1995; Peers and Price 2006; Allen et al. 2008; Lommer et al. 2012); the utilization of high affinity iron uptake systems (Maldonado and Price 2001; Shaked et al. 2005; Morrissey and Bowler 2012; Morrissey et al. 2015) and luxury uptake and storage of iron through the use of iron-sequestering mechanisms (Sunda and Huntsman 1995; Marchetti et al. 2009).

Iron storage in some diatoms is achieved through ferritins, a ubiquitous family of proteins found across all domains of life (Theil et al. 2006; Marchetti et al. 2009; Groussman et al. 2015). These proteins store large quantities of intracellular iron, thereby preventing iron toxicity. True ferritins are comprised of 24 subunits and may be up to 480 kDa in size. They can store up to 4,500 iron atoms as the insoluble iron oxide ferrihydrate within an inner core nano-cage subunit structure (Liu and Theil 2005). Gated pores control iron flow (as ferrous iron [Fe(II)]) into and out of the inner core (Theil et al. 2008). Recent investigation into the ferritin structure in the diatom *Pseudo-nitzschia multiseries* has demonstrated that oxidation of Fe(II) at the ferroxidase center in this protein occurs quickly, while subsequent mineralization of ferric iron [Fe(III)] occurs quite slowly, suggesting diatoms may have evolved a ferritin optimized for rapid sequestration and retrieval, which thus may function as an iron chaperone (Pfaffen et al. 2015).

Various functional roles for ferritin in microalgae have been described (Botebol et al. 2015; Pfaffen et al. 2015), one primary role being long-term iron storage (Marchetti et al. 2009). It has been suggested that diatoms living in chronically iron-limited environments that receive episodic iron inputs exhibit increased ferritin gene transcription and ferritin synthesis and are

thus able to store large reserves of iron (Marchetti et al. 2009). They then use this stored iron to support growth when surrounding seawater iron levels drop back to low ambient concentrations. This process ensures a steady intracellular supply of iron to support growth and cell division, and is thought to be the mechanism behind the numerical dominance of mostly ferritin-containing diatoms following iron fertilization events (Marchetti et al. 2009). In contrast, the green alga *Chlamydomonas reinhardtii* contains two distinct ferritin proteins with seemingly different functional roles. One exhibits a similar response to iron as observed in the marine pennate diatom *Pseudo-nitzschia*, where the protein is highly expressed under iron-replete conditions; the other increases expression under iron-limiting conditions, potentially serving as an intracellular iron buffer when iron is released from the degradation of iron-containing proteins during low-iron-induced stress (La Fontaine et al. 2002; Long et al. 2008). The green alga *Ostreococcus tauri* has recently been found to exhibit circadian behavior in ferritin expression: both transcript and protein abundance decrease during the day and increase at night, perhaps to store internal iron during darkness when iron-rich photosynthetic protein complexes are not as abundant (Botebol et al. 2015). However, a similar diel pattern in ferritin expression was not detected in the pennate diatom *Phaeodactylum tricornutum* (Smith et al. 2016). Given the variety of observed ferritin responses, it is likely that multiple functional roles for ferritin have evolved across, and perhaps within, algal lineages.

The two main lineages of diatoms, centrics and pennates, are estimated to have diverged relatively recently in geologic time – about 90 million years ago; yet they substantially differ in their genetic make-up (Bowler et al. 2008; Armbrust 2009). Pennate diatoms, such as those belonging to the genera *Pseudo-nitzschia* or *Fragilariopsis,* frequently dominate large blooms in iron-limited regions of the ocean following iron enrichment, and outcompete centric diatoms and

other phytoplankton groups present in the initial assemblages (Boyd et al. 2007). This tendency has been partially attributed to their use of ferritin (Marchetti et al. 2009). Although it was initially thought that only pennate diatoms contained ferritin, a recent community-wide transcriptomic sequencing effort has provided evidence that some centric diatoms also possess ferritin-like gene homologs (Groussman et al. 2015).

It remains unclear whether centric diatoms that contain ferritin can store iron to a similar extent as ferritin-containing pennate diatoms, and whether they depend on ferritin for long-term storage of iron to sustain growth and cell division following episodic iron input events. This study aims to examine whether ferritin-containing versus non-containing centric and pennate diatoms systematically differ in their iron storage capacities and associated ferritin gene expression in response to varying iron concentrations in their growth medium. A phylogenetically diverse group of diatoms was cultured under varying iron conditions from low, growth-limiting iron concentrations, to iron levels in excess of those needed to support maximum growth rates. Our findings provide evidence to support multiple distinct functional roles for ferritin among diatoms that may lead to differences in how these proteins influence cellular acclimation and adaptation to variations in iron supply and metabolic utilization.

Methods

Experimental design and diatom culturing methodology

Diatoms used in this study were selected on the basis of phylogeny and the availability of transcriptome sequence information. The pennate diatom, *Pseudo-nitzschia granii* UNC1102, was isolated from the Northeast Pacific Ocean in 2011 (Ocean Station Papa: 50°N, 145°W; Table 3.1). All other isolates were obtained from the Provasoli-Guillard National Center for Marine Algae and Microbiota (NCMA; East Boothbay, ME USA). Cultures of each isolate were grown using the semi-continuous batch culture technique, allowing cells to remain in the exponential growth phase throughout the experimental period. All culture work was performed using the synthetic seawater medium Aquil (Price *et al.*, 1988/89). The nitrate, phosphate, and silicic acid concentrations were 300 μmol L^{-1}, 10 μmol L^{-1}, and 100-200 μmol L^{-1}, respectively. Trace metals were buffered with 100 μmol L^{-1} ethylenediaminetetraacetic acid (EDTA) and the B-vitamins cobalamin, biotin and thiamine were supplied. Total iron was added as Fe:EDTA (1:1) chelates. Trace metal clean techniques were implemented while preparing the Aquil medium and during handling of cultures (Marchetti et al. 2015). All prepared Aquil media were allowed to equilibrate overnight before experimental use. Cultures were grown at 12, 14 or 20 °C (depending on their habitable ranges as provided by the NCMA or based on the location of isolation). Diatoms were grown under continuous light at an intensity of 100-150 μmol quanta m^{-2} s^{-1}, except for *Thalassionema frauenfeldii* which was grown under a 13/11 light/dark cycle due to an inability to grow under continuous light. Growth rates were determined from *in vivo* chlorophyll *a* fluorescence, monitored with a Turner designs 10-AU fluorometer, and calculated from linear regression of the natural log of fluorescence versus time (Brand et al. 1981). Isolate size dimensions were estimated using light microscopy (Leica DMI6000). Lengths and widths of

9-17 individual cells were measured and incorporated into calculations to determine biovolume (μm^3) from approximate geometric microalgal shapes (Hillebrand et al. 1999).

All cultures were grown at both high and low iron concentrations. The high concentration (1,370 nmol L^{-1} total iron [Fe_T]) was well in excess of that needed to achieve a maximum iron-saturated growth rate (μ_{max}). Diatoms were also grown at a low iron concentration (1.5 to 600 nmol L^{-1} depending on the species) in which the growth was mildly to moderately iron-limited [10-80% iron limitation of μ_{max} (Table 3.1)]. Experimental high and low iron treatments were determined by analyzing steady-state growth rate data from 28 mL cultures grown under decreasing iron concentrations until iron-limited growth was observed. Cultures were acclimated to their iron conditions for a minimum of three transfers before iron quotas were measured. Separate, parallel cultures were grown for iron quotas (28 mL) and RNA collections (500 mL) for isolates containing ferritin, except for *Amphora coffeaeformis* and *Thalassionema frauenfeldii,* which were grown independently due to logistical constraints. Differences in the maximal growth rates between the iron quota and RNA collection cultures were less than 20% for *Thalassionema frauenfeldii*, while maximal growth rates in *Amphora coffeaeformis* were roughly half those of the ferritin expression cultures. The growth rate data obtained from the gene expression experiments for these two isolates is presented in Table 3.1, and growth rate data corresponding to iron quota experiments is presented in Fig. 3.1, 3.4, and 3.5. For all other isolates, iron quota growth rates are presented in both Table 3.1 and Fig. 3.1, 3.4, and 3.5.

Isolate (strain ID)	Isolation location	Diatom Lineage	Biovolume (μm^3)	Temperature (°C)	μ_{max} (d^{-1})	μ μ_{max}^{-1} (low iron)	FTN copies
Pseudo-nitzschia granii (UNC1102)	Northeast Pacific 50˚N 145˚W (oceanic)	Raphid pennate	46 ±11	12	1.62 ± 0.11	0.69 ± 0.09	1
Amphora coffeaeformis (CCMP127)	North Atlantic 41.5˚N 70.7˚W (coastal)	Raphid pennate	500 ± 191	20	1.21 ± 0.32	0.22 ± 0.06	2
Thalassionema frauenfeldii (CCMP1798)	North Atlantic 18.5˚N 64.6˚W (coastal)	Araphid pennate	1305 ± 798	20	0.65 ± 0.03	0.78 ± 0.05	2
Grammatophora oceanica (CCMP410)	South Pacific 37.9˚S 144.9˚E (coastal)	Araphid pennate	860 ±273	20	0.31 ± 0.06	0.9 ± 0.26	ND
Minutocellus polymorphus (CCMP3303)	South Atlantic 17.5˚S 11.25˚E (coastal)	Bipolar centric	188 ±44	20	1.9 ±0.14	0.89 ± 0.1	1
Thalassiosira sp. (NH16)	North Pacific 45.7˚N 124.5˚W (coastal)	Bipolar centric	332 ±144	20	0.52 ±0.02	0.9 ± 0.16	1
Thalassiosira rotula (CCMP3096)	North Pacific 49.7˚N 127.4˚W (coastal)	Bipolar centric	7,525 ±3,609	14	0.45 ±0.02	0.73 ± 0.04	2
Thalassiosira weissflogii (CCMP1336)	North Atlantic 41.1˚N 72.1˚W (coastal)	Bipolar centric	741 ± 195	20	1.26 ±0.06	0.81 ± 0.05	ND
Thalassiosira pseudonana (CCMP1335)	North Atlantic 40.8˚N 72.8˚W (coastal)	Bipolar centric	93 ±70	20	1.49 ±0.23	0.82 ± 0.15	ND
Thalassiosira oceanica (CCMP1005)	North Atlantic 33.2˚N 65.3˚W (oceanic)	Bipolar centric	149 ±59	20	1.14 ±0.04	0.63 ± 0.03	ND
Corethron hystrix (CCMP308)	North Atlantic 58.5˚N 0.3˚W (coastal)	Radial centric	19,309 ± 5,695	14	0.56±0.03	0.5 ± 0.14	ND

Table 3.1. Diatom isolation locations, temperatures, biovolumes, and growth rates within culture experiments. Maximum growth rate (μ_{max}) under high iron conditions and the ratio of the iron-limited growth rate under the low iron conditions relative to the maximum growth rate (μ μ_{max}^{-1}) are provided along with the number of distinct *FTN* homologs identified within each isolate's transcriptome. ND = not detected. Separate, parallel cultures were simultaneously grown for iron quotas and RNA collections for all isolates except for *Amphora coffeaeformis* and *Thalassionema frauenfeldii*, and growth rates presented throughout the study correspond to iron quota cultures. For these two isolates, growth rate data obtained from the gene expression experiments are displayed here, while growth rate data corresponding to iron quota experiments is presented in Fig. 3.1, 3.4, and 3.5.

Cellular iron quotas

Iron quotas normalized to carbon (Fe:C) were obtained by growing triplicate cultures under the two iron conditions (i.e., high and low) using the $^{55}Fe/^{14}C$ dual labeling approach (Tortell et al. 1996; Marchetti et al. 2006). Cultures were grown in acid-cleaned, Milli-Q rinsed, and microwave sterilized 28 mL polycarbonate centrifuge tubes. For high-iron media, 1% of Fe_T was added as radiolabeled $^{55}FeCl_3$ with the remaining 99% consisting of non-labeled $FeCl_3$, while the low-iron medium was prepared by adding a range of radiolabeled $^{55}FeCl_3$ concentrations (15% to 100% of the total) depending on the target iron concentration. Approximately 2 x 10^{-3} μCi of $H^{14}CO_3^-$ was added to each 28 mL iron treatment to allow for measurement of cellular fixed carbon. Spiked media was allowed to equilibrate for 24 hours before inoculation with phytoplankton. Cultures were harvested when they reached mid- to late-exponential phase, allowing for approximately four to five cell divisions. Cells were filtered onto 47 mm polycarbonate filters (3 □m pore size) and were subsequently exposed to a titanium/citrate EDTA solution for 5 minutes to remove any externally-bound iron adsorbed on to the cell surface. This solution reduces Fe(III) to Fe(II) and thereby removes iron oxyhydroxides and iron adsorbed to the cell surface (Hudson and Morel 1989). The ^{14}C activity in seawater and titanium/citrate EDTA rinsed filters was similar, except for *Corethron hystrix* which lost up to 66% of its calculated carbon concentration after exposure to the later. The filters were transferred to scintillation vials and cellular ^{55}Fe and ^{14}C were determined via liquid scintillation counting with a dual-label protocol (Beckman). Cell associated ^{55}Fe and ^{14}C activity was corrected by subtracting counts in 0.2□m filtered inoculated media. Cell-free blanks were on average less than 10% of the total activity, with the exception of ^{14}C in *C. hystrix* in the low

iron treatment where the loss of carbon after the titanium/citrate EDTA rinse led to a 55% blank to total activity ratio.

To distinguish between the amount of intracellular iron incorporated into functional proteins needed to support growth from that of luxury iron storage, iron quotas were determined at two iron levels: at high iron concentration well in excess of that needed to support maximum growth rate (μ_{max}), and at iron concentrations low enough to cause a reduction in growth rate. Since it was difficult to obtain identical reductions in growth across species, the Fe:C ratio at the point where μ_{max} is first achieved was estimated by assuming a linear relationship between iron quota and growth rate as has been previously observed (Sunda and Huntsman, 1997; Fig. 3.1). According to Sunda and Huntsman (1997), plots of growth rate versus Fe:C ratio demonstrated mostly linear relationships for iron-limited cells that intersected the x-axis at a minimum Fe:C ratio, indicating a finite maintenance iron quota when growth rate is zero. The nearly linear relationship between iron-limited growth rate and cellular iron quota was similar for all four coastal species examined (two diatoms and two dinoflagellates) despite a >4-fold difference in the maximum growth rate (Sunda and Huntsman 1997).

In the present study x-intercepts were assumed to be 4 μmol Fe mol C^{-1} for most of the coastal isolates, consistent with previous data (Sunda and Huntsman 1997). The exceptions were for the species that were likely to have either lower or higher minimum iron quotas based on the growth rates and Fe:C ratios empirically measured under low-iron conditions (Fig. 3.1). For instance, since the measured Fe:C quotas for *A. coffeaeformis, T. frauenfeldii, T. sp NH16, M. polymorphus* and *T. oceanica* [based on Marchetti 2006]) under low iron conditions were already close to 4 μmol Fe mol C^{-1} (Fig. 3.1), the minimum iron quota was assumed to be 2 μmol Fe mol C^{-1}. Additionally the minimum iron quota for *P. granii* was set at 1 μmol Fe mol C^{-1} since the

growth rate was approximately 30% of its maximum at the measured Fe:C quota of 4.81 μmol Fe mol C^{-1}. For *C. hystrix*, the minimum iron quota was assumed to be approximately 20 μmol Fe mol C^{-1} due its cellular growth requirement for iron under low iron conditions being relatively high (Fig. 3.1). A higher minimum iron quota is hypothesized for this species based on the observation that when the amount of cellular iron needed to increase growth rate goes up, the maintenance iron does as well (Sunda and Huntsman 2011), as they are both dependent on cellular ATP generated from photosynthesis or respiration, two iron-intensive cellular processes. In any case, even if the minimum iron quotas were set to the lowest (zero) or highest (the empirically measured iron-limited iron quota) possible values, it would have no effect on the conclusion that the luxury iron storage capacity of *P. granii* is significantly higher than the other diatoms examined.

Using the assumed minimum iron quota values at growth rates of zero, and our empirically measured growth rates and iron quotas in the iron-limited diatoms grown under low-iron conditions, linear equations of growth rate as a function of Fe:C ratios were determined (see example for *P. granii* in Fig. 3.1). Solving for the iron quota when μ_{max} is achieved and then subtracting this value from the empirically measured iron quota under high iron conditions allowed for an estimate of Fe-Q_{store}. These values reflect the ability of the diatom species to take up iron at high external iron concentrations exceeding that required to support maximum growth rate. An exception was *T. oceanica* where the minimum Fe:C quota needed to support μ_{max} was estimated from previously reported data (Marchetti *et al.* 2006).

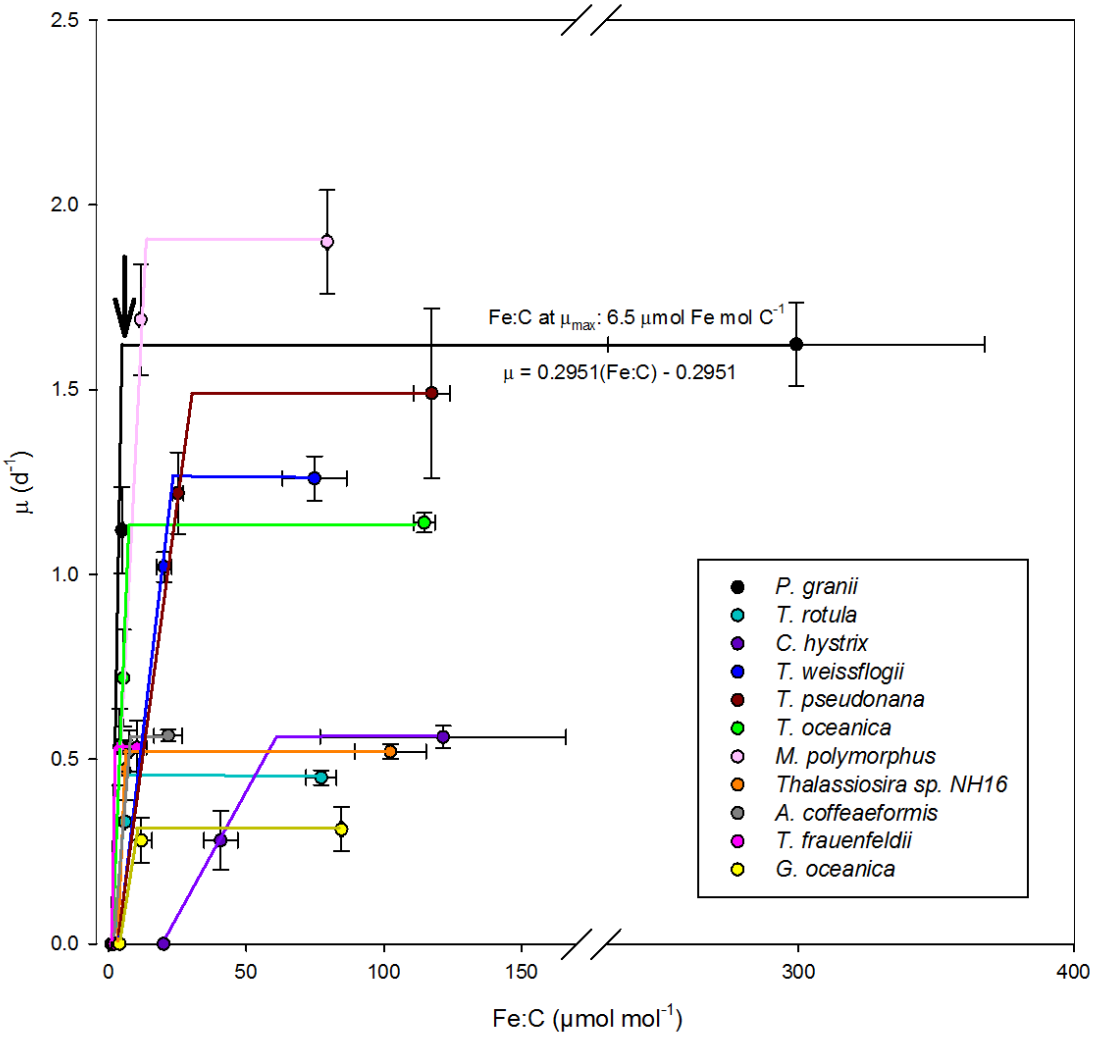

Fig. 3.1. Estimation of luxury iron storage capacity (Fe-Q_{store}) across isolates using an assumed linear relationship between specific growth rate (μ) and cellular iron quota (Fe:C) as described in the methods. As an example, the linear equation for the growth rate as a function of Fe:C and the estimated Fe:C at μ_{max} (indicated by the arrow) is provided for *P. granii* (black line). *T. oceanica* growth rates and iron quotas are from Marchetti et al. (2006).

Target gene sequence acquisition and phylogenetic analysis

P. granii ferritin (*FTN*) and actin (*ACT*) gene sequences were retrieved from a previously sequenced transcriptome library (accession number SRX0066451; Marchetti *et al.*, 2012). *ACT* was chosen as the housekeeping gene to determine relative gene expression due to its

constitutive expression under a variety of growth conditions (Alexander et al. 2012). Gene sequences for *FTN* and *ACT* from the isolates examined in this study were obtained through a sequence homology search using BLASTx v2.2.28 with *Pseudo-nitzschia granii* genes against the database Marine Microbial Eukaryote Transcriptome Sequencing Project (MMETSP) using an e-value cutoff of 10^{-5} (Altschul et al. 1990). In addition, *Pseudo-nitzschia multiseries* and *Fragilariopsis cylindrus* protein sequences used in the *FTN* phylogenetic tree were acquired from the publicly available JGI Genome Portal. Paired-end *FTN* read counts of the transcriptomes of MMETSP isolates in this study ranged from 277 to 1472 with a mean of 607, indicating that the gene is likely to be present at transcript levels substantial enough to be detected under iron-replete conditions (iMicrobe, MMETSP). Nevertheless it is possible that transcriptome sequencing depth did not capture the presence of *FTN* in the isolates where a *FTN* gene homolog was not identified. Therefore the assumption that the non-ferritin-containing isolates used in this study are truly without ferritin must be interpreted with caution. It is important to note that alternative sequence search methodology may uncover additional *FTN* copies present in transcriptomes unidentified by the search tools and settings used here.

For phylogenetic analysis, *FTN* sequences within the open reading frame were aligned using MUSCLE within Geneious v5.6.4 software (Edgar 2004). A Maximum-Likelihood tree was created with MEGA6 using the JTT matrix-based model, partial deletion of residues and 100 bootstrap replicates (Tamura et al. 2013). Diatoms were grouped into classes (i.e., raphid pennate, araphid pennate, bi-multipolar centric, or radial centric) based on chronograms from Sorhannus (2007).

Primer development, RNA extraction and gene expression

Primers were designed for each examined *FTN*-containing diatom individually using Primer3 v0.4.0 (Table 3.2, Untergasser *et al.*, 2012), tested via PCR and visualized through gel electrophoresis. Correct target amplification was confirmed through Sanger sequencing of the resulting PCR product. For RNA, triplicate 500 mL cultures were grown in autoclaved, acid-cleaned, Milli-Q rinsed polycarbonate bottles and harvested onto 25 or 47 mm polycarbonate filters (3 □m pore size) in mid- to late-exponential growth phase to achieve adequate biomass. Filters were flash frozen in liquid nitrogen and then stored at -80°C until RNA extraction. RNA extractions were performed using the RNAqueous 4-PCR kit (Ambion) followed by DNAsing at 37°C for 45 minutes with DNAse I (Ambion) according to the manufacturer's guidelines. Up to two µg of total RNA was used, or all of the total RNA obtained if the extracted yield was lower. The RNA was reverse transcribed using the SuperScript III First-Strand cDNA Synthesis kit with oligo-dT primers (Invitrogen). Real-time quantitative PCR (qPCR) was performed on synthesized cDNA with a Mastercycler ep gradient S thermal cycler (Eppendorf).

Relative gene expression of *P. granii FTN* normalized to *ACT* was estimated using two distinct methods. First, the ΔCt method [$2^{-(\Delta Ct)}$] (Pfaffl 2001), and second, using a series of standards for each gene ranging from 10 - 10^6 copies μL^{-1} (Marchetti et al. 2015; Ellis et al. 2017). The ΔCt method of obtaining relative transcript copy numbers requires the PCR primer efficiencies (E) be equal or close to 2, corresponding to the doubling of template for every increase in cycle (Pfaffl 2001). To test the efficiency of our primers on *P. granii*, dilutions ranging from full concentration to a ten-fold dilution of cDNA were plotted against the threshold cycle (Ct), which produced a linear curve. The validity of the ΔCt method was supported by comparison to the standard curve method for *P. granii*. Relative gene expression obtained

through either method was found to be similar (Fig. 3.2) and therefore the *FTN* gene expression analyses of the other isolates was performed using the ΔCt method.

Quantitative-PCR reaction protocols closely follow those outlined by Marchetti *et al.* (2015), with 20 µL triplicate reactions consisting of a 2 µL cDNA template, 10 µL KAPA SyberFast qPCR kit mix (Kapa), 1.6 µL forward and reverse primers, and 4.8 µL of UV-light treated Milli-Q water. For the creation of *P. granii FTN* and *ACT* standards, target DNA sequences were amplified by PCR at 94°C for 2 minutes, followed by 40 cycles for 30 seconds at 95°C, 30 seconds at the optimum annealing temperature specific to each primer set, and 1 minute at 72°C. PCR cocktail reactions consisted of 4 µL DNA template, 2 µL $MgCl_2$, 2 µL of Taq buffer (Promega), 0.8 µL of the forward and reverse primers, 0.15 µL Taq polymerase (Promega), and 9.25 µL of UV-light treated Milli-Q water (Marchetti *et al.,* 2015). Amplified products were transformed into competent *E. coli* cells using the TOPO TA Cloning Kit (Invitrogen). Kanamycin-resistant colonies containing the inserted vector and fragment were grown overnight in Luria Broth and plasmids were extracted using QIAprep Miniprep (Qiagen). Plasmids were linearized using the enzyme *SpeI* at 37°C for 1 hour, followed by 20 minutes at 80°C. Qubit RNA Assay Kit (Invitrogen) was used to quantify linearized plasmid and standards were created by diluting to 10 - 10^6 copies μL^{-1}. To test for statistical differences in gene expression between iron treatments, a one-way analysis of variance (ANOVA) was performed. Data sets were tested for normality, equal variance and a Holm-Sidak or Tukey pairwise multiple comparison test was performed using Sigmaplot 12.5. The level of significance was $p < 0.05$.

Organism	Gene	Forward Primer (5’ to 3’)	Reverse Primer (5’ to 3’)	Target Length
Minutocellus polymorphus	*FTN*	TTTGGGCGAAATCTTGAATC	GATCGAGGCTGAAGACAAGG	164
Minutocellus polymorphus	*ACT*	CCGGACTCGTCGTACTCTTC	AGGACCTGTACGCCAACATC	226
Thalassiosira sp. NH16	*FTN*	ATCCCAGTTCATGGTCAAGC	GGGGAGCAGGATAACACAAA	202
Thalassiosira sp. NH16	*ACT*	GCATGAGCAAGGAAATCACA	CACTTCCTGTGCACAATGCT	187
Thalassiosira rotula	*FTN1*	TTCCAGCGAGCGAAGTTATT	AATAAGACTCCGGGGTTGCT	192
Thalassiosira rotula	*FTN2*	CTGCGCTGTCTCA	CGCTTATTGGCAA	193
Thalassiosira rotula	*ACT*	TGAGGTCCTCTTCCAGCCTA	TAATAGATGCAGGGGCCAAC	203
Thalassionema frauenfeldii	*FTN1*	TACTCCTACACCCCGACAGG	CTTTCTTCGCCAGATTCGTC	183
Thalassionema frauenfeldii	*FTN2*	CGTAGTCATGCGCTCACATT	CAGCATCCGCAACATGATAG	175
Thalassionema frauenfeldii	*ACT*	GGTGCCACAATCTTGACCTT	AATGAACGTTTCCGATGTCC	242
Amphora coffeaeformis	*FTN1*	TGAAGCACTCATCTCGTTGG	ATTCGCCCATGGATTCAATA	132
Amphora coffeaeformis	*FTN2*	TGAATGCGTCGCAGCTATAC	CCAAATCAATGGGAAAATCG	159
Amphora coffeaeformis	*ACT*	ACACCGTCCATCTCAAGACC	TTACCGAGCGTGGTTATTCC	244
Pseudo-nitzschia granii	*FTN*	ATTGGGCTTTGTCGACTTG	GAAAAATCGTGGCATTCGTT	189
Pseudo-nitzschia granii	*ACT*	ACTCGTTGACTACCACCGCT	GGACATCTGAATCGCTCGTTT	181

Table. 3.2. Primer sequences for ferritin and actin genes used in gene expression analysis of the diatom isolates.

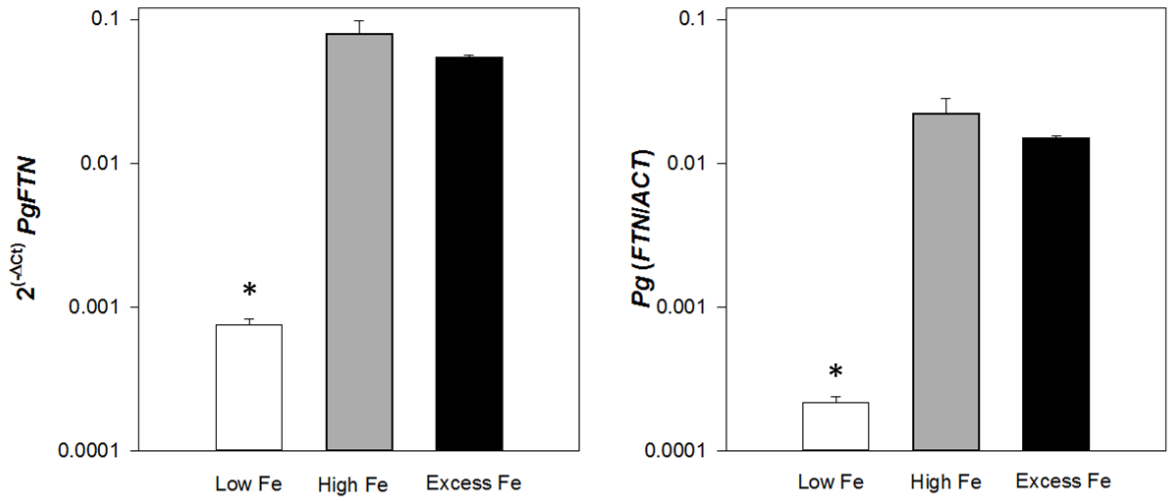

Fig. 3.2. A comparison between the ΔCt (left) and qPCR standards methods (right) for determining *FTN* transcript abundance in the diatom *P. granii*. Standard error bars represent the variation among triplicate cultures. Asterisk indicates significantly lower expression under iron-limited condition as compared to all other treatments (ANOVA, $p < 0.05$). Low Fe indicates growth at an iron concentration of 1.5 nmol L^{-1} Fe_T, High Fe of 1,370 nmol L^{-1} Fe_T, and Excess Fe of 8,410 nmol L^{-1} Fe_T.

Biogeographical distribution of FTN possession

Patterns of *FTN* possession were biogeographically represented by using *P. granii* and MMETSP strain isolation locations, when available, retrieved from either the MMETSP iMicrobe database or the NCMA website using a custom Matlab script. Annual mean surface nitrate concentrations were obtained from the World Ocean Atlas 2009 (Garcia et al. 2010). Fisher's exact test was used to compare the distribution of genes that were present or absent in diatoms isolated from non-HNLC regions and HNLC regions (equatorial Pacific, Northeast Pacific, and Southern Ocean; Moore *et al.*, 2002), of which the Southern Ocean was the only location with adequate transcriptome representation.

Results

Ferritin phylogenetic analysis of centric and pennate diatoms

The recent transcriptome sequencing of 78 diatoms as part of MMETSP has provided an opportunity to determine the prevalence of ferritin throughout the diatom lineage. Through querying this database, along with additional publicly available diatom transcriptomes and genomes, we found that over 85% of the sequenced pennate diatoms contain at least one *FTN* homolog compared to 41% of centric diatoms (Fig. 3.3A). The majority of putatively ferritin-containing diatoms within the database are pennates (62% pennates versus 38% centrics), despite centric diatoms making up the majority of sequenced isolates (centrics: n=44, pennates: n=34).

Within the centric diatom lineage, bi-multipolar diatoms are better represented than radial centrics, and the majority of them (65%) do not contain a *FTN* homolog. There are approximately equal proportions of radial centrics with and without a *FTN* homolog within their transcriptomes. The pennate lineage is mostly represented by raphid as compared to araphid

pennates, of which all but one (*Stauroneis constricta* or 96% of the total) contain at least one *FTN* homolog. Similarly, most araphid pennate diatoms (67%) contain *FTN*.

The high number of diatom transcriptome sequences also provided the opportunity to examine the phylogenetic relatedness of *FTN* within this algal group. Centric and pennate diatoms do not form exclusive subgroups like those commonly observed through phylogenetic analysis of evolutionarily conserved genes such as ribosomal RNA genes (e.g., 18S rDNA). Rather, distinct clades exist consisting of mixtures from both diatom lineages and all four subgroups (Fig. 3.3B). Additionally, some diatom strains contain more than one *FTN* homolog (Fig 3.3B: denoted with 1 & 2 following strain ID). These ferritins varied in degree of similarity, from being quite distinct and located in different clades within the phylogenetic tree (e.g., *Thalassionema frauenfeldii* CCMP1798 1 and 2), to being similar and clustering closely together (e.g., *Thalassiosira rotula* CCMP3096 1 and 2).

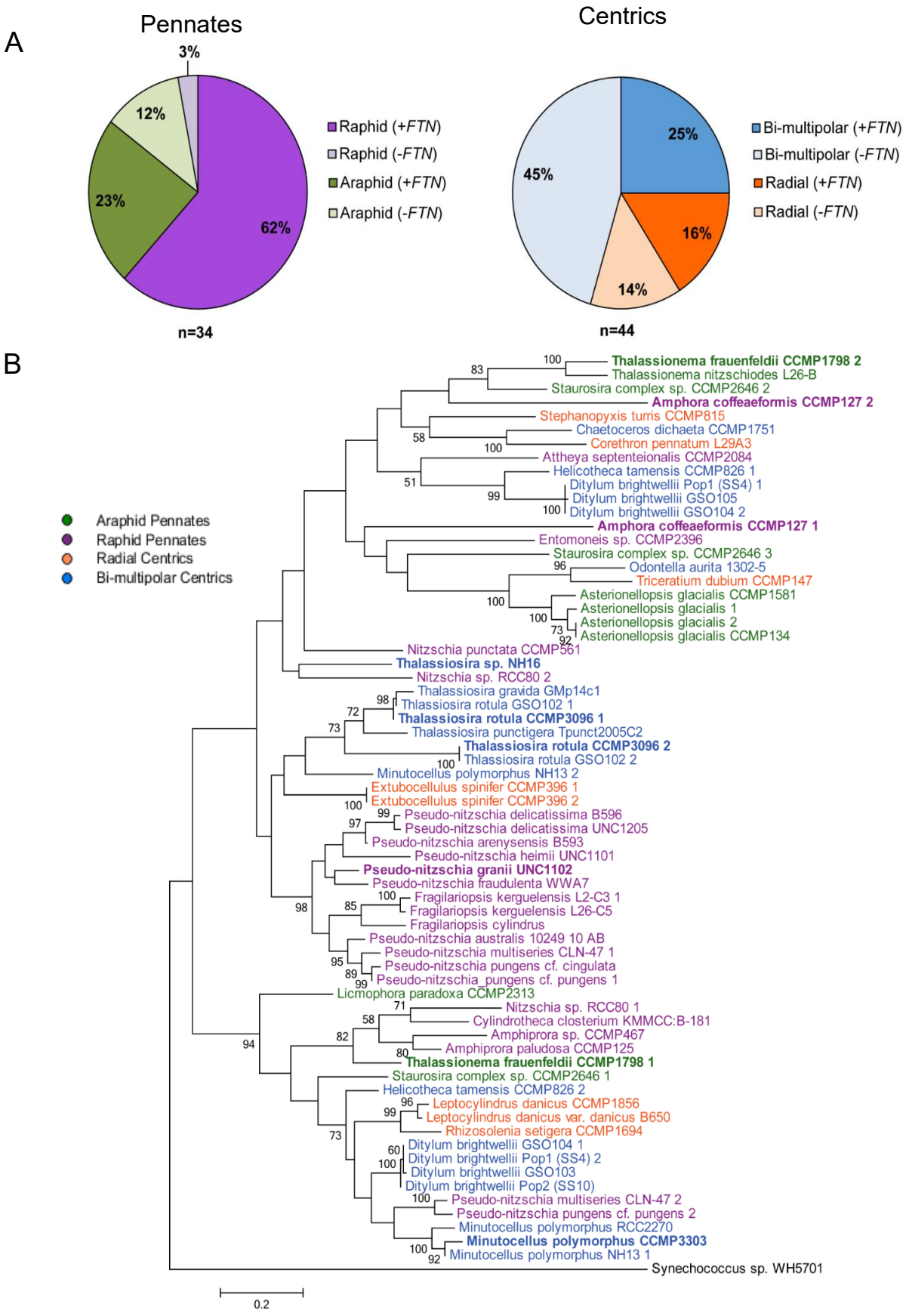
A
Pennates
3%
12%
23%
62%
Raphid (+FTN)
Raphid (-FTN)
Araphid (+FTN)
Araphid (-FTN)
n=34
Centrics
25%
45%
16%
14%
Bi-multipolar (+FTN)
Bi-multipolar (-FTN)
Radial (+FTN)
Radial (-FTN)
n=44
B
Araphid Pennates
Raphid Pennates
Radial Centrics
Bi-multipolar Centrics
Thalassionema frauenfeldii CCMP1798 2
Thalassionema nitzschiodes L26-B
Staurosira complex sp. CCMP2646 2
Amphora coffeaeformis CCMP127 2
Stephanopyxis turris CCMP815
Chaetoceros dichaeta CCMP1751
Corethron pennatum L29A3
Attheya septenteionalis CCMP2084
Helicotheca tamensis CCMP826 1
Ditylum brightwellii Pop1 (SS4) 1
Ditylum brightwellii GSO105
Ditylum brightwellii GSO104 2
Amphora coffeaeformis CCMP127 1
Entomoneis sp. CCMP2396
Staurosira complex sp. CCMP2646 3
Odontella aurita 1302-5
Triceratium dubium CCMP147
Asterionellopsis glacialis CCMP1581
Asterionellopsis glacialis 1
Asterionellopsis glacialis 2
Asterionellopsis glacialis CCMP134
Nitzschia punctata CCMP561
Thalassiosira sp. NH16
Nitzschia sp. RCC80 2
Thalassiosira gravida GMp14c1
Thlassiosira rotula GSO102 1
Thalassiosira rotula CCMP3096 1
Thalassiosira punctigera Tpunct2005C2
Thalassiosira rotula CCMP3096 2
Thlassiosira rotula GSO102 2
Minutocellus polymorphus NH13 2
Extubocellulus spinifer CCMP396 1
Extubocellulus spinifer CCMP396 2
Pseudo-nitzschia delicatissima B596
Pseudo-nitzschia delicatissima UNC1205
Pseudo-nitzschia arenysensis B593
Pseudo-nitzschia heimii UNC1101
Pseudo-nitzschia granii UNC1102
Pseudo-nitzschia fraudulenta WWA7
Fragilariopsis kerguelensis L2-C3 1
Fragilariopsis kerguelensis L26-C5
Fragilariopsis cylindrus
Pseudo-nitzschia australis 10249 10 AB
Pseudo-nitzschia multiseries CLN-47 1
Pseudo-nitzschia pungens cf. cingulata
Pseudo-nitzschia_pungens cf. pungens 1
Licmophora paradoxa CCMP2313
Nitzschia sp. RCC80 1
Cylindrotheca closterium KMMCC:B-181
Amphiprora sp. CCMP467
Amphiprora paludosa CCMP125
Thalassionema frauenfeldii CCMP1798 1
Staurosira complex sp. CCMP2646 1
Helicotheca tamensis CCMP826 2
Leptocylindrus danicus CCMP1856
Leptocylindrus danicus var. danicus B650
Rhizosolenia setigera CCMP1694
Ditylum brightwellii GSO104 1
Ditylum brightwellii Pop1 (SS4) 2
Ditylum brightwellii GSO103
Ditylum brightwellii Pop2 (SS10)
Pseudo-nitzschia multiseries CLN-47 2
Pseudo-nitzschia pungens cf. pungens 2
Minutocellus polymorphus RCC2270
Minutocellus polymorphus CCMP3303
Minutocellus polymorphus NH13 1
Synechococcus sp. WH5701
0.2

Fig. 3.3. **A**. *FTN* presence and absence within MMETSP transcriptomes. The pennate diatom classes, Bacillariophyceae (raphid) and Fragilariophyceae (araphid) are shown in purple and green, respectively, while the centric diatom classes, Mediophyceae (bi-multipolar) and Coscinodiscophyceae (radial) are shown in blue and orange, respectively. Darker colors represent fractions of species within the transcriptome database containing FTN, while lighter shades of colors indicate proportions of diatom species without an identified FTN homolog. **B.** Maximum-Likelihood tree of FTN among the four classes of diatoms. Numbers beside nodes indicate bootstrap values; only bootstraps above 50 are included. *Synechococcus sp* WH5701 was used as the outgroup. Strains examined in this study are indicated in bold. Isolates containing *FTN* but excluded from the tree due to only partial amino acid sequences available include *Chaetoceros neogracile* CCMP1317, *Fragilariopsis kerguelensis* L2-C3, *Thalassiothrix antarctica* L26-D1, and *Synedropsis recta* CCMP1620.

Ferritin gene expression as a function of iron storage capacity

Among the diatom isolates examined, μ_{max} under high-iron conditions varied 8-fold, ranging from a high of 1.9 ± 0.14 d^{-1} in *Minutocellus polymorphus* to 0.45 ± 0.02 d^{-1} in *Thalassiosira rotula* (Table 3.1). In general, diatoms with large biovolumes had lower μ_{max} values compared to those with smaller biovolumes, consistent with established phytoplankton physiological patterns (Fig. 3.4; Finkel, 2007). However, there were exceptions. For example, *Thalassiosira sp*. NH16 (cell volume = 332 ± 144 μm^3) grew at a similar μ_{max} as the much larger *T. rotula* (volume = 7,525 ± 3,609 μm^3) despite the 23-fold difference in cell volume. Growth rates were reduced by an average of 28 ± 21% in the low iron conditions relative to the growth saturating values under the high iron conditions, indicating mild to moderate iron limitation in most cases (Table 3.1). However severe growth reduction occurred in the gene expression experiments with *Amphora coffeaeformis* (78%; Table 3.1) although not in the separately conducted iron quota culture experiments (8%; Fig. 3.1, 3.4. 3.5).

Relative *FTN* expression levels varied among species, with transcript abundance substantially lower for *FTN*1 in the coastal pennate *Thalassionema frauenfeldii* than in the other diatom isolates (Fig. 3.6). Trends in *FTN* expression in response to iron status significantly differed among the diatoms (Fig. 3.6). The oceanic pennate *P. granii* contained only a single *FTN* gene and its expression increased by 100-fold with increasing iron quota (ANOVA: *p*=

0.006; Fig. 3.6). Similarly, expression of the single *FTN* gene in *Thalassiosira sp.* NH16 increased at high cellular iron quota, although to a much lesser extent than *P. granii* (2-fold; ANOVA: $p = 0.01$), consistent with the lower cellular Fe:C ratio in the high iron culture. The opposite iron-response pattern was observed in one of the two *FTN* genes in the coastal diatoms *Amphora coffeaeformis* and *Thalassiosira rotula*. In these genes, *A. coffeaeformis* (*FTN*1) and *T. rotula* (*FTN*2), *FTN* expression was 6- and 160-fold higher under low-iron conditions when cellular Fe:C quotas were reduced (ANOVA: $p = 0.003$ and $5x10^{-5}$, respectively; Fig. 3.6; Fig. 3.7). However, the second *FTN* gene in both species was constitutively expressed and showed no change with variations in iron status and cellular iron quota. In addition, variations in iron quotas and iron limitation of growth rate had no significant effect on *FTN* expression levels in *Minutocellus polymorphus* and *T. frauenfeldii* (ANOVA: $p > 0.05$; Fig. 3.7).

In order to examine whether *FTN* expression may be affected by other growth conditions, cultures of *P. granii* were grown under varying iron conditions, light levels, and macronutrient starvation (see Marchetti et al. submitted for details on experimental design). Here, *FTN* expression was affected only by iron status and was unaltered by macronutrient starvation or light limitation (Fig. 3.8). These results demonstrate that decreased *FTN* expression is not simply a function of growth rate reduction or a general response to resource limitation.

Growth rate reductions in the iron quota experiments varied across isolates; on average, iron-limited diatoms decreased their growth rate by approximately 20% relative to μ_{max}, with *Corethron hystrix* displaying the greatest reduction in growth rate (50% of μ_{max}). Under high iron conditions, the cellular Fe:C ratios in the examined diatoms ranged by over 30-fold, from 10 ± 3.4 μmol Fe mol C^{-1} in the coastal pennate diatom *Thalassionema frauenfeldii* to 300 ± 68 μmol Fe mol C^{-1} in the oceanic pennate diatom *Pseudo-nitzschia granii* (Fig. 3.7). Under the-low iron

conditions, minimum iron quotas ranged 10-fold, from 4 ± 0.8 µmol Fe mol C^{-1} in *Thalassionema frauenfeldii* to 41 ± 6 µmol Fe mol C^{-1} in *Corethron hystrix* (Fig. 3.7). Prior to beginning cell quota culture experiments *Thalassionema frauenfeldii* cultures displayed a 10% growth reduction in the low iron treatment containing 450 nmol L^{-1} Fe_T, but during the experimental period growth reduction was not observed despite the 60% decrease in iron quota (Fig. 3.5).

Based on the iron quota measurements, the largest estimated luxury iron storage capacity (Fe-Q_{store}) was achieved in *P. granii* (293 µmol Fe mol C^{-1}), with the next largest belonging to *T. oceanica* (110 µmol Fe mol C^{-1}; Fig. 3.7). The smallest Fe-Q_{store} values (6.3 and 13.7 µmol Fe mol C^{-1}), were observed in *T. frauenfeldii* and *A. coffeaeformis,* respectively. There were no apparent differences in the Fe-Q_{store} between *FTN*-containing and non-containing centric and pennate diatoms (Fig. 3.7). Rather, *P. granii* exhibited the highest Fe-Q_{store} due to a combination of having the highest Fe:C under high-iron conditions and one of the lowest estimated Fe:C ratios needed to achieve μ_{max}. Consistent with its exceptionally large iron storage capacity, *P. granii* was the only examined diatom to exhibit an appreciable increase in relative *FTN* expression at high Fe concentration, whereas expression of *FTN* in the other diatoms either did not change appreciably or decreased under high-iron conditions (Fig. 3.7).

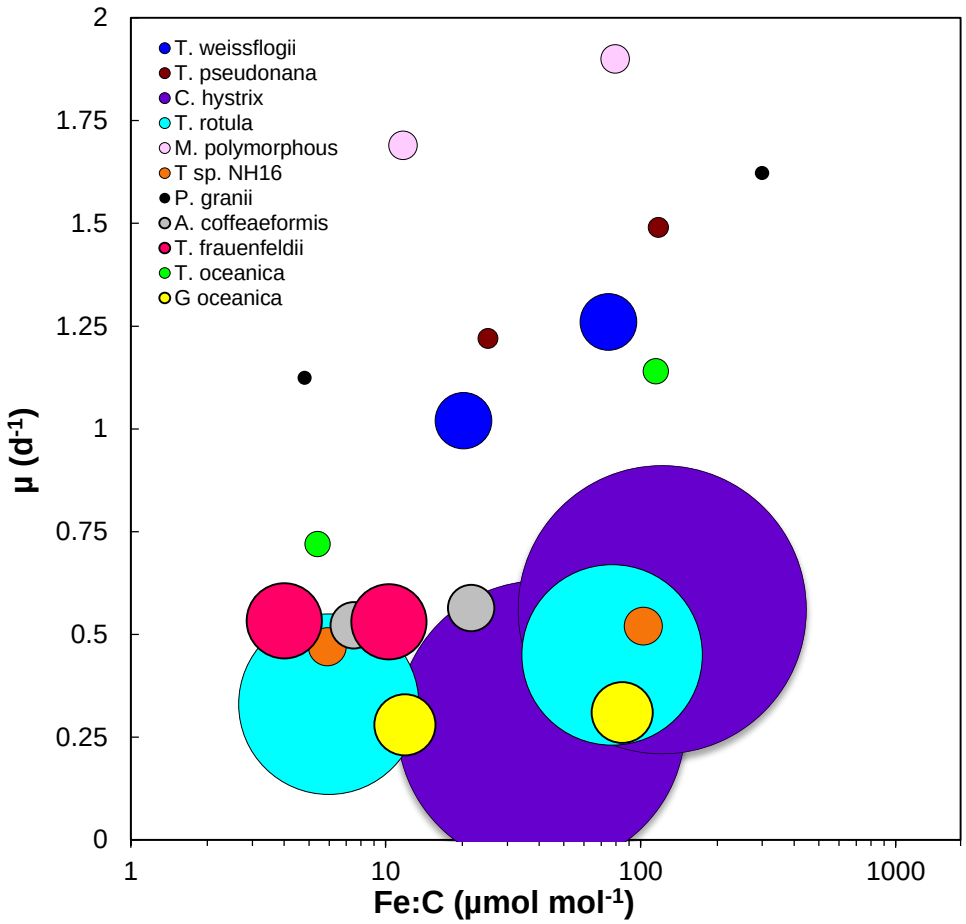

Fig. 3.4. A. Diatom growth rates (μ) as a function of measured intracellular iron quotas (Fe:C) under the different iron conditions shown on a linear-$\log_{10}$ scale. Sizes of circles scale to diatom biovolumes (μm^3) where the largest circle indicates a volume of 19,309 μm^3 (*C. hystrix*) and the smallest circle indicates a volume of 46 μm^3 (*P. granii*). *T. oceanica* growth rates and iron quotas are from Marchetti *et al.* (2006).

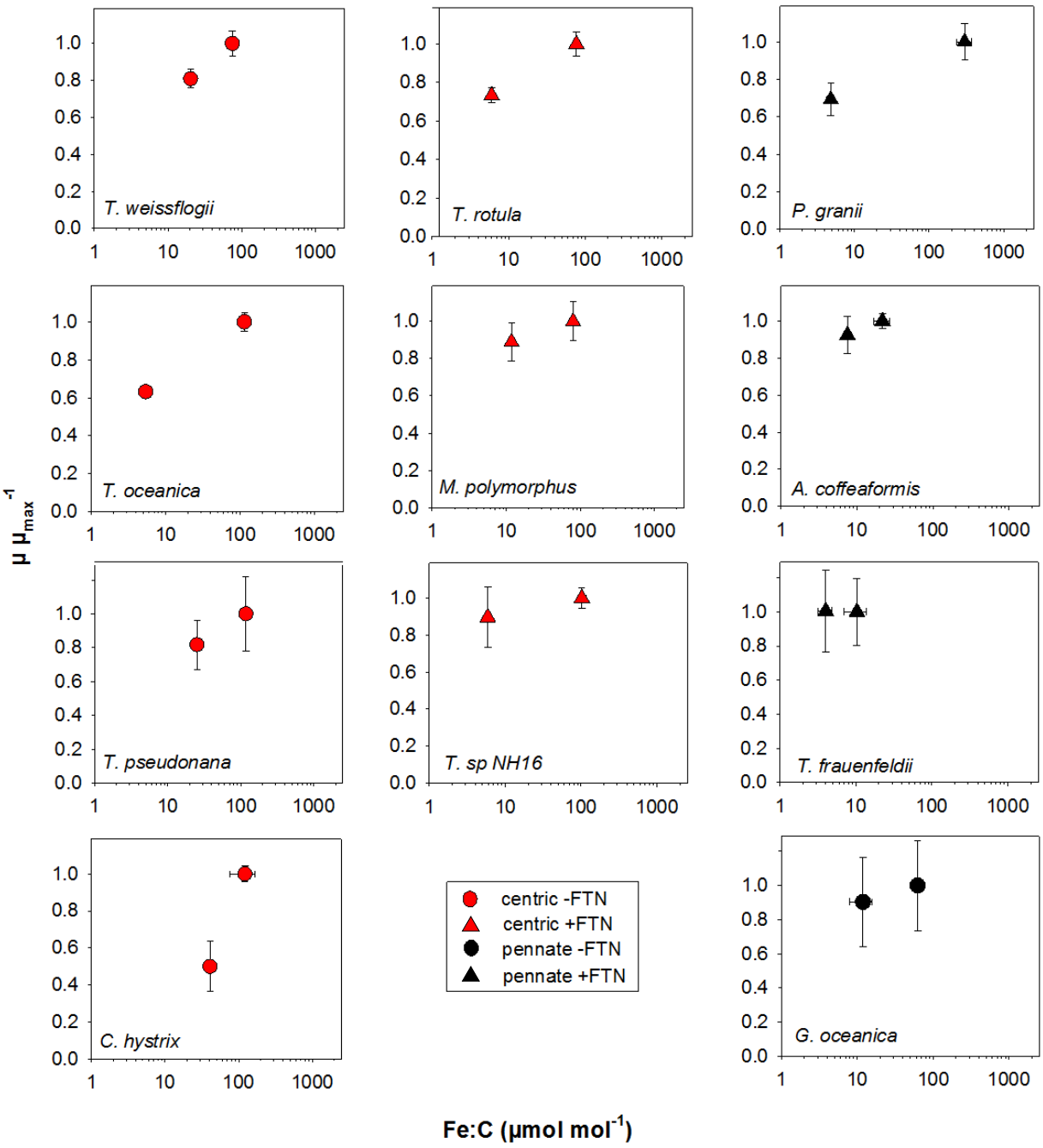

Fig. 3.5. Ratio of growth rate under low iron conditions (1.5 - 600 nmol L^{-1} Fe_T) to maximum growth rate under high iron conditions (μ μmax^{-1}; 1,370 nmol L^{-1} Fe_T) plotted as a function of the intracellular iron quotas (Fe:C) for each diatom isolate. Shown are data for pennate (black symbols) and centric (red symbols) diatoms where at least one *FTN* gene homolog was present (triangles) or absent (circles) in their transcriptomes. Error bars represent the standard deviation of triplicate cultures. T. oceanica growth rates and iron quotas are from Marchetti et al. (2006).

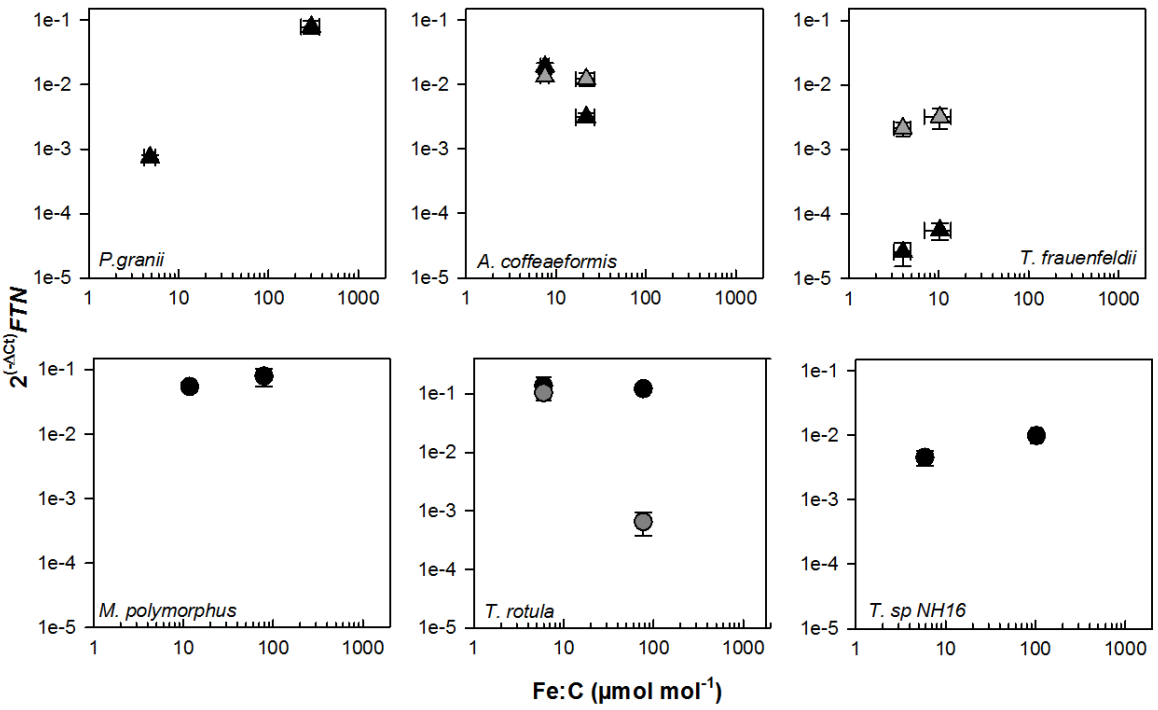

Fig. 3.6. Relative *FTN* transcript abundance ($2^{(-\Delta Ct)}$*FTN*) for each of the *FTN*-containing diatoms shown as a function of the cellular iron quota (Fe:C) under high and low iron conditions. Pennate diatoms are depicted as triangles while centric diatoms are depicted as circles. Second *FTN* gene copies in select isolates are shown in gray. Standard error bars represent the variation in iron quotas (horizontal) and gene expression (vertical) among triplicate cultures.

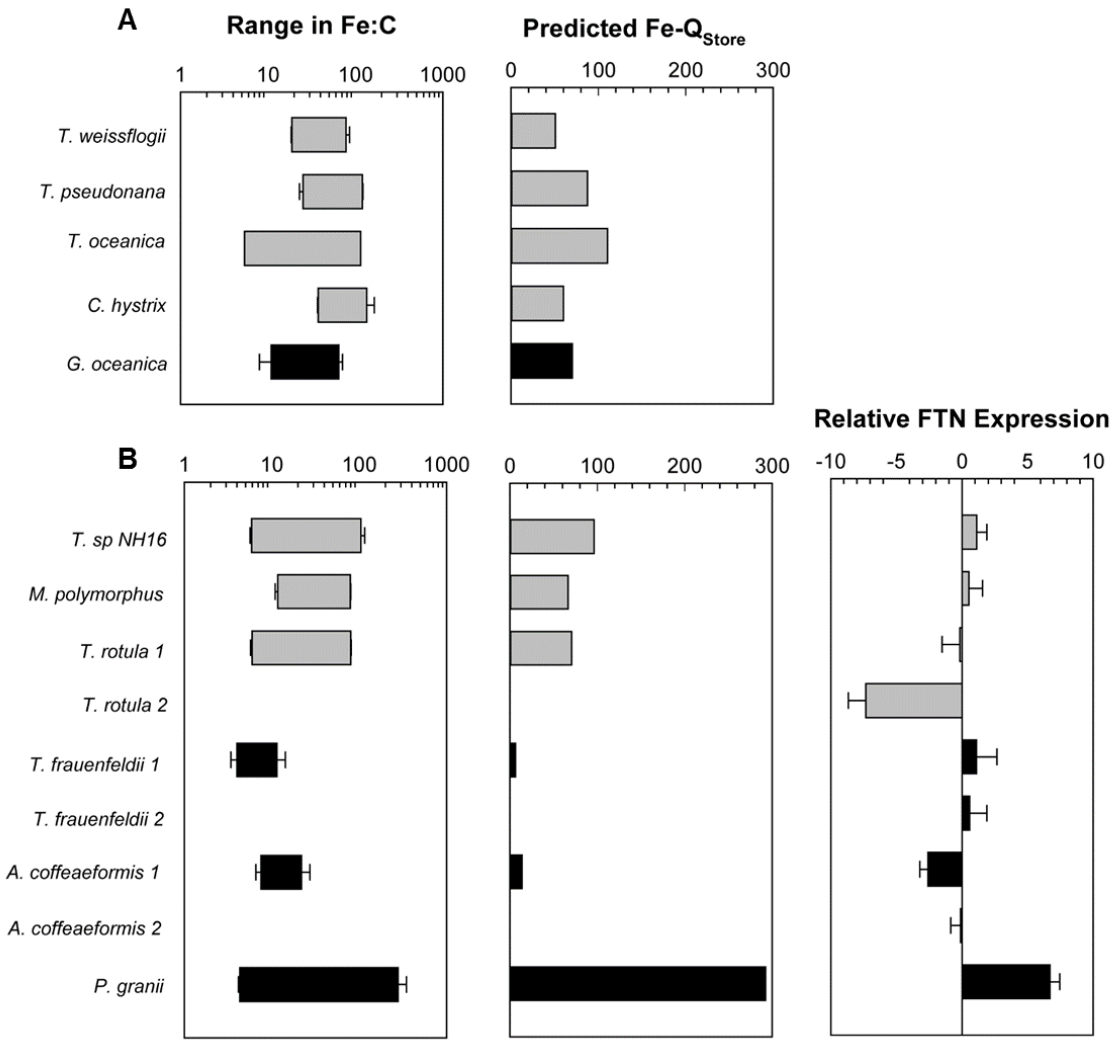

Fig. 3.7. Comparison of intracellular iron quota (Fe:C) ranges empirically measured, estimated luxury iron storage (Fe-Q_{Store}), and *FTN* expression among phylogenetically distinct diatom isolates grown under high and low iron conditions. Diatoms are separated by whether a *FTN* gene is **A**) absent or **B**) present within their transcriptomes. Pennate diatoms are displayed in black, centrics in grey. Bar plots display ranges in Fe:C ratios (µmol Fe mol C^{-1}) depicted on a log (base 10) scale. The estimated Fe-Q_{Store} displayed on a linear scale are calculated by subtracting empirically measured iron quotas under high iron conditions by estimated iron quotas at μ_{max} (Sunda and Huntsman, 1997; see methods). *T. oceanica* iron quota measurements are from Marchetti *et al.* (2006). Relative *FTN* expression represents the ratio of actin-normalized *FTN* expression under the high iron conditions compared to the expression under low iron conditions shown on a log (base 2) transformed scale. Multiple *FTN* copies are denoted by 1 and 2. Standard error bars represent variation among triplicate cultures. Positive values indicate a higher number of *FTN* transcripts under high iron conditions, while negative values indicate higher *FTN* expression under low iron conditions.

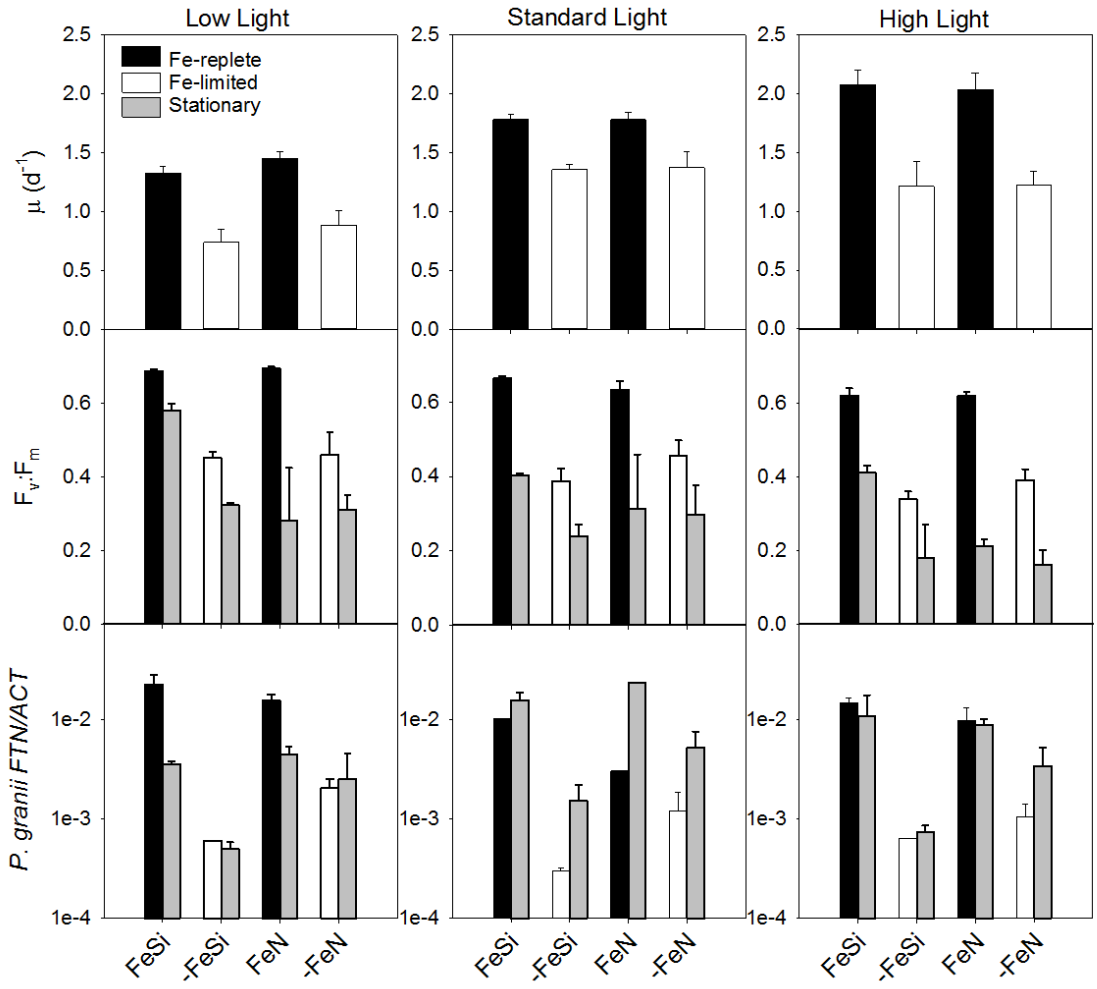

Fig. 3.8. Growth rates, F_v:F_m, and *FTN:ACT* expression in *P. granii* under a variety of growth conditions. Low light = 40 µmol quanta $m^{-2}s^{-1}$, standard light = 150 µmol quanta $m^{-2}s^{-1}$, high light = 400 µmol quanta $m^{-2}s^{-1}$. Si = silica-starved at stationary phase, N = nitrate-starved at stationary phase. Fe = iron-replete growth, -Fe = iron-limited growth. Standard error bars represent the variation among triplicate cultures.

Biogeographical analysis of ferritin among diatoms

The origins of the diatom isolates used in the analysis of FTN distributions ranged from tropical to polar regions, with the majority being obtained from coastal waters (Fig. 3.9). Many bi-multipolar centric isolates containing *FTN* were isolated from the northwest coast of the US, including the isolates *Thalassiosira sp.* NH16 and *T. rotula*. There were no significant differences in *FTN* presence between HNLC and non-HNLC pennate or centric diatoms (Fig. 3.9; $p \geq 0.5$) with 57% of sequenced diatoms from HNLC regions containing at least one *FTN* gene and 51% from other regions also containing a *FTN* (Fig. 3.9). These trends are mainly based on diatom *FTN* presence and absence within the Southern Ocean, the primary HNLC region containing a sufficient number of diatom isolates with sequenced transcriptomes (Fig. 3.9). For each of the two other iron-limited HNLC regions (e.g., Northeast Pacific and equatorial Pacific Ocean) there were too few isolates to draw any definitive conclusions on the distribution of *FTN* genes, with only a single isolate from each location (both raphid pennates). While *P. granii* UNC1102 from the Northeast Pacific Ocean contains a *FTN* homolog, the gene was absent from the transcriptome of the equatorial Pacific diatom *Stauroneis constricta* CCMP1120.

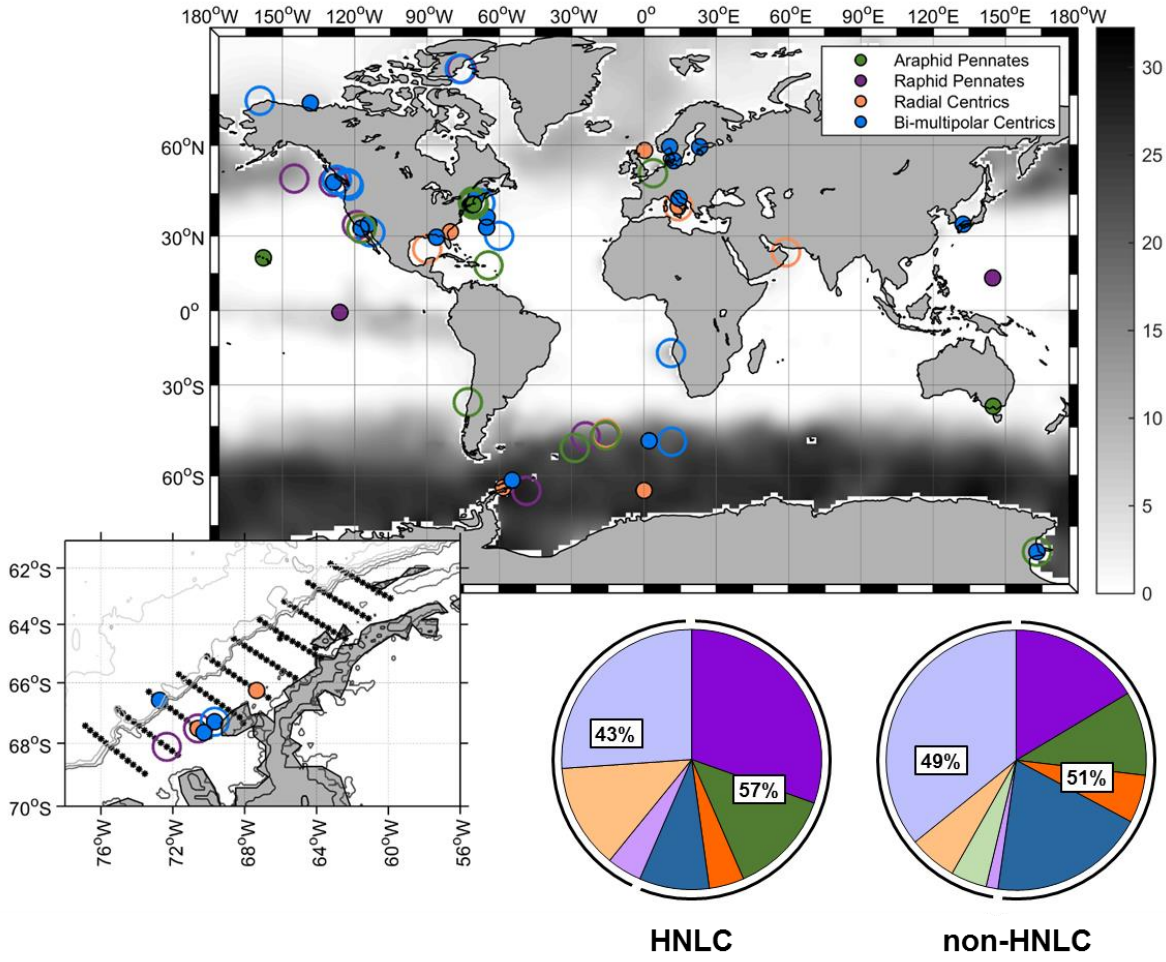

Fig. 3.9. Global distribution of diatom strains where a *FTN* homolog is present (open circles) or absent (closed circles) within available diatom transcriptome sequences. Background grayscale variation represents mean annual surface nitrate concentrations (μmol L^{-1}) World Ocean Atlas; (Garcia et al. 2010)]. Inset displays the Western Antarctic Peninsula region with the Palmer Long Term Ecological Research (LTER) grid where additional sequenced diatom isolates not contained within MMETSP were obtained. Pie charts represent percentage of isolates within the HNLC versus non-HNLC regions containing *FTN* or having no *FTN* sequence identified within their transcriptomes. The pennate diatom classes, Bacillariophyceae (raphid) and Fragilariophyceae (araphid) are shown in purple and green, respectively, while the centric diatom classes, Mediophyceae (bi-multipolar) and Coscinodiscophyceae (radial) are shown in blue and orange, respectively. Darker colors represent fractions of isolates containing *FTN*, while lighter corresponding shades indicate proportions without an identified *FTN* homolog.

Discussion

Iron storage in diatoms

Our study verifies that centric and pennate diatoms display varied capacities to store iron irrespective of whether they contain ferritin. It is consistent with previous reports that diatoms such as *T. weissflogii* and *T. pseudonana*, which do not contain ferritin, perform luxury iron uptake at high iron concentrations (Sunda and Huntsman, 1995; Nuester *et al.*, 2012). In addition to ferritin, iron is stored in vacuoles in yeast through its incorporation into polyphosphates (Raguzzi et al. 1988). Natural resistance associated macrophage proteins (NRAMPs), which transfer divalent metals (including ferrous iron) out of vacuolar storage in plants, are highly expressed in iron-limited *T. pseudonana* (Lanquar et al. 2005; Kustka et al. 2007), consistent with vacuolar storage of iron as an alternative to ferritin for diatoms as well.

In the present study, alternative iron storage mechanisms in the non-ferritin-containing diatoms allowed for similar maximum iron quotas as those achieved in most of the ferritin-containing diatoms under very high iron conditions, demonstrating possession of ferritin alone does not confer an overall enhanced ability to store high levels of non-metabolic cellular iron. Furthermore, *T. frauenfeldii* contained the lowest estimated luxury iron storage capacity under high-iron conditions (6.3 μmol Fe mol C^{-1}; Fig. 3.7B) despite containing two distinct *FTN* genes. Both the identity of these alternative iron storage mechanisms and the mechanisms that regulate the transfer of iron between storage pools and functional iron proteins remain unclear at present. Most importantly, because our experiments were conducted under acclimated growth conditions, it is unclear how the efficacy of ferritin-mediated iron storage compares to non-ferritin iron storage mechanisms during rapid transitions between conditions of high and low iron availability.

Biogeographical patterns in ferritin acquisition

Within the examined diatoms, there were no apparent differences in the luxury iron storage capacities between ferritin-containing and non-ferritin containing diatoms when grown under the same high iron concentrations. What did become apparent was the exceptional iron storage capacity of the oceanic pennate diatom *P. granii*. A large maximum quota at high iron concentrations combined with a low cellular iron quota needed to achieve μ_{max} resulted in a remarkable ability of *P. granii* to store iron. Consequently, cells containing luxury iron could undergo at least eight cellular divisions solely on their internal iron reserves (Marchetti et al. 2009). This ability for continued growth on stored iron supports previous claims as to how iron storage mediated through ferritin likely contributes towards the success of this diatom genera in dominating large blooms in HNLC regions following experimental iron enrichment (Marchetti et al. 2009).

The capacity of *P. granii* to substantially decrease the cellular iron needed to support relatively fast growth rates highlights how well-adapted this species is to growing in the iron-limited region from which it was isolated. To gain a biogeographical perspective on diatom *FTN* distributions and determine whether possession of ferritin preferentially occurs in diatoms residing in HNLC regions, we searched sequenced transcriptomes of diatoms isolated from throughout the ocean, taking advantage of the geographical coverage offered by isolates sequenced as part of the MMETSP (Keeling et al. 2014). Both HNLC and non-HNLC diatoms possess *FTN* transcripts, and they appear to be common throughout the world's oceans with no clear biogeographical pattern associated with its presence in diatoms. This suggests that ferritin may have a role in both environments experiencing chronic iron limitation and in regions with higher, but perhaps more variable iron levels, such as coastal upwelling environments. Although

not addressed in this study, there may be a relationship between ferritin possession in diatoms residing in regions with variable iron inputs compared to those in areas with a more consistent iron supply, as the storage protein could be critical in maintaining intracellular iron homeostasis in regions with rapidly changing external iron concentrations.

Structure, taxonomy and phylogeny of diatom ferritin

The protein structure of ferritin may provide clues regarding its utilization in phytoplankton. The coastal marine diatom *Pseudo-nitzschia multiseries* has an isoform of ferritin that seems to be optimized for rapid iron sequestration and release. This diatom contains a glutamic acid residue in a region of the ferroxidase center (Glu130) that complexes and stabilizes ferric iron (Fe[III]) following oxidation of Fe(II). This complexation reduces the rate of subsequent Fe(III) transfer to the protein core and storage as ferrihydrate. By contrast, substitution of Glu130 with a non-Fe coordinating residue allows for quicker Fe(III) mineralization and storage (Pfaffen et al. 2015). Interestingly, aside from *Pseudo-nitzschia granii*, none of the other ferritin-containing diatoms examined in our study contain a glutamic acid or other charged amino acid at site 130, but instead have an alanine, serine or glycine (Fig. 3.10). In addition, all but one of these diatoms (*Thalassiosira* sp NH16) have ferritins with gene expression patterns that differed compared to *P. multiseries* (Marchetti et al. 2009) and *P. granii*, which was the only isolate to substantially increase *FTN* expression (by 100-fold) under high iron conditions in this study (Fig. 3.7B). The presence of glutamic acid in this key position at the ferroxidase center in *P. granii* is puzzling, however, as its presence suggests a retarded transfer of Fe(III) between the ferroxidase site in ferritin and the site of ferrihydrate deposition, which one might argue would retard rather than facilitate long-term storage of iron. Clearly further

work is needed to understand the ecological importance of these ferritin isoforms and whether differences in functional roles can result from minor variations in key amino acid residues in the ferroxidase centers.

Furthermore we report that taxonomically related diatoms contain ferritins with different expression patterns in response to iron concentrations. Variable ferritin expression patterns among diatom isolates are perhaps explained by multiple lateral gene transfer events or by gene mutation within the diatom lineage (Marchetti et al. 2009; Groussman et al. 2015). Within the *Thalassiosira* genus, *Thalassiosira* sp. NH16 significantly increased *FTN* expression under high iron conditions, while *T. rotula* contains one *FTN* gene whose transcription significantly increased under low iron conditions and another with no change in expression. In addition *A. coffeaeformis* contains two *FTN* genes that are phylogenetically similar, yet display trends similar to those observed in *T. rotula*. Given that closely related taxa may contain ferritins with different expression patterns, the functional roles of ferritins should not be based on taxonomic relatedness. In other words, phylogeny does not dictate ferritin functionality.

In addition, ferritin genes in *T. rotula* (*FTN*2) and *A. coffeaeformis* (*FTN*1) displayed similar gene expression responses to low iron conditions in which expression increased in one of two *FTN* genes, but their predicted ferritin protein sequences differ substantially. In diatoms and other microalgae, there are two distinct clades of ferritin based on sequence homology in the C-terminus region. The subgroup with high bootstrap support (94%) and distinct sequence homology has been named FTN-II, whereas all other ferritins are known as FTN-I (see Fig 3.3B; Groussman *et al.*, 2015). Our findings suggest caution should be used in assuming that these phylogenetically determined clades can be used to predict a similarity in ferritin functional role within each clade. *Pseudo-nitzschia granii* and *Thalassiosira* sp. NH16 both exhibit increased

FTN expression under high iron conditions while *T. rotula (FTN*2*)* and *A. coffeaeformis* (*FTN*1) increased *FTN* expression under iron limiting conditions, yet all of these ferritins group within the FTN-I clade. Furthermore, as noted previously, a single residue substitution could substantially change ferritin functionality, suggesting that ferritin sequence homology alone may be an inaccurate indicator of ferritin function (Pfaffen et al. 2015).

A

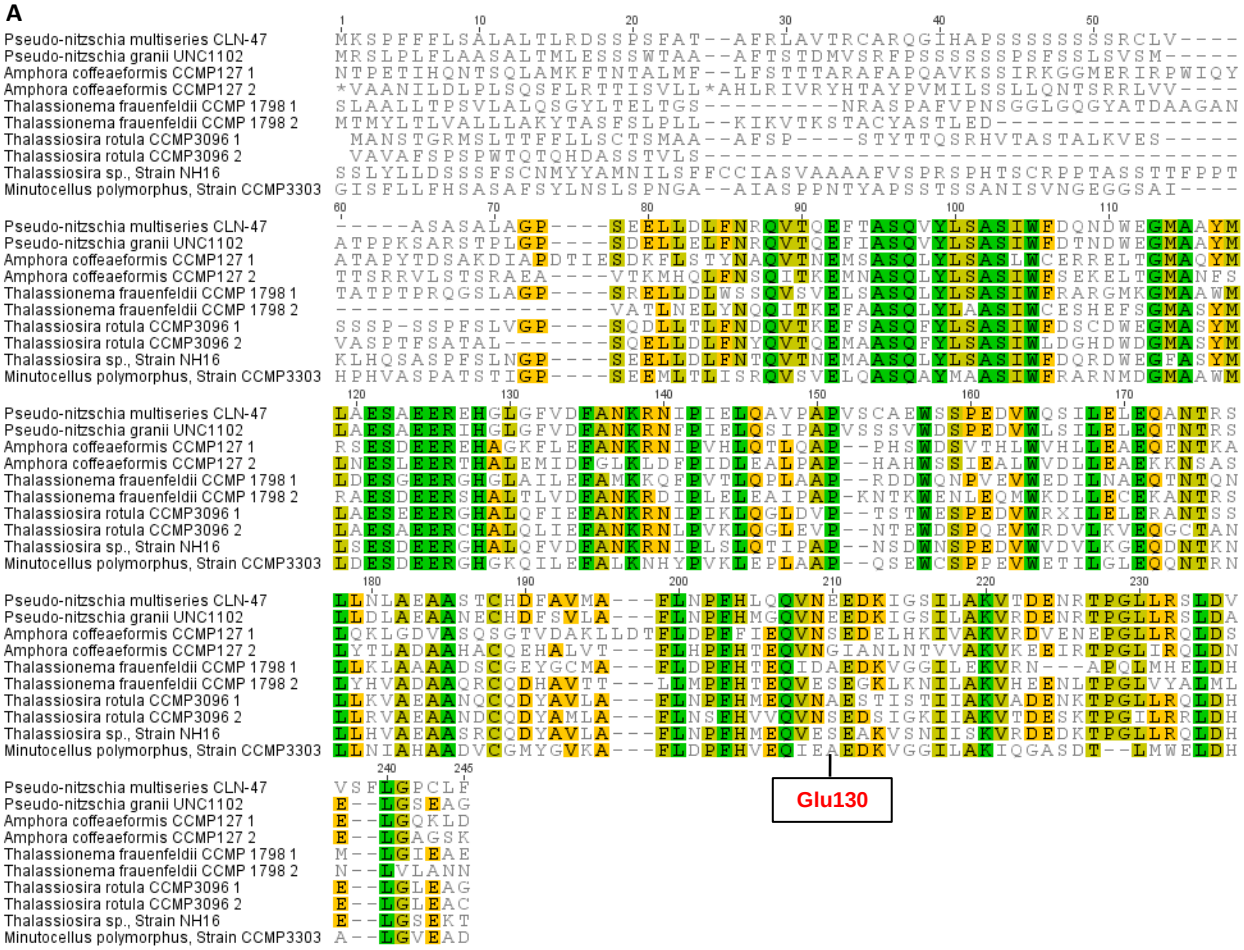

B

	P. multiseries	*P. granii*	*A.coffeaeformis 1*	*A. coffeaeformis 2*	*T. frauenfeldii 1*	*T. frauenfeldii 2*	*T. rotula 1*	*T. rotula 2*	*T. sp. NH16*	*M. polymorphus*
P. multiseries		67.2	34.6	37.2	38.6	38.3	51.8	46.8	47.5	40.1
P. granii	67.2		37.3	34.9	39.7	38.4	55.7	46.1	48.7	43.9
A. coffeaeformis 1	34.6	37.3		34	32.6	30.4	35.7	32.4	38.2	29.3
A. coffeaeformis 2	37.2	34.9	34		32.1	38.1	38	34.1	34.2	27.8
T. frauenfeldii 1	38.6	39.7	32.6	32.1		27.9	38.2	38.8	40.2	50
T. frauenfeldii 2	38.3	38.4	30.4	38.1	27.9		39	36.6	39.6	30.1
T. rotula 1	51.8	55.7	35.7	38	38.2	39		54.1	52.8	39.2
T. rotula 2	46.8	46.1	32.4	34.1	38.8	36.6	54.1		48.1	36.6
T. sp. NH16	47.5	48.7	38.2	34.2	40.2	39.6	52.8	48.1		39.7
M. polymorphus,	40.1	43.9	29.3	27.8	50	30.1	39.2	36.6	39.7	

Fig. 3.10. Alignment of ferritin amino acid sequences among diatom isolates presented in this study (**A**) obtained from either the *P. granii* sequence transcriptome library (Marchetti et al. 2012) or the MMETSP database. Alignment was created using MUSCLE within Geneious version 5.6.4 (Edgar 2004; Tamura et al 2013). Residues are color-coded by blosum62 score matrix similarity (threshold = 5); residues with 100% similarity are represented in green, 80-100% in gold, 60-80% in yellow, and less than 60% in white. The glutamic acid at position 130 is indicated. **B**. Percent similarity of amino acids residues between isolates in A.

Multiple functional roles for diatom ferritins

Gene expression patterns found in this study provide compelling evidence for multiple functional roles of ferritin within diatoms. One role is for long-term storage during periods of high iron bioavailability, allowing for use of these iron reserves to support cell growth and division when iron in the surrounding environment drops back to low, growth-limiting concentrations. Such a role is consistent with the iron storage capacities and gene expression patterns observed in *P. granii*, which also appear to be independent of light or macronutrient status. *FTN* expression also increases under high iron conditions in *Thalassiosira* sp. NH16, albeit to a much lower degree. These diatoms may have evolved ferritins specialized for long-term iron storage over multiple cell divisions.

For many of the other diatom ferritins examined in this study there was no significant change in gene expression with variations in iron quota. These included those in the diatoms *M. polymorphus*, *T. rotula* (*FTN*1), *A. coffeaeformis* (*FTN*2) and *T. frauenfeldii* (*FTN*1&2). A similar pattern has been observed in the green alga *Ostreococcus tauri*, where *FTN* gene expression did not significantly change in response to iron limitation of growth, but rather was strongly regulated by diel light cycles (Botebol et al. 2015). Further studies investigating ferritin signaling pathways, regulation factors, and ferritin localization under low iron stress could provide a more comprehensive understanding of the mechanisms behind ferritin transcript regulation in these diatoms.

In contrast to *P. granii* and *Thalassiosira* sp. NH16, the diatoms *T. rotula* and *A. coffeaeformis* significantly increased expression of one of their two *FTN* genes under iron limitation of growth rate, suggesting that there is a role for ferritin under iron-limiting conditions that may be widespread. One possibility may be as a proactive safety mechanism to protect cells

against intracellular iron toxicity when high affinity iron uptake systems, which are upregulated under low iron conditions (Shaked and Lis 2012), encounter pulses of elevated iron. By utilizing ferritin as a short-term storage mechanism under low-iron conditions, cells would be protected against possibly lethal doses of iron influx, and would be able to utilize the accumulated iron to support subsequent cellular growth. Alternatively, or in addition, ferritins may store iron released by cellular degradation of iron-containing proteins and protein complexes such as ferredoxin and photosystem I during acclimation to low-iron conditions (La Fontaine et al. 2002; Long et al. 2008). Further supporting the important role of ferritins in iron-limited cells, in ferritin knock-out experiments within the green alga *Ostreococcus tauri*, cells without ferritin were less tolerant of low-iron conditions than their wild-type counterparts (Botebol et al. 2015). It is possible that diatoms exhibiting increased *FTN* expression when iron quotas are lowest have adapted to environments with large fluctuations in bioavailable iron, and have thus benefitted from this putative functional role of their ferritins. We conclude that diatom ferritin may be a versatile protein for storing intracellular iron as needed to correct for temporal differences between cellular iron supply and metabolic demand on both short and long timescales. Thus it is likely a contributing factor to the success of many diatoms in the marine environment.

CHAPTER 4: A COUPLED TRANSCRIPTOMIC AND PROTEOMIC COMPARISON OF THE RESPONSE TO IRON LIMITATION IN THE OCEANIC PENNATE DIATOM *PSEUDO-NITZSCHIA GRANII*[4]

Introduction

Pseudo-nitzschia is a cosmopolitan bloom-forming genus of marine pennate diatoms (Hasle 2002). Members commonly form dense blooms in coastal waters where they contribute to the base of the food chain that supports productive fisheries. In addition to being a dominant bloom-forming genus, *Pseudo-nitzschia* is known as a harmful algal blooming (HAB) taxon due to its production of the neurotoxin, domoic acid (DA). Toxic blooms of *Pseudo-nitzschia* have been documented around the world (Lelong et al. 2012). In the NE Pacific Ocean, high phytoplankton biomass is typically fueled by upwelling of nutrient-rich deep ocean waters and merging of complementary water masses. *Pseudo-nitzschia* blooms at the intersection of coastal nitrate-poor yet iron-rich waters with oceanic nitrate-rich yet iron-poor waters (Ribalet et al. 2010). Further offshore, in the middle of the Alaskan Gyre, chronic iron limitation of phytoplankton growth is well-characterized, with occasional blooms occurring when ephemeral iron inputs to surface waters occur via atmospheric deposition of continental dust from arid regions or from volcanic activity (Lam et al. 2006; Lam and Bishop 2008). Iron fertilization experiments have demonstrated that the introduction of bioavailable iron to these high-nutrient, low-chlorophyll (HNLC) waters creates diatom-dominated phytoplankton blooms, often

[4]This chapter is a manuscript draft in progress that will be modified before submission for publication. The working citation is: Cohen NR, Gong W, Saito M, Marchetti A. A coupled proteomic and transcriptomic comparison of the response to iron limitation in the pennate diatom *Pseudo-nitzschia granii*. NRC and AM designed the study; WG contributed bioinformatic support; MS generated the proteomic data; NRC and AM wrote the manuscript.

comprised of *Pseudo-nitzschia*, with the potential to transport large amounts of carbon to the ocean's interior (de Baar et al. 2005; Boyd et al. 2007; Marchetti et al. 2012; Smetacek et al. 2012).

The success of *Pseudo-nitzschia* in forming large blooms in the NE Pacific Ocean following iron addition has been in part attributed its competitive growth characteristics. Oceanic diatoms have numerous strategies for decreasing their cellular iron demand compared to coastal diatoms (Sunda and Huntsman 1995; Strzepek and Harrison 2004; Marchetti et al. 2006; Sutak et al. 2012). The HNLC diatom *Pseudo-nitzschia granii* maintains more rapid growth rates under iron-limiting conditions even when compared to other (non-HNLC) oceanic diatoms. Growth rates under iron limitation of *P. granii*, the (non-HNLC) oceanic diatom *Thalassiosira oceanica*, and the coastal diatoms *Thalassiosira rotula* and *Thalassiosira sp.* NH16 have been measured by Marchetti et al. (2006) and Cohen et al. (submitted). *P. granii* grows at a specific growth rate of 1.12 day^{-1} under the low iron conditions that result in substantial reduction in intracellular iron quota (Fig. 4.1). By contrast, the other isolates examined maintained maximum specific growth rates ≥30% lower under iron limitation. We therefore propose *P. granii* as a model pennate diatom species when investigating iron limitation-induced changes in molecular physiology, due to its exceptional ability to sustain growth under iron limitation, even when compared to species from non-HNLC oceanic regions.

Investigation of the molecular physiology of *Pseudo-nitzschia* has additionally provided key insights into this species' competitiveness for growth in low iron environments. In particular, *P. granii* highly expresses the gene encoding the iron storage protein, ferritin, under iron-replete conditions. This enables *P. granii* to take up and store iron during pulses of high iron availability and then use these reserves for subsequent cell growth and division once iron in the surrounding

environment drops back to growth-limiting concentrations. As a result, this species can sustain 8 cellular divisions using its stored iron reserves (Marchetti et al. 2009). Most other phylogenetically diverse diatoms investigated in recent laboratory studies did not exhibit *P. granii*'s pattern of increased ferritin gene expression under iron-replete conditions and did not have iron storage capacities quite as large (Cohen et al. submitted). Thus, *P. granii* is able to both substantially decrease the amount of cellular iron needed to support growth rates under iron limitation and to store large amounts of cellular iron during periods of iron availability. These strategies in part allow *P. granii* to form large blooms in HNLC regions following natural and artificial iron enrichment (Marchetti et al. 2009, 2012; Cohen et al. in press).

In this study we examine the transcriptomic and proteomic responses of the oceanic pennate diatom *P. granii* isolated from an iron-limited region of the NE Pacific Ocean to changes in iron status. Our primary objective was to elucidate the molecular bases behind the exceptional ability of *P. granii* to cope under low iron conditions and elicit a rapid response to iron resupply. Furthermore we report key differences between the immediate and prolonged effects of iron enrichment on cellular metabolism of initially iron-limited *P. granii* cells.

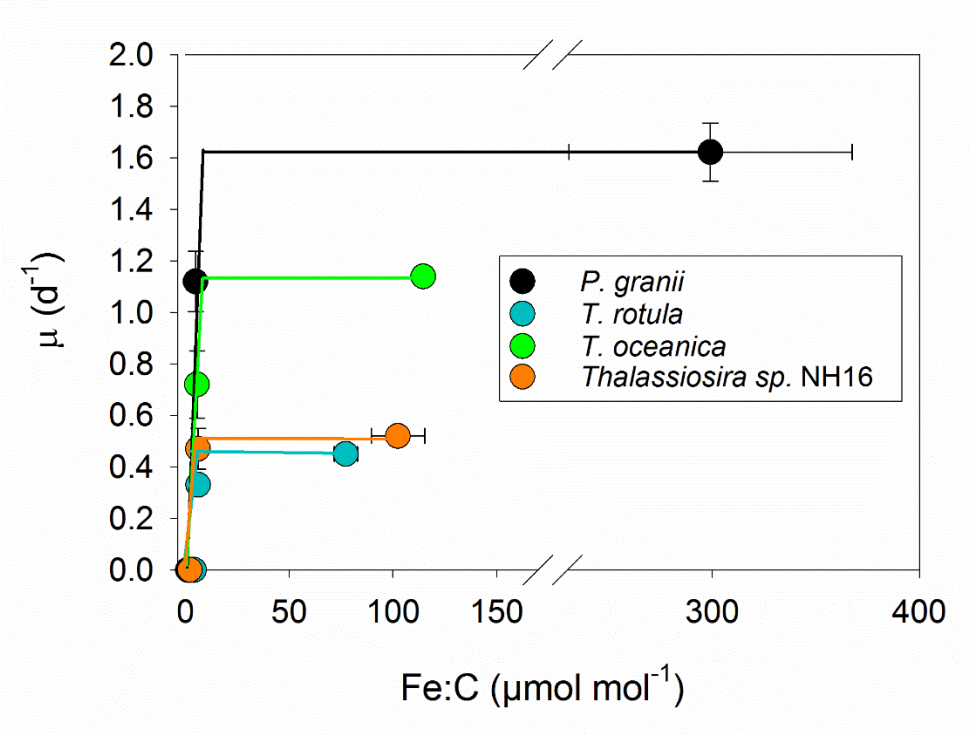

Fig. 4.1. Specific growth rates (μ) as a function of cellular iron quota (Fe:C) in the diatom species *Pseudo-nitzschia granii* (black), *Thalassiosira oceanica* (green), *Thalassiosira rotula* (blue), and *Thalassiosira sp.* NH16 (orange). Data from Marchetti et al. (2006) and Cohen et al. submitted.

Methods

Acclimated iron-replete and iron-limited culture conditions

The pennate diatom *Pseudo-nitzschia granii* (UNC1102) was isolated from naturally iron-limited waters of the Northeast Pacific Ocean at Ocean Station Papa (OSP; 50°N, 145°W) in 2011. The isolate was identified through sequencing of the 18S and ITS1 regions (accession numbers KJ866907 and EU051654, respectively). Cultures were maintained in the artificial seawater medium Aquil using trace metal clean (TMC) techniques according to Marchetti et al. (2006). For media preparation, 2 L aliquots of Aquil were placed into acid-cleaned, Milli-Q (18.2 MΩ·cm) H_2O-rinsed polycarbonate bottles. Dispensed seawater was supplemented with filter-sterilized (0.2-μm Acrodisc) ethylenediaminetetraacetic acid (EDTA)-trace metals (without iron) and vitamins (cobalamin, thiamine and biotin) according to Price et al. (1989). Trace metal

concentrations were buffered using 100 μmol L^{-1} of EDTA. Aquil medium macronutrient concentrations were 300 μmol L^{-1} nitrate, 10 μmol L^{-1} phosphate, and 100 μmol L^{-1} silicic acid.

In iron-replete treatments (+Fe), 1,370 nmol L^{-1} of Fe_T was added in a 1:1 Fe:EDTA solution corresponding to a dissolved inorganic iron (Fe') concentration of 2.7 nmol L^{-1} (Marchetti et al. 2009). In order to growth limit *P. granii* by iron (-Fe), 200 nmol L^{-1} of the iron chelator desferroxiamine B (DFB) was added to 1.5 nmol L^{-1} Fe_T, yielding an Fe' concentration of approximately 0.02 pmol L^{-1} (Strzepek et al. 2012). The Fe:DFB solution was allowed to equilibrate overnight before being added to medium, and the final Aquil medium was allowed to chemically equilibrate overnight before use. Cells were grown in 28 mL acid-cleaned polycarbonate centrifuge tubes for a minimum of three growth cycles using the semi-continuous culture approach in order to pre-acclimate cells to the treatment conditions. For large culture experiments, acclimated cells were inoculated into Aquil medium that was dispensed into 4 L acid-cleaned, Milli-Q H_2O-rinsed polycarbonate bottles.

All experiments were inoculated when seed cultures were in mid-exponential growth phase. Cultures were grown under a continuous, saturating photon flux density of 110 μmol photons m^{-2} s^{-1}. The length of experiments was typically between 5 and 15 days, depending on iron treatment. Cultures were maintained at 12°C and stirred for the duration of the pre-acclimation and experimental periods to prevent cells from settling. Subsamples were withdrawn daily under a TMC laminar flow hood to monitor growth rates and changes in cell density, as well as to ensure cells remained in the exponential growth phase throughout the experimental period.

Iron status was determined through measuring growth rates and maximum photochemical yields of PSII (F_v:F_m). Growth rates (μ) were calculated by measuring changes in the natural log

of *in vivo* fluorescence over time using a Turner Designs model 10-AU fluorometer, as described in (Brand et al. 1981). F_v:F_m was obtained by measuring fluorescence induction with a Satlantic FIRe fluorometer (Gorbunov and Falkowski 2005). Before each measurement, a subsample (5 mL) of each culture was placed in the dark for 20 minutes. A short, saturating pulse of blue light (450 nm) was applied to dark-acclimated phytoplankton for a 100 µs duration to measure fluorescence induction from minimum (F_o) to maximum (F_m) fluorescence yields. F_o and F_m were used to estimate F_v:F_m from $(F_m - F_o) F_m^{-1}$. Values were calculated for each culture upon harvesting during the mid-exponential growth phase. Measurements were performed using multiple-turnover flash (MTF).

Transcriptomic analysis of acclimated experiments

P. granii cells in 500 mL of culture medium were harvested for RNA analysis from both acclimated iron-replete and iron-limited conditions. Cells were directly collected onto 3 µm polycarbonate filters (Millipore; 25 mm) using vacuum filtration. Filters were immediately stored at-80°C until RNA extractions were performed using the RNAqueous 4-PCR kit (Ambion) following manufacturer's protocols. To remove DNA contamination, RNA was incubated with deoxyribonuclease (DNase) I at 37°C for 45 minutes and purified with DNase inactivation reagent (Ambion). RNA concentrations were measured using a NanoDrop spectrophotometer, and samples containing concentrations <100 ng μL^{-1} were concentrated using the RNeasy MinElute Cleanup Kit (Qiagen). Quantitative PCR (qPCR) with the RNA samples was performed to test for DNA contamination levels, and samples with amplification of DNA products were given an additional round of the DNase incubation.

For transcriptomic sequencing, total RNA was prepared with the Illumina TruSeq Stranded mRNA Library Preparation Kit. RNA from three replicate cultures within iron-replete treatments and two replicate cultures from iron-limited treatments were separately prepared for sequencing. Barcoded samples were sequenced on a single lane of Illumina MiSeq (150 bp, paired-end). Sequencing statistics are provided in Table 4.1.

Raw reads were trimmed of poor quality bases and adapters using Trimmomatic v0.32 (paired-end mode, adaptive quality trim with 40 bp target length and strictness of 0.6, minimum length of 36bp; Bolger et al. 2014). Trimmed reads were assembled using Trinity v2.2.0 (Grabherr et al. 2011). Read counts were obtained by quasi-mapping raw reads to contigs with Salmon v0.6.0 (ISF library type; Patro et al. 2015). Our *P. granii* transcriptome completeness was estimated to be 66% via BUSCO (Simão et al. 2015). Protein-coding regions were predicted using GeneMark-S-T (Tang et al. 2015). Functional annotations were assigned based on sequence homology to proteins in the Kyoto Encyclopedia of Genes and Genomes database (KEGG; Release 75) via BLASTp v2.3.0 with an Expect (E)-value cutoff of 10^{-3} (Altschul et al. 1990).

All read counts corresponding to identical genes, or KEGG Orthology (KO), were summed together. For genes without KO assignments but possessing an annotated gene definition according to KEGG or NCBI (e.g. *ISIPs, RHO),* read counts corresponding to these definitions were summed. The R package edgeR v3.12.0 was used to calculate normalized counts, fold change, and counts-per-million (CPM) from pairwise comparisons between iron-replete and iron-limited samples. For determining differential expression, the edgeR exact test was performed, which uses a similar statistical procedure to the Fisher exact test (Robinson and Smyth 2008; Robinson et al. 2010).

Table 4.1. Sequencing statistics of Illumina Miseq run with acclimated cultures (left) or 454/SOLiD run with iron-resupply cultures (right). (+Fe) = iron-replete, (-Fe) = iron-limited. Replicate transcriptomes are denoted with the replicate number beside the treatment label.

	Assembly	**+Fe (1)**	**+Fe (2)**	**+Fe (3)**	**-Fe (1)**	**-Fe (2)**	**Assembly**	**+Fe**	**-Fe**
Read data									
No. of paired-end reads post filtering		6,125,358	6,357,880	5,024,008	6,580,188	5,264,142		14,670,144	9,721,565
Avg length of trimmed forward read (bp)		125.6	124.9	118.9	125.0	124.7		47	47
Assembly									
No. of contigs	69,581						14,989		
N50	1,199						835		
Mapping rate		99.2%	99.1%	98.0%	98.9%	98.2%		33%	32%
Quality									
BUSCO (complete and complete/single-copy)	66%						21%		
KEGG annotation									
No. of contigs with functional annotation	16,431 (24%)						3,717 (25%)		

Iron resupply experiments and transcriptomic analysis

The diatom *Pseudo-nitzschia granii* was again used in iron resupply experiments. This diatom was also obtained and isolated from iron-enriched OSP surface waters, though three years earlier (2008) than the isolate used in acclimated experiments. Therefore iron resupply experiments were conducted with a different species strain (UWOSP1E) than those of acclimated experiments (UNC1102). Iron-limited cells were achieved by culturing in Aquil media containing a premixed Fe-EDTA (1:1) solution at a Fe_T concentration of 1.5 nmol L^{-1}. Cells were acclimated to these low iron conditions using the semi-continuous batch culture technique until growth rates did not vary by more than 10% (4-5 transfers). Acclimated iron-limited *P. granii* cells were inoculated into 20 L of Aquil medium and grown at similar temperature and light conditions as described previously. Upon entering the mid-exponential growth phase, 15 L of the iron-limited culture medium was removed, cells were filtered onto Millipore Supor membrane filters (0.45 µm, 47 mm), and immediately flash-frozen and stored at -80°C. A pulse iron addition (resupply) was then performed by adding 1,370 nmol L^{-1} Fe_T to the remaining 5 L of iron-limited cell culture. Photophysiology was assessed through F_v:F_m prior to and following the iron resupply. Following 24 h, the cells remaining in the medium were harvested as previously described.

RNA extractions from individual filters were performed using kits and protocols as described previously. A combination of sequencing approaches were used on this mRNA, resulting in a single 454 sequence library from iron-resupplied cells and SOLiD sequence libraries from both iron-limited and iron-resupplied cells. To obtain enough mRNA for the 454 pyrosequencing and SOLiD sequencing, three 20 L culture experiments were performed and the mRNA from each experiment was pooled. For 454 pyrosequencing, 10 µg of iron-replete *P.*

granii mRNA was reverse transcribed into ds cDNA and sequenced. For SOLiD sequencing, 2.1 µg (iron-limited) and 1.4 µg (iron-resupplied) of *P. granii* ds cDNA was fragmented to an average size of 125 bp using a Covaris S2 System sonicator. The cDNA was then end-repaired using Polishing Enzymes 1 and 2 (Applied Biosystems) to create blunt ends according to the SOLiD protocol. P1 and P2 adaptors were ligated to the cDNA, and the cDNA was Nick-translated. PCR amplification was performed using 5 cycles and 2 cycles for iron-enriched and iron-limited *P. granii* cDNA, respectively. The amplified cDNA fragments were purified using the PureLink PCR Purification Kit (Invitrogen). Each sample was diluted to 60 pg μl^{-1}. Two and four emulsion PCRs were performed for iron-resupplied and iron-limited *P. granii* cDNA, respectively. Forty-one million beads of each sample were loaded on to two spots of an eight spot slide, and run on an Applied Biosystems SOLiD sequencer version 3 Plus.

Functional annotation of genes was determined with the iron-resupplied 454 reads using the methodology described previously. Iron-limited and iron-resupplied SOLiD reads were mapped to 454 reads using the aligner BWA v.0.5. Differential gene expression was performed with edgeR v3.12.0 as described previously, with the exception of no sequence replicates. Sequencing statistics are provided in Table 4.1.

Global proteomic analysis of steady-state cultures

For proteomic analysis, *P. granii* cultures were grown in duplicate 4 L acid-cleaned polycarbonate bottles under acclimated iron-replete and iron-limited conditions using the culture methodology described previously. After reaching mid to late exponential growth phase, cells were filtered onto 0.45 um polyethersulfone filters (0.45 µm, 42 mm), re-suspended in 5 mL of

Aquil filtrate, and centrifuged (12,000 rpm) into pellets that were immediately frozen at -80°C until analysis.

Protein digestion was performed according to Cox and Saito (2013). Briefly, pellets were exposed to 100 mM ammonium bicarbonate buffer solution at pH 8 (AMBIC). Sonication was performed with a Branson sonifier 450, and samples were centrifuged at 14,000g and 4°C for 35 min. Approximately 200 µL of supernatant was precipitated overnight with acetone at -20°C. The precipitated samples were centrifuged at 14,000g and 4°C for 30 min, and 100 µL of 7.5M urea in AMBIC was added to the acetone-precipitated pellet. Next a series of incubation steps was performed consisting of 200 mM dithiothreitol (DTT), 200 mM iodacetamide, and an additional 200 mM DTT (Cox and Saito 2013). Protein yield was determined using the BioRad DS Protein Assay. Trypsin was added in a trypsin:protein ratio of 1:50. The samples were mixed and incubated for approximately 16 hours at 37°C. The digested material was analyzed via liquid chromatography tandem mass spectrometry (LC/MS) using a Paradigm MS4 HPLC system with reverse phase chromatography and Thermo LTQ ion trap mass spectrometer (2µL min^{-1} flow rate, C18 column). Mass spectra were processed using SEQUEST software. Relative protein abundance was determined by calculating a spectral counting score with Scaffold 3 Proteome Software using a peptide false discovery rate of 5%.

Proteome mass spectra were matched to the *P. granii* UWOSP1E transcriptome. Open reading frames were predicted using FragGeneScan (Rho et al. 2010), and functional annotation of peptides were assigned based on sequence homology to the KEGG database via BLASTp v2.3.0 and an E-value cutoff of 10^{-3}. Differential expression in pairwise comparisons was determined using the Fisher exact test ($p < 0.05$), and peptides with low spectral counts (<2) were filtered out.

It is important to note that detected mass spectra could only be functionally assigned to a protein if a complete match to a translated amino acid sequence derived from the transcriptome was possible. Since the reference transcriptome used here was obtained from a different strain (*P. granii* UWOSP1E) than used in the proteomic study (*P. granii* UNC1102), it is possible that proteins predicted to be expressed were not able to be identified due to 454/SOLiD sequencing errors or strain-specific differences in amino acid sequences. In addition, we are unable to quantify the abundance of one protein relative to another based on normalized total spectral counts. This is due to tryptic peptide biases that are introduced during protein digestion; large proteins with many tryptic peptides have higher counts associated with them compared to similar abundances of small proteins with few tryptic peptides, therefore it is difficult to quantitatively compare relative abundances across proteins.

Results and Discussion

Comparison of the transcriptome and proteome under acclimated conditions

P. granii UNC1102 cultures grown for transcriptomic and proteomic analysis experienced iron limitation of growth, with average relative growth rates significantly reduced by >2-fold ($p < 0.02$; Fig. 4.2). Individual cultures grown for transcriptomic assessment grew at 1.77 ± 0.03 day^{-1} under iron-replete conditions and 0.67 ± 0.13 day^{-1} when iron-limited (Fig. 4.3A), while separate cultures grown for proteomic assessment reached a maximum rate of 2.16 ± 0.12 day^{-1} under iron-replete conditions and 0.97 ± 0.03 day^{-1} when iron-limited (Fig. 4.3B). These differences in specific growth rates may be attributed to the time between culturing experiments (two years). Similar to the iron-limited growth rates, F_v:F_m values significantly

decreased under iron limitation by approximately 10% ($p < 0.03$; Fig. 4.2). In addition, the cell morphology of *P. granii* was visually distinct under iron limitation. Iron-limited diatoms decrease in biovolume by elongating in length and decreasing their width, because this increases their surface area to volume ratio (Pahlow et al. 1997; Marchetti and Cassar 2009), and this phenomenon was consistently observed via light microscopy over the duration of these experiments.

Comparative transcriptomic analysis yielded the detection of 3,324 transcripts with functional annotations to KEGG Orthology (KO) genes, of which 338 were considered preferentially expressed under acclimated iron-replete conditions and 230 preferentially expressed under acclimated iron-limited conditions ($p < 0.05$; Fig. 4.4A). Proteomic analysis detected 545 proteins corresponding to KOs (Fig. 4.5). Approximately 239 of these peptides were significantly differentially expressed between acclimated iron-replete and iron-limited conditions, but KEGG annotations were not available for 114 of them (48%), and their cellular function is unclear. Of these peptides with KEGG annotations, 63 significantly increased under iron-replete conditions and 62 significantly increased under iron limitation ($p < 0.05$; Fig. 4.5; Zhang et al. 2006).

Certain iron-related genes and proteins of interest showed strong agreement between transcriptomic and proteomic expression responses to iron treatments (HSP70: heat shock protein 70; FBA class I: fructose biphosphate class I; FLDA: flavodoxin; ISIP1: Iron starvation induced protein 1; Fig. 4.6). However, others demonstrated little coherence (HSP90: heat shock protein 90; ISIP2A: Iron starvation induced protein 2A; PETE: plastocyanin; Fig. 4.6). Possible causes of this discrepancy include post-transcriptional regulation and differential mRNA and protein stability. A Pearson correlation coefficient of ~0.4 has been reported between mRNA

transcript and protein abundance based on averages from available data sets, suggesting transcript abundance may only explain 40% of the variation in protein expression (Vogel and Marcotte 2012). A similar correlative analysis was not possible with our transcriptomic and proteomic data sets, given that the global proteomic approach does not allow for quantitative abundance estimates across distinct peptides. Nevertheless the two methods have been shown to be congruent with regards to nutrient stress biomarkers in diatoms; both transcripts and proteins corresponding to components of phosphate metabolism are elevated under phosphate-limited conditions (Dyhrman et al. 2012), and both vitamin B_{12}-acquisition transcripts and proteins are abundant in response to vitamin B_{12}-limitation (CBA1; Bertrand et al. 2012). We add here the agreement between gene and protein expression of HSP70, ISIP1, FBA class I, and FLDA in *P. granii* under iron limitation (see further discussion below).

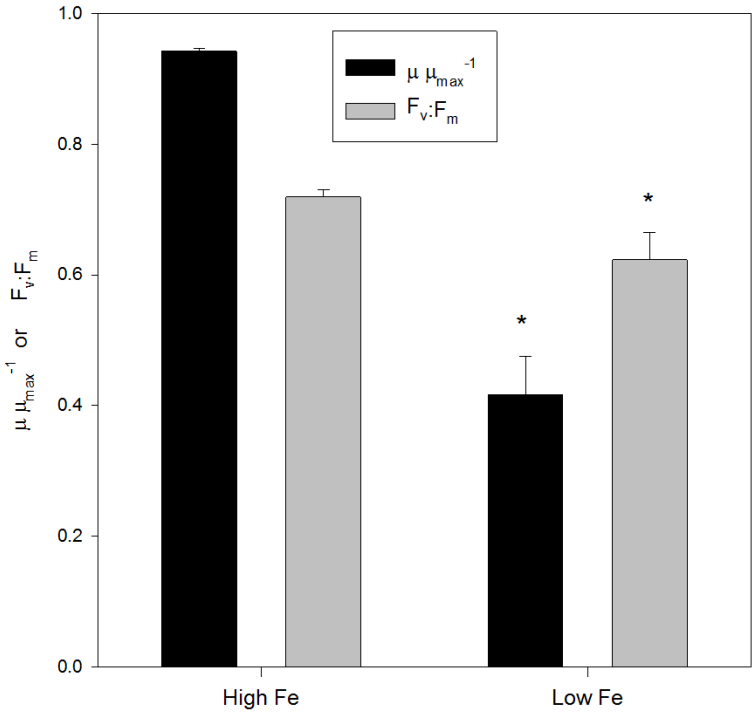

Fig. 4.2. Relative growth rates (μ μmax^{-1}) and maximum photochemical yield of PSII (F_v:F_m) within acclimated iron-replete and iron-limited cultures of *P. granii*. Values are averaged between transcriptomic (*n* = 3) and proteomic cultures (*n* = 3). Asterisks (*) represent a significant decrease in measurements as compared to iron-replete conditions ($p < 0.05$).

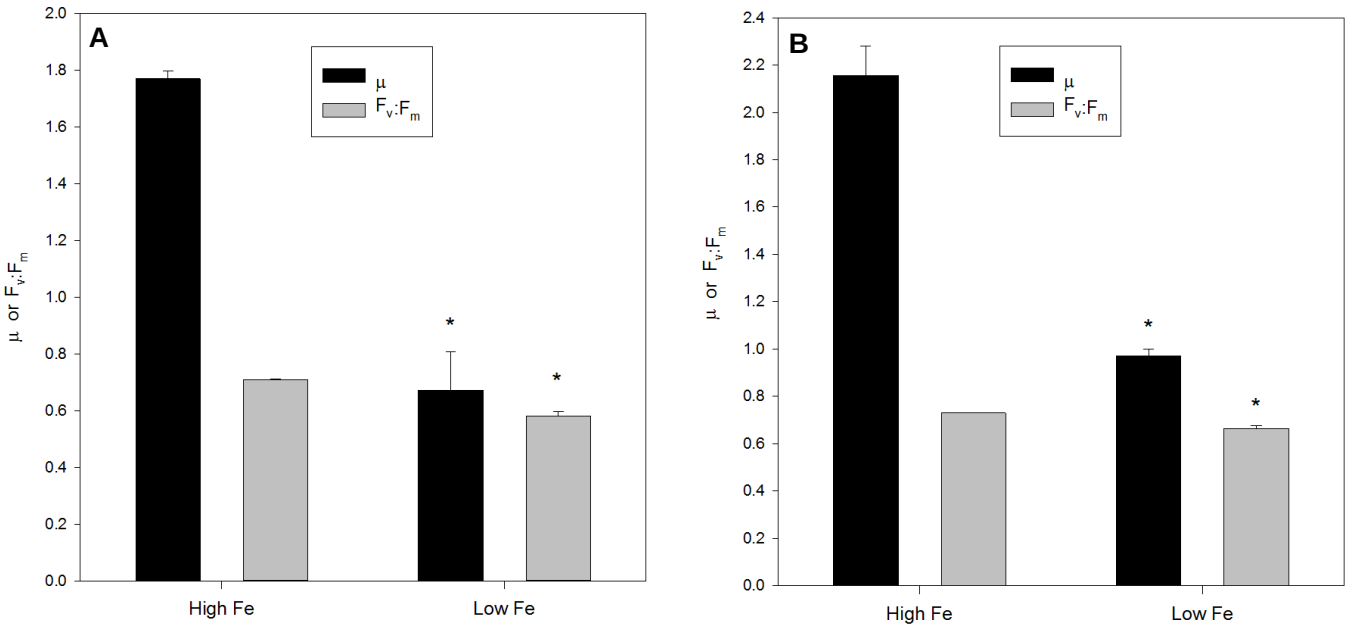

Fig. 4.3. Specific growth rates of acclimated iron-replete and iron-limited *P. granii* and maximum photochemical yield of PSII (F_v:F_m) measured within cultures grown for transcriptomic (**A**) or proteomic analysis (**B**). Asterisks (*) represent a significant decrease in measurements as compared to iron-replete conditions ($p < 0.05$).

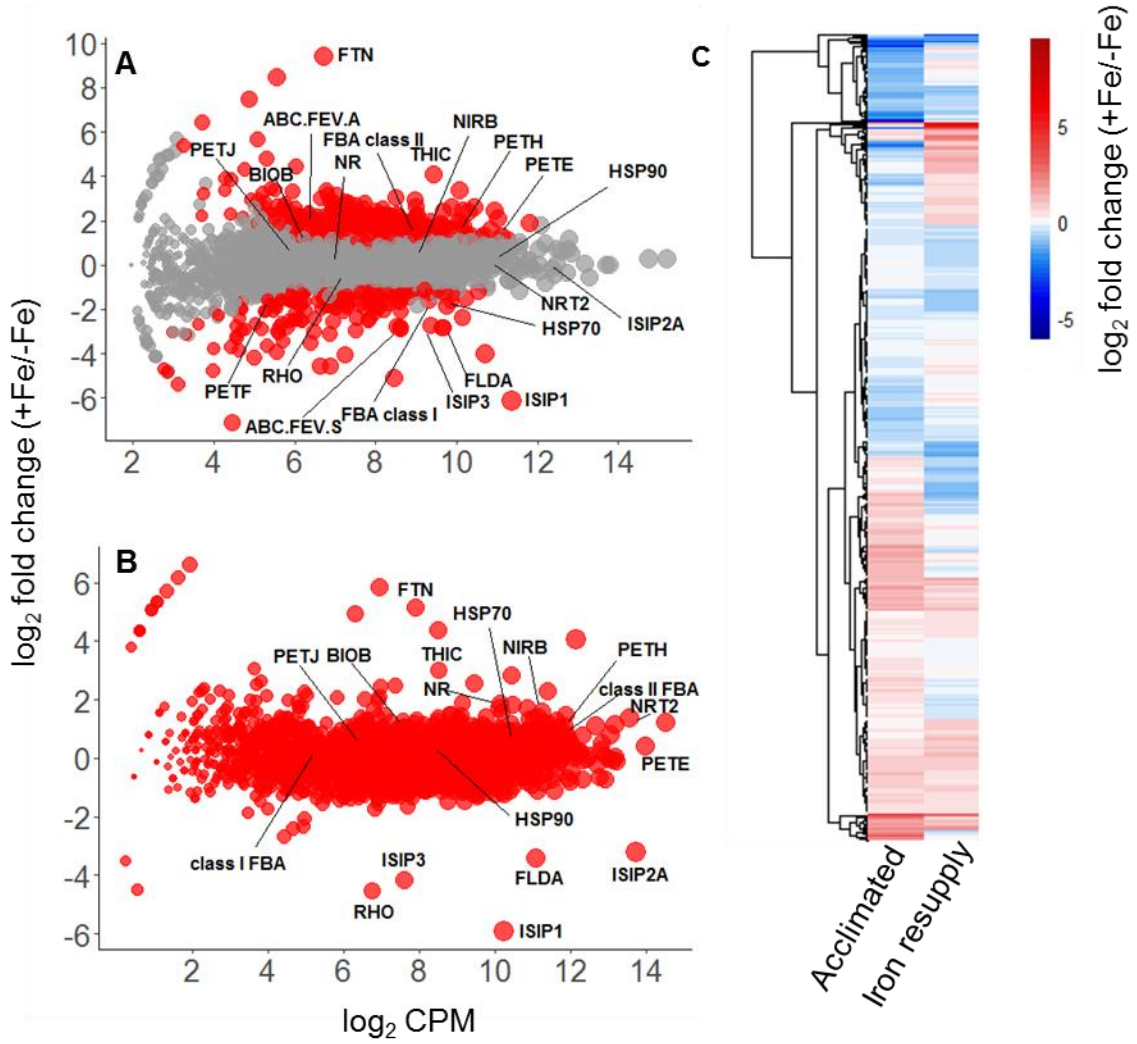

Fig. 4.4. Transcriptomic response in *P. granii* in relation to iron status. **A**) MA plot depicting the differential expression of genes between acclimated iron-replete (+Fe) relative to iron-limited (-Fe) cells. Each point corresponds to a unique gene (KO). Points are colored in red if significantly differentially expressed between treatments ($p < 0.05$). **B**) MA plot depicting the differential expression of genes following iron resupply (+Fe) relative to iron-limited (-Fe) cells. **C**) Heatmap displaying the $\log_2$ fold change between iron-replete (+Fe) and iron-limited (-Fe) conditions, within acclimated and iron resupply experiments. The dendrogram reflects similarity in expression responses among genes and was created using Euclidean distance and hierarchical clustering. *PETJ*: cytochrome c_6; *PETH*: ferredoxin-NADP+ reductase; *PETE*: plastocyanin; *PETF*: ferredoxin; *FLDA*: flavodoxin; *ABC.FEV.S*: iron complex transport system substrate-binding protein; *ABC.FEV.A*: iron(III) dicitrate transport ATP-binding protein; *FTN*: ferritin; *RHO*: proteorhodopsin; *FBA class I/II*: fructose biphosphate aldolase I/II; *ISIP*: iron starvation induced protein; *NR*: nitrate reductase; *NIRB*: nitrite reductase; *NRT2*: nitrate transporter; *BIOB*: biotin synthase; *THIC*: phosphomethylpyrimidine synthase; *HSP*: heat shock protein.

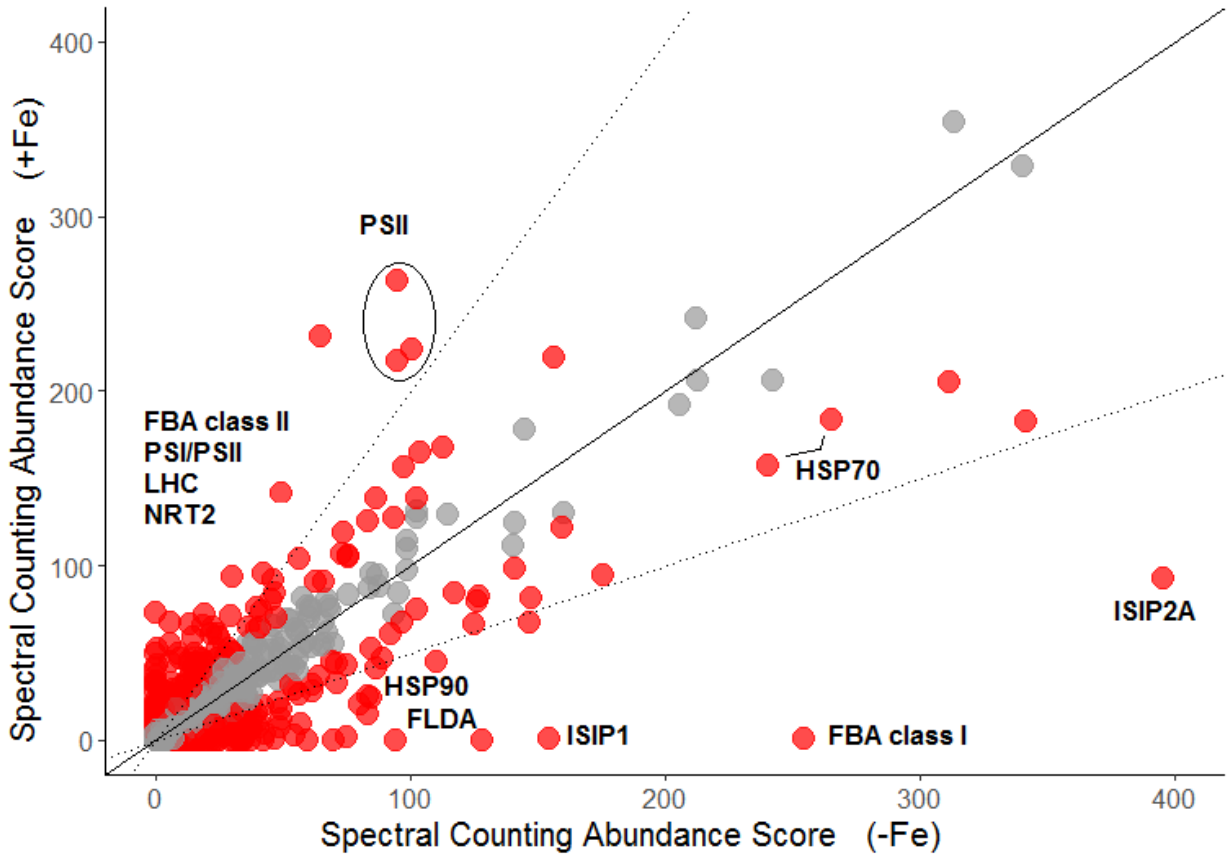

Fig. 4.5. Proteome response in *P. granii* under acclimated iron-replete (+Fe) or iron-limited (-Fe) conditions. Both peptides with and without functional annotations (KEGG, NCBI) are shown. Peptides are colored red if significantly differentially expressed between treatments as determined with the Fisher's exact test ($p < 0.05$). The solid line represents a 1:1 relationship between treatments, and dotted lines represent a 2:1 relationship, or relative 2-fold change. Spectral counting abundance scores should not be used to compare relative abundances across peptides. PSI/II: photosynthetic proteins and complexes; LHC: light harvesting complex; FLDA: flavodoxin; FBA class I/II: fructose biphosphate aldolase I/II; ISIP: iron starvation induced protein; NRT2: nitrate transporter; HSP: heat shock protein.

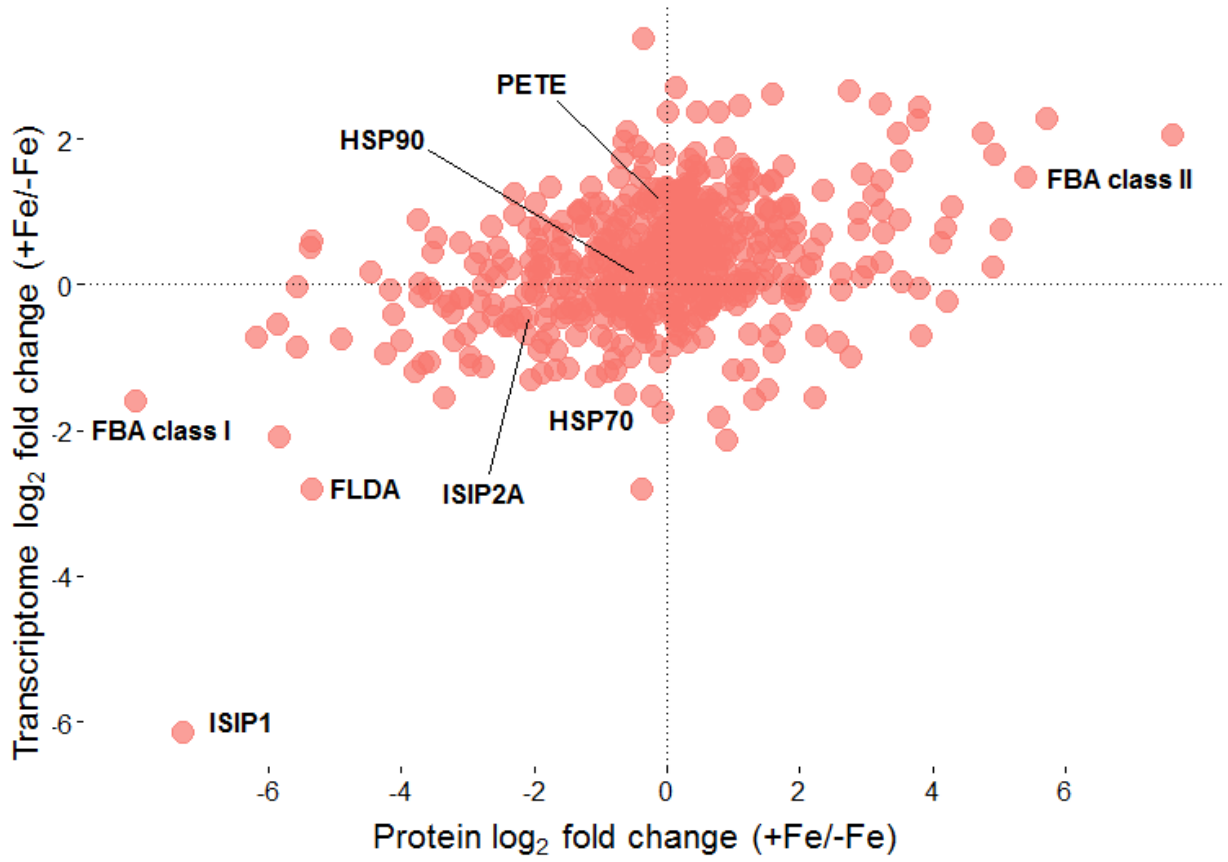

Fig. 4.6. Comparison of differentially expressed genes and proteins in *P. granii*. Depicted are the $\log_2$ fold change in gene and protein expression under acclimated iron-replete relative to iron-limited conditions (+Fe/-Fe). Only genes and proteins with KEGG annotations are shown. Genes of interest are annotated. PETE: plastocyanin; FLDA: flavodoxin; FBA class I/II: fructose biphosphate aldolase I/II; ISIP: iron starvation induced protein; HSP: heat shock protein.

Comparison of the transcriptomes under acclimated and iron-resupply conditions

P. granii UWOSP1E cells experienced iron limitation prior to the iron resupply, and growth rate and F_v:F_m rapidly increased immediately following the iron addition event (Fig. 4.7). The transcriptome under acclimated iron-replete conditions was compared to the transcriptome obtained directly following iron resupply. Among the 1,728 genes that were detected in both acclimated and iron resupply experiments, only 38 were consistently more highly expressed by >2-fold under iron-replete conditions in both experiments. This notably included ferritin (*FTN*; 678-fold in acclimated conditions; 35-fold following iron resupply) and the thiamine synthesis gene phosphomethylpyrimidine synthase (*THIC*; 17-fold in acclimated conditions; 8-fold following iron resupply). Similarly under iron limitation, only 19 genes were differentially expressed by >2-fold in both experiments, including flavodoxin (*FLDA*: 7-fold in acclimated conditions; 11-fold following iron resupply), iron starvation induced protein 3 (*ISIP3*; 6-fold in acclimated conditions; 18-fold following iron resupply) and iron starvation induced protein 1 (ISIP1; 69-fold in acclimated conditions; 60-fold following iron resupply). Furthermore, 370 genes showed highly divergent expression patterns with a >2-fold increase or decrease in expression that was not shared between the acclimated and iron resupply experiments (Fig. 4.4C). These relatively few genes with overlapping expression responses suggests substantial differences in cellular reorganization as a consequence of resupply versus acclimated growth variations with iron status.

Interestingly, the gene encoding proteorhodopsin (*RHO)*, an iron-independent, light-driven proton pump capable of generating ATP, was differentially expressed under iron limitation by 23-fold as compared to when cells were resupplied with iron, but was not differentially expressed under acclimated conditions (Fig. 4.4A-B). RHO proteins were not

detected in the proteome. This may suggest that *RHO* is only temporarily downregulated following pulse iron addition and once the iron demand is met, *RHO* expression may once again increase. Similar *RHO* transcript abundance between acclimated iron-replete and iron-limited conditions may furthermore indicate *RHO* is valuable in supplementing photosynthetic ATP production under both high and low iron concentrations.

Furthermore, transcripts for proteins involved in nitrate uptake and assimilation were elevated directly following the resupply of iron to iron-limited cells, with this response again not shared by cells exposed to acclimated iron-replete conditions (Fig. 4.4A-B). The gene encoding a nitrate uptake transporter, *NRT2*, increased in expression by 2-fold following iron resupply, though transcripts were not differentially expressed under acclimated iron-replete conditions. Furthermore genes encoding the nitrate assimilation proteins nitrate reductase (*NR*) and nitrite reductase (*NIRB*) increased in expression by >3-fold following iron resupply, but were similarly not differentially expressed between acclimated conditions (<1.6-fold change; $p \geq 0.97$; Fig. 4.4A-B). This tendency can be attributed to selective partitioning of iron resources, in which newly acquired iron is shuffled into iron-requiring pathways that were previously constrained by low iron availability. Such responses have been observed following iron fertilization in natural phytoplankton communities of the HLNC NE Pacific Ocean, with genes encoding nitrate assimilation proteins increasing in expression following iron enrichment (Cohen et al., in press; Marchetti et al. 2012). In contrast, the diatom *Phaeodactylum tricornutum* continues to highly express nitrate assimilation genes under acclimated iron-replete conditions (Allen et al. 2008).

A disconnect in transcript and protein expression was observed with the 2.7-fold higher protein expression of NRT2 under acclimated iron-replete conditions ($p = 0.04$; Fig. 4.5). NR similarly demonstrated 2-fold higher protein expression under acclimated iron-replete conditions

(although this was not statistically significant [$p = 0.11$]) whereas NIRB proteins were not detected. Given that *P. granii* cells under acclimated iron-replete conditions constitutively express nitrate uptake and assimilation genes, yet higher peptide abundances are observed, we conclude that the large increase in these transcripts following iron resupply is likely a temporary, immediate response with these transcripts later decreasing in abundance once adequate protein levels are levels of reduced amine nitrogen are reached.

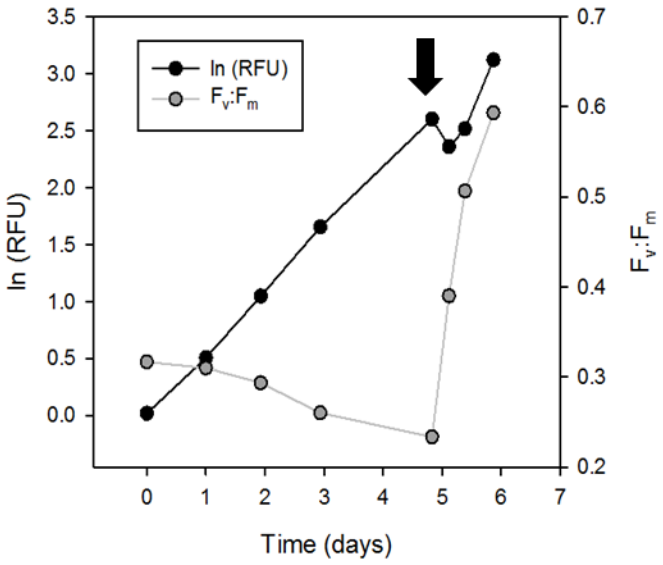

Fig. 4.7. *Pseudo-nitzschia granii* UWOSP1E growth dynamics and maximum photochemical yield of PSII (F_v:F_m) within non-acclimated iron resupply experiments. The natural log of the fluorescence units (lnRFU; black) and F_v:F_m (gray) are plotted as a function of time (days). The black arrow indicates the point in time in which the iron resupply was administered to iron-limited cells. Figure modified from Marchetti et al. (In press).

Bioindicators of iron status

Transcripts and proteins corresponding to fructose biphosphate aldolases (*FBA*), functioning in gluconeogenesis, glycolysis, and in the Calvin cycle, were identified with class II and class I forms differentially expressed depending on iron status. Transcripts for both genes were considered abundant (log_2CPM = 9.2; Fig. 4.4A). Transcripts for *class II FBA* were >3-fold

(p = 0.009) and proteins 40-fold ($p = 1x10^{-13}$) more abundant under iron-replete conditions, while *class I FBA* transcripts were 3-fold (p = 0.002) and proteins 250-fold ($p = 1.8x10^{-77}$) more abundant under iron-limited conditions. FBA class I uses Schiff-based catalysis, not requiring a metal cofactor, while class II depends on metal catalysis (Horecker et al. 1972). The patterns we observed are consistent with laboratory cultures of *T. oceanica* and *P. tricornutum* grown under varying iron states, and has additionally been observed in naturally iron-limited diatom assemblages before and after iron addition (Lommer et al. 2012; Allen et al. 2012; Cohen et al. unpublished). Class II FBA is therefore hypothesized to contain iron as a metal cofactor.

Several genes demonstrated characteristic expression responses to iron status, consistent with established trends in other examined diatoms. Ferritin (*FTN*), an iron storage protein involved in maintaining iron homeostasis (Marchetti et al. 2009; Botebol et al. 2015), was one of the most differentially expressed genes in both resupply (34-fold) and acclimated iron-replete conditions (690-fold; $p = 2.8x10^{-12}$; Fig. 4.4; Fig. 4.8), whereas ferritin proteins were not detected. This pattern of increased *FTN* under iron enrichment is consistent with ferritin playing a role in long-term iron storage in this diatom (Marchetti et al. 2009; Cohen et al. submitted). Similarly, the ABC-type iron-binding transporter gene *ABC.FEV.A* was more highly expressed under acclimated iron-replete conditions by >2-fold (p = 0.047; Fig. 4.4B), suggesting this transporter may assist in the transfer of iron into the cell under high iron concentrations (Naka et al. 2013).

Changes in expression of a group of mostly uncharacterized, yet iron responsive, protein-encoding genes were also examined. *ISIP1* transcripts were abundant (log_2CPM = 11.4) and one of the most differentially expressed genes (by 64-fold; $p = 1.7x10^{-20}$) under acclimated iron-limited conditions, following similar trends to ISIP1 protein expression under iron limitation

(150-fold; $p = 3.4x10^{-47}$; Fig. 4.8). *ISIP3* gene expression similarly increased by 6-fold and 18-fold under iron limitation in both acclimated ($p = 3.4x10^{-7}$) and iron resupply experiments, respectively, though was not detected in the proteome. Both ISIP1 and ISIP3 have been observed to increase under iron stress though their function is not clear (Allen et al. 2008; Marchetti et al. 2012). *ISIP2A*, which is thought to function in iron acquisition (Morrissey et al. 2015), was not differentially expressed on the transcript level but was abundant ($p = 0.43$, $\log_2$CPM = 12.4), while the protein was 3-fold more abundant under iron limitation ($p = 6x10^{-46}$). *ISIP2B*, a gene also differentially expressed under iron limitation in some diatoms (Allen et al. 2008), was not detected in the *P. granii* transcriptome or proteome. The ABC-type iron-binding transporter *ABC.FEV.S* was 7-fold more highly expressed under iron limitation ($p = 2.5x10^{-8}$), but similarly not detected in the proteome. These proteins likely play important roles in maintaining growth during periods of iron limitation, given their high transcript and protein abundances and sensitivity to iron status observed within both laboratory and field analyses, although additional characterization is needed to clarify their exact cellular functions.

Iron limitation also appeared to result in an overall induced stress response in *P. granii*, with heat shock proteins among the most differentially expressed peptides identified in the proteome under acclimated iron-limited conditions (HSP70 and HSP90; $p < 0.01$; Fig. 4.5). *HSP70* was significantly more highly expressed under iron limitation ($p = 0.01$), although *HSP90* was constitutively expressed (Fig. 4.4A). Similar to *P. granii*, *Phaeodactylum tricornutum* increased expression of nine genes encoding heat shock proteins under acclimated iron-limiting conditions (Allen et al. 2008). The gene encoding HSP90 has been demonstrated to bind iron (Kovár et al. 2004) and along with HSP70 is actively involved in senescence, with increases in transcripts occurring during stationary and declining growth phases in the diatom

Skeletonema marinoi (Lauritano et al. 2015). These proteins therefore may directly aid in iron acquisition during periods of iron stress and/or aid in protecting the cell from unfavorable growth conditions by regulating cell cycle, hormones, and signaling pathways (Jackson 2013).

Collectively these results demonstrate that *P. granii* highly expresses certain iron-related genes under iron limitation (*HSP70, ABC.FEV.S, ISIP1, ISIP2A, ISIP3, FBA class I*) and conversely highly expresses others under iron-replete conditions (*FTN, ABC,FEV.A*). These trends are consistent with metatranscriptomic observations within natural *Pseudo-nitzschia* assemblages, and are likely adequate bioindicators of iron status for this genus in the natural environment (Fig. 4.6; Cohen et al. unpublished; Marchetti et al. submitted). These strategies aid in our understanding of how *P. granii* acquires iron externally, maintains growth under iron stress, and efficiently stores iron intracellularly when it becomes bioavailable.

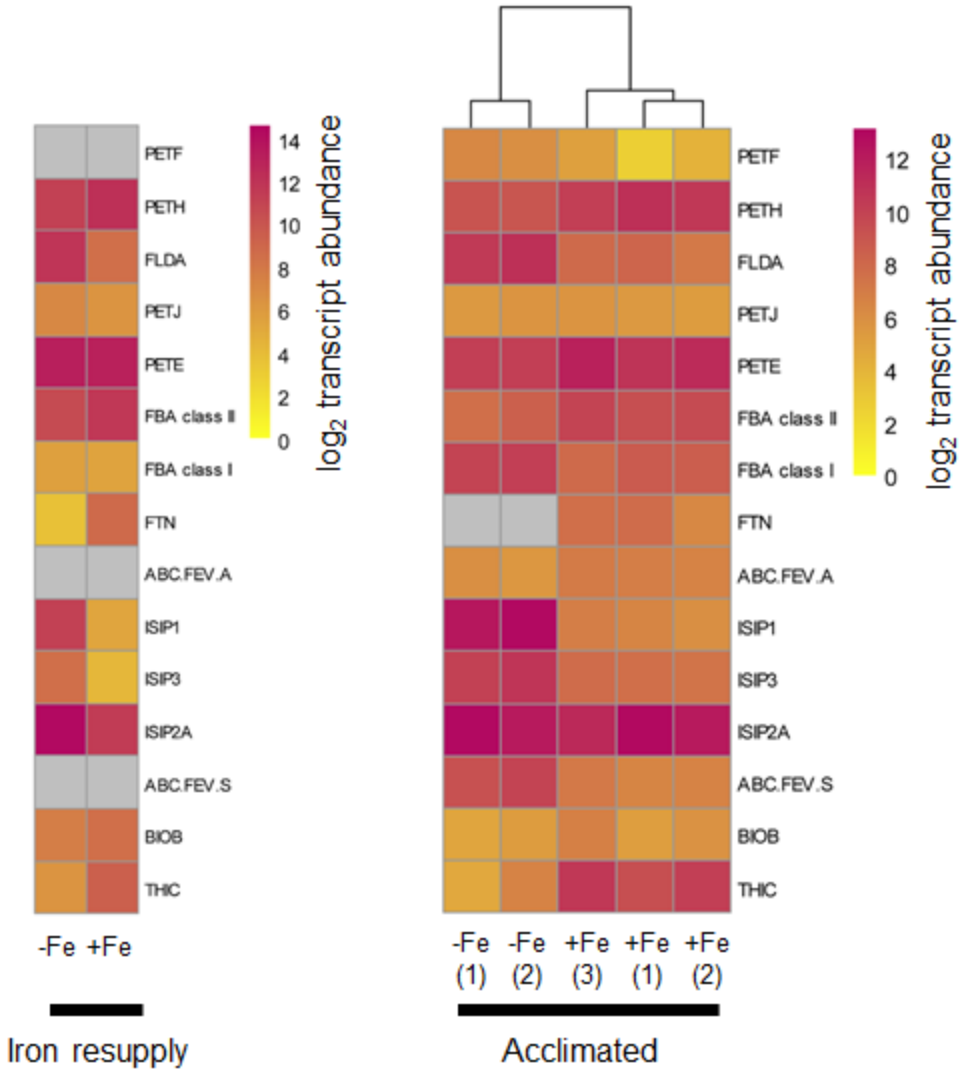

Fig. 4.8. Heatmap displaying log_2 normalized transcript counts (abundance) for genes of interest across iron-replete (+Fe) and iron-limited (-Fe) conditions, within acclimated and iron resupply experiments. Replicate transcriptomes are denoted with a number under the treatment. Gray indicates no transcripts were detected in the transcriptome. *PETF*: ferredoxin; *PETH*: ferredoxin-NADP+ reductase; *FLDA*: flavodoxin; PETJ: cytochrome c_6; PETE: plastocyanin; *FBA class I/II*: fructose biphosphate aldolase I/II; *FTN*: ferritin; *ABC.FEV.A*: iron(III) dicitrate transport ATP-binding protein; *ISIP*: iron starvation induced protein; *ABC.FEV.S*: iron complex transport system substrate-binding protein; *BIOB*: biotin synthase; *THIC*: phosphomethylpyrimidine synthase.

Photosynthesis-related protein substitutions

Several genes encoding iron-independent proteins known to function as replacements for iron-dependent proteins were detected in the *P. granii* transcriptomes, with varying gene and protein expression responses (Fig. 4.4A). The replacement of iron-dependent ferredoxin (PETF)

for iron-independent flavodoxin (FLDA) during electron transport under iron limitation has been documented in several diatom laboratory studies (LaRoche et al. 1995; Douchette et al. 1996; Erdner and Anderson 1999; McKay et al. 1999; Allen et al. 2008). Although *FLDA* transcripts and proteins were more highly expressed in the acclimated iron-limited cells by 5-fold ($p = 3.8x10^{-7}$) and 38-fold ($p = 3.7x10^{-20}$) respectively, a replacement of *FLDA* with *PETF* under acclimated iron-replete conditions was not apparent in *P. granii*. Instead, *PETF* transcript abundance was low compared to *FLDA* transcripts (log_2CPM = 5.5 for *PETF* versus 9.6 *FLDA*), and the PETF protein was not detected under either condition. This is in contrast to most laboratory studies demonstrating *PETF* transcripts to be orders of magnitude more abundant than *FLDA* in the diatom genus *Thalassiosira* (Whitney et al. 2011). In addition, iron-dependent *PETF* transcripts were actually 2-fold more highly expressed under acclimated iron-limited conditions ($p = 0.01$; Fig. 4.4A; Fig. 4.8). PETF proteins have also been reported to be more highly expressed under iron limitation in the pennate diatom *Phaeodactylum tricornutum* (Graff van Creveld et al. 2016), and this pattern is again consistent with field observations of *Pseudo-nitzschia*-dominated natural assemblages (Cohen et al., unpublished). However, constitutive expression of *PETF* transcripts in response to iron status has been reported within the centric diatoms *Thalassiosira pseudonana* and *Thalassiosira weissflogii* (Whitney et al. 2011). Together these results support a role of PETF under iron-limited conditions in the pennate diatoms, with perhaps a constitutive function in the centric diatoms.

Interestingly, the gene encoding ferredoxin-NADP+ oxidoreductase (*PETH*), an enzyme that received electrons from either reduced PETF or FLDA and thereby converts $NADP^+$ to NADPH (Kurisu et al. 2001), showed higher expression under acclimated iron-replete conditions ($p = 0.008$; Fig. 4.4A). Furthermore *PETH* transcripts were abundant in either transcriptome

(log_2CPM = 10.2), though protein expression was constitutive. Assuming transcript abundance equates to protein abundance, an alternative to PETF could be primarily responsible for receiving electrons from PSI and transferring them to PETH for the production of reducing equivalents under iron-replete conditions. An amino acid alignment of the PETF identified in this transcriptome compared to characterized PETFs from other model diatoms *P. tricornutum*, *T. pseudonana* and *T. oceanica* demonstrates that the *P. granii* PETF sequence resembles that of the HNLC Southern Ocean diatom *Fragilariopsis cylindrus* (71% similarity; Fig. 4.9). Further investigation into functional roles of PETF within HNLC diatoms vs. non-HNLC diatoms is required to determine if amino acid sequence differences equate to differences in functional roles.

The gene encoding cytochrome c_6 (*PETJ*), an iron-containing protein involved in photosynthetic electron transport, was neither differentially expressed (p = 0.97), nor abundant (log_2CPM = 5.7; Fig. 4.4A) under either high or low iron acclimated conditions and furthermore was not detected in the proteome. Transcripts of the gene encoding the copper-containing functional replacement for this protein, plastocyanin (*PETE),* were significantly more abundant under iron-replete conditions (p = 0.05; Fig. 4.4A), and 40-fold more abundant than *PETJ* transcripts (log_2CPM = 11; Fig. 4.8), although PETE was not differentially expressed in the proteome (p = 0.65). These *PETE* transcript and protein expression patterns suggest that *P. granii* is adapted to a chronically iron-limited environment and utilizes iron-independent plastocyanin even under acclimated iron-replete conditions, and not as a temporary replacement under iron limitation as demonstrated with *FLDA*. This finding is consistent with previous observations of *PETE* being constitutively expressed within other oceanic diatoms regardless of iron status (Peers and Price 2006; Lommer et al. 2012). We conclude that certain photosynthetic

substitutions in *P. granii* are temporary and based on iron status, while others appear to be permanent.

Influence of iron status on vitamin synthesis

Iron is hypothesized to influence vitamin B_1 (thiamine) and B_7 (biotin) metabolism due to the presence of iron-sulfur (Fe-S) clusters in enzymes involved in the production of these vitamins. Although biotin is biosynthesized by *P. granii* (Cohen et al. in press), it is unclear whether this diatom species biosynthesizes thiamine. Growth media used in laboratory experiments presented here contained thiamine, biotin, and cobalamin at concentrations specified by Price et al. (1988/89), which are generally in concentrations orders of magnitude higher levels measured in the coastal ocean (Sañudo-Wilhelmy et al. 2012). Many marine heterokonts are thiamine producers that do not require exogenous thiamine to grow; *P. multiseries* does not require thiamine in the growth medium, whereas *P. pungens* does (Tang et al. 2010; Sañudo-Wilhelmy et al. 2014).

The thiamine biosynthesis gene *THIC* (phosphomethylpyrimidine synthase), encoding an enzyme containing 4Fe-4S clusters, was one of the most differentially expressed genes under iron-replete conditions in both acclimated and iron resupply experiments. *THIC* gene expression was >3.5-fold higher in the acclimated high iron cultures ($p = 6.8 \times 10^{-8}$) and transcripts were generally abundant (Fig. 4.4A-B), although the enzyme was not detected in the proteome. Other thiamine biosynthetic transcripts were also detected and likewise highly expressed under acclimated iron-replete conditions, including hydroxymethylpyrimidine kinase (*THIDE*; 2.8-fold; $p = 0.003$) and thiamine-phosphate pyrophosphorylase (*THIE;* 2.6-fold; $p = 0.04$). Although transcripts of the biosynthetic gene thiazole synthase (*THIG*) were detected and abundant ($\log_2$CPM = 12.1), transcript levels were not different between iron conditions ($p =$

0.19). Remaining genes involved in thiamine biosynthesis (Paerl et al. 2015) were not identified in the transcriptome, either due to lack of sequencing depth, low transcript abundance, or possible absence from the genome. Overall, the thiamine biosynthesis KEGG module was more highly expressed under iron replete conditions by 16-fold and was one of the most differentially expressed modules detected (Fig. 4.10).

The continued expression of thiamine biosynthesis genes despite thiamine being added to the culture medium could be explained by one of the following possibilities: a) *P. granii* does not have a mechanism to take up thiamine from the environment, or b) thiamine and/or vitamin B_{12}(cobalamin) was depleted in the *P. granii* culture, with cobalamin-limitation perhaps causing an increase in *THIC* expression through S-adenosyl methionine (AdoMet) starvation (Bertrand et al. 2012), and/or c) *P. granii* takes up only thiamine intermediates and biosynthesizes the final product. If *P. granii* does not possess the complete biosynthetic machinery necessary to produce thiamine, it may be able to incorporate intermediates available in seawater to fulfill its requirement, as has been demonstrated in the coccolithophore *Emiliana huxleyi* (McRose et al. 2014). Depletion of vitamins from the culture medium is unlikely, given that growth rates did not decrease over the course of the experiments, with cells remaining in the exponential phase of growth.

Similar to thiamine, many chlorophytes, haptophytes and heterokonts (including diatoms) are capable of biotin biosynthesis, although there is significant variation even within a group. For example, *P. pungens* is auxotrophic for biotin in addition to thiamine, while *P. multiseries* and *P. granii* are able to survive without exogenous biotin (Tang et al. 2010; Sanudo-Wilhelmy et al. 2014). Biotin serves as a cofactor in carboxylation enzymes, most notably those involved in fatty acid synthesis, and is produced through a series of reactions beginning with the compound

pimeloyl-coenzyme A (Streit and Entcheva 2003). The last enzyme in the biotin pathway, BIOB, is an iron-dependent enzyme containing 4Fe-4S and 2Fe-2S clusters that facilitate binding of the precursor, dethiobiotin, and donate a sulfur atom to the biotin molecule itself (Jarrett 2005). *BIOB* gene expression in both the acclimated iron-replete and iron resupplied treatments increased by 2-fold relative to the iron-limited treatment (Fig. 4.4A-B). Although *BIOB* transcript abundance was relatively high within iron resupplied cultures (log_2CPM = 8.2), it was not in the acclimated cells (log_2CPM = 5.9; $p = 0.15$), nor was BIOB protein detected in the proteome. The biotin biosynthesis KEGG module, comprised of all biotin synthesis genes, exhibited 2-fold higher expression under acclimated iron-replete conditions compared to that observed in iron-limited culture (Fig. 4.10). Thus, the increased gene expression was likely due to a combination of iron being available for biosynthesis as well as increased growth rates that result in additional vitamins needed to support elevated rates of growth and metabolism.

A

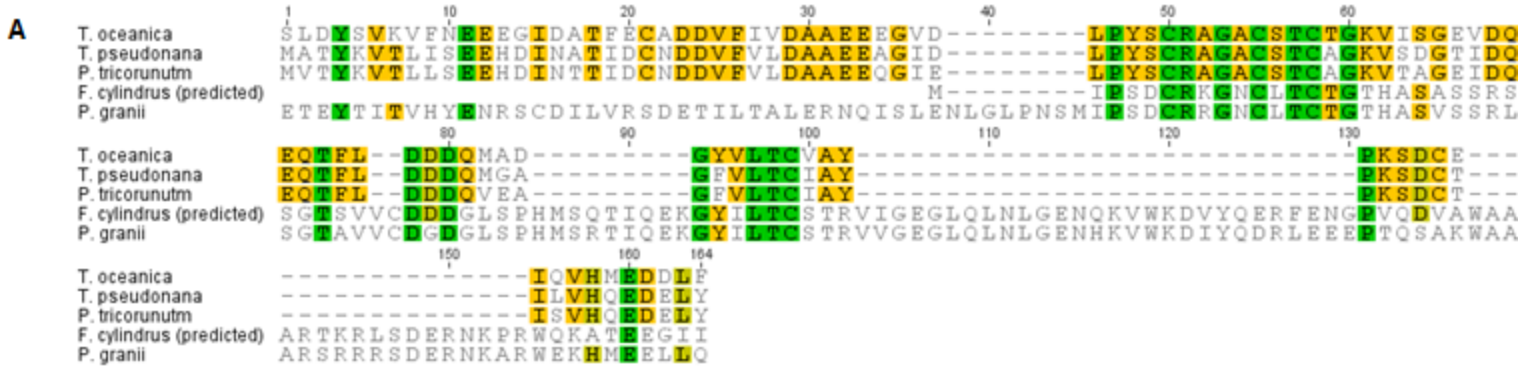

B

	T. oceanica	T. pseudonana	P. tricorunutm	F. cylindrus	P. granii
T. oceanica	100	67.7	65.7	20	11.6
T. pseudonana	67.7	100	88.9	16.7	13.4
P. tricorunutm	65.7	88.9	100	16.7	14
F. cylindrus	20	16.7	16.7	100	61.6
P. granii	11.6	13.4	14	61.6	100

Fig. 4.9. **A**. Alignment of ferredoxin (PETF) amino acid sequence identified within the *P. granii* transcriptome compared to PETF from other model diatom species Alignment was created using MUSCLE within Geneious version 5.6.4 (Edgar 2004; Tamura et al 2013). Residues are color-coded by blosum62 score matrix similarity (threshold = 5); residues with 100% similarity are represented in green, 80-100% in gold, 60-80% in yellow, and less than 60% in white. **B**. Percent similarity of amino acids residues between isolates in A.

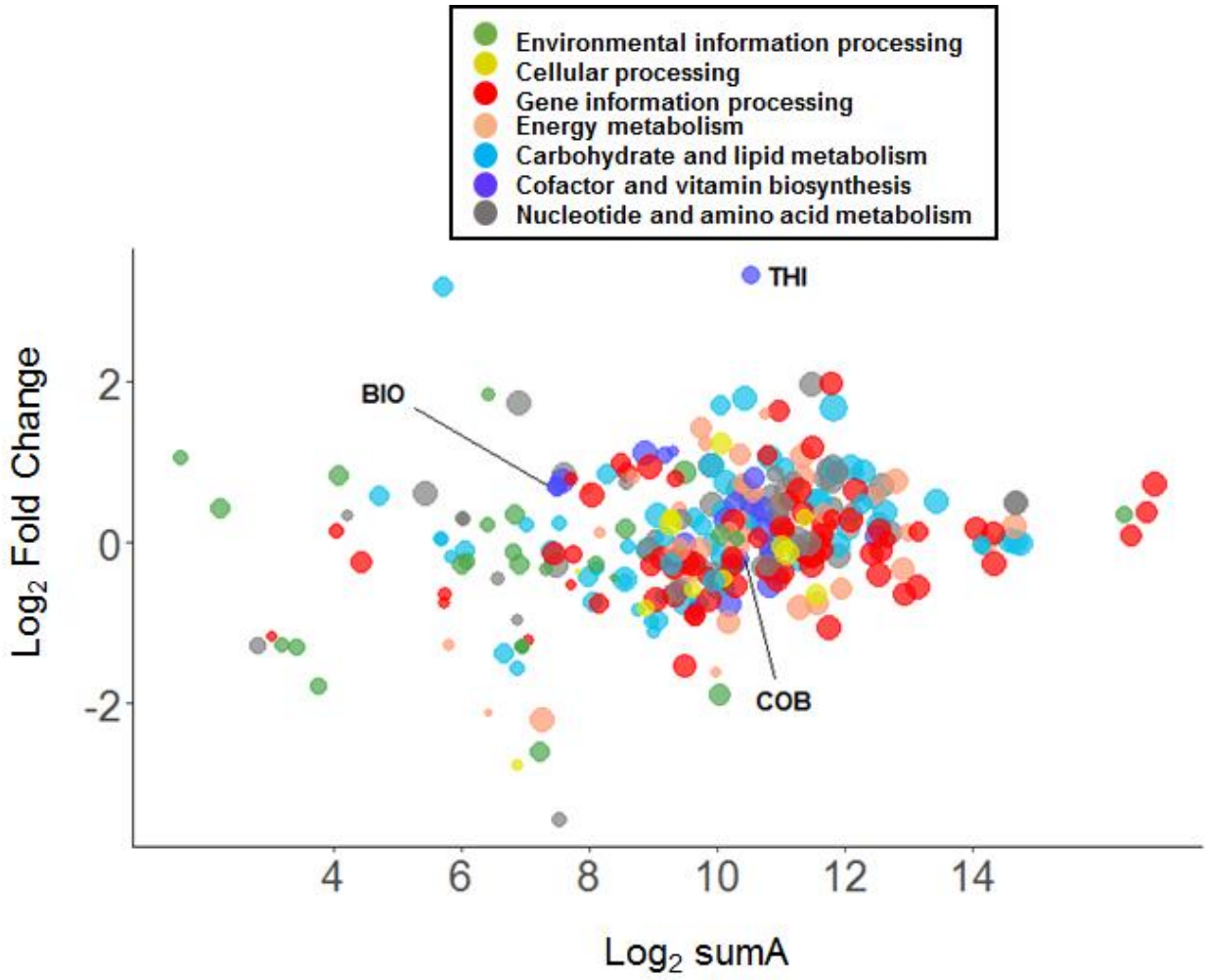

Fig. 4.10. MA plot displaying module expression between acclimated iron-replete (+Fe) and iron-limited (-Fe) transcriptomes. Normalized counts corresponding to individual genes (KOs) were summed by module; each point on the plot corresponds to a unique KEGG module. Modules are colored based on class2 and class3 KEGG groupings. Log_2 fold change represents the fold change between iron-replete and iron-limited conditions (+Fe/-Fe), while log_2 sumA represents the average normalized counts between treatments. Points increase in size with higher percentages of module completeness. COB: cobalamin synthesis; BIO: biotin synthesis; THI: thiamine synthesis.

Conclusion

We conclude the HNLC diatom *P. granii* has multiple strategies for sustaining growth at low iron levels and for rapidly blooming once iron becomes available in the environment. Notable cellular responses to iron status were observed with both transcript and protein levels, including the increase in flavodoxin (FLDA) and iron-starvation-induced-proteins (ISIPs) under acclimated iron-limiting conditions, and the differential production of two distinct forms of

fructose biphosphate aldolases (FBAs) depending on the cellular iron status. Furthermore, several genes were differentially expressed only in iron-resupplied cells as compared to the acclimated iron-replete cells, including the increase in expression of proteorhodopsin (RHO) and nitrate assimilation genes. However there were also gene expression patterns that were consistent between acclimated and non-acclimated iron-replete conditions including the increased expression of genes encoding ferritin (FTN) and those involved in vitamin synthesis. Collectively these strategies contribute to our understanding of how *P. granii* sustains growth during periods of chronic iron limitation and may then rapidly restructure its transcriptome and proteome in response to iron pulse events to quickly become a dominate member of the iron-induced phytoplankton community in the NE Pacific Ocean in response to episodic increases in iron availability.

CONCLUSION

The findings presented in this dissertation have contributed to our understanding of how diatom species can restructure their iron metabolism to respond to iron scarcity in the coastal and open ocean. Each of the aforementioned studies could benefit from additional analyses to further substantiate the impacts of changes in iron availability on natural phytoplankton communities, and these are discussed below. Furthermore, the studies presented here may prove useful in guiding and interpreting future field analyses, in identifying diatom biomarkers of environmental stress, and in predicting ocean productivity using taxa-specific physiological traits.

Findings from microcosm incubation experiments performed in the NE Pacific Ocean indicate iron bioavailability influences B-vitamin production and utilization dynamics, with decreases in gene expression of biotin synthase, the final enzyme involved in the biotin biosynthetic pathway, under iron limitation. In addition, increases in B_{12}-independent methionine synthase (METE) and cobalamin acquisition 1 (CBA1) transcripts were detected following iron enrichment in natural diatom communities, suggesting NE Pacific Ocean phytoplankton communities may be driven into B_{12}-limitation following iron enrichment. Shifts in phytoplankton community composition as a result of iron-induced B_{12}-limitation did not occur, though they may have become apparent if the experimental incubation period had continued past 96 hours. Since macronutrient drawdown was negligible following this incubation period, future experiments are recommended to proceed for 144 hours to capture changes in phytoplankton community composition. Assessing community shifts with metatranscriptomics may be misleading, as certain organisms may produce disproportionately large amounts of mRNA

relative to their abundance in the community. It is therefore recommended to use 18S amplicon sequencing approaches in combination with light microscopy to determine eukaryotic community composition shifts due to iron and vitamin pulse additions. Furthermore, given that iron-induced B_{12} consumption by phytoplankton has now been identified in both the Southern Ocean and NE Pacific Ocean (Bertrand et al. 2011; Cohen et al. in press), it is possible that a similar dynamic exists in the remaining HNLC region to be investigated: the equatorial Pacific Ocean. B_{12} stress biomarkers METE and CBA1 could easily be detected via global proteomic approaches or metatranscriptomic sequencing, on both the ambient phytoplankton communities and following iron enrichment.

Investigations into the responses of natural diatom assemblages to varying iron status within the subarctic NE Pacific Ocean and the California Upwelling Zone have highlighted the different nutrient strategies invoked by chronically iron-limited oceanic diatoms as compared to coastal regions with inherently larger and more variable iron supplies. This analysis would be significantly strengthened by the incorporation of an additional oceanic site, as only one was represented in this study. It could then be determined which iron-related strategies are shared among chronically low-iron-adapted diatoms, versus the ones that are specific to unique physiochemical environments (e. g. Southern Ocean vs. NE Pacific Ocean). Additionally, our findings suggest that genes of interest involved in iron and nitrate metabolism at times exhibit divergent expression patterns between the genetically diverse diatom genera investigated, *Pseudo-nitzschia* and *Thalassiosira*, despite these taxa residing in identical environments. Laboratory culture experiments with *Pseudo-nitzschia* and *Thalassiosira* CUZ isolates could easily be designed to further explore this phenomenon, using qPCR to target several of these genes exhibiting highly divergent expression responses between the two taxa: ferredoxin- and

NADPH-requiring nitrite reductases, ferritin, and ferredoxin. Differences in the functional roles of these proteins may indicate these two taxa have evolved distinct metabolisms optimized for differing nutrient regimes, or that they use different metabolic strategies to adapt to their environment. This may be responsible for their co-existence in the same environment. An example of this has previously been observed within cyanobacterial populations of the equatorial Pacific Ocean, with *Synechococcus* experiencing nitrate stress while *Prochlorococcus* in the same community does not (Saito et al. 2014, 2015), likely due to differences in their nitrate requirements and acquisition and storage strategies.

The final two chapters of this dissertation hone in on an ecologically relevant diatom genus commonly abundant in the NE Pacific Ocean, *Pseudo-nitzschia*. Gene expression analyses and iron quota measurements within laboratory experiments have demonstrated that *P. granii* is unique in its broad iron quota range and gene expression patterns of ferritin, consistent with this species achieving high levels of long-term iron storage. Gene expression data suggest ferritin serves fundamentally different functional roles between *P. granii* and the other diatom species isolated from non-HNLC marine environments. Although these gene expression findings are suggestive of altered ferritin pools as a function of iron status, mRNA abundance does not always equate to protein levels, and it is recommended to confirm these trends with quantifiable protein expression approaches. The frequency of ferritin being used for short-term iron storage under low iron in the natural environment is furthermore unclear, and metatranscriptomic field analyses are recommended to better understand the prevalence of ferritin transcripts and proteins under iron stress. It is additionally unknown whether the *Pseudo-nitzschia* lineage is unique in its utilization of ferritin for long-term iron storage, or whether only certain species within this genus (*P. granii* and *P. multiseries*) have evolved this function. Additional field-based studies could

clarify whether the majority of coastal *Pseudo-nitzschia* sp. utilize ferritin for long-term storage under iron-replete conditions, similar to oceanic *P. granii*, or whether coastal *Pseudo-nitzschia* are also more likely to possess multiple ferritin homologs, with at least one being more highly expressed under low iron, as observed in the coastal diatoms *Amphora coffeaeformis* and *Thalassiosira rotula*.

Finally, comparing the proteome and transcriptome of *P. granii* under acclimated iron-replete and iron-limited conditions has provided insights into this species' competitiveness for growth in its low iron environment. The molecular strategies used by this diatom include constitutive expression of plastocyanin, coordinated use of class I and II fructose biphosphate aldolases, utilization of flavodoxin, iron starvation induced proteins, and iron acquisition machinery under iron stress. Under iron enrichment, *P. granii* stores large amounts of iron and upregulates thiamine and biotin synthesis, allowing this species to rapidly proliferate and sustain growth once iron becomes available. Interestingly, low-iron acclimated *P. granii* that receives a pulse addition of iron demonstrate highly divergent gene expression patterns compared to acclimated iron-replete cells. For example, iron-resupplied cells increase expression of proteorhodopsin and nitrate assimilation machinery, whereas acclimated *P. granii* do not, suggesting a temporal component to transcript production. However, both the *P. granii* strains (UNC1102 vs. UWOSP1E) and sequencing approaches (454/SOLiD vs. Illumina Miseq) differed between acclimated and non-acclimated iron resupply experiments, with the physiological and bioinformatic implications of these differences unclear. Comparisons between acclimated and iron resupply conditions would be substantially strengthened by repeating experiments with identical strains and sequencing approaches.

Interpreting findings from laboratory-based experiments and applying these insights to observations from the natural environment may substantially strengthen our mechanistic understanding of how diatom communities respond to nutrient stress, such as low iron or vitamin availability. For example, the *P. granii* transcriptome obtained from laboratory cultures indicates genes within the cobalamin synthesis module are not overexpressed under prolonged iron enrichment, whereas this phenomenon was definitively observed with natural assemblages of diatoms in the NE Pacific Ocean following iron addition. This implies that the cobalamin synthesis module is not simply upregulated to fuel increased growth during high iron conditions. We can therefore attribute the increases in gene expression following iron enrichment in the NE Pacific Ocean to growth-induced cobalamin consumption and subsequent depletion, likely resulting in a need for diatoms to incorporate and process cobalamin intermediates from the environment. It is my hope that the extensive laboratory and field data presented here will be similarly useful in guiding future interpretations of natural diatom community responses to changing nutrient availability.

Several of the genes identified in these studies could serve as useful biomarkers for vitamin, iron and nitrate stress in diatoms. These include biotin synthase (BIOB), B_{12}-independent methionine synthase (METE), flavodoxin (FLDA), iron-starvation-induced-proteins (ISIP), a nitrate transporter (NRT2), and an ammonium transporter (AMT). Certain putative bioindicator genes investigated in the these studies, including ferritin (FTN), ferredoxin (PETF) and RubisCO (RBCL), have demonstrated inconsistent expression patterns in response to iron status among diverse diatom taxa and/or geographical regions, rendering them less useful as bioindicators, but interesting as candidates to further explore functional diversity in diatom assemblages.

The aforementioned gene and protein expression patterns, diatom community composition shifts, and physiological responses observed as a function of changing iron status increase our understanding of how diatoms metabolically respond to iron limitation, and in turn regulate the chemistry and physics of their marine environment. Understanding these iron-specialized intracellular processes driving phytoplankton community composition and bloom dynamics is critical as we begin to predict how the changing climate will affect our oceans – which will likely include changes in iron bioavailability and supply (Shi et al. 2010; Hutchins and Boyd 2016). Future research studies will ideally build off of the findings presented here, and will continue to advance our understanding of diatom ecophysiology in response to changes in iron status.

APPENDIX I: TRANSCRIPT COUNTS OF GENES (KOS) ENCOMPASSED WITHIN KEGG VITAMIN MODULES

The following tables represent EdgeR-normalized transcript counts of genes (KOs) encompassed within KEGG vitamin biosynthetic modules. Genes not identified within metatranscriptomes are denoted with an asterisk (*), and pathway-related genes identified but not encompassed within KEGG biosynthetic modules or incorporated into Fig. 1.8. are denoted with a dagger (†)

A. Methionine biosynthesis (KEGG M00017)

KEGG KO	Gene name	Control	B_7	B_{12}	Iron	Iron/B_7	Iron/B_{12}	Taxonomic assignment of contig with most number of reads mapped	Contig ID
K00928	lysC (aspartate kinase)	18.54	36.38	16.14	29.18	32.67	54.78	Chaetoceros	k32.11609416
K12524	thrA bifunctional aspartokinase / homoserine dehydrogenase	363.62	376	331.67	438.9	444.3	375.98	Pseudo-nitzschia	k78.8602
K00133	asd (aspartate-semialdehyde dehydrogenase)	300.88	206.2	301	366.9	350.38	354.33	Pseudo-nitzschia	k55.7837707
K00003	homoserine dehydrogenase	192.51	188	242.9	375.6	395.3	289.83	Pseudo-nitzschia	k78.1443060
K00651	metA (homoserine O-succinyltransferase)	5.7	0	0	0	1.63	0	Fragilariopsis	k78.1188573
K01739	metB (cystathionine gamma-synthase)	19.96	26.28	23.4	34.77	19.6	26.51	Pseudo-nitzschia	k78.3427204
K01760	metC (cystathionine beta-lyase)	9.98	28.3	12.1	20.49	24.5	12.81	Pseudo-nitzschia	k55.7694532
K00548	metH (cobalamin-dependent methionine synthase)	2571.04	2444	2761.5	2824	2233.8	2591.66	Pseudo-nitzschia	k102.1421651
K00549	metE (cobalamin-independent methionine synthase)	35.65	34.36	13.72	1118	1075.6	14.14	Attheya	k102.906889

B. Aerobic cobalamin (B_{12}) biosynthesis (KEGG M00122) and Warren at al. 2002

KEGG KO	Gene name	Control	B_7	B_{12}	Iron	Iron/B_7	Iron/B_{12}	Taxonomic assignment of contig with most number of reads mapped	Contig ID
K02303*	cobA (uroporphyrin-III C-methyltransferase)	-	-	-	-	-	-	-	-
K03394*	cobI-cbiL (precorrin-2/cobalt-factor-2 C20-methyltransferase)	-	-	-	-	-	-	-	-
K02229*	cobG (precorrin-3B synthase)	-	-	-	-	-	-	-	-
K05934*	cobJ (precorrin-3B C17-methyltransferase)	-	-	-	-	-	-	-	-
K05934*	cobM (precorrin-3B C17-methyltransferase)	-	-	-	-	-	-	-	-
K02228*	cobF (precorrin-6A synthase)	-	-	-	-	-	-	-	-
K05895*	cobK-cbiJ (precorrin-6A/cobalt-precorrin-6A reductase)	-	-	-	-	-	-	-	-
K00595*	cobL (precorrin-6Y C5,15-methyltransferase)	-	-	-	-	-	-	-	-
K06042*	cobH-cbiC (precorrin-8X/cobalt-precorrin-8 methylmutase)	-	-	-	-	-	-	-	-
K02224†	cobB-cbiA (cobyrinic acid a,c-diamide synthase)	0	0	8.88	13.04	14.7	9.28	Fragilariopsis	k55.5081093
K02230†	cobN (cobaltochelatase)	64.17	84.89	34.7	56.5	49.82	28.27	Pseudo-nitzschia	k102.457980

K09882*	cobS (cobaltochelatase)	-	-	-	-	-	-	-	-
K09883*	cobT (cobaltochelatase)	-	-	-	-	-	-	-	-
K13786*	cobR (cob(II)yrinic acid a,c-diamide reductase)	-	-	-	-	-	-	-	-
K00798	MMAB (cob(I)alamin adenosyltransferase)	14.26	40.43	10.49	35.39	26.14	19	Pseudo-nitzschia	k78.1875219
K19221	cobA (cob(I)alamin adenosyltransferase)	0	12.13	3.23	6.83	1.63	6.19	Proboscia	k102.630702
K02232	cobQ-cbiP (adenosylcobyric acid synthase)	11.41	16.17	31.47	35.39	15.52	38.88	Pseudo-nitzschia	k78.1072180
K02225*	cobC1 (cobalamin biosynthetic protein)	-	-	-	-	-	-	-	-
K02227	cobD-cbiB (adenosylcobinamide-phosphate synthase)	5.7	12.13	0	6.21	12.25	3.53	Pseudo-nitzschia	k32.6793699
K02231	cobP/cobU (adenosylcobinamide kinase / adenosylcobinamide-phosphate guanylyltransferase)	61.32	48.51	104.1	107.4	134.76	80.41	Pseudo-nitzschia	k78.3347784
K00768	cobT/cobU (nicotinate-nucleotide--dimethylbenzimidazole phosphoribosyltransferase)	47.06	36.38	17.75	82.57	66.97	45.51	Pseudo-nitzschia	k55.4762687
K02226*	cobC (alpha-ribazole phosphatase)	-	-	-	-	-	-	-	-
K02233	cobS/cobV (adenosylcobinamide-GDP ribazoletransferase)	5.7	4.04	10.49	8.07	8.17	13.25	Pseudo-nitzschia	k32.16560201

D. Biotin (B_7) biosynthesis (KEGG M00123)

KEGG KO	Gene name	Control	B_7	B_{12}	Iron	Iron/B_7	Iron/B_{12}	Taxonomic assignment of contig with most number of reads mapped	Contig ID
K00652	bioF (8-amino-7-oxononanoate synthase)	77	36.38	63.75	62.71	65.34	73.78	Pseudo-nitzschia	k32.9349273
K00833	bioA (adenosylmethionine---8-amino-7-oxononanoate aminotransferase)	14.26	64.68	71.01	70.78	72.69	99.41	Pseudo-nitzschia	k32.16632481
K01935*	bioD (dethiobiotin synthetase)	-	-	-	-	-	-	-	-
K19562	BIO3-BIO1 (bifunctional dethiobiotin synthetase)	0	0	0	3.73	3.27	2.65	Chaetoceros	k32.10502853
K01012	bioB (biotin synthase)	72.72	74.79	94.42	175.7	191.11	143.15	Pseudo-nitzschia	k102.1421793

C. Pyridoxine (B_6) biosynthesis (KEGG M00124)

KEGG KO	Gene name	Control	B_7	B_{12}	Iron	Iron/B_7	Iron/B_{12}	Taxonomic assignment of contig with most number of reads mapped	Contig ID
K03472*	epd (D-erythrose 4-phosphate dehydrogenase)	-	-	-	-	-	-	-	-
K03473*	pdxB (erythronate-4-phosphate dehydrogenase)	-	-	-	-	-	-	-	-
K00831	serC (phosphoserine aminotransferase)	215.32	159.7	200.94	376.2	342.84	334.86	Pseudo-nitzschia	k78.1512013
K00097*	pdxA (4-hydroxythreonine-4-phosphate dehydrogenase)	-	-	-	-	-	-	-	-
K03474*	pdxJ (pyridoxine 5-phosphate synthase)	-	-	-	-	-	-	-	-
K00275	pdxH (pyridoxamine 5'-phosphate oxidase)	2.85	0	1.61	0	5.3	7.35	Proboscia	k32.4683187

E. Riboflavin (B_2) biosynthesis (KEGG M00125)

KEGG KO	Gene name	Control	B_7	B_{12}	Iron	Iron/B_7	Iron/B_{12}	Taxonomic assignment of contig with most number of reads mapped	Contig ID
K01497	ribA (GTP cyclohydrolase II)	82.71	60.64	39.54	3.73	8.17	9.28	Extubocellulus	k102.415465
K14652	ribBA (3,4-dihydroxy 2-butanone 4-phosphate synthase / GTP cyclohydrolase II)	175.4	115.2	176.73	213.6	157.63	209.42	Pseudo-nitzschia	k55.7841422
K11752	ribD (diaminohydroxyphosphoribosylaminopyrimidine deaminase)	18.54	30.32	16.14	18.63	39.2	14.14	Pseudo-nitzschia	k32.6651024
K00794	ribH (6,7-dimethyl-8-ribityllumazine synthase)	102.67	141.5	123.47	194.3	264.62	166.12	Pseudo-nitzschia	k55.7845127
K00793	ribE (riboflavin synthase)	142.6	80.85	101.68	169.5	164.16	132.98	Pseudo-nitzschia	k55.5372907
K00861	RFK (riboflavin kinase)	141.17	99.04	146.06	217.9	213.98	205.88	Pseudo-nitzschia	k78.3035101
K00953	FLAD1 (FAD synthetase)	158.28	125.3	250.97	347.1	269.52	360.08	Pseudo-nitzschia	k78.3438120

F. Thiamine (B_1) biosynthesis (KEGG M00127) and Paerl et al. 2015

KEGG KO	Gene name	Control	B_7	B_{12}	Iron	Iron/B_7	Iron/B_{12}	Taxonomic assignment of contig with most number of reads mapped	Contig ID
K14153	thiDE (hydroxymethylpyrimidine kinase)	48.48	40.43	37.12	37.25	48.19	34.46	Pseudo-nitzschia	k55.7846018
K00941	thiD (hydroxymethylpyrimidine/phosphomethylpyrimidine kinase)	0	0	4.03	0	2.45	3.53	Extubocellulus	k78.2340
K00788	thiE (thiamine-phosphate pyrophosphorylase)	22.82	16.17	8.07	18	24.5	14.14	Pseudo-nitzschia	k78.3195155
K18278†	thi5 (pyrimidine precursor enzyme)	0	0	1.61	1.2	1.63	5.3	Proboscia	k55.7074135
K03147	thiC (phosphomethylpyrimidine synthase)	51.34	50.53	66.98	83.81	104.54	80.41	Tryblionella	k55.4049062
K03146*	thi4 (thiamine thiazole synthase)	-	-	-	-	-	-	-	-
K00878*	thiM (hydroxyethylthiazole kinase)	-	-	-	-	-	-	-	-
K03149†	thiG (thiazole synthase)	9.98	24.26	4.04	5.59	6.53	5.3	Extubocellulus	k55.2262329
K00946*	thiL (thiamine-monophosphate kinase)	-	-	-	-	-	-	-	-

APPENDIX II: BIOTIN UPTAKE EXPERIMENTS

Certain biotin-producing organisms are capable of both biosynthesis and uptake from the surrounding environment (Shakoury-elizeh et al. 2004), though it is unclear if both are performed in the ecologically-relevant oceanic diatom *Pseudo-nitzschia granii*. In *E.coli* each biotin biosynthesis enzyme biotin synthase (BIOB) performs only one reaction converting dethiobiotin to biotin under low-iron conditions, since the sulfur atom from an iron-sulfur cluster within the enzyme is donated to form the sulfur ring of the biotin molecule itself. However, the enzyme can repair itself and thus perform multiple reactions under high-iron conditions (Reyda et al. 2008). In terms of turnover rate, the biotin synthase enzyme is able to produce approximately 120 molecules of biotin in one day ($k \approx 0.08\ min^{-1}$; Choi-Rhee and Cronan 2005).

Information regarding biotin auxotrophy and uptake mechanisms in diatoms is limited. One member of the *Pseudo-nitzschia* diatom genus, the coastal diatom *Pseudo-nitzschia pungens,* is auxotrophic for biotin and requires the vitamin to be added in growth medium, while another coastal species, *P. multiseries,* does not require external biotin to grow (Tang et al. 2010). We therefore hypothesized that other members of the *Pseudo-nitzschia* genus may be able to import biotin from the environment. This was tested through radiolabeled (^{3}H)-biotin uptake experiments performed with laboratory cultures of *P. granii*. Furthermore, we sought to determine whether iron status influences biotin uptake activity, as it does biotin synthase transcript production (Fig. 1.1). Using this information, we investigated how the intracellular biotin quota may be changing as a function of iron status through its relationship with growth rate, biotin uptake, and biotin synthesis.

Methods

Tritium-labeled biotin (^{3}H-biotin) was added to growth medium prepared as described in Chapter 1. However to avoid having iron precipitate and form colloids that could bind to ^{3}H, less iron was added to these experiments while still ensuring cells were under iron-replete conditions. The high iron treatment was prepared with 42 nmol L^{-1} of total iron and approximately 84 pmol L^{-1} of unchelated iron (Aquil pFe 20.5, Marchetti et al. 2009). The low-iron treatment was prepared in 200:1.5 nM DFB:Fe ratios yielding ~0.02 pmol L^{-1} unchelated iron (Strzepek et al. 2012), identical to the large-culture experimental conditions discussed in Chapter 1. Duplicate antibiotic-treated and steady-state acclimated +Fe/+B_7 and –Fe/+B_7 cells were inoculated into 30 mL of Aquil with 1 nmol L^{-1} ^{3}H-biotin (corresponding to half of the Aquil recipe biotin concentration), almost an order of magnitude above values naturally observed along the coast of California (Sañudo-Wilhelmy et al. 2012). Once the maximum exponential phase fluorescence was reached, cultures were filtered onto 3 µm filters and the filtrate was re-passed through 0.2 µm filters to determine uptake by residual free-living bacteria. Filters were rinsed with seawater three times before PerkinElmer Ultra Gold liquid scintillation cocktail was combined with the filters directly into scintillation vials. Filtration glassware was cleaned using detergent, HCl and Milli-Q. Radioactivity was detected using a scintillation counter and monitoring ^{3}H. DPMs were subtracted from a 30 mL filtered Aquil blank and are normalized to estimated cell counts and growth rates from each culture. Cell counts were estimated from fluorescence values using the linear relationship between the two parameters empirically obtained from acclimated iron-limited and iron-replete *P. granii* cultures.

Antibiotic-treated cultures were prepared by following an antibiotic cocktail created by Uwe John and modified by Shady Amin (University of Washington), as described in Chapter 1.

Bacterial presence was detected by the use of bacteriological peptone broth in conjunction with SYBR green staining and epifluorescent microscopy, and cultures were deemed axenic when bacteriological peptone broth remained clear after 3 days and a substantial reduction in bacterial cells could be observed following SYBR staining.

It may be important to note that the amount of ^{3}H derived from the original ^{3}H-biotin molecules that were metabolized by cells during these experiments (3-7 days) and excreted in a dissolved form is unknown, and our estimates for biotin uptake could therefore be artificially low. Only ^{3}H-labaled material that was collected onto 3 µm filters (e.g. contained within the organic fraction or adsorbed onto cells/filters) was included in this analysis. Therefore, any biologically-processed ^{3}H material that was in the dissolved fraction would not have been quantified.

Results

Uptake rates of the diatom fraction (> 3 µm) were on average 2-fold higher in iron-replete cells (4.1×10^{-13} pg cell^{-1} d^{-1}) as compared to iron-limited cells (2.1×10^{-13} pg cell^{-1} d^{-1}; Appendix Fig. 1.1). Uptake rates of the free-living bacterial fraction (<3 µm and >0.2 µm) were indistinguishable from background. This suggests that acclimated iron- and biotin-replete (+Fe/+B_7) *P. granii* cells are importing more biotin than their iron-limited (-Fe/+B_7) counterparts. It is possible only healthier cells can afford to put energy towards uptake, with growth-limited cells unable to acquire external resources. It is unclear whether biotin-deficient cultures take up external biotin since only cultures acclimated to biotin-replete conditions were used in this study.

Most importantly, uptake of external biotin under steady-state +B_7-conditions appear to be negligible in comparison to the total biotin requirement, as the amount removed from the

medium over the period of one day was several orders of magnitude lower than the amount predicted to be contained within diatoms [$Q \approx 2.5 \times 10^{-4}$ pg cell^{-1}, as determined with *Phaeodactylum tricornutum* biotin quotas obtained by Carlucci and Bowes (1972), and the estimated per cell carbon amount 144 pg C cell^{-1} (Mullin et al. 1966)].

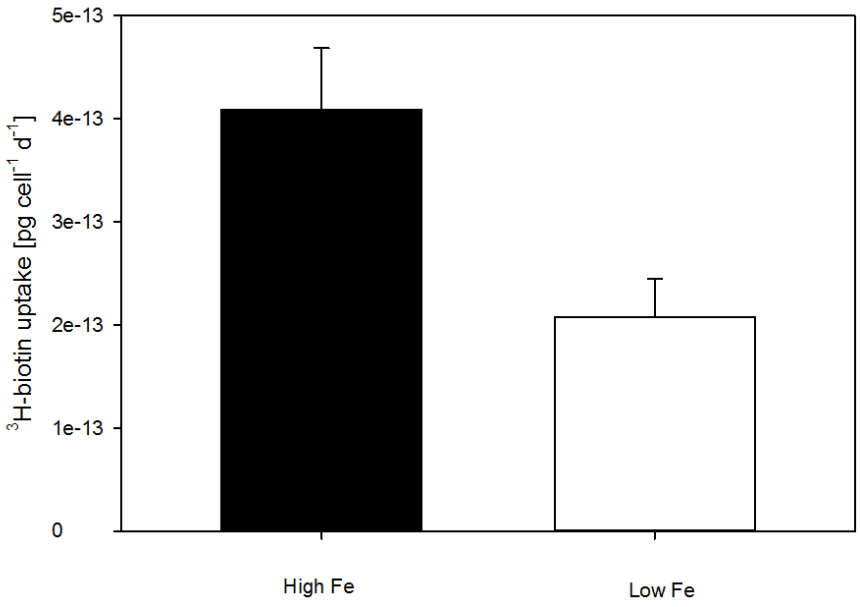

Appendix Fig. 1.1. Uptake of biotin by iron replete (left) and iron-limited (right) *P. granii* cells under acclimated growth conditions. Standard error bars reflect the variation between duplicate 28 mL cultures.

Discussion

The relationship between biotin uptake and biotin synthesis could potentially provide information about intracellular biotin quotas when incorporated into a theoretical framework using a modified Droop equation (Droop 1968) (Eq. 1).

$\rho = Q^*\mu$, under steady-state conditions (Droop, 1968) Eq. 1

Here we assume that imported biotin (ρ) is combined with biotin synthesis (P) to fulfill the biotin requirement (Qμ) (Eq. 2).

$$\rho = Q^*\mu - P, \text{ or } Q^*\mu = \rho + P \quad \text{Eq. 2}$$

Key assumptions are that diatoms possess the transporters/uptake mechanisms for acquiring biotin from the environment and that diatoms are not producing biotin in excess of their cellular requirement. However, the proportion of biotin being taken up into the cell under acclimated biotin-replete conditions appears to be negligible compared to the predicted cellular biotin quota. It is unclear whether larger amounts of biotin uptake would occur within acclimated biotin-deficient treatments, or within environmental diatom communities under non-steady-state conditions. Given that our acclimated biotin-replete experiments show very little uptake is occurring, we assume uptake to be several orders smaller than production and forgo the term, and proceed to examine the relationship between growth rate, quota and production in our cultures.

if $\rho << Q$, then

$$Q^*\mu \approx P \quad \text{Eq. 3}$$

In order to maintain cellular processes under iron limitation, and since uptake seems to be minimal, we hypothesize that iron-limited cells acclimated conditions decrease their biotin Q. As the growth rate of iron-limited cells decreases by up to 50%, possibly resulting in a reduction in Q, P would be expected to decrease appreciably and is consistent with observed decreases in biotin synthase transcript abundance under iron limitation. The alternative possibility, in which Q stays constant under iron limitation, would imply production of biotin is only a function of growth rate. This is likely not the case as light-limited cultures (when growth is reduced due to light availability, yet iron is available) exhibit relatively high abundance of biotin synthase

transcripts, similar to iron-replete cultures (Fig. 1.2). A large assumption being made is that transcript abundance equates to protein expression, which was not able to be confirmed given that the peptide was not detected in the *P. granii* proteome.

Unfortunately we were not able to empirically measure Q under acclimated iron-replete and iron-limited conditions using an attempted LC/MS quantification method due to our limits of detection being too large to confidently detect the sub-pg concentrations of biotin within *P. granii* cells. The method consisted of vitamin extraction, using Carlucci and Bowes (1972) as a reference, followed by LC/MS analysis with a Thermo Scientific TSQ Quantum Ultra triple quadrupole mass spectrometer using electrospray ionization with an Acquity UPLC system. Other method details included the use of a Thermo Hypersil Gold column, injection rates of ~250 µL min^{-1}, and 10 µL injection volumes. The 245.1/123.1 transition was monitored for quantification. Further method development achieving lower limits of detection is necessary to quantify biotin quotas in *P. granii* and to determine whether our hypothesis, that intracellular biotin quotas are reduced under acclimated iron-limited conditions, is correct.

REFERENCES

Agusti, S., J. Gonzalez-Gordillo, D. Vaque, M. Estrada, M. I. Cerezo, G. Salazar, J. M. Gasol, and C. M. Duarte. 2015. Ubiquitous healthy diatoms in the deep sea confirm deep carbon injection by the biological pump. Nat. Commun. **6**: 1–8. doi:10.1038/ncomms8608

Alexander, H., B. D. Jenkins, T. A. Rynearson, M. A. Saito, M. L. Mercier, and S. T. Dyhrman. 2012. Identifying reference genes with stable expression from high throughput sequence data. Front. Microbiol. **3**: 385. doi:10.3389/fmicb.2012.00385

Alexander, H., M. Rouco, S. T. Haley, S. T. Wilson, D. M. Karl, and S. T. Dyhrman. 2015. Functional group-specific traits drive phytoplankton dynamics in the oligotrophic ocean. Proc. Natl. Acad. Sci. **112** : E5972–E5979.

Allen, A. E., J. LaRoche, U. Maheswari, and others. 2008. Whole-cell response of the pennate diatom Phaeodactylum tricornutum to iron starvation. Proc. Natl. Acad. Sci. U. S. A. **105**: 10438–10443. doi:10.1073/pnas.0711370105

Allen, A. E., A. Moustafa, A. Montsant, A. Eckert, P. G. Kroth, and C. Bowler. 2012. Evolution and Functional Diversification of Fructose Bisphosphate Aldolase Genes in Photosynthetic Marine Diatoms. Mol. Biol. Evol. **29** : 367–379.

Altschul, S. F., W. Gish, W. Miller, E. W. Myers, and D. J. Lipman. 1990. Basic local alignment search tool. J. Mol. Biol. **215**: 403–10. doi:10.1016/S0022-2836(05)80360-2

Anderson, P. J., J. Lango, C. Carkeet, A. Britten, B. Kra, B. D. Hammock, and J. R. Roth. 2008. One Pathway Can Incorporate either Adenine or Dimethylbenzimidazole as an ⎵ -Axial Ligand of B 12 Cofactors in Salmonella enterica □. J. Bacteriol. **190**: 1160–1171. doi:10.1128/JB.01386-07

Andersson, I., and A. Backlund. 2008. Structure and function of Rubisco. Plant Physiol. Biochem. **46**: 275–291. doi:http://dx.doi.org/10.1016/j.plaphy.2008.01.001

Armbrust, E. V. 2009. The life of diatoms in the world ' s oceans. Nature **459**: 185–192. doi:10.1038/nature08057

de Baar, H. J. W., P. W. Boyd, K. H. Coale, and others. 2005. Synthesis of iron fertilization experiments: From the iron age in the age of enlightenment. J. Geophys. Res. C Ocean. **110**: 1–24. doi:10.1029/2004JC002601

Barwell-Clarke, J., F. Whitney, and P. B. of Ocean Sciences. 1996. Institute of Ocean Sciences Nutrient Methods and Analysis, The Institute.

Behrenfeld, M. J., E. Boss, D. A. Siegel, and D. M. Shea. 2005. Carbon-based ocean productivity and phytoplankton physiology from space. Global Biogeochem. Cycles **19**: 1–14. doi:10.1029/2004GB002299

Behrenfeld, M. J., and A. J. Milligan. 2013. Photophysiological Expressions of Iron Stress in Phytoplankton. Annu. Rev. Mar. Sci **5**: 217–46. doi:10.1146/annurev-marine-121211-172356

Bender, S., C. Durkin, C. Berthiaume, R. Morales, and E. V. Armbrust. 2014. Transcriptional responses of three model diatoms to nitrate limitation of growth. Front. Mar. Sci. **1**: 3. doi:10.3389/fmars.2014.00003

Bertrand, E. M., A. E. Allen, C. L. Dupont, T. M. Norden-krichmar, J. Bai, and R. E. Valas. 2012. Influence of cobalamin scarcity on diatom molecular physiology and identification of a cobalamin acquisition protein. Proc. Natl. Acad. Sci. U. S. A. **109**: 1762–1771. doi:10.1073/pnas.1201731109

Bertrand, E. M., J. P. McCrow, A. Moustafa, and others. 2015. Phytoplankton-bacterial interactions mediate micronutrient colimitation at the coastal Antarctic sea ice edge. Proc. Natl. Acad. Sci. U. S. A. **112**: 9938–43. doi:10.1073/pnas.1501615112

Bertrand, E. M., M. A. Saito, P. A. Lee, R. B. Dunbar, P. N. Sedwick, and G. R. Ditullio. 2011. Iron limitation of a springtime bacterial and phytoplankton community in the Ross Sea: Implications for vitamin B12 nutrition. Front. Microbiol. **2**: 1–12. doi:10.3389/fmicb.2011.00160

Bertrand, E. M., M. A. Saito, J. M. Rose, C. R. Riesselman, M. C. Lohan, A. E. Noble, P. a. Lee, and G. R. DiTullio. 2007. Vitamin B12 and iron colimitation of phytoplankton growth in the Ross Sea. Limnol. Oceanogr. **52**: 1079–1093. doi:10.4319/lo.2007.52.3.1079

Biller, D. V, and K. W. Bruland. 2012. Analysis of Mn, Fe, Co, Ni, Cu, Zn, Cd, and Pb in seawater using the Nobias-chelate PA1 resin and magnetic sector inductively coupled plasma mass spectrometry (ICP-MS). Mar. Chem. **130–131**: 12–20. doi:http://dx.doi.org/10.1016/j.marchem.2011.12.001

Birol, I., S. D. Jackman, C. B. Nielsen, and others. 2009. De novo transcriptome assembly with ABySS. Bioinformatics **25**: 2872–2877. doi:10.1093/bioinformatics/btp367

Bolger, A. M., M. Lohse, and B. Usadel. 2014. Trimmomatic: A flexible trimmer for Illumina sequence data. Bioinformatics **30**: 2114–2120. doi:10.1093/bioinformatics/btu170

Botebol, H., E. Lesuisse, R. Sutak, and others. 2015. Central role for ferritin in the day/night regulation of iron homeostasis in marine phytoplankton. Proc. Natl. Acad. Sci. **112**: 1–6. doi:10.1073/pnas.1506074112

Bowler, C., A. E. Allen, J. H. Badger, and others. 2008. The Phaeodactylum genome reveals the evolutionary history of diatom genomes. Nature **456**: 239–244. doi:10.1038/nature07410

Boyd, P., J. A. Berges, and P. J. Harrison. 1998. In vitro iron enrichment experiments at iron-rich and -poor sites in the NE subarctic Pacific. J. Exp. Mar. Bio. Ecol. **227**: 133–151. doi:http://dx.doi.org/10.1016/S0022-0981(97)00264-5

Boyd, P. W., T. Jickells, C. S. Law, and others. 2007. Mesoscale Iron Enrichment Experiments 1993 – 2005: Synthesis and Future Directions. Science (80-.). **315**: 612–618.

Brand, L. E., R. R. L. Guillard, and L. S. Murphy. 1981. A method for the rapid and precise determination of acclimated phytoplankton reproduction rates. J. Plankt. Res. **3** : 193–201.

Brown, K. L., K. I. Twing, and D. L. Robertson. 2009. Unraveling the regulation of nitrogen assimilation in the marine diatom Thalassiosira pseudonana (Bacillariophyceae): Diurnal variations in transcript levels for five genes involved in nitrogen assimilation. J. Phycol. **45**: 413–426. doi:10.1111/j.1529-8817.2009.00648.x

Bruland, K. W., E. L. Rue, and G. J. Smith. 2001. Iron and macronutrients in California coastal upwelling regimes : Implications for diatom blooms. Limnol. Oceanogr. **46**: 1661–1674.

Brzezinski, M. A., J. W. Krause, R. M. Bundy, K. A. Barbeau, P. Franks, R. Goericke, M. R. Landry, and M. R. Stukel. 2015. Enhanced silica ballasting from iron stress sustains carbon export in a frontal zone within the California Current. J. Geophys. Res. Ocean. **120**: 4654–4669. doi:10.1002/2015JC010829

Carlucci, A. F., and P. M. Bowes. 1972. Vitamin B12, thiamine, and biotin contents of marine phytoplankton. J. Phycol. **8**: 133–137. doi:10.1111/j.1529-8817.1972.tb04013.x

Chappell, P. D., L. P. Whitney, J. R. Wallace, A. I. Darer, S. Jean-Charles, and B. D. Jenkins. 2015. Genetic indicators of iron limitation in wild populations of Thalassiosira oceanica from the northeast

Pacific Ocean. Isme J **9**: 592–602. doi:10.1038/ismej.2014.171

Chase, Z., B. Hales, T. Cowles, R. Schwartz, and A. van Geen. 2005. Distribution and variability of iron input to Oregon coastal waters during the upwelling season. J. Geophys. Res. C Ocean. **110**: 1–14. doi:10.1029/2004JC002590

Chauton, M. S., P. Winge, T. Brembu, O. Vadstein, and A. M. Bones. 2013. Gene Regulation of Carbon Fixation, Storage, and Utilization in the Diatom Phaeodactylum tricornutum Acclimated to Light/Dark Cycles. Plant Physiol. **161**: 1034–1048. doi:10.1104/pp.112.206177

Choi-Rhee, E., and J. E. Cronan. 2005. Biotin Synthase Is Catalytic In Vivo, but Catalysis Engenders Destruction of the Protein. Chem. Biol. **12**: 461–468. doi:http://dx.doi.org/10.1016/j.chembiol.2005.02.006

Cox, A. D., and M. A. Saito. 2013. Proteomic responses of oceanic Synechococcus WH8102 to phosphate and zinc scarcity and cadmium additions. Front. Microbiol. **4**: 387. doi:10.3389/fmicb.2013.00387

Croft, M. T., A. D. Lawrence, E. Raux-deery, M. J. Warren, and A. G. Smith. 2005. Algae acquire vitamin B 12 through a symbiotic relationship with bacteria. Nature **438**: 90–93. doi:10.1038/nature04056

Croft, M. T., M. J. Warren, and A. G. Smith. 2006. MINIREVIEWS Algae Need Their Vitamins †. Eukaryot. Cell **5**: 1175–1183. doi:10.1128/EC.00097-06

Doucette, G., D. Erdner, M. Peleato, J. Hartman, and A. MD. 1996. Quantitative analysis of iron-stress related proteins in Thalassiosira weissflogii: measurement of flavodoxin and ferredoxin using HPLC. Mar. Ecol. Prog. Ser. **130**: 269–276.

Droop, M. R. 1968. Vitamin B12 and Marine Ecology. IV. The Kinetics of Uptake, Growth and Inhibition in Monochrysis Lutheri. J. Mar. Biol. Assoc. United Kingdom **48**: 689–733.

Du, X., and W. T. Peterson. 2014. Seasonal Cycle of Phytoplankton Community Composition in the Coastal Upwelling System Off Central Oregon in 2009. Estuaries and Coasts **37**: 299–311. doi:10.1007/s12237-013-9679-z

Dyhrman, S. T., B. D. Jenkins, T. A. Rynearson, and others. 2012. The Transcriptome and Proteome of the Diatom Thalassiosira pseudonana Reveal a Diverse Phosphorus Stress Response. PLoS One **7**: 1–10. doi:10.1371/journal.pone.0033768

Edgar, R. C. 2004. MUSCLE: multiple sequence alignment with high accuracy and high throughput. Nucleic Acids Res. **32**: 1792–1797.

Ellis, K. A., N. R. Cohen, C. Moreno, and A. Marchetti. 2017. Cobalamin-independent Methionine Synthase Distribution and Influence on Vitamin B12 Growth Requirements in Marine Diatoms. Protist **168**: 32–47. doi:http://dx.doi.org/10.1016/j.protis.2016.10.007

El-Sabaawi, R., and P. J. Harrison. 2006. Interactive effects of irradiance and temperature on the photosynthetic physiology of the diatom Pseudo-nitzschia granii (Bacillariophyceae) from the northeast subarctic Pacific. J. Phycol. **42**: 778–785. doi:10.1111/j.1529-8817.2006.00246.x

Erdner, D. L., and D. M. Anderson. 1999. Ferredoxin and flavodoxin as biochemical indicators of iron limitation during open-ocean iron enrichment. Limnol. Oceanogr. **44**: 1609–1615. doi:10.4319/lo.1999.44.7.1609

Finkel, Z. V. 2007. Does Phytoplankton Cell Size Matter?: The Evolution of Modern Marine Food Webs,.

La Fontaine, S., J. M. Quinn, S. S. Nakamoto, M. D. Page, V. Göhre, J. L. Moseley, J. Kropat, and S. Merchant. 2002. Copper-Dependent Iron Assimilation Pathway in the Model Photosynthetic

Eukaryote Chlamydomonas reinhardtii. Eukaryot. Cell **1** : 736–757.

Garcia, H. E., R. A. Locarnini, T. P. Boyer, J. I. Antonov, M. M. Zweng, O. K. Baranova, and D. R. Johnson. 2010. World Ocean Atlas 2009, Volume 4: Nutrients (phosphate, nitrate, silicate), Ed. NOAA A. S. Levitus [ed.]. U.S. Government Printing Office.

Gobler, C. J., C. Norman, C. Panzeca, G. T. Taylor, and S. A. Sañudo-Wilhelmy. 2007. Effect of B-vitamins (B1, B12) and inorganic nutrients on algal bloom dynamics in a coastal ecosystem. Aquat. Microb. Ecol. **49**: 181–194. doi:10.3354/ame01132

Grabherr, M. G., B. J. Haas, M. Yassour, and others. 2011. Full-length transcriptome assembly from RNA-Seq data without a reference genome. Nat Biotech **29**: 644–652.

Graff van Creveld, S., S. Rosenwasser, Y. Levin, and A. Vardi. 2016. Chronic iron limitation confers transient resistance to oxidative stress in marine diatoms. Plant Physiol. **172**: 968–979.

Groussman, R. D., M. S. Parker, and E. V. Armbrust. 2015. Diversity and Evolutionary History of Iron Metabolism Genes in Diatoms. PLoS One **10**: e0129081.

Harris, S. L., D. E. Varela, F. W. Whitney, and P. J. Harrison. 2009. Nutrient and phytoplankton dynamics off the west coast of Vancouver Island during the 1997/98 ENSO event. Deep Sea Res. Part II Top. Stud. Oceanogr. **56**: 2487–2502. doi:http://dx.doi.org/10.1016/j.dsr2.2009.02.009

Harrison, G. I., and F. M. M. Morel. 1986. Response of the marine diatom Thalassiosira weissflogii to iron stress1. Limnol. Oceanogr. **31**: 989–997. doi:10.4319/lo.1986.31.5.0989

Harrison, P. J., F. A. Whitney, A. Tsuda, H. Saito, and K. Tadokoro. 2004. Nutrient and plankton dynamics in the NE and NW Gyres of the subarctic Pacific Ocean. J. Oceanogr. **60**: 93–117. doi:10.1023/B:JOCE.0000038321.57391.2a

Hasle, G. R. 2002. Are most of the domoic acid-producing species of the diatom genus Pseudo-nitzschia cosmopolites? Harmful Algae **1**: 137–146. doi:http://dx.doi.org/10.1016/S1568-9883(02)00014-8

Heal, K. R., L. T. Carlson, A. H. Devol, E. V. Armbrust, J. W. Moffett, D. A. Stahl, and A. E. Ingalls. 2014. Determination of four forms of vitamin B 12 and other B vitamins in seawater by liquid chromatography / tandem mass spectrometry. Rapid Commun. Mass Spectrom. **28**: 2398–2404. doi:10.1002/rcm.7040

Heal, K. R., W. Qin, F. Ribalet, and others. 2017. Two distinct pools of B12 analogs reveal community interdependencies in the ocean. Proc. Natl. Acad. Sci. **114** : 364–369.

Helliwell, K. E., A. D. Lawrence, A. Holzer, and others. 2016. Cyanobacteria and Eukaryotic Algae Use Different Chemical Variants of Vitamin B12. Curr. Biol. 999–1008. doi:10.1016/j.cub.2016.02.041

Helliwell, K. E., G. L. Wheeler, K. C. Leptos, R. E. Goldstein, and A. G. Smith. 2011. Insights into the evolution of vitamin B 12 auxotrophy from sequenced algal genomes. Mol. Biol. Evol. **28**: 2921–2933. doi:10.1093/molbev/msr124

Hillebrand, H., C.-D. Dürselen, D. Kirschtel, U. Pollingher, and T. Zohary. 1999. Biovolume calculation for pelagic and benthic microalgae. J. Phycol. **35**: 403–424. doi:10.1046/j.1529-8817.1999.3520403.x

Honjo, S., S. J. Manganini, R. A. Krishfield, and R. Francois. 2008. Particulate organic carbon fluxes to the ocean interior and factors controlling the biological pump: A synthesis of global sediment trap programs since 1983. Prog. Oceanogr. **76**: 217–285. doi:http://dx.doi.org/10.1016/j.pocean.2007.11.003

Horecker, B. L., O. Tsolas, and C. Y. Lai. 1972. 6 Aldolases, p. 213–258. *In* P.D. Boyer [ed.]. Academic

Press.

Hutchins, D. A., and P. W. Boyd. 2016. Marine phytoplankton and the changing ocean iron cycle. Nat. Clim. Chang. **6**: 1072–1079.

Hutchins, D. A., G. R. DiTullio, Y. Zhang, and K. W. Bruland. 1998. An iron limitation mosaic in the California upwelling regime. Limnol. Oceanogr. **43**: 1037–1054. doi:10.4319/lo.1998.43.6.1037

Hutchins, D. A., C. E. Hare, R. S. Weaver, and others. 2002. Phytoplankton iron limitation in the Humboldt Current and Peru Upwelling. **47**: 997–1011.

Jackson, S. E. 2013. Hsp90: Structure and Function, p. 155–240. *In* S. Jackson [ed.], Molecular Chaperones. Springer Berlin Heidelberg.

Jarrett, J. T. 2005. The novel structure and chemistry of iron–sulfur clusters in the adenosylmethionine-dependent radical enzyme biotin synthase. Arch. Biochem. Biophys. **433**: 312–321. doi:10.1016/j.abb.2004.10.003

Johnson, K. S., F. P. Chavez, and G. E. Friederich. 1999. Continental-shelf sediment as a primary source of iron for coastal phytoplankton. Nature **398**: 697–700.

Johnson, Z. I., R. Shyam, A. E. Ritchie, C. Mioni, V. P. Lance, J. W. Murray, and E. R. Zinser. 2010. The effect of iron- and light-limitation on phytoplankton communities of deep chlorophyll maxima of the western Pacific Ocean. J. Mar. Res. **68**.

Keeling, P. J., F. Burki, H. M. Wilcox, and others. 2014. The Marine Microbial Eukaryote Transcriptome Sequencing Project (MMETSP): Illuminating the Functional Diversity of Eukaryotic Life in the Oceans through Transcriptome Sequencing. PLoS Biol. **12**. doi:10.1371/journal.pbio.1001889

King, A. L., and K. Barbeau. 2007. Evidence for phytoplankton iron limitation in the southern California Current System. Mar. Ecol. Prog. Ser. **342**: 91–103.

King, A. L., S. a Sañudo-Wilhelmy, K. Leblanc, D. a Hutchins, and F. Fu. 2011. CO2 and vitamin B12 interactions determine bioactive trace metal requirements of a subarctic Pacific diatom. ISME J. **5**: 1388–96. doi:10.1038/ismej.2010.211

Koch, F., T. K. Hattenrath-lehmann, J. A. Goleski, S. Sañudo-Wilhelmy, N. S. Fisher, and C. J. Gobler. 2012. Vitamin B 1 and B 12 uptake and cycling by plankton communities in coastal ecosystems. Front. Microbiol. **3**: 1–11. doi:10.3389/fmicb.2012.00363

Kovár, J., H. Stýbrová, P. Novák, and others. 2004. Heat Shock Protein 90 Recognized as an Iron-Binding Protein Associated with the Plasma Membrane of HeLa Cells. Cell. Physiol. Biochem. **14**: 41–46.

Kromkamp, J. C., and R. M. Forster. 2003. The use of variable fluorescence measurements in aquatic ecosystems: differences between multiple and single turnover measuring protocols and suggested terminology. Eur. J. Phycol. **38**: 103–112. doi:10.1080/0967026031000094094

Kurisu, G., M. Kusunoki, E. Katoh, T. Yamazaki, K. Teshima, Y. Onda, Y. Kimata-Ariga, and T. Hase. 2001. Structure of the electron transfer complex between ferredoxin and ferredoxin-NADP+ reductase. Nat Struct Mol Biol **8**: 117–121.

Kustka, A. B., A. E. Allen, and F. M. M. Morel. 2007. Sequence analysis and transcriptional regulation of iron acquisition genes in two marine diatoms. J. Phycol. **43**: 715–729. doi:10.1111/j.1529-8817.2007.00359.x

Lam, P. J., and J. K. B. Bishop. 2008. The continental margin is a key source of iron to the HNLC North Pacific Ocean. Geophys. Res. Lett. **35**: 1–5. doi:10.1029/2008GL033294

Lam, P. J., J. K. B. Bishop, C. C. Henning, M. A. Marcus, G. A. Waychunas, and I. Y. Fung. 2006. Wintertime phytoplankton bloom in the subarctic Pacific supported by continental margin iron. Global Biogeochem. Cycles **20**: 1–12. doi:10.1029/2005GB002557

Langmead, B., and S. L. Salzberg. 2012. Fast gapped-read alignment with Bowtie 2. Nat Methods **9**: 357–359. doi:10.1038/nmeth.1923

Lanquar, V., F. Lelièvre, S. Bolte, and others. 2005. Mobilization of vacuolar iron by AtNRAMP3 and AtNRAMP4 is essential for seed germination on low iron. EMBO J. **24**: 4041–4051. doi:10.1038/sj.emboj.7600864

LaRoche, J., H. Murray, M. Orellana, and J. Newton. 1995. Flavodoxin expression as an indicator of iron limitation in marine diatoms. J. Phycol. **31**: 520–530. doi:10.1111/j.1529-8817.1995.tb02545.x

Lauritano, C., I. Orefice, G. Procaccini, G. Romano, and A. Ianora. 2015. Key genes as stress indicators in the ubiquitous diatom Skeletonema marinoi. BMC Genomics **16**: 411. doi:10.1186/s12864-015-1574-5

Lelong, A., H. Hégaret, P. Soudant, and S. S. Bates. 2012. Pseudo-nitzschia (Bacillariophyceae) species, domoic acid and amnesic shellfish poisoning: revisiting previous paradigms. Phycologia **51**: 168–216. doi:10.2216/11-37.1

Li, H., B. Handsaker, A. Wysoker, and others. 2009. The Sequence Alignment/Map format and SAMtools. Bioinformatics **25**: 2078–2079. doi:10.1093/bioinformatics/btp352

Li, S., and J. E. Cronan. 1993. Growth Rate Regulation of Escherichia coli Acetyl Coenzyme A Carboxylase , Which Catalyzes the First Committed Step of Lipid Biosynthesis. J. Bacteriol. **175**: 332–340.

Liu, X., and E. C. Theil. 2005. Ferritins: Dynamic Management of Biological Iron and Oxygen Chemistry. Acc. Chem. Res. **38**: 167–175. doi:10.1021/ar0302336

Lohmann, A., M. A. Schottler, C. Brehelin, F. Kessler, R. Bock, E. B. Cahoon, and P. Dormann. 2006. Deficiency in phylloquinone (vitamin K1) methylation affects prenyl quinone distribution, photosystem I abundance, and anthocyanin accumulation in the Arabidopsis AtmenG mutant. J. Biol. Chem. **281**: 40461–40472. doi:10.1074/jbc.M609412200

Lommer, M., A.-S. Roy, M. Schilhabel, S. Schreiber, P. Rosenstiel, and J. LaRoche. 2010. Recent transfer of an iron-regulated gene from the plastid to the nuclear genome in an oceanic diatom adapted to chronic iron limitation. BMC Genomics **11**: 718. doi:10.1186/1471-2164-11-718

Lommer, M., M. Specht, A.-S. Roy, and others. 2012. Genome and low-iron response of an oceanic diatom adapted to chronic iron limitation. Genome Biol. **13**: R66. doi:10.1186/gb-2012-13-7-r66

Long, J. C., F. Sommer, M. D. Allen, S.-F. Lu, and S. S. Merchant. 2008. FER1 and FER2 Encoding Two Ferritin Complexes in Chlamydomonas reinhardtii Chloroplasts Are Regulated by Iron. Genetics **179**: 137–147. doi:10.1534/genetics.107.083824

Maldonado, M. T., and N. M. Price. 2001. Reduction and transport of organically bound iron by Thalassiosira oceanica (Bacillariophyceae). J. Phycol. **37**: 298–310. doi:10.1046/j.1529-8817.2001.037002298.x

Malviya, S., E. Scalco, S. Audic, and others. 2016. Insights into global diatom distribution and diversity in the world's ocean. Proc. Natl. Acad. Sci. **348**: in review. doi:10.1073/pnas.1509523113

Marchetti, A., and N. Cassar. 2009. Diatom elemental and morphological changes in response to iron limitation: a brief review with potential paleoceanographic applications. Geobiology **7**: 419–431.

doi:10.1111/j.1472-4669.2009.00207.x

Marchetti, A., D. Catlett, B. M. Hopkinson, K. Ellis, and N. Cassar. 2015. Marine diatom proteorhodopsins and their potential role in coping with low iron availability. ISME J **9**: 2745–2748. doi:10.1038/ismej.2015.74

Marchetti, A., and P. J. Harrison. 2007. Coupled changes in the cell morphology and elemental (C, N, and Si) composition of the pennate diatom Pseudo-nitzschia due to iron deficiency. Limnol. Oceanogr. **52**: 2270–2284. doi:10.4319/lo.2007.52.5.2270

Marchetti, A., M. T. Maldonado, E. S. Lane, and P. J. Harrison. 2006. Iron requirements of the pennate diatom Pseudo-nitzschia: Comparison of oceanic (high-nitrate, low-chlorophyll waters) and coastal species. Limnol. Oceanogr. **51**: 2092–2101. doi:10.4319/lo.2006.51.5.2092

Marchetti, A., M. S. Parker, L. P. Moccia, and others. 2009. Ferritin is used for iron storage in bloom-forming marine pennate diatoms. Nature **457**: 467–470. doi:10.1038/nature07539

Marchetti, A., D. M. Schruth, C. A. Durkin, and others. 2012. Comparative metatranscriptomics identi fi es molecular bases for the physiological responses of phytoplankton to varying iron availability. Proc. Natl. Acad. Sci. doi:10.1073/pnas.1118408109

McKay, R. M. L., J. La Roche, A. F. Yakunin, D. G. Durnford, and R. J. Geider. 1999. Accumulation of ferredoxin and flavodoxin in a marine diatom in response to Fe. J. Phycol. **35**: 510–519. doi:10.1046/j.1529-8817.1999.3530510.x

McRose, D., J. Guo, A. Monier, and others. 2014. Alternatives to vitamin B1 uptake revealed with discovery of riboswitches in multiple marine eukaryotic lineages. ISME J. **8**: 2517–29. doi:10.1038/ismej.2014.146

Moore, J. K., S. C. Doney, D. M. Glover, and I. Y. Fung. 2002. Iron cycling and nutrient-limitation patterns in surface waters of the World Ocean. Deep. Res. II **49**: 463–507.

Morrissey, J., and C. Bowler. 2012. Iron Utilization in Marine Cyanobacteria and Eukaryotic Algae. Front. Microbiol. **3**: 43. doi:10.3389/fmicb.2012.00043

Morrissey, J., R. Sutak, J. Paz-Yepes, and others. 2015. A Novel Protein, Ubiquitous in Marine Phytoplankton, Concentrates Iron at the Cell Surface and Facilitates Uptake. Curr. Biol. **25**: 364–371. doi:http://dx.doi.org/10.1016/j.cub.2014.12.004

Mullin, M. M., P. R. Sloan, and R. W. Eppley. 1966. Relationship between carbon content, cell volume, and area in phytoplankton. Limnol. Oceanogr. **11**: 307–311. doi:10.4319/lo.1966.11.2.0307

Muralla, R., E. Chen, C. Sweeney, J. A. Gray, A. Dickerman, B. J. Nikolau, and D. Meinke. 2008. A Bifunctional Locus (BIO3-BIO1) Required for Biotin Biosynthesis in Arabidopsis. Plant Physiol. **146**: 60–73. doi:10.1104/pp.107.107409

Naka, H., M. Liu, and J. H. Crosa. 2013. Two ABC transporter systems participate in siderophore transport in the marine pathogen Vibrio anguillarum 775 (pJM1). FEMS Microbiol. Lett. **341**: 79–86. doi:10.1111/1574-6968.12092

Nakajima, K., A. Tanaka, and Y. Matsuda. 2013. SLC4 family transporters in a marine diatom directly pump bicarbonate from seawater. Proc. Natl. Acad. Sci. **110** : 1767–1772.

Nelson, D. M., D. J. DeMaster, R. B. Dunbar, and W. O. Smith. 1996. Cycling of organic carbon and biogenic silica in the Southern Ocean: Estimates of water-column and sedimentary fluxes on the Ross Sea continental shelf. J. Geophys. Res. **101**: 18519. doi:10.1029/96JC01573

Nelson, D. M., P. Tréguer, M. A. Brzezinski, A. Leynaert, and B. Quéguiner. 1995. Production and

dissolution of biogenic silica in the ocean: Revised global estimates, comparison with regional data and relationship to biogenic sedimentation. Global Biogeochem. Cycles **9**: 359–372. doi:10.1029/95GB01070

Noble, R. T., and J. A. Fuhrman. 1998. Use of SYBR Green I for rapid epifluorescence counts of marine viruses and bacteria. Aquat. Microb. Ecol. **14**: 114–118.

Nuester, J., S. Vogt, and B. S. Twining. 2012. Localization of iron within centric diatoms of the genus Thalassiosira. J. Phycol. **48**: 626–634. doi:10.1111/j.1529-8817.2012.01165.x

Paerl, R. W., E. M. Bertrand, A. E. Allen, B. Palenik, and F. Azam. 2015. Vitamin B1 ecophysiology of marine picoeukaryotic algae: Strain-specific differences and a new role for bacteria in vitamin cycling. Limnol. Oceanogr. **60**: 215–228. doi:10.1002/lno.10009

Pahlow, M., U. Riebesell, and D. A. Wolf-Gladrow. 1997. Impact of cell shape and chain formation on nutrient acquisition by marine diatoms. Limnol. Oceanogr. **42**: 1660–1672. doi:10.4319/lo.1997.42.8.1660

Pan, Y., D. V. Subba Roa, K. H. Mann, R. G. Brown, and R. Pocklington. 1996. Effects of silicate limitation on production of domoic acid , a neurotoxin , by the diatom Pseudo- nitzschia m ultiseries . I . Batch culture studies. Mar. Ecol. Prog. Ser. **131**: 225–233. doi:10.3354/meps131235

Parker, C. E., M. T. Brown, and K. W. Bruland. 2016. Scandium in the open ocean: A comparison with other group 3 trivalent metals. Geophys. Res. Lett. **43**: 2758–2764. doi:10.1002/2016GL067827

Parsons, T. R., Y. Maita, and C. M. Lalli. 1984. A manual of chemical and biological methods for seawater analysis, Pergamon Press.

Patro, R., G. Duggal, and C. Kingsford. 2015. Salmon: Accurate, Versatile and Ultrafast Quantification from RNA-seq Data using Lightweight-Alignment. bioRxiv. doi:10.1101/021592

Peers, G., and N. M. Price. 2006. Copper-containing plastocyanin used for electron transport by an oceanic diatom. Nature **441**: 341–344.

Pejchal, R., and M. L. Ludwig. 2005. Cobalamin-Independent Methionine Synthase (MetE): A Face-to-Face Double Barrel That Evolved by Gene Duplication R.M. Stroud [ed.]. PLoS Biol. **3**: e31. doi:10.1371/journal.pbio.0030031

Pfaffen, S., J. M. Bradley, R. Abdulqadir, M. R. Firme, G. R. Moore, N. E. Le Brun, and M. E. P. Murphy. 2015. A Diatom Ferritin Optimized for Iron Oxidation but Not Iron Storage. J. Biol. Chem. **290** : 28416–28427.

Pfaffl, M. W. 2001. A new mathematical model for relative quantification in real-time RT–PCR. Nucleic Acids Res. **29** : e45–e45.

Price, N. M., G. I. Harrison, J. G. Hering, R. J. Hudson, P. M. V. Nirel, B. Palenik, and F. M. M. Morel. 1989. Preparation and Chemistry of the Artificial Algal Culture Medium Aquil. Biol. Oceanogr. **6**: 443–461. doi:10.1080/01965581.1988.10749544

Provasoli, L. 1963. Organic regulation of phytoplankton fertility. sea **2**: 165–219.

Raguzzi, F., E. Lesuisse, and R. R. Crichton. 1988. Iron storage in Saccharomyces cerevisiae. FEBS Lett. **231**: 253–258. doi:10.1016/0014-5793(88)80742-7

Reinfelder, J. R. 2011. Carbon Concentrating Mechanisms in Eukaryotic Marine Phytoplankton. Annu. Rev. Mar. Sci **3**: 291–317. doi:10.1146/annurev-marine-120709-142720

Reyda, M. R., R. Dippold, M. E. Dotson, and J. T. Jarrett. 2008. Loss of Iron Sulfur Clusters from Biotin

Synthase as a Result of Catalysis Promotes Unfolding and Degradation. Arch. Biochem. Biophys. **471**: 32–41. doi:10.1016/j.abb.2007.12.001

Rho, M., H. Tang, and Y. Ye. 2010. FragGeneScan: predicting genes in short and error-prone reads. Nucleic Acids Res. **38** : e191–e191.

Ribalet, F., A. Marchetti, K. A. Hubbard, and others. 2010. Unveiling a phytoplankton hotspot at a narrow boundary between coastal and offshore waters. Proc. Natl. Acad. Sci. **107** : 16571–16576.

Robertson, G., J. Schein, R. Chiu, and others. 2010. De novo assembly and analysis of RNA-seq data. Nat. Methods **7**: 909–12. doi:10.1038/nmeth.1517

Robinson, M. D., D. J. McCarthy, and G. K. Smyth. 2010. edgeR: A Bioconductor package for differential expression analysis of digital gene expression data. Bioinformatics **26**: 139–140. doi:10.1093/bioinformatics/btp616

Robinson, M. D., and G. K. Smyth. 2008. Small-sample estimation of negative binomial dispersion, with applications to SAGE data. Biostatistics **9**: 321–332. doi:10.1093/biostatistics/kxm030

La Roche, J., P. W. Boyd, R. M. L. McKay, and R. J. Geider. 1996. Flavodoxin as an in situ marker for iron stress in phytoplankton. Nature **382**: 802–805.

Rogato, A., A. Amato, D. Iudicone, M. Chiurazzi, M. I. Ferrante, and M. R. d'Alcalà. 2015. The diatom molecular toolkit to handle nitrogen uptake. Mar. Genomics **24, Part 1**: 95–108. doi:http://dx.doi.org/10.1016/j.margen.2015.05.018

Saito, M. A., A. E. Noble, A. Tagliabue, T. J. Goepfert, C. H. Lamborg, and W. J. Jenkins. 2013. Slow-spreading submarine ridges in the South Atlantic as a significant oceanic iron source. Nat. Geosci. **6**: 775–779. doi:10.1038/ngeo1893

Sañudo-Wilhelmy, S. a, L. S. Cutter, R. Durazo, and others. 2012. Multiple B-vitamin depletion in large areas of the coastal ocean. Proc. Natl. Acad. Sci. U. S. A. **109**: 14041–14045. doi:10.1073/pnas.1208755109

Sañudo-Wilhelmy, S. A., L. Gómez-Consarnau, C. Suffridge, and E. A. Webb. 2014. The role of B vitamins in marine biogeochemistry. Annu. Rev. Mar. Sci **6**: 339–67. doi:10.1146/annurev-marine-120710-100912

Sanudo-Wilhelmy, S. A., G. Laura, C. Suffridge, and E. A. Webb. 2014. The Role of B Vitamins in Marine Biogeochemistry.doi:10.1146/annurev-marine-120710-100912

Sarmiento, J. L., and M. Bender. 1994. Carbon biogeochemistry and climate change. Photosynth. Res. **39**: 209–234. doi:10.1007/BF00014585

Schuback, N., C. Schallenberg, C. Duckham, M. T. Maldonado, and P. D. Tortell. 2015. Interacting Effects of Light and Iron Availability on the Coupling of Photosynthetic Electron Transport and CO_2-Assimilation in Marine Phytoplankton. PLoS One **10**: e0133235.

Shaked, Y., A. B. Kustka, and F. M. M. Morel. 2005. A general kinetic model for iron acquisition by eukaryotic phytoplankton. Limnol. Oceanogr. **50**: 872–882. doi:10.4319/lo.2005.50.3.0872

Shaked, Y., and H. Lis. 2012. Disassembling Iron Availability to Phytoplankton. Front. Microbiol. **3**: 123. doi:10.3389/fmicb.2012.00123

Shakoury-elizeh, M., J. Tiedeman, J. Rashford, and others. 2004. Transcriptional Remodeling in Response to Iron Deprivation in Saccharomyces cerevisiae □. Mol. Biol. Cell **15**: 1233–1243. doi:10.1091/mbc.E03

Shi, D., Y. Xu, B. M. Hopkinson, and F. M. M. Morel. 2010. Effect of Ocean Acidification on Iron Availability to Marine Phytoplankton. Science (80-.). **327**: 676–679. doi:10.1126/science.1183517

Simão, F. A., R. M. Waterhouse, P. Ioannidis, E. V Kriventseva, and E. M. Zdobnov. 2015. BUSCO: assessing genome assembly and annotation completeness with single-copy orthologs. Bioinforma. .

Smetacek, V., C. Klaas, V. H. Strass, and others. 2012. Deep carbon export from a Southern Ocean iron-fertilized diatom bloom. Nature **487**: 313–319. doi:10.1038/nature11229

Smith, S. R., J. T. F. Gillard, A. B. Kustka, and others. 2016. Transcriptional Orchestration of the Global Cellular Response of a Model Pennate Diatom to Diel Light Cycling under Iron Limitation. PLOS Genet. **12**: e1006490.

Sorhannus, U. 2007. A nuclear-encoded small-subunit ribosomal RNA timescale for diatom evolution. Mar. Micropaleontol. **65**: 1–12. doi:http://dx.doi.org/10.1016/j.marmicro.2007.05.002

Stein, A. F., R. R. Draxler, G. D. Rolph, B. J. B. Stunder, M. D. Cohen, and F. Ngan. 2015. NOAA's HYSPLIT Atmospheric Transport and Dispersion Modeling System. Bull. Am. Meteorol. Soc. **96**: 2059–2077. doi:10.1175/BAMS-D-14-00110.1

Streit, W. R., and P. Entcheva. 2003. Biotin in microbes, the genes involved in its biosynthesis, its biochemical role and perspectives for biotechnological production. Appl Microbiol Biotechnol **61**: 21–31. doi:DOI 10.1007/s00253-002-1186-2

Strzepek, R. F., and P. J. Harrison. 2004. Photosynthetic architecture differs in coastal and oceanic diatoms. Nature **431**: 689–692.

Strzepek, R. F., K. A. Hunter, R. D. Frew, P. J. Harrison, and P. W. Boyd. 2012. Iron – light interactions differ in Southern Ocean phytoplankton. Limnol. Oceanogr. **57**: 1182–1200. doi:10.4319/lo.2012.57.4.1182

Sunda, W. G., and S. A. Huntsman. 1995. Iron uptake and growth limitation in oceanic and coastal phytoplankton. Mar. Chem. **50**: 189–206. doi:http://dx.doi.org/10.1016/0304-4203(95)00035-P

Sunda, W. G., and S. A. Huntsman. 1997. Interrelated influence of iron, light and cell size on marine phytoplankton growth. Nature **390**: 389–392.

Sunda, W. G., and S. A. Huntsman. 2011. Interactive effects of light and temperature on iron limitation in a marine diatom: Implications for marine productivity and carbon cycling. Limnol. Oceanogr. **56**: 1475–1488. doi:10.4319/lo.2011.56.4.1475

Sutak, R., H. Botebol, P.-L. Blaiseau, T. Léger, F.-Y. Bouget, J.-M. Camadro, and E. Lesuisse. 2012. A Comparative Study of Iron Uptake Mechanisms in Marine Microalgae: Iron Binding at the Cell Surface Is a Critical Step. Plant Physiol. **160** : 2271–2284.

Tamura, K., G. Stecher, D. Peterson, A. Filipski, and S. Kumar. 2013. MEGA6: Molecular Evolutionary Genetics Analysis version 6.0. Mol. Biol. Evol. .

Tang, S., A. Lomsadze, and M. Borodovsky. 2015. Identification of protein coding regions in RNA transcripts. Nucleic Acids Res. .

Tang, Y. Z., F. Koch, and C. J. Gobler. 2010. Most harmful algal bloom species are vitamin B 1 and B 12 auxotrophs. Proc. Natl. Acad. Sci. U. S. A. **107**: 20756–20761. doi:10.1073/pnas.1009566107

Taylor, F. J. R., and R. Haigh. 1996. Spatial and temporal distributions of microplankton during the summers of 1992–1993 in Barkley Sound, British Columbia, with emphasis on harmful species. Can. J. Fish. Aquat. Sci. **53**: 2310–2322. doi:10.1139/f96-181

Taylor, R. L., D. M. Semeniuk, C. D. Payne, J. Zhou, J.-É. Tremblay, J. T. Cullen, and M. T. Maldonado. 2013. Colimitation by light, nitrate, and iron in the Beaufort Sea in late summer. J. Geophys. Res. Ocean. **118**: 3260–3277. doi:10.1002/jgrc.20244

Thamatrakoln, K., and M. Hildebrand. 2008. Silicon Uptake in Diatoms Revisited: A Model for Saturable and Nonsaturable Uptake Kinetics and the Role of Silicon Transporters. Plant Physiol. **146**: 1397–1407.

Theil, E. C., X. S. Liu, and T. Tosha. 2008. Gated pores in the ferritin protein nanocage. Inorganica Chim. Acta **361**: 868—874. doi:10.1016/j.ica.2007.08.025

Theil, E. C., M. Matzapetakis, and X. Liu. 2006. Ferritins: iron/oxygen biominerals in protein nanocages. JBIC J. Biol. Inorg. Chem. **11**: 803–810. doi:10.1007/s00775-006-0125-6

Tortell, P. D., M. T. Maldonado, and N. M. Price. 1996. The role of heterotrophic bacteria in iron-limited ocean ecosystems. Nature **383**: 330–332.

Tortell, P. D., G. H. Rau, and M. M. Morel. 2000. Inorganic carbon aquisition in coastal Pacific phytoplankton communities. Limnol. Ocean. **45**: 1485–1500.

Untergasser, A., I. Cutcutache, T. Koressaar, J. Ye, B. C. Faircloth, M. Remm, and S. G. Rozen. 2012. Primer3—new capabilities and interfaces. Nucleic Acids Res. **40** : e115–e115.

Varela, D. E., and P. J. Harrison. 1999. Effect of ammonium on nitrate utilization by Emiliania huxleyi , a coccolithophore from the oceanic northeastern Pacific. Mar. Ecol. Prog. Ser. **186**: 67–74.

Vogel, C., and E. M. Marcotte. 2012. Insights into the regulation of protein abundance from proteomic and transcriptomic analyses. Nat Rev Genet **13**: 227–232.

Warren, M. J., E. Raux, H. L. Schubert, and J. C. Escalante-Semerena. 2002. The biosynthesis of adenosylcobalamin (vitamin B_{12}). Nat. Prod. Rep. **19**: 390–412. doi:10.1039/b108967f

Webb, M. E., A. Marquet, R. R. Mendel, F. Rebeille, and A. G. Smith. 2007. Elucidating biosynthetic pathways for vitamins and cofactors. Nat Prod Rep **24**: 988–1008. doi:10.1039/b703105j

Whitney, L. P., J. J. Lins, M. P. Hughes, M. L. Wells, P. D. Chappell, and B. D. Jenkins. 2011. Characterization of Putative Iron Responsive Genes as Species-Specific Indicators of Iron Stress in Thalassiosiroid Diatoms. Front. Microbiol. **2**: 234. doi:10.3389/fmicb.2011.00234

Young, J. N., A. M. C. Heureux, R. E. Sharwood, R. E. M. Rickaby, F. M. M. Morel, and S. M. Whitney. 2016. Large variation in the Rubisco kinetics of diatoms reveals diversity among their carbon-concentrating mechanisms. J. Exp. Bot. **67**: 3445–3456. doi:10.1093/jxb/erw163

Zhang, B., N. C. VerBerkmoes, M. A. Langston, E. Uberbacher, R. L. Hettich, and N. F. Samatova. 2006. Detecting Differential and Correlated Protein Expression in Label-Free Shotgun Proteomics. J. Proteome Res. **5**: 2909–2918. doi:10.1021/pr0600273

Zhang, H., Y. Zhuang, J. Gill, and S. Lin. 2013. Proof that Dinoflagellate Spliced Leader (DinoSL) is a Useful Hook for Fishing Dinoflagellate Transcripts from Mixed Microbial Samples: Symbiodinium kawagutii as a Case Study. Protist **164**: 510–527. doi:10.1016/j.protis.2013.04.002

Zöllner, E., H.-G. Hoppe, U. Sommer, and K. Jürgens. 2009. Effect of zooplankton-mediated trophic cascades on marine microbial food web components (bacteria, nanoflagellates, ciliates). Limnol. Oceanogr. **54**: 262–275. doi:10.4319/lo.2009.54.1.0262